

DOCTORAL THESIS

Development of
Spray-Pyrolysis-Synthesised
TiO₂ Thin Films for Photocatalytic
Degradation of Volatile Organic
Compounds in Air

Jekaterina Sydorenko

TALLINN UNIVERSITY OF TECHNOLOGY
DOCTORAL THESIS
6/2023

**Development of Spray-Pyrolysis-
Synthesised TiO₂ Thin Films for
Photocatalytic Degradation of Volatile
Organic Compounds in Air**

JEKATERINA SYDORENKO



TALLINN UNIVERSITY OF TECHNOLOGY

School of Engineering

Department of Materials and Environmental Technology

This dissertation was accepted for the defence of the degree 07/02/2023

Supervisor:

Prof. Ilona Oja Acik
School of Engineering
Tallinn University of Technology
Tallinn, Estonia

Co-supervisor:

Dr. Marina Kritševskaja
School of Engineering
Tallinn University of Technology
Tallinn, Estonia

Opponents:

Prof. Didier Robert
Institute of Chemistry and Process for Energy,
Environment and Health
University of Strasbourg
Strasbourg, France

Prof. Aile Tamm
Institute of Physics
University of Tartu
Tartu, Estonia

Defence of the thesis: 17/03/2023, Tallinn

Declaration:

Hereby I declare that this doctoral thesis, my original investigation and achievement, submitted for the doctoral degree at Tallinn University of Technology has not been submitted for doctoral or equivalent academic degree.

Jekaterina Sydorenko

signature



European Union
European Regional
Development Fund



Investing
in your future

Copyright: Jekaterina Sydorenko, 2023

ISSN 2585-6898 (publication)

ISBN 978-9949-83-954-4 (publication)

ISSN 2585-6901 (PDF)

ISBN 978-9949-83-955-1 (PDF)

Printed by Koopia Niini & Rauam

TALLINNA TEHNIKAÜLIKOOL
DOKTORITÖÖ
6/2023

**Pihustuspürolüüsiga sünteesitud TiO₂
õhukeste kilede väljatöötamine lenduvate
orgaaniliste ühendite fotokatalüütiliseks
lagundamiseks õhus**

JEKATERINA SYDORENKO

Contents

List of Publications.....	7
Author's Contribution to the Publications.....	8
Introduction.....	9
Abbreviations, Terms, and Symbols	11
1 Literature overview	12
1.1 Photocatalysis.....	12
1.2 Photocatalysts	13
1.2.1 TiO ₂	15
1.2.2 TiO ₂ powder	15
1.2.3 TiO ₂ thin films.....	16
1.2.4 Precursor solution for TiO ₂ film deposition using chemical methods...	18
1.2.5 State-of-the-art development of photocatalytic TiO ₂ thin films by chemical spray pyrolysis	20
1.2.6 Trends in photocatalytic activity enhancement of TiO ₂ thin films	21
1.3 Applications based on TiO ₂ photocatalytic oxidation	23
1.4 Gas-phase photocatalytic oxidation	25
1.4.1 Indoor air pollution	25
1.4.2 Design of photocatalytic reactor	26
1.4.3 Parameters affecting the gas-phase photocatalytic oxidation process	27
1.4.4 Outlook and practical applicability of TiO ₂ films to indoor air treatment .	30
1.5 Summary of literature overview and the aim of the study	31
2 Experimental method	33
2.1 Deposition and characterisation of the TiO ₂ thin films	33
2.2 Estimation of photocatalytic activity of the TiO ₂ thin films	34
2.2.1 Stearic acid photocatalytic oxidation	35
2.2.2 Gas-phase photocatalytic oxidation of VOCs	35
2.2.3 Photocatalytic inactivation of <i>E. coli</i> bacteria and H1N1 virus.....	37
3 Results and Discussion.....	38
3.1 Characterisation of the TiO ₂ thin films	38
3.1.1 Structural and optical properties	38
3.1.2 Chemical composition and wettability	40
3.1.3 Surface properties.....	42
3.2 Photocatalytic activity of the TiO ₂ thin films	45
3.2.1 Stearic acid photocatalytic oxidation	46
3.2.2 Gas-phase photocatalytic oxidation of VOCs	47
3.2.3 Photocatalytic inactivation of <i>E. coli</i> bacteria and H1N1 virus.....	56
Conclusion	58
References.....	61
Acknowledgements	76
Abstract	77
Lühikokkuvõte	79

Appendix 1.....	81
Appendix 2.....	145
Curriculum vitae	150
Elulookirjeldus	153

List of Publications

The list of author's publications, on the basis of which the thesis has been prepared:

- I **J. Spiridonova**, A. Katerski, M. Danilson, M. Krichevskaya, M. Krunks, I. Oja Acik. "Effect of the titanium isopropoxide:acetylacetone molar ratio on the photocatalytic activity of TiO₂ thin films", *Molecules*, 24(23), 4326, 2019, doi.org/10.3390/molecules24234326.
- II **J. Spiridonova**, A. Mere, M. Krunks, M. Rosenberg, A. Kahru, M. Danilson, M. Krichevskaya, I. Oja Acik. "Enhanced visible and ultraviolet light-Induced gas-phase photocatalytic activity of TiO₂ thin films modified by increased amount of acetylacetone in precursor solution for spray pyrolysis", *Catalysts*, 10(9), 1011, 2020, doi.org/10.3390/catal10091011.
- III T. Dittrich, **J. Sydorenko**, N. Spalatu, H. N. Nickel, A. Mere, M. Krunks, I. Oja Acik. "Synthesis Control of Charge Separation at Anatase TiO₂ Thin Films Studied by Transient Surface Photovoltage Spectroscopy", *ACS Applied Materials & Interfaces*, 14(38), 43163-43170, 2022, doi.org/10.1021/acsami.2c09032.
- IV **J. Sydorenko**, A. Mere, M. Krunks, M. Krichevskaya, I. Oja Acik. "Transparent TiO₂ thin films with high photocatalytic activity for indoor air purification", *RSC Advances*, 12(55), 35531-35542, 2022, https://doi.org/10.1039/D2RA06488J.

Author's Contribution to the Publications

Contribution to the papers in this thesis are:

- I Deposition of the TiO₂ thin films by ultrasonic spray pyrolysis; characterization of structural, optical and wettability properties; measuring of self-cleaning properties of the films; data analysis; visuals; major role in writing.
- II Deposition of the TiO₂ thin films by ultrasonic spray pyrolysis; performing of gas-phase photocatalytic activity tests; data analysis; visuals; major role in writing.
- III Deposition of the TiO₂ thin films by ultrasonic spray pyrolysis; minor role in writing.
- IV Performing of gas-phase photocatalytic activity tests; data analysis; visuals; major role in writing.

Introduction

The lifestyle of modern society is leading to a situation in which people spend a significant amount of time indoors. The digital revolution and evolving technologies have driven us to work and study from home and occupy ourselves by spending much time on computers and phones. Typically, a person spends 90% of the day indoors on average, i.e. only 2 h per day outdoors. Hence, poor indoor air quality could be a reason behind acute health problems and symptoms of the sick building syndrome.

Nearly 200 pollutants are present in indoor air, most of which are volatile organic compounds (VOCs) that are emitted to the indoor air from regularly used products. The concentration of VOCs in indoor air is typically low (less than 1 ppm). Traditional treatment methods are neither sufficient nor cost-effective for the purification of indoor air containing various VOCs in low concentrations. For example, thermal incineration requires high temperatures and is unsuitable for domestic use. Through absorption and adsorption, the pollutants move to another phase but do not get degraded. Natural and mechanical ventilation help to reduce indoor pollution, but they also do not destroy the pollutants. Thus, the technology can be optimised by combining ventilation with a destructive air-purification technique.

Photocatalysis is a promising method for addressing the above-mentioned requirements. The catalyst remains unchanged after the treatment, and direct solar radiation can be used for the activation, thereby resulting in savings and simplifying the process.

TiO₂ is the most commonly used photocatalyst because of its high photocatalytic activity and excellent stability. The indoor air quality can be considerably improved by integrating thin film photocatalysts (e.g. TiO₂ thin films) with the surrounding environment. For practical applications, transparent TiO₂ films with good adhesion properties and a high photocatalytic activity under visible light should be deposited onto large, well-illuminated surfaces (e.g. windowpanes). Moreover, the TiO₂ surface possesses disinfectant properties, rendering it suitable for implementation in closed-loop ventilation systems.

TiO₂ has been extensively researched for its photocatalytic properties. However, some challenges and gaps exist in the field of material development, which limit its practical application. First, most studies focus on thick coatings prepared from commercial TiO₂ powders, while the photocatalytic activity of synthesised thin films is insufficient. Second, the preparation of visible (VIS) light-active TiO₂ using a facile wet-chemical deposition method remains a challenge. Moreover, a better understanding of gas-phase photocatalysis is essential for ensuring its practical applicability; thus, the parameters influencing the performance and causing the deactivation of thin films should be studied systematically.

The aim of this study is to develop a photocatalytic, low-material-quantity, transparent TiO₂ thin film by modifying the precursor solution. The novelty of this work is constituted by the following aspects: the systematic study of TiO₂ spray-pyrolysis-synthesised films by changing the molar ratio of acetylacetone (AcacH) in the precursor and the comprehensive analysis of changes in the material properties and their effects on the photocatalytic performance of the films. The results of this study provide a method for developing of ultraviolet (UV-A) and visible (VIS) light photocatalytically active thin films, thereby broadening the application range of thin film photocatalysts.

To realise this aim, TiO₂ thin films containing different molar ratios of titanium (IV) isopropoxide (TTIP):acetylacetone (AcacH) in the precursor solution were deposited by ultrasonic spray pyrolysis. The effect of increasing amount of AcacH in the precursor solution on the structural, optical, chemical, and morphological properties of the obtained films was studied. Moreover, the charge separation towards the external surface was investigated using surface photovoltage (SPV) measurements. The optimal molar ratio of TTIP:AcacH was investigated by the photocatalytic oxidation of the stearic acid (SA) layer. The gas-phase photocatalytic activity of the film with an optimal molar ratio was analysed under UV-A and VIS light at different operating conditions. The disinfectant properties of the film surfaces were also assessed.

This thesis is based on four published articles and is divided into three main chapters. The first chapter consists of a literature review, which includes the fundamentals of photocatalysis and the main deposition techniques used for thin film preparation. The benefits of ultrasonic spray pyrolysis and the importance of the composition of the precursor solution in preparing high-photocatalytic-activity films are highlighted. In addition, the application of the films, especially to the treatment of VOCs in indoor air, is discussed. The most widely used reactors and the effects of operating parameters on the efficiency of the photocatalytic process are described. The literature review summarises the challenges in the field and states the aims and objectives of this thesis. The second chapter describes the experimental details and characterisation methods used in this study. The third chapter elaborates on the results and discussion of the study and is divided into two sections. The first section describes the material properties of the TiO₂ films obtained at different TTIP:AcacH molar ratios. The second section summarises the photocatalytic and disinfectant properties of the films. The degradation of the stearic acid layer and different VOCs in the gas phase was monitored. Furthermore, the ability to inactivate surface-attached *E. coli* bacteria and H1N1 virus was evaluated.

This study was jointly conducted by two research groups. It is directly related to the research topics and projects of the Laboratory of Thin Film Chemical Technologies and the Laboratory of Environmental Technology, which focusses on developing TiO₂ thin films using wet-chemical methods for environmental remediation. The surface photovoltage measurements were performed in collaboration with the Helmholtz Zentrum in Berlin. Atomic force microscopy was conducted at The Arctic University of Norway. The antibacterial experiments were performed in collaboration with the National Institute of Chemical Physics and Biophysics. The antiviral experiments were conducted at the University of Tartu. This study was financially supported by The Estonian Ministry of Education and Research Institutional Research Funding projects IUT 19-4 'Thin films and nanomaterials wet-chemical methods for a new generation of photovoltaic devices', and PRG627 'Antimony-chalcogenide thin films for the next generation of semi-transparent solar cells for use in power-producing windows', the Estonian Centre of Excellence project TK141 (TAR16016EK) 'Advanced materials and high-technology devices for energy recuperation systems', and the European Commission's H2020 programme under the ERA Chair project 5GSOLAR grant agreement No 952509. In addition, this study was partially supported by ASTRA 'TUT Institutional Development Programme for 2016-2022' Graduate School of Functional Materials and Technologies (2014-2020.4.01.16-0032), Dora Plus program (activity 1), and Tallinn City Council (Raestipendium).

Abbreviations, Terms, and Symbols

A	Band area
AcacH	Acetylacetone
AFM	Atomic force microscopy
BE	Binding energy
CA	Contact angle
CB	Conduction band
CFU	Colony-forming unit
E _g	Band gap
FFU	Focus-forming unit
FTIR	Fourier-transform infrared spectroscopy
FWHM	Full width at half maximum
HOPG	Highly oriented pyrolytic graphite
IR	Infrared
ISO	International Organization for Standardization
K	Adsorption constant
k _r	Reaction rate constant
LMCT	Ligand-to-metal-charge transfer
LOQ	Limit of quantification
NHE	Normal hydrogen electrode
PCO	Photocatalytic oxidation
PEG	Polyethylene glycol
ppb	Parts per billion
ppm	Parts per million
Re	Reynolds number
RH	Relative humidity
RMS	Root mean square
r ₀	Initial reaction rate
ROS	Reactive oxygen species
SA	Stearic acid
SKPM	Scanning Kelvin probe microscopy
SPV	Surface photovoltage
t	Time
TTIP	Titanium (IV) isopropoxide
UV	Ultraviolet
UV–VIS	Ultraviolet–Visible light spectroscopy
VB	Valence band
VIS	Visible
VOCs	Volatile organic compounds
XPS	X-ray photoelectron spectroscopy
XRD	X-ray diffraction
ΔCPD	Contact potential difference

1 Literature overview

This chapter presents a brief overview of the fundamentals of photocatalysis, describes commonly used powder and thin film photocatalysts, lists the various methods of thin film deposition, and introduces potential applications of photocatalysis in different fields. This chapter primarily focusses on TiO₂ thin films as the most promising materials for the photocatalytic purification of indoor air. The challenges in TiO₂ thin film preparation for photocatalysis and the applications of TiO₂ thin films in gas-phase treatment are discussed.

1.1 Photocatalysis

Photocatalysis is an advanced oxidation process involving the formation of hydroxyl radicals and other reactive oxygen species (ROS), in the presence of a semiconductor, under suitable light irradiation. In 1972, Fujishima and Honda reported that, in photoelectrochemical cells, TiO₂ can split water into H₂ and O₂ under irradiation by ultraviolet (UV) light. Following this discovery, photocatalysis has garnered significant attention of scientists and engineers [1,2].

The photocatalysis can be divided into six steps: absorption of photons and photogeneration of electron–hole pairs, formation of the ROS, transfer of the reagents to photocatalyst surface, adsorption of the reagents, photochemical reactions on the surface/mineralisation of the organic species, and desorption and diffusion of the photocatalytic products from the photocatalyst surface [3].

The main step of the photocatalysis is the photogeneration of electron–hole pairs in the bulk of photocatalyst, when it absorbs light with an energy equal to or greater than the band gap of the material (Reaction 1.1) [4]. To initiate photocatalytic reactions on the TiO₂ surface, the photogenerated electrons and holes shall be separated and transferred to the surface-active sites. The photogenerated electrons and holes on the surface-active sites of the photocatalyst are responsible for the photocatalytic reduction (or inhibition of oxidation) or oxidation (or inhibition of reduction) of the adsorbed species, respectively (Figure 1.1) [5,6].



The hydroxyl groups adsorbed on the TiO₂ surface act as reducing agents, whereas the adsorbed oxygen acts as an oxidising agent. The transformation reactions yield hydroxyl radicals ($\bullet\text{OH}$) (Reactions 1.2–1.5), which can non-selectively mineralise almost all organic compounds adsorbed on the surface or present near the surface. Occasionally, the adsorbed organics can directly function as reducing agents; however, this situation mostly occurs in a dry atmosphere [6]. The formation of electron–hole pairs is a reversible process. The surface and bulk recombination of electron–hole pairs occur in the absence of suitable adsorbates or because of lattice defects. Energy and/or light are released during the recombination [7].



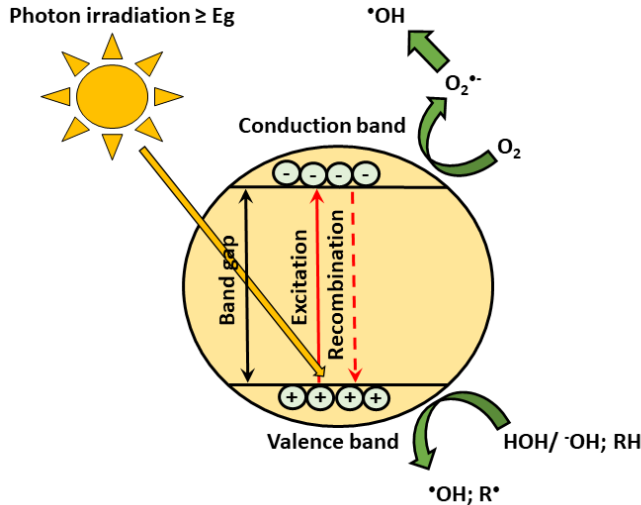
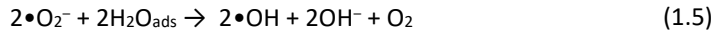


Figure 1.1. Processes occurring on the surface and in the lattice of TiO_2 . Modified from ref. [7].

Application of photocatalysis for photocatalytic oxidation (PCO) of air pollutants affords several useful extra features for traditional indoor air treatment methods, such as ventilation and filtration [8]:

- It is a destructive technique that does not generate any secondary pollution.
- It operates under ambient pressure and temperature conditions.
- The semiconductors used as photocatalyst are relatively inexpensive and can be reused for a long duration without any activity loss.
- Photocatalysis can occur under direct solar radiation.
- The process operation is facile and can be autonomous.
- PCO can occur even at low concentrations with the non-selective oxidation of organic pollutants.

Based on the above-mentioned aspects, photocatalysis can be widely applied to environmental remediation (abatement of air and water pollution), energy production, as multi-functional surfaces (e.g. self-cleaning, anti-fungal, and anti-fogging), and medicine (e.g. antibacterial, antiviral, and odour control) [4]. The detailed application of TiO_2 as a photocatalyst in different fields is introduced in Section 1.3.

1.2 Photocatalysts

In general, photocatalysts are semiconductors, that function as hosts for photocatalytic processes under suitable illumination [9].

The properties of potential photocatalysts are as follows [9–11]:

- A suitable energy band gap (E_g) to facilitate efficient absorption of the light throughout the solar spectrum.
- High mobility and long lifetime of charge carriers to reduce the recombination rate of the electron–hole pairs.
- Suitable positions of the band edges for redox reactions to produce both $\bullet\text{OH}$ and $\bullet\text{O}_2^-$ radicals from the adsorbed water and oxygen (Figure 1.2).
- A high concentration of surface-active sites (oxygen vacancies and defects) to enhance the reactivity of the photocatalyst with the adsorbed molecules.
- A large surface area to enable excellent adsorption of substances.
- Non-toxicity, low cost, and excellent mechanical and thermal stabilities to allow for environmental and economic profitability.

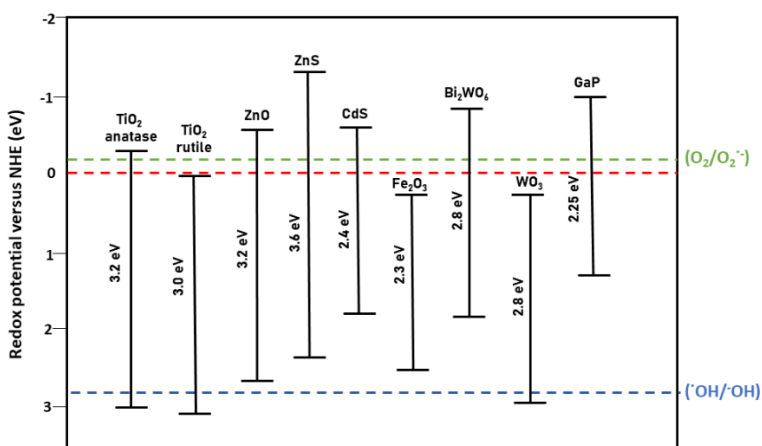


Figure 1.2. Band gaps and valence band and conduction band edges of some semiconductors compared with the standard redox potentials of the $(\text{O}_2/\text{O}_2^{\bullet-})$ and $(\bullet\text{OH}/\text{OH})$ redox couples versus normal hydrogen electrode (NHE) [7,12,13].

Nearly 190 compounds have been used as photocatalysts [8], including single-phase semiconductors (e.g. TiO₂, ZnO, NiO, CdS, Fe₂O₃, and Bi₂WO₆) and, bifunctional hybrids of two or more semiconductor materials (e.g. CdS/ZnS, CdS/TiO₂, CuFe₂O₄/TiO₂, and CdS/Au/TiO₂) [14]. ZnO shows a high photocatalytic activity; however, it is prone to photocorrosion [8]. Bi₂WO₆ also demonstrates a high photocatalytic activity, but it is unstable at low pH values [8]. ZnS has been studied as a photocatalyst due to its good physicochemical properties; however, its large band gap of 3.7 eV slightly limits its applicability [15].

Among all photocatalysts, TiO₂ has been investigated the most, owing to its chemical stability, high photoactivity, non-toxicity, and relatively low cost. Moreover, the position of valence band (VB) and conduction band (CB) edges of anatase TiO₂ render it suitable for redox reactions (Figure 1.2) [7]. Nearly 80% of the scientific literature related to oxide semiconductor photocatalysts from 1990 to 2010 is focussed on TiO₂ [8]. Furthermore, TiO₂ is the prevailing photocatalyst at present because no suitable alternative has been discovered yet.

1.2.1 TiO₂

TiO₂ is mainly prepared in the form of pigments [16]. In 2020, 1 million tons of TiO₂ pigment was produced in the USA [17]. The pigment is mostly used in the production of paints (including lacquers and varnishes; 60%), plastics (20%), and paper (5%). The remaining 15% of the produced TiO₂ pigments are used in catalysis, ceramics, coated textiles, etc. [17]. Owing to its white colour, TiO₂ is widely used in cosmetics and as a food additive (E171). However, from 2021 onwards, the European Food Safety Authority does not consider E171 to be safe for use in food because of the potential genotoxicity of TiO₂ nanoparticles with a size < 30 nm [18].

TiO₂ is an important n-type semiconductor with an indirect band gap. TiO₂ occurs in nature mainly in three crystal polymorphs: anatase (tetragonal), rutile (tetragonal), and brookite (orthorhombic). The rutile phase is the most thermally stable, whereas brookite is the most metastable phase and rarest among the natural TiO₂ polymorphs [19]. Thus, the rutile (E_g = 3.0 eV) and anatase (E_g = 3.2 eV) phases are mostly used for photocatalytic applications. Anatase is also a metastable phase that transforms into rutile upon processing in the temperature range 600–700 °C [20]. However, the anatase phase is considered more photocatalytically active than the rutile phase owing to the following reasons [2]:

- A wider band gap (3.2 eV).
- A higher concentration of surface oxygen vacancies, which increases the charge separation efficiency.
- A lower recombination rate of the electron–hole pairs.
- A higher position of the VB edge (Figure 1.2) than redox potential of the •OH/⁻OH redox couple, which allows for the oxidation of ⁻OH groups to •OH, and a lower position of the CB edge than the O₂/O₂•⁻ redox couple, allowing for the reduction of O₂ to O₂•⁻. Thus, anatase TiO₂ has favourable band-edge positions for photocatalytic redox reactions, which could facilitate the complete mineralisation of pollutants to CO₂ and H₂O [8,21].

TiO₂ can be used in photocatalysis as nanopowders in the form of suspended fluids (slurry) in a liquid medium, as highly dispersed fine particles on different supports (i.e. nanopowdered coatings), or as polycrystalline thin films [17].

1.2.2 TiO₂ powder

TiO₂ is mostly used as a nanopowder in photocatalytic applications.

Various TiO₂ powders are commercially available. The most popular powder is AEROXIDE® TiO₂ P 25 (Evonik), which is used in many photocatalytic applications as a standard titania photocatalyst owing to its high photoactivity, availability, and relatively low cost [22–25]. P 25 TiO₂ is composed of an approximately 80:20 ratio mixture of the anatase and rutile phases [18]. Cristal Global manufactures Millennium PC500 powder, whose particle size is two times lower but specific surface area (350 m² g⁻¹) is significantly greater than those of P 25 (50 ± 15 m² g⁻¹).

For water remediation, TiO₂ powder is commonly used in a simple suspended form (slurry). The photocatalyst is freely dispersed in the water phase, leading to good contact between the catalyst and water pollutants. However, the freely dispersed nanopowder should be separated from the treated fluid, which significantly increases the cost of purification [26,27]. Currently, layers of TiO₂ powder immobilised on different supports (nanopowdered coatings) are used more frequently [28]. In gas-phase

PCO, fluidised bed photocatalytic reactors containing TiO_2 powders or granules and immobilised layers of TiO_2 powders are commonly used [29]. PCO systems with immobilised catalysts exhibit a lower photocatalytic activity than non-immobilised systems as they have a fewer surface-active sites available for reaction with the pollutants [27,30]. Moreover, Verbruggen et al. [24] demonstrated the significance of the specific surface area of the nanopowders; the degradation rate of acetaldehyde on PC500 was ca 1.3 times higher than that on P25 [24].

Various PCO-based purifiers are available in the market [25]. Typically, the TiO_2 modules used in the purifiers are equipped with an UV-C lamp (Figure 1.3). For example, TiO_2 photocatalytic modules can be prepared by immobilising TiO_2 nanopowder on the surface of an aluminium honeycomb [31].

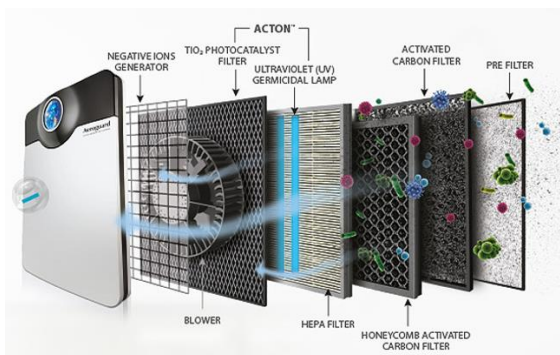


Figure 1.3. Schematic of an air purifier with a TiO_2 filter [32]. This is one example application of TiO_2 ; the detailed application of TiO_2 as a photocatalyst in different fields is introduced in Section 1.3.

The above-mentioned purifiers effectively remove numerous VOCs, get rid of unpleasant odours, and neutralise bacteria and viruses with an efficiency of up to 99.99%. Owing to the low adhesion strength of the TiO_2 nanoparticles in the filter module, it is recommended to replace the filters biennially [31,32].

To solve the problem of particle loss from the photocatalytic coatings and to broaden the application scope of photocatalysis, polycrystalline TiO_2 thin films on different supports can be used instead of TiO_2 nanopowders or nanopowdered coatings.

1.2.3 TiO_2 thin films

TiO_2 thin films have a high optical transmittance in the visible light region, a high dielectric constant (20–50), a high refractive index (anatase: 2.54, rutile: 2.75), excellent mechanical and chemical stabilities, and photoinduced superhydrophilicity (water contact angle ≈ 0) [33–37]. Owing to these properties, various TiO_2 -based thin films have been developed and used in several applications, such as solar cells, gas sensors, antireflective coatings, and photocatalysis [37].

The deposition of TiO_2 thin films onto the substrate affords a transparent layer with the thickness ranging from a few nanometres to several micrometres, depending on the fabrication method and deposition parameters [38–40].

The main advantages of TiO_2 thin films over nanopowdered coatings are as follows [41–43]:

- Low material quantity;
- Transparency;
- High mechanical resistivity;
- Excellent adhesion properties;
- Homogeneous surface coverage;
- Long-term stability;
- Reusability;
- Photoswitchable surface wettability;
- Surface multi-functionality (e.g. self-cleaning, anti-fungal, and anti-fogging).

To date, the main limitation of TiO₂ thin films is the insufficient photocatalytic activity, leading to the research on material development and in-depth analyses of the material properties [34].

The properties and photocatalytic performance of the films strongly depend on their degree of crystallinity, crystallite size, surface chemical composition, surface area, and electronic structures [36,44]. It is important to control the TiO₂ phase structure during the growth because the characteristic properties of the obtained film depend on the crystal structure, orientation, and morphology [36]. As mentioned in Section 1.2.1, TiO₂ generally crystallises in three structures: anatase, rutile, and brookite [2]. The phase transformation is determined by the process of thin film growth and is influenced by the defect concentration, grain boundary concentration, and particle packing.

Thin films can be deposited using physical or chemical methods, which comprise many sub-methods (Figure 1.4) [45].

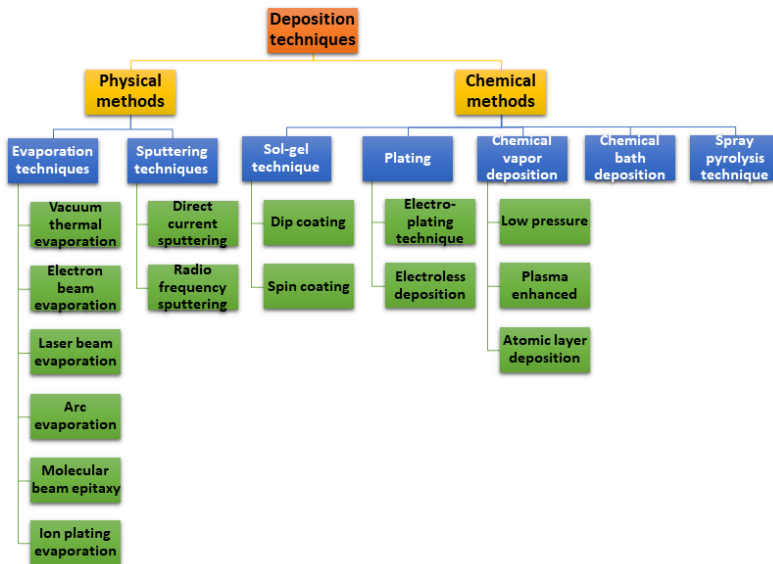


Figure 1.4. Methods of thin film deposition.

Sputtering and evaporation are the common physical methods for preparing thin films; the photocatalytic activities of such films have been tested in VOCs PCO in several studies [46,47] (Appendix 2).

For example, Garliso and Palmisano prepared a 20 nm thick TiO₂ film by electron beam evaporation, which could oxidise approximately 40% of toluene (5 ppm) in 30 min under UV-A irradiation in a gas-phase batch reactor [46]. In another study, 100 nm thick TiO₂ films fabricated by physical evaporation oxidised 80.5% of acetaldehyde (40 ppm) in 20 s [47].

Table 1.1 in Appendix 2 shows that the TiO₂ films fabricated using physical and chemical methods have similar photocatalytic activities. Since the preparation of thin films using physical methods is more expensive than that using chemical methods, owing to the requirements of high-purity reagents and vacuum, chemical methods are widely used for fabrication of photocatalysts [48].

The photocatalytic properties of the thin films obtained using chemical deposition techniques strongly depend on the chemistry of the solution (e.g. concentration, pH value, and viscosity), deposition parameters, and post-deposition treatment conditions (e.g. temperature, time, and environment) [34,49].

The most common wet-chemical deposition methods are sol-gel dip/spin coating, chemical batch deposition, and spray pyrolysis (Figure 1.4) [50]. Among all the deposition methods, the sol-gel-synthesised spin-/dip-coated thin films have been researched the most [49,51,52]. According to the Web of Science database, approximately 20% of the papers on TiO₂ thin films discuss films synthesised by sol-gel spin/dip coating. Thin films prepared by the sol-gel process have been applied to the PCO of various VOCs such as toluene, acetaldehyde, formaldehyde, and ethanol. [49,51].

For example, Hernandez-Alonso [53] reported a toluene conversion efficiency of 60% (initial concentration = 192 ppm) by a sol-gel dip-coated 470 nm thick TiO₂ film in 2 h under UV-A irradiation [53]. In their study on sol-gel dip-coated 350 nm thick TiO₂ film, Quici et al. [54] achieved a toluene conversion efficiency of 78% (initial concentration = 155 ppb) in ca 1 s under UV-C irradiation [54] (Appendix 2).

The selection of the deposition technique is crucial to the formation of stable thin films with the desired properties. For future manufacturing applications, the chosen method should be cost-effective, easily scalable, and operable at relatively low temperatures and pressures. To obtain high-photocatalytic-activity films, the synthesis method should allow for the control of the film microstructure, deposition rate, and formation of the adhesive film.

1.2.4 Precursor solution for TiO₂ film deposition using chemical methods

As mentioned in the previous section, in wet-chemical methods, the choice of the precursor solution and its composition and concentration influence the properties of the thin films. Solution preparation in these methods is often based on sol-gel process. In the sol-gel process, an oxide network is formed during the polymerisation reactions of the precursor dissolved in the liquid media [55]. Titanium alkoxides are commonly used as Ti precursors in sol-gel chemistry. Dulian et al. [56] prepared TiO₂ films by sol-gel dip-coating using two different Ti precursors, namely, titanium (IV) isopropoxide (TTIP) and titanium (IV) butoxide dissolved in anhydrous ethanol; HCl was added to avoid precipitation [56]. They observed that the films obtained from the TTIP solution had smaller grains and a higher photocatalytic activity in methylene orange PCO than those obtained from titanium (IV) butoxide [56].

Metal alkoxide precursors exhibit a high reactivity towards water, thereby producing titanium-oxo/hydroxo precipitates [57]. Chemical additives or so-called chelating ligands are used to retard the fast hydrolysis of the precursor. Chelating ligands are resistant to

hydrolysis and block hydrolysis-condensation sites [58]. Additives such as stabilising agents (e.g. acetylacetonate, diethanolamine, and polyethylene glycol) [39] [55,58–60], acids (e.g. HCl, acetic acid, and citric acid) [55,58], bases (e.g. NaOH) [61], and solvents (e.g. 2-methoxyethanol) [62] can be used to stabilise the solution. The choice of the chemical additives and their concentration could affect the properties of the final material [58,63,64].

Acetylacetonate (AcacH) is a strong chelating agent that behaves as a nucleophilic reactant and replaces the alkoxy group in metal alkoxides, forming stable transparent complexes [57,58,61,63,65]. The formation of complexes upon the reaction of TTIP with AcacH in an ethanol solution is shown in Figure 1.5. Dimeric $[\text{Ti}(\text{OR})_3(\text{AcacH})]_2$ structure and monomeric *cis*- $\text{Ti}(\text{OR})_2(\text{AcacH})_2$ structure were formed when TTIP ($\text{Ti}(\text{OR})_4$) was reacted with AcacH in molar ratios of 1:1 and 1:2, respectively [57,63].

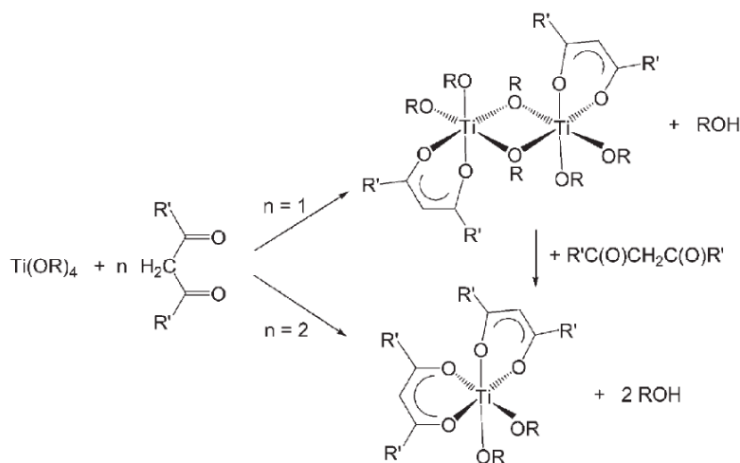


Figure 1.5. Modification of TTIP ($\text{Ti}(\text{OR})_4$) by AcacH in 1:1 and 1:2 molar ratios [57].

The role of the chelating ligand concentration in the material and photocatalytic activity of the synthesised TiO_2 has been explained in several studies [66–70]. Juma et al. [58] studied the formation of a TTIP:AcacH complex by infrared spectroscopy and the effect of TTIP:AcacH molar ratios (1:1, 1:2, 1:3, and 1:4) in the precursor solution on the morphological, structural, and optical properties of TiO_2 thin films [58]. The FTIR spectra revealed that complete chelation occurred for the solution with a TTIP:AcacH molar ratio of 1:2. At a molar ratio of 1:3, in addition to the complex formation, excess AcacH was detected in the solution, as proven by the appearance of the peaks of the carbonyl groups not involved in chelation [58]. The Raman spectra and XRD diffractogram showed that the transformation to rutile phase occurred at lower annealing temperatures; for the TTIP:AcacH molar ratios of 1:2 and 1:3, the peaks of the rutile phase started to appear at 800 and 700 °C, respectively [58].

Away et al. [70] studied the effects of three additives (diethanolamine, lactic acid, and citric acid) on TiO_2 films prepared by sol-gel dip coating [70]. They found that all the stabilising agents prevented solution precipitation; the films obtained from different sols had similar structural and morphological properties and could oxidise ca 90% of methylene blue in 120 min under UV irradiation [70]. Imao et al. [63] prepared TiO_2 nanocrystalline films by the addition of two hydrolysis inhibitors, namely AcacH

and polyethylene glycol (PEG) [63]. They discovered that thin films with a narrow particle size distribution can be prepared by increasing the amount of PEG in solution; consequently, the adsorption of organics could be improved [63]. Kajitvichyanukul et al. [64] determined the effect of AcacH on the photocatalytic activity of TiO₂ films in Cr (VI) PCO [64]. The change in the titanium (IV) butoxide:AcacH molar ratio from 1:0 to 1:2 resulted in a smoother surface and enhanced adhesion properties [64]. Kaltsum et al. [71] studied the role of AcacH in the PCO to reduce the quantity of degradation products such as free fatty acids and peroxide in used frying oil [71]. They found that when the TTIP:AcacH molar ratio was increased from 1:1 to 2:3, the obtained TiO₂ films had a higher crystallite size, film thickness, and photocatalytic activity [71]. Yu et al. [68] studied the effect of AcacH molar ratio on the corrosion properties of a silane–zirconium sol–gel coating. They observed that an increase in the AcacH molar ratio from 1 to 3 narrowed the particle size distribution, thereby making the surface smoother and more compact and increasing the corrosion potential [68].

Acetylacetone, benzoylacetone, and urea are used as fuel additives in combustion film synthesis [72,73]. Thus, excess AcacH in the precursor solution can be used as a fuel. The combustion of organic precursors during the film growth can result in a decrease in the number of oxygen vacancies on the surface of the obtained film [72,73]. In contrast, as a chelating ligand, excess of AcacH can be a source of carbon impurities, which can be incorporated into the TiO₂ lattice and grain boundaries [69]. The electrons in the highest occupied molecular orbital of the chelating ligand can directly make a transition to the CB of TiO₂ [69]. Consequently, the chelating ligands and TiO₂ bonds exhibit the ligand-to-metal charge transfer (LMCT) mechanism, which facilitates the efficient photogeneration of •O₂⁻ under VIS light irradiation.

The influence of chelating agents on the properties of the TiO₂, has been studied extensively; however, to the best of our knowledge, the effects of excess AcacH in the precursor solution, after complete formation of complex, on the growth and photocatalytic activity of the film have not been investigated systematically. Moreover, there is a literature gap between the material and photocatalytic properties of TiO₂ thin films with respect to changes in the AcacH molar ratio in the precursor solution.

1.2.5 State-of-the-art development of photocatalytic TiO₂ thin films by chemical spray pyrolysis

Spray pyrolysis is a wet-chemical method based on the deposition of a sol (spray solution) on a heated substrate.

The main benefits of spray pyrolysis over other wet-chemical methods are as follows [74,75]:

- Uniform and large area coverage,
- Facile control of the film thickness,
- Good reproducibility of the films,
- In-line production with a high throughput, and
- High material utilisation, i.e. low material wastage.

Despite their advantages, spray-pyrolysis-synthesised TiO₂ thin films have been studied less than spin- and dip-coated films, as discussed in Section 1.2.4 [49,52,59]. The main reason is that in addition to the precursor solution, the process parameters of spray pyrolysis must be optimised [39,76,77].

The pyrolysis process begins by nebulising the precursor solution into a liquid aerosol and generating droplets. Then, aerosol is transported to the hot substrate, on which

the dispersed precursor decomposes forming a thin film. All the processing parameters during this period affect the properties of the final material.

The droplet diameter or volume, initial concentration and composition of the precursor solution, deposition rate, and temperature determine the final properties of the obtained material, such as the average particle size and distribution, phase composition, and homogeneity [75,78–81].

Therefore, all the deposition parameters and the precursor solution composition and preparation technology must be optimised for obtaining TiO₂ thin films with a high photocatalytic activity.

Atay et al. [82] synthesised 240 nm thick TiO₂ films from a TiCl₄ precursor by ultrasonic spray pyrolysis at 300 °C. The preferential orientation (004) significantly influenced the structural, optical, and surface properties of the obtained films, resulting in a low refractive index, which may be beneficial for potential applications in photocatalysis [82]. Cao et al. [83] prepared TiO₂ thin films by ultrasonic spray pyrolysis using N₂, O₂, or a mixture of these gases as carriers. The TiO₂ film obtained in the nitrogen atmosphere exhibited a pyramidal morphology and had a lower photoluminescence intensity, resulting in a lower recombination rate of the electron–hole pairs [83]. The photocatalytic activity of the film in paraoxon pesticide PCO under visible light irradiation increased owing to the presence of oxygen vacancy defects and Ti³⁺ species, which led to a red shift in the adsorption edge [83].

TiO₂ thin-film preparation for photocatalytic applications via optimisation of the deposition parameters of ultrasonic spray pyrolysis was previously studied at the Department of Materials and Environmental Technology, Tallinn University of Technology. In these studies [39,59,77,84], the TTIP:AcacH molar ratio in the solution was set to 1:4, and the effect of the deposition temperature in the range 250–450 °C was investigated. A deposition temperature of 350 °C along with post-annealing in air for 1 h at 500 °C was optimal for photocatalytic thin-film preparation because of the presence of numerous OH[−] groups and oxygen vacancies on the film surface [84]. These thin films could oxidise up to 7.5, 9.3, and 4.8 ppm of acetaldehyde, acetone, and heptane, respectively, as individual air pollutants with an initial concentration of 10 ppm, for a catalyst surface area of 600 cm² under UV-A irradiation (Appendix 2) [77,84].

In this study, the precursor solution was optimised to enhance the photocatalytic activity of the TiO₂ films.

1.2.6 Trends in photocatalytic activity enhancement of TiO₂ thin films

The photocatalytic activity of TiO₂ thin films has been increased using several fabrication strategies. The major challenges regarding the efficient photocatalytic activity of TiO₂ thin films have also been discussed. First, TiO₂ has relatively wide band gaps of 3.2 and 3.0 eV for the anatase and rutile phases, respectively, which implies the requirement of ultraviolet light irradiation. Second, the high recombination rate of the charge carriers results in the low quantum efficiency of the process. Third, TiO₂ is a non-porous material with a polar surface; hence, only a few non-polar organic pollutants can be adsorbed [85]. Accordingly, several studies on TiO₂ photocatalysis are focussed on overcoming these challenges and modifying TiO₂ to increase its photocatalytic activity [85].

Doping is one approach to overcome the fast recombination of the electron–hole pairs and shift the activity of the material to the visible-light region [37]. TiO₂ can be modified by metal dopants such as Fe, Nb, Zr, Co, Sm, Pt, Ag, and Au or non-metal

dopants such as N, S, C, B, and F [37]. Xu et al. [86] prepared Fe-doped TiO₂ films with Fe:Ti atomic ratios ranging 0% to 20% by sol-gel drain coating. The film with an Fe:Ti molar ratio of 3% exhibited the highest photocatalytic activity in the PCO of Rhodamine B owing the generation of defect states, which prolong the lifetime of the electron-hole pairs. However, at a molar ratio of 5%, these defect states behave as recombination centres, thereby decreasing the PCO [86]. Single doping with a metal or non-metal resulted in excellent performance and decreased the recombination rate of the charge carriers, but there were thermal stability issues, and some dopants could be lost during the preparation process. Thus, co- or tri-doping has been used in some studies. For example, Alotaibi et al. [87] prepared Zn and N co-doped TiO₂ thin films by chemical vapour deposition. The dopants addition resulted in a prolonged charge carrier lifetime and high concentration of the formed superoxide, which enhanced the photocatalytic and antibacterial activities of the films [87]. Jiang et al. [88] studied the PCO of benzene under visible light irradiation on F, Fe, and N tri-doped TiO₂ thin films prepared by sol-gel spin coating. The maximum conversion efficiency (36.27%) was achieved by the film with 5, 0.03, and 7 atomic percent of F, Fe, and N, respectively; the efficiency of the undoped film was significantly lower (approximately 2.5%) [88]. Other methods for modifying TiO₂ are dye sensitisation, fabrication of composites with other materials, and surface modification. Zhang et al. [89] investigated the PCO of a TiO₂/reduced graphene oxide multilayer film. The PCO rate of the obtained layer against Rhodamine B dye was $2.6 \times 10^{-2} \text{ min}^{-1}$, which is 13 times higher than that of the TiO₂/poly(styrene sulfonate) nanocomposite film. The PCO rate increased owing to the formation of Ti-O-C bonds, which bridged TiO₂ and reduced graphene to enable efficient charge separation and transfer, thereby increasing the number of •O₂⁻ surface-active sites [89].

Generation of various point defects, such as misplaced lattice atoms/ions, vacancies, and foreign atoms/ions, and dislocations is another strategy to increase the photocatalytic activity of TiO₂ films. Polycrystalline materials have defects owing to their grain and crystallite boundaries. The location of a defect strongly depends on its nature. Defects can form energy levels within the band gap of the material, referred to as 'trap sites'. Depending on the location, trap sites can be permanent (deep location) or temporary (shallow location), and a charge carrier can be bound. In the first case, the charge carriers are strongly bonded and not available to participate in the redox reaction; in the second case, the trap sites increase the separation of the electron-hole pairs. Therefore, defects can enhance as well as inhibit the photocatalytic activity of TiO₂ [48]. Abdullah et al. [90] used photoluminescence spectroscopy to study the trap-state defects in TiO₂ thin films deposited by magnetron sputtering at different temperatures [90]. They observed that an increase in the deposition temperature decreased the number of oxygen vacancies, which are the predominant defect states facilitating the PCO process [90]. Carey and McKenna [91] added dopants such as Zr and Hf to TiO₂ to optimise the mobility of the charge carriers and prevent electron trapping [91].

The higher the degree of crystallinity of TiO₂, the better its PCO performance because less defects are present in bulk TiO₂ [48]. Thus, the calcination temperature can be increased to enhance the crystallinity; however, high temperatures lead to crystal growth in anatase TiO₂, resulting in grain growth and the phase transformation of anatase to rutile. To limit the aggregation of TiO₂ particles, additives can be used, e.g. SiO₂. Zhou et al. [92] prepared a film by the sol-gel process and observed enhanced PCO of Rhodamine B owing to its lower crystallite size [92].

Another approach to increase the photocatalytic activity of the films is to control the surface states and facet orientations, which determine the adsorption of reactants and charge carrier transfer during the photocatalysis [93,94]. TiO_2 nanoparticles are usually dominated by (101) facets with small amount of the highly oriented and energetic (001) facets. Stefanov et al. [94] observed that the PCO rate of acetaldehyde in the gas-phase was on the order of magnitude higher on the (001) facets than on the (101) facets. Moreover, they found that the film with the preferred orientation (001) was less affected by changes in the relative humidity (RH) compared to those with a random orientation [94]. However, Pan et al. [93] observed that (100) facets have approximately ten times higher density of surface-active sites than (001) facets [93].

Most of the above-mentioned strategies are expensive because they require the incorporation of additional materials. Therefore, the choice of the deposition technique and precursor and the determination of optimal parameters for film deposition are crucial for obtaining cost-effective thin films with a high photocatalytic activity. Moreover, the adaption of new advanced characterisation techniques to explain changes in the surface of the films is necessary for a deeper understanding of the enhancement of photocatalytic properties.

1.3 Applications based on TiO_2 photocatalytic oxidation

During photocatalysis, solar energy is converted to chemical energy. The ability of TiO_2 to oxidise or reduce molecules via its chemical energy can be harnessed in various applications, such as environmental remediation, energy production, medicine and functional surfaces in construction (Figure 1.6) [95].

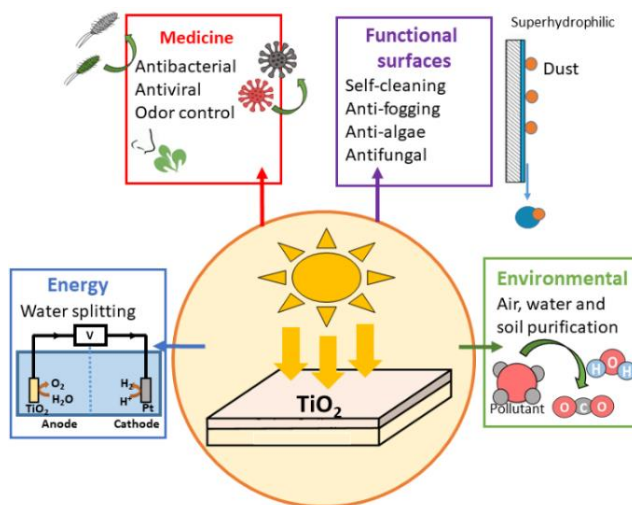


Figure 1.6 Applications of TiO_2 in different fields of photocatalysis.

TiO_2 was used in construction in the 1910s as a pigment and opacifier in building materials because of its white colour and excellent optical properties [96]. The photoirradiation of titania electrodes for water splitting by Fujishima and Honda in 1972 considerably impacted the field of photocatalysis [1] [97]. Hydrogen production via water splitting is a promising application of TiO_2 because it allows for the production of electric energy in fuel cell systems without CO_2 emissions [98].

Since the discovery of the photocatalytic properties of TiO₂, its application range has expanded rapidly. The use of TiO₂ powders in the PCO of organic pollutants for air and wastewater treatment began in 1980s. A few years later, the ability of TiO₂ to kill microorganisms such as *Lactobacillus acidophilus*, *Saccharomyces cerevisiae*, and *Escherichia coli* was discovered, following which the application of TiO₂ to medicine began attracting the interest of researchers [96,99]. In 1994, Sierka and Sjogren found out that the ROS formed on the TiO₂ surface under light irradiation destroyed the shells of viruses, leading to their inactivation [100]. Recent papers have demonstrated that TiO₂ thin films can inactivate *E. coli* cells in 90 min under UV irradiation [101], and the films modified with carbon nanomaterials can inactivate *E. coli* bacteria at a rate constant of 0.01 min⁻¹ under VIS light irradiation [102]. Sol-gel synthesised TiO₂ films can inactivate 99% of influenza virus in 15 and 30 min under UV and fluorescent lamp irradiation, respectively [103], and SARS-CoV-2 virus after 5 h under ambient laboratory light irradiation [104].

The application of TiO₂ as a functional surface originated from the discovery of its light-induced reversible hydrophilic properties by Wang et al. in 1997 [105]. They observed that the water contact angle of the as-prepared TiO₂ film was 72°±1°; upon UV irradiation, the TiO₂ film surface became superhydrophilic, exhibiting a water contact angle of 0°±1° [105]. This finding has initiated the use of TiO₂ coatings as self-cleaning and anti-fogging surfaces. In 2001, Pilkington Glass Company developed the first commercial self-cleaning glass. Pilkington Activ™ is a glass with a 15 nm thick TiO₂ film deposited by atmospheric pressure chemical vapour deposition; it is still available in the market [106]. The quantum efficiency of stearic acid PCO on Pilkington Activ™ at 365 nm was 0.7 × 10⁻⁵ molecules per photon, and the material became superhydrophilic after prolonged UV irradiation, deeming it a suitable reference material for semiconductor film photocatalysis [107].

Currently, TiO₂ is widely used in construction in the form of nanoparticles or nanometre-sized thin films to prepare photoactive TiO₂-based building materials. This technology is applied in exterior construction materials (e.g. tiles, paints, glass, and tents), interior furnishing materials (e.g. windows, wallpaper, and paints), and road construction materials (e.g. lamp coatings, traffic signs, and tunnel walls) [96,108]. An example application of the addition of TiO₂ photocatalysts in construction is the 'Dives in Misericordia' Church in Italy [109]. Another example is a TiO₂ photocatalytic pavement block, with an area of 10,000 m², on a parking line in Antwerp, Belgium, which was built within the framework of the pilot project. The on-site measurements revealed a decrease in the NO_x concentration and long-term activity; however, a precise interpretation of results is difficult owing to the influence of traffic, wind speed, light intensity, and RH [108,110].

As discussed in Section 1.2.2, TiO₂ powders have been applied to indoor air PCO treatment as a module in air purifiers (Figure 1.3). The application of TiO₂ thin films to indoor air purification has been studied, and some success has been achieved at the scientific level [111]. However, the significant gap between the laboratory-scale academic research and production demand should be bridged to realise the practical application of PCO technology, as discussed in Section 1.4.4. In addition to the preparation of durable photocatalyst, a comprehensive study of the gas-phase PCO is essential. Moreover, the analysis of the ability of TiO₂ thin films to oxidize mixtures of organic pollutants in air under VIS light irradiation remains a challenge.

1.4 Gas-phase photocatalytic oxidation

The application of photocatalysis using TiO_2 to the decomposition of air pollutants was first studied in the early 1970s; the partial PCO of paraffins was published by Teichner et al. [111,112]. The research interest in indoor air purification using TiO_2 emerged in the 2010s [108]. Photocatalysis is a cost-effective technology for purifying indoor air consisting of a wide spectrum of VOCs. Although the PCO via TiO_2 has been studied by various researchers for nearly 50 years, certain limitations impede its commercial application to indoor air treatment. The nanopowdered TiO_2 coatings that have been extensively investigated in the literature are not safe because nanoparticles could enter the human body owing to their poor adhesion properties, resulting in adverse health effects [108]. Therefore, it is crucial to prepare TiO_2 thin films with excellent adhesion properties and a PCO ability similar to that of powders. In addition to the improvement in the material properties of thin films, the gas-phase photocatalytic activity of the thin films in the PCO of air pollutants under different operating parameters must be researched extensively.

1.4.1 Indoor air pollution

Indoor air quality is an important issue because it is strongly related to the health and comfort of the residents [113]. Today people spend more than 90% of their time indoors. Indoor air pollutants include particulate matter, inorganic compounds, VOCs, and biological factors, all of which can negatively impact the human health.

VOCs are present in the indoor air because of the daily use of products such as cosmetics, air fresheners, and furniture; they constitute a major fraction of indoor air pollutants [114]. Indoor air can contain up to 200 different VOCs with individual concentrations of less than 10 ppb [25]. The concentrations of VOCs in the buildings depend on the RH, building age, and wealth status of the families [115]. Moreover, modern construction and renovation strategies are directed towards energy-efficient buildings. Immense attention to the energy savings often goes against the maintenance of the recommended VOCs levels in the indoor air. Insolation of buildings can lead to poor air infiltration; if the intentional ventilation is insufficient, it can result in higher VOCs concentrations [116]. For example, the mean concentration of total VOCs in energy-efficient buildings in Switzerland is 384 ppb [115]. However, according to the European Commission, the comfort range of total VOCs is less than 200 ppb [117]. If the concentration of total VOCs indoors exceeds 25 ppm, the indoor air is considered toxic [117].

Airborne bacteria, viruses, and fungi are present in the indoor air. Bioaerosols can cause human diseases, whereas others are beneficial to organisms. Jo and Seo [118] calculated that, on average, humans inhale 5×10^6 and 9×10^5 virus- and bacteria-like particles, respectively, from the indoor air every day [118]. Currently, owing to COVID-19, there is a growing concern regarding viral pandemics. Therefore, purification of air from bacteria and viruses has attracted scientific attention [119].

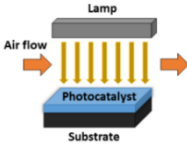
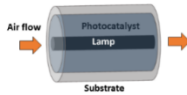
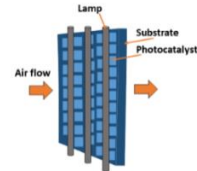
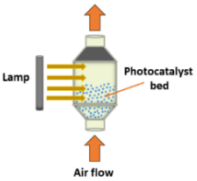
The control of VOCs concentrations and disinfection of indoor air can enhance the working productivity and reduce the health effects [117]. However, not all treatment technologies are suitable for domestic use. Photocatalysis is a prospective and cost-effective technology that can be easily applied to indoor air purification [111].

1.4.2 Design of photocatalytic reactor

The modelling and design of photocatalytic reactors should consider the fluid hydrodynamics, lamp emission models, radiation transport, and kinetics [111].

The major types of gas-phase reactor construction for photocatalysis are plate, annular, honeycomb monolith, and fluidised bed reactors. The characteristic features of the main reactor design for gas-phase photocatalysis are listed in the Table 1.1.

Table 1.1. Major types of gas-phase photocatalytic reactors [111,122].

Type of the reactor	Scheme	A short description of the reactor	Advantages	Limitations
Plate		Square or rectangular box. The catalyst is located at the bottom of the reactor. Can be equipped with an inner or outer source of irradiation.	Simplicity of the design. Small pressure drop. Possibility of obtaining a high reaction rate.	Small reaction area. Low mass transfer. Not commercially feasible.
Annular		Cylindrical tube. The catalyst is coated onto the inner surface. The lamp is located at the centre of the reactor.	Simplicity of the design. Small pressure drop. High linear velocity of the air.	Small reaction area. Not commercially feasible
Honeycomb monolith		Contains a certain number of channels. The catalyst is coated onto the walls of the channels as a thin layer.	Large reaction area, high mechanical strength, compact structure. High area-to-volume ratio.	Low photon utilisation rate.
Fluidised bed		Gas goes through a transparent container, which is filled with the catalyst.	High gas-feed rate. Small pressure drop. Good contact of the pollutant with the catalyst.	Difficulties in control. Loss and removal of the catalyst.

Photocatalytic reactors can operate in batch, continuous, or recyclable regimes. Conventionally, the batch regime is used in laboratory gas-phase PCO because it affords facile scalability of the reactor system and study of the reaction kinetics [120]. However, the continuous-flow regime provides more information for potentially commercial applications because it mimics the operation of air purification systems [120,121].

The important parameters in a photocatalytic reactor design are the gas flow type (streamline or turbulent), gas flow rate (volume and pressure drop), gas residence time in the reactor, distance between the light source and photocatalyst, and mass transfer between the photocatalyst and contaminants [122]. The reactor design should offer good conditions for PCO reactions. The main limitations of the photocatalytic reactor design are mass and photon transfer. Therefore, the reactor should be compact while affording a large throughput, a low pressure drop, an optimal use of radiation, and no loss of catalyst [84].

As shown in Table 1.1, all reactor constructions have advantages and limitations. Therefore, the basic designs of the reactor construction have been modified to optimise the process performance. Tokode et al. [123] studied the performance of a photocatalytic impeller reactor in toluene PCO to overcome the mass-transfer limitations. The catalyst was immobilised on modified Rushton impellers such that the reactor could be operated as a stirred tank reactor [123]. Micro- and milli-reactors are gaining popularity owing to their unique feature of microspace. These reactors solve the problems of photocatalyst coating, mass transfer, and illumination [124]. Da Costa Filho et al. [125] studied the PCO of n-decane in a multi-photoreactor coated with a TiO₂-P 25 thin coating. The catalyst-coated surface area per reactor volume was 990 m² m⁻³, and the gas streams were fed to alternate chambers, which resulted in good contact between the pollutant and the catalyst [125].

1.4.3 Parameters affecting the gas-phase photocatalytic oxidation process

The operating parameters, such as the air flow rate, initial concentration of the pollutants, oxygen concentration, RH, temperature, and irradiance, can strongly affect the performance of PCO. Therefore, the optimisation of these parameters is instrumental in the process design.

Air flow regime

Air flow rate is the main parameter that affects the mass transfer; it also determines the residence time of the pollutants in the reactor and the amount of treated air per unit time or volume of the catalyst. An increase in the air flow rate may have a dual antagonistic effect on PCO. Mass transfer improves with an increase in the air flow rate, whereas the contact time between the pollutant and catalyst surface decreases. At low gas flow rates, the mass transfer may limit the PCO efficiency, wherein, the efficiency would increase with an increase in the gas flow rate. At intermediate gas flow rates, the PCO of VOCs is not affected by changes in the gas flow rate, and the reaction kinetics on the photocatalyst surface is the limiting factor. At high gas flow rates, the residence time in the reactor is insufficient for the PCO of VOCs on the photocatalyst surface; the efficiency of the PCO would increase with decreasing gas flow rate. The reactor configuration and reaction kinetics on the photocatalyst surface should be considered while determining the optimal gas flow regime [7]. Air moves in the reactor at ambient room temperature and pressure, which indicates that air is a Newtonian incompressible

fluid with uniform physical properties [111]. The Reynolds number (Re) can be used to describe the mass transfer (Equation 1) [126]. Obee [127] found that, for a TiO_2 glass-plate photocatalytic reactor with a catalyst surface area of 39 cm^2 , the PCO rate of toluene with an initial concentration of 0.71 ppm increased up to an Re value of 300 , after which the effect of mass transfer was negligible [127].

$$Re = \frac{\rho u L}{\mu} \quad (1)$$

where ρ is the density of air, kg m^{-3} ,
 u is the air flow speed, m s^{-1} ,
 L is the characteristic linear dimension of the reactor, m ,
and μ is the dynamic viscosity of the air, $\text{Pa}\cdot\text{s}$.

Quici et al. [54] studied the PCO of toluene (500 ppb) in a benchtop plug-flow photocatalytic reactor, wherein the TiO_2 catalyst was coated onto the Raschig rings by sol-gel dip coating. They observed a decrease in the toluene conversion efficiency from 90% to 30% with an increase in the air flow rate from 0.125 to 4 L min^{-1} , and the residence time in the reactor decreased from 1920 to 129 ms [54]. Sleiman et al. [128] also observed a decrease in the toluene conversion efficiency with an increase in the air flow rate [128]. Liang et al. [129] observed an increase in the efficiency of the acetone PCO from 18% to 78% with an increase in the air flow rate from 1 to 3 L min^{-1} ; however, a further increase in the air flow rate resulted in a decrease in the PCO efficiency [129].

Initial concentration of the pollutants

The PCO rate on the photocatalyst surface is affected by the initial concentration of VOCs, oxygen concentration, RH, temperature, and intensity of the irradiation source [7].

The initial concentration of VOCs can affect the efficiency of pollutant PCO in three ways. At low concentrations, the PCO rate strongly depends on the concentration, and the PCO of VOCs follows first-order reaction kinetics, that is, the PCO rate increases linearly with an increase in the concentration. The high density of surface-active sites leads to rapid PCO [130]. At intermediate concentrations, the PCO rate continues to increase with increasing VOCs concentration, but the rate of increase is small and non-linear. At high concentrations, the PCO rate starts to decrease because of insufficient number of surface-active sites. At a certain point between the intermediate and high concentrations, the PCO rate is independent of the concentration, during which the PCO follows zero-order reaction kinetics [7]. Li et al. [131] investigated the toluene PCO in a continuous-flow reactor using a $g\text{-C}_3\text{N}_4/TiO_2$ composite catalyst and observed an increase in the toluene conversion efficiency with an increase in the initial toluene concentration from 90 to 200 ppm ; the maximum efficiency was 93% . A further increase in the concentration resulted in a decrease in the conversion efficiency up to 25% at an initial toluene concentration of 1000 ppm [131]. Debono et al. [132] studied toluene PCO in a 120 L batch reactor using a $100\text{ mg } TiO_2$ catalyst load and observed a decrease in reaction rate constant with an increase in the initial toluene concentration from 50 to 250 ppb [132].

Oxygen concentration

Oxygen plays several roles in the photocatalysis. Adsorbed molecular oxygen is an electron-trapping species. Therefore, the presence of oxygen reduces the recombination rate of the electron-hole pairs. Moreover, the reduction reactions on the TiO₂ surface afford O₂•⁻, which enhances the formation of •OH [7]. Kim et al. [133] studied the gas-phase PCO of trichloroethylene, acetone, methanol, and toluene in pure nitrogen, synthetic air (~20.9 vol% O₂), and pure oxygen atmospheres. They observed that, in the nitrogen atmosphere, the PCO rates of all pollutants were lower than those in synthetic air and pure oxygen atmospheres. However, the PCO rates in air and pure oxygen atmospheres were similar. Their study proved that the amount of oxygen in air (~21%) is adequate for efficient PCO [133].

Relative humidity

The effect of water vapour depends on its concentration and the type and concentration of VOCs in the polluted air. A high RH enhances the formation of •OH. However, water adsorption on the catalyst surface can deteriorate the adsorption of VOCs, thereby decreasing the efficiency of the process. At high initial concentrations of VOCs, competitive adsorption with water is slightly significant. Additionally, a high RH helps to prolong the lifetime of the photocatalyst because the presence of water vapour decreases the deactivation rate [7]. In several studies, the negative effect of water vapour on the PCO of isopropanol, trichloroethylene, and acetone was reported; a high RH exerted a positive effect on the PCO of toluene and formic acid but no significant effect on the PCO of l-butanol [133].

Raillard et al. [134] studied the effect of water vapour on the adsorption and PCO of methyl ethyl ketone on four different TiO₂ photocatalysts, two of them were powdered TiO₂ deposited onto supports, whereas the other two were thin films coated onto glass substrate. They found out that an increase in the RH from 0% to 30% variably affected the PCO of methyl ethyl ketone, depending on the form of the photocatalyst. For the powdered photocatalysts, the adsorption constant decreased at a high RH owing to the competitive adsorption between the water and pollutant molecules, whereas the reaction rate constant increased because of the increase in the quantity of hydroxyl radicals. For the thin film photocatalysts, the converse was observed: the adsorption constant increased and the reaction rate constant decreased at a high RH. The presence of a large amount of water on the film surface resulted in the formation of a water film; therefore, the pollutants were dissolved in the water layer, whereby the water molecules inhibited the diffusion of the pollutant to the catalyst surface [134].

Operating temperature

Theoretically, the operating temperature can affect both the adsorption-desorption processes and the conversion of pollutants during the PCO reactions. However, several papers have demonstrated that the kinetics of photocatalytic reactions are insensitive to small variations in the temperature [7]. Kim et al. [133] studied the VOC PCO at 25, 45, and 75 °C. The optimal temperature for the PCO of trichloroethylene, acetone, and methanol was 45 °C. For toluene, the PCO was the most efficient at 25 °C [133]. Jiang and Yu [135] studied the effect of air temperature on toluene PCO over N-doped TiO₂ coatings. They observed a slight increase in the PCO rate with an increase in the temperature from 5 to 35 °C because of increased diffusion velocity. However, despite the increase in the removal efficiency with increasing temperature, practical

applications under room-temperature conditions are more beneficial because additional heating would increase the room temperature, which can result in occupant discomfort and higher heating costs [135].

Irradiation source

The intensity of the irradiation source is another parameter that affects the photocatalytic reaction kinetics. An increase in the irradiation source intensity increases the number of photons, thereby generating more electron–hole pairs. However, only a fraction of the electron–hole pairs participate in the photocatalysis; the remaining pairs undergo the recombination process. The photocatalysis process can be enhanced by an increase in the light intensity, if the generated electron–hole pairs are consumed more intensively in the redox reactions than in the recombination process. This typically occurs at high initial concentrations of VOCs. At low initial concentrations of VOCs, an increase in the intensity could increase the recombination rate [7]. Dillert et al. [136] studied the effect of light intensity on the PCO of NO with an initial concentration ranging 0.05–1.3 ppm on TiO₂ photocatalyst. The light intensity was varied from 0 to 1.5 mW cm⁻² by changing the distance between the UV-A lamp and the photoreactor. At a high photon flux (light intensity > 1.3 mW cm⁻²), the PCO rate increased almost linearly with the concentration growth, whereas at a low photon flux (light intensity < 0.7 mW cm⁻²), the PCO rate increased with the concentration until it reached a limiting value, which was governed by the photon flux [136].

1.4.4 Outlook and practical applicability of TiO₂ films to indoor air treatment

Despite the substantial researches in the field of photocatalysis, the gas-phase PCO is still less understood compared to that of the PCO of aqueous pollutants [137].

Gas–solid reactions are complex and occur primarily at the interface between the adsorbed pollutants and the solid photocatalyst surface. Both the adsorption and degradation of pollutant molecules are affected by the molecular structure of the pollutants, catalyst surface, and operating parameters (e.g. reactor system, air flow rate, and humidity). Thus, the reaction kinetics of gas-phase PCO has been studied less than that of PCO in aqueous environments [138] [139]. Moreover, various gas-phase reactor systems, wide range of pollutants with different concentrations and, different photocatalysts have been reported. The comparison of the results in the literature is difficult because of the unavailability of a standard methodology and reference material [52,140].

Another research topic is the lifetime of the photocatalytic thin films. Photocatalyst deactivation has been frequently reported for gas-phase PCO reactions. If in an aqueous environment, water can help to remove the adsorbed intermediates from the catalyst surface, than in the gas-phase regeneration is needed. Washing with water, UV cleaning under an air stream, heat treatment, or ozonation can be performed. A further in-depth exploration of the deactivation mechanism of the catalyst will help in preparing efficient and durable photocatalysts [138,139].

PCO testing under real indoor conditions remains one of the biggest challenges in the field. The performance of TiO₂ thin films is typically evaluated for the PCO of a single pollutant. Overall, indoor can contain various VOCs in low concentrations (ppb). Several studies have been conducted on the PCO of VOCs mixtures on powders and coatings prepared from P 25 [52,121,141]. However, thin films have been used for the PCO of multi-component air mixtures only in a few studies [142]. Certain VOCs can

inhibit the PCO of other pollutants. For example, toluene intermediates can be adsorbed on the photocatalyst surface, blocking the surface-active sites [121,143]. In contrast, some VOCs can produce radicals with a high oxidation potential during partial PCO. For example, $\bullet\text{Cl}$ is produced during trichloroethylene PCO [140,144]. The competitive adsorption of VOCs in the mixture on the catalyst surface must be focussed in particular. For example, Chen and Zhang [141] observed the interference effect between VOCs in the mixture; molecules with a higher affinity to the catalyst were adsorbed more easily on the surface-active sites and oxidised faster [141]. A similar observation of the sequential PCO of VOCs, which was related to the competitive adsorption of different compounds on the photocatalyst surface was reported by Debono et al. [132]. A systematic study of the PCO of pollutant mixtures and their interactions under real conditions will provide a solid foundation for the practical application of TiO_2 thin films to indoor air treatment [137–139].

From a socioeconomic viewpoint, photocatalytic air treatment has a significant potential. In 2000, a review paper estimated that up to 200 billion United States dollars can be saved annually in the USA by improving the indoor air quality [145]. Thus, during the development of photocatalysts, it is vital to consider the final cost of the film, especially the commercial prospects [140].

1.5 Summary of literature overview and the aim of the study

Photocatalysis is an advanced oxidation process that can be widely applied to environmental remediation. The incorporation of TiO_2 photocatalysts in the field of construction, in the form of thin film coatings, will be beneficial for air purification via destruction of VOCs, bacteria, and viruses. However, the significant gap between academic research and industrial applications needs to be bridged.

Despite the availability of many catalytic materials, TiO_2 is the most promising material for photocatalysis and continues to be of interest to many researchers. The main challenges are preparing VIS light-driven TiO_2 photocatalysts and reducing the recombination of the photoinduced charges. These challenges can be overcome using several strategies, such as metal/non-metal or multiple-ion doping, formation of heterojunctions with other semiconductors, dye sensitisation, and preparation of composites. The modification of TiO_2 leads to the formation of impurity energy levels and defect states, which affect the grain size. However, 99% of the studies focus on pre-fabricated nanopowders or thick non-transparent coatings. Thus, there is a gap between the development of thin transparent polycrystalline TiO_2 films with low material quantities and the demonstration of high photocatalytic activity under UV and VIS light irradiation.

The film preparation method significantly affects the properties of the resultant film. The application of physical methods affords high-purity films; however, these methods are relatively expensive. Thus, the optimisation of chemical methods would be beneficial for manufacturing cost-effective films. Ultrasonic spray pyrolysis is an efficient, cost-effective, and easily scalable method for the production of films on the laboratory and industrial scales. Temperature, mist generation, aerosol flow, and other deposition parameters influence the film properties. Moreover, the composition and concentration of the precursor solution play a major role in determining the final properties of the synthesised films. Acetylacetone (AcacH) is a widely used stabilising agent in TiO_2 thin-film preparation. The molar ratio of the Ti precursor and chelating agent affect the crystallite size, phase composition, and surface of the film and

decrease the recombination rate of electron–hole pairs, consequently influencing the photocatalytic properties. However, to the best of our knowledge, the effects of changes in the TTIP:AcacH molar ratio in the solution on the photocatalytic properties have not been systematically investigated thus far.

Prior to applying TiO₂ films to indoor air treatment, their photocatalytic properties must be understood comprehensively. Batch reactors have been used in most studies; however, continuous-flow reactors are preferable to mimic real applications. The operating parameters, such as the air flow rate, initial concentration of the pollutants, and RH, can strongly influence the PCO. Hence, it is important to study the effects of operating parameters on the reaction kinetics. Moreover, indoor air can contain mixtures of hundreds of VOCs in low concentrations. Thus, synergy between VOCs with different molecular structures and polarities should be considered. To the best of our knowledge, this is the first study in which a transparent polycrystalline TiO₂ film was investigated in a continuous-flow reactor for the photocatalytic oxidation (PCO) of multi-component VOCs mixtures under different operating conditions.

Based on the literature review and the aforementioned gaps in the literature, the following hypothesis is formulated: An increase in the amount of AcacH in the precursor solution will result in a larger amount of organic additive in the solution, which in turn will lead to an increased carbon content in the obtained film. Moreover, excess AcacH in the precursor solution and carbon incorporation will affect the material properties of the TiO₂ thin films, such as the structural and morphological features and the chemical composition. The changes in the material properties of the TiO₂ films with increasing amount of AcacH will affect the photocatalytic performance.

Therefore, the main aim of this thesis is to fabricate transparent TiO₂ thin films by varying the amount of AcacH in the precursor solution and to explain the corresponding variations in the properties of the TiO₂ thin films and their effect on the photocatalytic activity of the films. A comprehensive study of the TiO₂ thin films with different TTIP:AcacH molar ratios in the precursor solution and their corresponding photocatalytic air-cleaning properties was performed.

The objectives of this thesis are as follows:

1. To deposit TiO₂ thin films with different TTIP:AcacH molar ratios in the precursor solution using the cost-effective, easily scalable technique of ultrasonic spray pyrolysis. To study the structural, optical, morphological, and surface properties of the obtained films.
2. To determine the TiO₂ thin films with optimal TTIP:AcacH molar ratio in the precursor solution for the PCO of an 8.8 mM stearic acid (SA) layer.
3. To systematically investigate the photocatalytic activities of the selected films in oxidising VOCs (e.g. acetone, acetaldehyde, heptane, and toluene), mimicking the real indoor air pollution conditions under UV-A and VIS light irradiation in the continuous mode. To study the PCO of individual VOCs and VOCs in mixtures under different operating conditions (initial concentration of the pollutants, RH, and air flow rate).
4. To test the antibacterial and antiviral activities of the TiO₂ film surface against *E. coli* bacteria and H1N1 virus under UV-A irradiation.

2 Experimental method

In this chapter, the experimental methods applied in the studies pertaining to Papers I, II, III, and IV for TiO₂ thin-film preparation; characterisation; and measurements of the self-cleaning, gas-phase photocatalytic, antibacterial, and antiviral activities are summarised.

2.1 Deposition and characterisation of the TiO₂ thin films

TiO₂ thin films were deposited onto borosilicate glass substrates by ultrasonic spray pyrolysis at 350 °C (Figure 2.1) and annealed for 1 h at 500 °C in air. A titanium (IV) isopropoxide (TTIP) solution (0.2 M) was used as the precursor. Acetylacetonate (AcacH) and ethanol were used as the additive and solvent, respectively. Only the amount of AcacH in the precursor solution was varied in the entire film-preparation process. The molar ratio of TTIP:AcacH was varied from 1:1 to 1:20. Additional details regarding the film preparation are available in Paper I.

Ultrasonic mist generation is superior to other mist generation techniques (e.g. pneumatic) because it consumes less energy, and the generated droplets are much smaller and have a lower velocity [146]. A schematic of the ultrasonic spray pyrolysis setup is presented in Figure 2.1. The piezoceramic element in the ultrasonic generator generates mechanical vibrations that get transported to the liquid, producing capillary waves. The generated waves break the liquid into small droplets without applying pressure or compressed air. Subsequently, the fine mist is transported by the compressed air to the heated surface, on which it decomposes, forming a thin film [75].

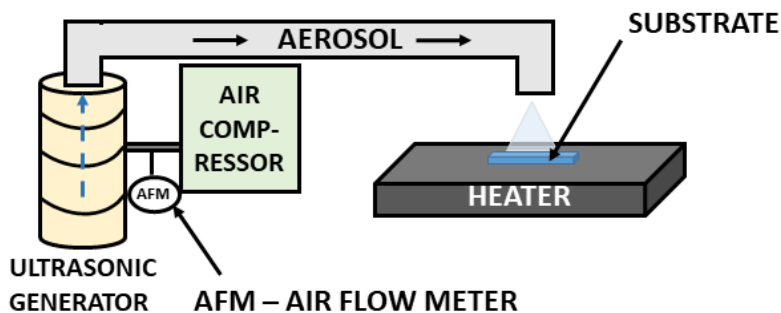


Figure 2.1 Schematic of the ultrasonic spray pyrolysis setup.

The methods used for characterising the obtained thin films are listed in Table 2.1. Unless otherwise specified, the measurements were performed at the Department of Materials and Environmental Technology, Tallinn University of Technology.

Table 2.1. Methods used for the characterisation of TiO₂ thin films.

Properties	Characterisation methods	Apparatus	Ref.
Phase composition and crystallite size	XRD	Rigaku Ultima IV	I
Transmittance, reflectance, film thickness, and band gap	UV-VIS	Jasco V-670	I
Chemical composition of the film surface	XPS	Kratos Analytical Axis Ultra DLD	I
Wettability	Water contact angle measurement	DSA 25 (KRÜSS Instrument)	I
Topography	AFM	MFP-3D AFM from Asylum Research ^a	[147]
Surface contact potential difference	Kelvin probe	Kelvin Probe, Besocke delta phi ^b	III
Charge separation	Transient SPV	Nd:YAG laser (NT230-50, $\lambda = 216\text{--}2600$ nm) that is equipped with a spectral cleaning unit, EKSPLA ^b	III

^a ARC-Arctic Centre for Sustainable Energy, Department of Physics and Technology, UiT The Arctic University of Norway, Tromsø, Norway.

^b Helmholtz Zentrum Berlin für Materialien und Energie GmbH, Institut für Silizium-Photovoltaik, Berlin, Germany.

2.2 Estimation of photocatalytic activity of the TiO₂ thin films

First, the photocatalytic activities of all films were estimated by the photocatalytic oxidation (PCO) of stearic acid (SA) layer, referred to as the SA test [I]. Second, selected films were tested for their activity in oxidising VOCs in the gas phase [II, IV]. Finally, the ability of the film with an optimal TTIP:Acach molar ratio to inactivate *Escherichia coli* bacteria and H1N1 virus was tested [II].

The photocatalytic experiments were conducted using UV-A and VIS light sources. Before each experiment, the films were pre-treated with UV-A light for at least 30 min. The UV-A lamps used in the photocatalytic experiments for SA and VOCs PCO had the following characteristics: UV Philips Actinic BL 15 W irradiance 3.5 mW cm⁻² with a reflector (integrated in the range of 180–400 nm, with maximum emission at 365 nm, UV-B/UV-A ratio < 0.2%). The parameters of the VIS light lamps were as follows: VIS Philips TL-D 15 W, irradiance 3.3 mW cm⁻² with reflector (integrated in the range of 180–700 nm, UV/UV-VIS ratio < 5%) [I, II, IV].

2.1.1 Stearic acid photocatalytic oxidation

The PCO of a thin layer of SA deposited onto a TiO₂ film is a common method for assessing the self-cleaning properties of the films. In this study [I], 100 μL of an 8.8 mM SA solution was deposited atop the film with a catalyst surface area of 4 cm² by spin coating. The PCO of the SA layer as a function of the irradiation time was monitored by Fourier-transform infrared spectroscopy (FTIR, PerkinElmer, Beaconsfield) in the wavenumber range of 3200–2500 cm⁻¹. The integrated area of the two typical SA bands centred at 2853 and 2923 cm⁻¹ was used to measure the PCO rate. The PCO rate of SA was assumed to follow first-order kinetics. Equation 2 represents the relationship between the integrated band area (A) and time (t).

$$A(t) = A_0e^{-kt} \quad (2)$$

The values of the reaction rate constant (k) were determined from the slope of the linear fit of the plot ln(A/A₀) versus t.

2.1.2 Gas-phase photocatalytic oxidation of VOCs

The gas-phase PCO of VOCs as individual pollutants [II, IV] and in mixtures [IV] on the sprayed TiO₂ films was studied in a continuous-flow multi-section reactor (Figure 2.2).

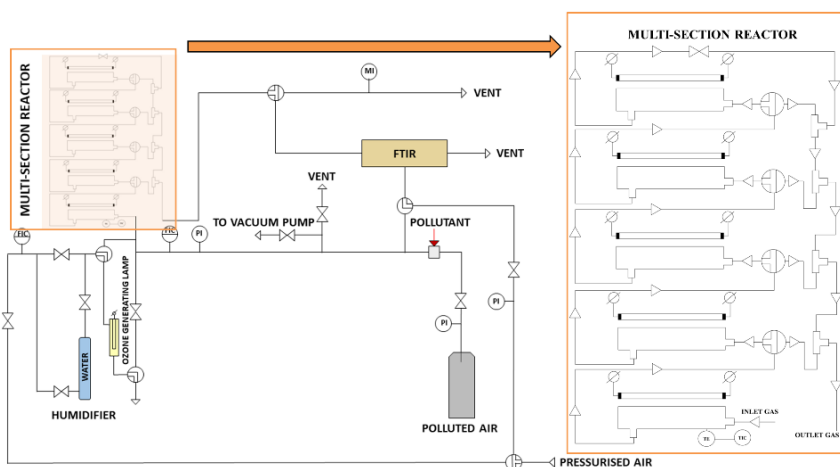


Figure 2.2. The schematic of the photocatalytic setup. Modified from ref. [121]. FIC – gas flow controller, PI – manometer, MI – gas humidity meter.

The reactor contained five sequentially connected sections. Each section had a volume of 130 mL and a catalyst surface area of 120 cm² (the catalyst surface area was equal to the surface area of the borosilicate glass substrate). Thus, the five sections collectively provided a catalyst surface area of 600 cm². TiO₂ films were placed inside each section of the reactor. UV-A or VIS lamps were placed over each section of the reactor, 6 cm away from the surface of the photocatalytic films. The temperature in the reactor sections was checked by a temperature controller containing a thermocouple (Omega, CN9000A); the value was determined as 40 ± 2 °C. The air temperature in the

reactors was higher than the ambient owing to the heating by lamps. The air flow rates were regulated by mass flow controllers and varied from 0.5 to 1 L min⁻¹, resulting in changes in the residence time in the reactor from 15.6 to 7.8 s per reactor section. A gas humidifier was used to change the relative humidity (RH) from 6% to 40%.

Information on the experimental conditions is presented in Table 2.2. Detailed descriptions can be found in papers II and IV.

Table 2.2. Consolidated table of gas-phase photocatalytic oxidation (PCO) experiments with VOCs.

VOC PCO as individual air pollutants						
Photo-catalyst	Pollutant	Concentration, ppm	RH, %	Air flow rate, L min ⁻¹	Irradiation source	Ref
TiO ₂ film with TTIP:AcacH 1:8	Acetaldehyde	5, 10, 40	6, 40	0.5, 1	UV-A, VIS	II
	Acetone	5, 10, 40	6, 40	0.5, 1	UV-A, VIS	
	Heptane	5, 10, 40	6, 40	0.5, 1	UV-A, VIS	IV
	Toluene	5, 10, 40	6, 40	0.5, 1	UV-A, VIS	
TiO ₂ film with TTIP:AcacH 1:5	Acetaldehyde	10	6	0.5	UV-A	II
	Acetone	10	6	0.5	UV-A	
Pilkington Activ™	Acetaldehyde	10	6	0.5	UV-A	
	Acetone	10	6	0.5	UV-A	
VOCs PCO in mixtures						
TiO ₂ film with TTIP:AcacH 1:8	Acetaldehyde, acetone, heptane	9 (3+3+3)	6, 40	0.5, 1	UV-A, VIS	IV
	Acetaldehyde, acetone, heptane	9 (3+3+3)	6, 40	0.5, 1	UV-A, VIS	

Four model pollutants were used as representatives of different groups of VOCs, namely, acetaldehyde, acetone, heptane, and toluene. The oxidation of VOCs as individual air pollutants in the concentration range 5–40 ppm was studied. Moreover, the oxidation of the two VOC mixtures with an initial concentration of 9 ppm was monitored. The first mixture contained 3 ppm each of acetaldehyde, acetone, and heptane. The second mixture comprised 3 ppm each of acetaldehyde, acetone, and toluene. An INTERSPEC 200-X FTIR spectrometer with an 8 m gas cell (Specac Tornado) and a 20 m gas cell (Specac Atmos) was used to analyse the concentration of VOCs as individual pollutants and VOC mixtures, respectively. Interspec version 3.40 Pro and

Essential FTIR software were used to acquire and process the air spectra. All the spectra were recorded at least thrice. The average conversion efficiency was calculated with a standard deviation of < 5%. Acetaldehyde, acetone, heptane, and toluene were quantified at the IR bands of 1170–1060, 1250–1180, 3020–2790, and 2975–2850 cm^{-1} , respectively.

2.1.3 Photocatalytic inactivation of *E. coli* bacteria and H1N1 virus

The antibacterial activity of the TiO_2 film against *Escherichia coli* was studied in the Laboratory of Environmental Toxicology, National Institute of Chemical Physics and Biophysics, using an in-house protocol based on the modified ISO 27,447 and ISO 22,196 standards [II]. A bacterial suspension of 5×10^4 cells per cm^2 was prepared in a nutrient broth, and 15 μL of the suspension was applied to the TiO_2 surface with a catalyst surface area of 4 cm^2 , which was then covered with a polyethylene film. The samples were then exposed to UV-A with an irradiance of 0.26–0.33 mW cm^{-2} . After the UV-A exposure, the film was washed with 2 mL of toxicity neutralising solution, diluted in a phosphate-buffered physiological saline, and drop-plated for counting after 24 h of incubation. A statistical analysis was performed to detect statistically significant differences in the viable bacterial counts. Further experimental details are presented in Paper II.

The antiviral activity of the TiO_2 film against H1N1 was studied at the Institute of Technology, University of Tartu, using a modified ISO 21702:2019 protocol. A viral suspension of 10^7 – 10^8 FFU mL^{-1} was prepared in a phosphate-buffered saline, and 300 μL of the suspension was applied to the TiO_2 surface with a catalyst surface area of 12.25 cm^2 , followed by coverage with a polyvinyl chloride film. The samples were exposed to UV-A with an irradiance of 0.2–0.3 mW cm^{-2} . The virus titre was determined using the TCID50 method, and the titres were calculated as FFU mL^{-1} using the Spearman–Karber algorithm.

3 Results and Discussion

In this chapter, the results of the study on sprayed TiO₂ thin films are presented and discussed. This chapter is divided into two sections. The first part concerns the material characterisation. The second part focusses on the photocatalytic activity of the films (i.e. self-cleaning, gas-phase, and disinfectant properties of the film surface). These results have been published in Papers I, II, III, and IV.

3.1 Characterisation of the TiO₂ thin films

Herein, the effects of the amount of acetylacetone (AcacH) in the precursor solution on the structural, optical, and surface properties; wettability; and chemical composition of the films were studied. The results of this study are published in Papers I, II, and III. The results of the atomic force microscopy (AFM) measurements were published in [147].

TiO₂ thin films with TTIP:AcacH molar ratios from 1:1 to 1:20 were deposited onto borosilicate glass substrates by ultrasonic spray pyrolysis at a deposition temperature of 350 °C and were annealed for 1 h in air atmosphere at 500 °C.

3.1.1 Structural and optical properties

The crystallinity, phase composition, and mean crystallite size of the TiO₂ thin films were estimated by X-ray diffraction (XRD). The XRD diffractograms in Figure 3.1 a show the peaks at 2 theta values of 25.3°, 37,0°, 37.8°, 38.6°, 48.1°, 53.9°, and 55°, which correspond to the reflection planes (101), (103), (004), (112), (200), (105), and (211), respectively (JCPDS 01-070-6826). The peaks belonging to the rutile or brookite phase were not detected. This confirms that all the TiO₂ films, regardless of the amount of acetylacetone in the precursor solution, consist of the anatase phase only. However, the magnified XRD patterns of the (101) main peak of anatase TiO₂ indicated a shift from 2 theta value of 25.38° for TTIP:AcacH 1:3 to 25.43° for TTIP:AcacH 1:20 (Figure 3.1 b). This shift indicates that carbon impurities could be incorporated into the lattice and probably accumulated at the grain boundaries of TiO₂. The incorporation of carbon atoms into the lattice of anatase TiO₂ can occur through a substitutional mechanism at the oxygen sites [146] or by occupying an interstitial site [148].

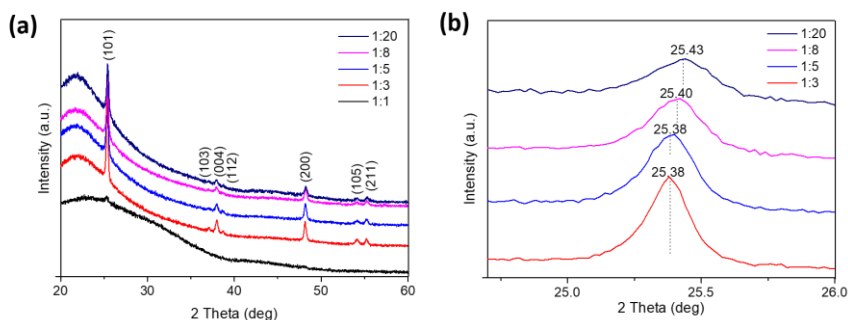


Figure 3.1. X-ray diffraction (XRD) patterns (a) and magnified patterns of the (101) main peak (b) of anatase TiO₂ thin films deposited with TTIP:AcacH molar ratios from 1:1 to 1:20.

The mean crystallite size was calculated using the Scherrer formula from the full width at half maximum (FWHM) of the most intense (101) peak; it decreased from 50 to 31 nm with increasing amount of acetylacetonate in the solution (Table 3.1) [11]. This decrease in the mean crystallite size confirms the incorporation of carbon into the film, which hinders the crystallite growth [149].

As discussed in Section 1.2.4, an increase in the amount of AcacH in the precursor solution can influence the phase transformation from anatase to rutile and enhance the crystallisation process. In this study, all the films were annealed at 500 °C, and no phase transformation occurred upon increasing the AcacH molar ratio.

Table 3.1 Summary of the structural and optical properties of the TiO₂ thin films.

TTIP:AcacH	Mean crystallite size, nm	Thickness, nm	Band gap, eV
1:1	< LOQ*	130	3.5
1:3	50	400	3.3–3.4
1:5	42	380	
1:8	38	370	
1:10	28	380	
1:20	31	280	

* - Less than the limit of quantification

The optical properties of the films were measured by UV–VIS spectroscopy (Figure 3.2 a). The total transmittance spectra of the TiO₂ thin films showed that the transparency of the films in the visible range was approximately 80%, irrespective of the amount of AcacH in the precursor solution. The thickness of all the films, calculated using the Swanepoel’s method, was ~380 nm, except for the film with a molar ratio of 1:1 (Table 3.1).

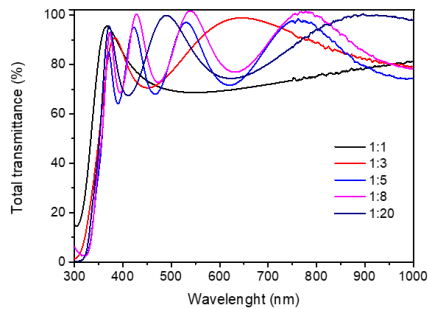


Figure 3.2. Total transmittance spectra of the TiO₂ thin films deposited with TTIP:AcacH molar ratios from 1:1 to 1:20.

The differences in the structural and optical properties of the film with TTIP:AcacH 1:1 is due to the incomplete complex formation during precursor solution preparation. AcacH replaces the alkoxy group, retarding the hydrolysis of TTIP and forming a stable complex [65]. A molar ratio of 1:1 is insufficient for complex formation; a complex is formed at a molar ratio of 1:2, and at molar ratios $\geq 1:3$, excess AcacH appears in the solution [58].

The transmittance was used to calculate the indirect optical band gaps of the TiO₂ films using a Tauc plot. The band gaps of all the films were in the range 3.3–3.4 eV (Table 3.1) [I], which corresponds to the values reported for synthesised anatase TiO₂ films [150].

The results demonstrate that an increase in the amount of AcacH in the precursor solution shift the (101) main peak of anatase TiO₂ to higher 2 theta values and decrease the mean crystallite size from 50 to 30 nm, which could indicate the incorporation of carbon impurities into the obtained TiO₂ thin film.

3.1.2 Chemical composition and wettability

The chemical composition and bonding structure of the obtained TiO₂ thin films were studied by X-ray photoelectron spectroscopy (XPS). The XPS spectra of the O1s and C1s core levels are shown in Figure 3.3.

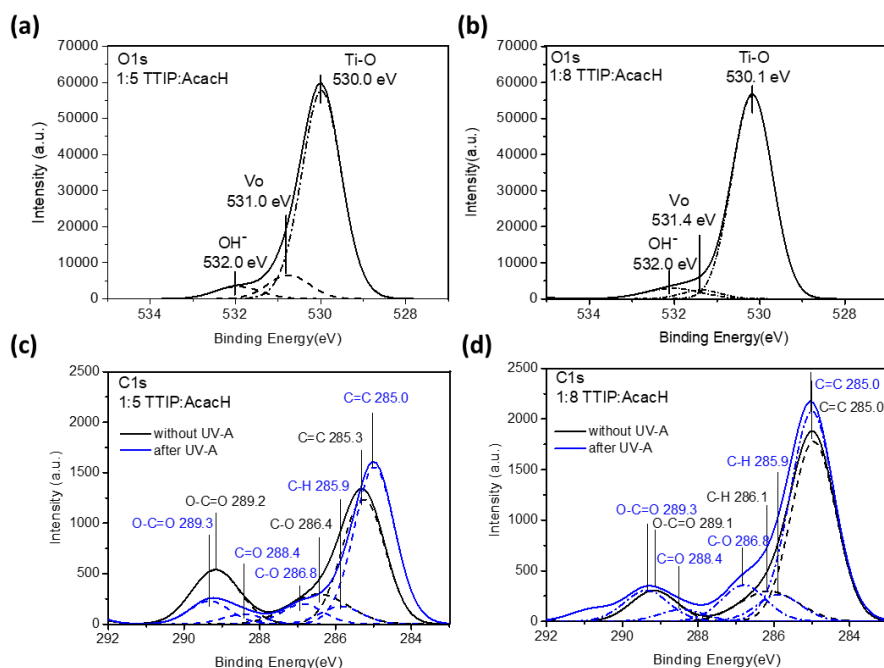


Figure 3.3. X-ray photoelectron spectroscopy (XPS) spectra of O1s core level for films with TTIP:AcacH molar ratios 1:5 (a) and 1:8 (b) after UV-A pre-treatment. XPS spectra of C1s core level for films with TTIP:AcacH molar ratios 1:5 (c) and 1:8 (d) as-prepared and after 24 h of UV-A pre-treatment.

The O1s core-level spectra consisted of three peaks (Figure 3.3 a and b). The peak with the highest intensity at a binding energy (BE) of 530.0 eV corresponds to the Ti–O bond. The peak at a BE of 531.0 eV indicates the O²⁻ ions in the oxygen-deficient regions within the matrix of TiO₂ [151], which can be associated with the oxygen vacancies (Vo); the peak corresponding to a BE of 532.0 eV is ascribed to the hydroxyl groups adsorbed on the surface [152]. The integrated peak areas were used to calculate the atomic concentrations of the chemical constituents. There was no significant difference between the atomic ratios of (OH)/(Ti–O) and (Vo)/(Ti–O) (I). As mentioned

in Section 1.2.5., Dundar et al. [59] showed that the oxygen defects and the number of hydroxyl groups on the surface depend on the deposition temperature however, the deposition temperature was maintained constant herein. Thus, the increase in the amount of AcacH in the precursor solution did not impact the number of oxygen vacancies and hydroxyl groups [59].

The XPS spectra of the films with TTIP:AcacH 1:5 and 1:8 for the C1s core levels before and after UV-A pre-treatment are shown in Figure 3.3 c and d, respectively. The amount of total carbon increased from 6.95% to 12.00 at% when TTIP:AcacH was changed from 1:5 to 1:8 for the films pre-treated with UV-A for 24 h. The dominant peak with a binding energy (BE) of 285.0 eV corresponds to the C–C bond, and the peak with a BE of 285.9 is attributed to the C–H bond. These non-oxygenated carbons are contaminants adsorbed on the TiO₂ surface [152]. However, some researchers have proposed that such carbon species may exist in the grain boundaries of TiO₂ and therefore, act as photosensitisers [148,153]. The other peaks belong to the oxygen-containing carbon species (Figure 3.3). These peaks confirm the incorporation of carbon into the lattice in place of the Ti atoms, i.e. interstitial carbon doping [148,153]. The presence of a large amount of hydrocarbon species on the film surface is attributed to the contamination from the ambient environment [152]. However, as shown in Figure 3.3, the carbon content of the freshly prepared and annealed samples and that of the same sample after 24 h of UV-A pre-treatment were almost the same (black and blue lines in Figure 3.3 c and d). Since the intensities of the peaks denoting the bonds of non-oxygenated carbon species do not decrease after UV-A pre-treatment, the carbon bonds are not a consequence of the contamination of the surface. The carbon species probably existed in the grain boundaries of TiO₂.

The incorporated carbon species on the TiO₂ surface may function as photosensitisers and absorb VIS light [153] [154]. Moreover, the incorporation of carbon atoms can lead to the formation of localised occupied states within the band gap of TiO₂, which can reduce the recombination rate of the electron–hole pairs [148].

To understand the effect of carbon incorporation on the electronic structure, the density of states was evaluated using the valence band (VB) XPS spectra (Figure 3.4 a) [156].

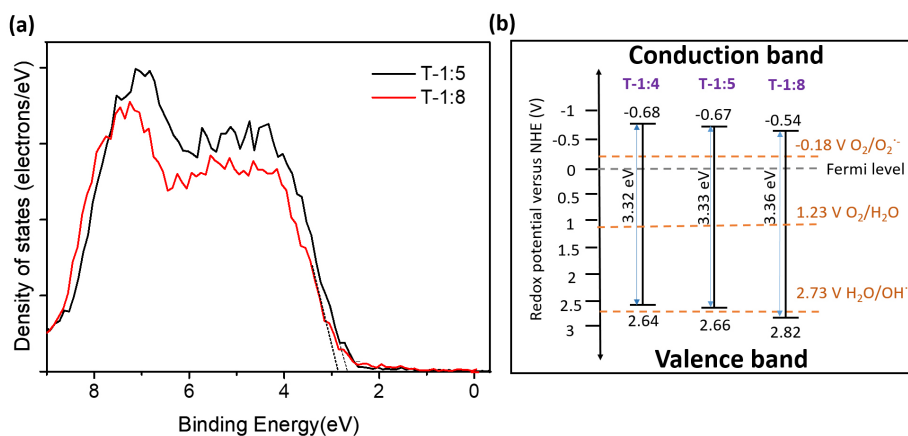


Figure 3.4. XPS valence band spectra (a) and valence and conduction band edges (b) of the TiO₂ thin films with TTIP:AcacH 1:5 and 1:8 molar ratios.

The maximum energies of the VB edges of the films with TTIP:AcacH 1:5 and 1:8 were ~ 2.66 and ~ 2.82 eV, respectively (Figure 3.4 a). Thus, the VB edge of the film with a molar ratio of 1:8 downshifted upon increasing the amount of AcacH. The downshift in the VB top edge can be related to the incorporation of carbon [148].

The band structure of the TiO₂ films was schematised (Figure 3.4 b) by combining the values of band gaps and VB edges determined from the UV–VIS (Section 3.1.1) and XPS spectra, respectively. Figure 3.4 b shows that owing to the downshift in the VB edge, the redox potential of the film with TTIP:AcacH 1.8 was more positive than the redox potential of the H₂O/•OH couple [157], thereby rendering the position of the band edges more favourable for photocatalytic redox reactions, as discussed in Section 1.2.

The surface wettability of the films was evaluated by measuring the water contact angles (CA) (Table 3.2) (I). Table 3.2 shows that all the as-prepared films, irrespective of the amount of AcacH, were hydrophilic (water CA < 90°). After 15 min of UV-A pre-treatment, all the films became superhydrophilic with water CA < 5°.

Table 3.2. Wettability results of the TiO₂ thin films.

TTIP:AcacH	Water contact angle, °	
	As-prepared samples	After 15 min of UV-A treatment
1:1	3 ± 0.5	3 ± 0.5
1:3	24 ± 0.5	4 ± 0.5
1:5	13 ± 0.5	4 ± 0.5
1:8	20 ± 0.5	~0
1:10	11 ± 0.5	~0
1:20	9 ± 0.5	~0

The reverse superhydrophilic properties of the TiO₂ surface are closely related to the photoinduced metastable TiO₂ surface, which was formed during the UV-A pre-treatment. The pre-treatment of the TiO₂ surface in the presence of oxygen and adsorbed water enhanced the photocatalytic performance; the enhancement is applicable to VIS-light-responsive photocatalysts as well [158].

The results demonstrated that the increase in the amount of AcacH in the precursor solution led to more carbon content on the surface of the films. The incorporation of carbon into the film influences the electronic structure of the material. The VB edge shifted upon increasing the amount of AcacH, thereby enhancing the production of •OH.

3.1.3 Surface properties

The morphology of the TiO₂ films was studied by atomic force microscopy (AFM) in the non-contact mode, and the results were published in [147]. The topographies of the films with TTIP:AcacH molar ratios of 1:1, 1:5, 1:8, and 1:10 are shown in Figure 3.5.

The TiO₂ films deposited with a larger amount of AcacH in the spray solution had a fine-grain structure, unlike the TiO₂ films deposited with a smaller amount of AcacH in the spray solution. A larger amount of AcacH in the precursor solution facilitates the formation of a film with a more uniform surface, resulting in a denser TiO₂ film [159]. The root mean square (RMS) roughness decreased from 2.6 to 0.9 nm with the change in the TTIP:AcacH molar ratio from 1:5 to 1:20.

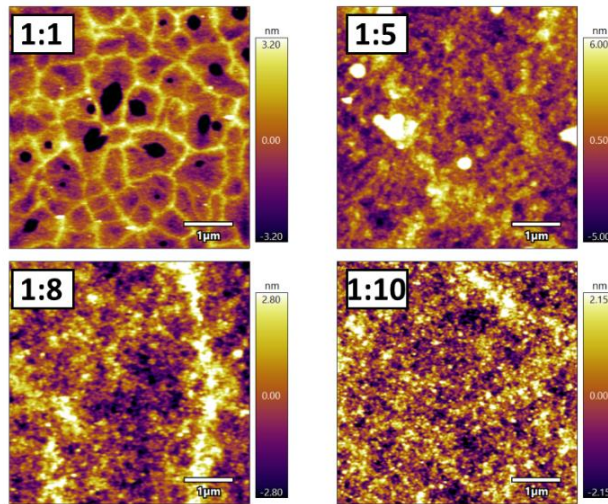


Figure 3.5. Atomic force microscopy topography maps of the TiO_2 thin films with different TTIP:AcacH molar ratios [147].

For a deeper understanding of the changes in the surface of the films, surface photovoltage (SPV) measurements were studied in the Paper III. The spectra of the contact potential difference (ΔCPD) for the TiO_2 films with TTIP:AcacH molar ratios of 1:1, 1:4, 1:5, 1:8, 1:10, and 1:20, measured using the Kelvin probe, are shown in Figure 3.6.

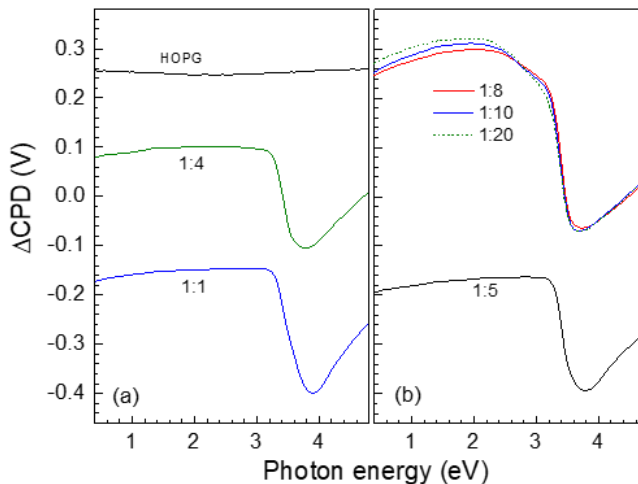


Figure 3.6. Spectra of the contact potential difference (ΔCPD) for the TiO_2 thin films with different TTIP:AcacH molar ratios. The spectrum of highly oriented pyrolytic graphite (HOPG) is shown for comparison [III].

The spectrum of highly oriented pyrolytic graphite (HOPG) is shown for comparison. The Δ CPD of HOPG did not indicate the influence of illumination; it was approximately 0.26 V, which corresponds to the work function (WF) of HOPG. At low photon energies, the Δ CPD of the TiO₂ films changed from -0.17 to 0.273 V when the TTIP:AcacH molar ratio was changed from 1:1 to 1:20. The WF of HOPG in air (4.475 eV) can be used as a reference [160]. Thus, the WF of TiO₂ films changed from 4.045 to 4.488 eV with TTIP:AcacH molar ratio alteration from 1:1 to 1:20 [III]. The changes in the WF of TiO₂ thin films is in qualitative agreement with the shift of the VB in XPS spectra (Section 3.1.2 Figure 3.4).

The intense change in the Δ CPD signal at a photon energy of \sim 3.2 eV is correlated to the band gap of anatase TiO₂ [2]. The maximum Δ CPD was measured for photon energies ranging 3.7–3.9 eV, as inferred from the signals; Δ CPD was high for the films with TTIP:AcacH 1:8, 1:10, and 1:20. This signifies that the charge separation was stronger for a larger amount of AcacH. However, the overall charge separation does not provide specific information about the fast and local charge separation processes, which are crucial to photocatalysis.

Starting from the TTIP:AcacH with a molar ratio of 1:8, the Δ CPD signal exhibited a slight linear change in the photon energy region 2.6–3.2 eV before the intense change at 3.2 eV [III]. This slight change can be associated with the Urbach tail and indicates the ionisation of excitons by internal electric microfields formed by lattice disorders, charged impurities, etc., which may be ascribed to the incorporated carbon [150].

The maps of the colour-coded SPV signals (photon energy versus time) for the TiO₂ thin films are shown in Figure 3.7 [III].

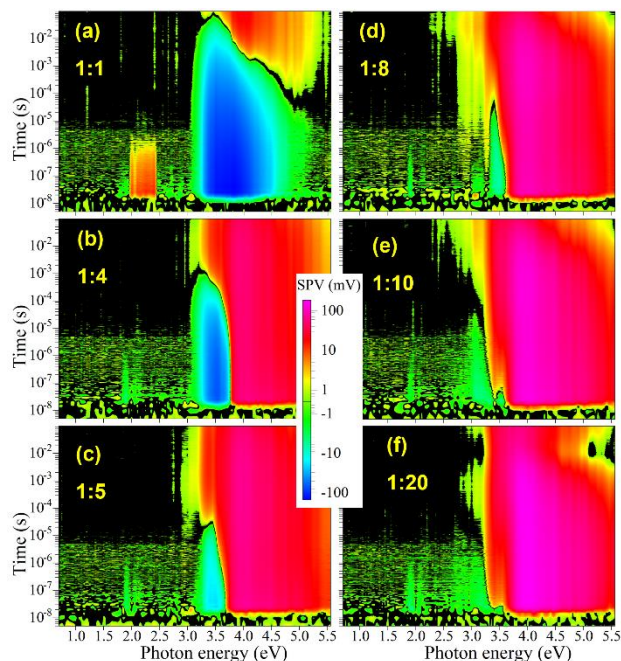


Figure 3.7. Contour plots of transient surface photovoltage (SPV) spectroscopy of the TiO₂ thin films with different TTIP:AcacH molar ratios [III].

For the TiO₂ film with a TTIP:AcacH molar ratio of 1:1, negative SPV signals were observed at a photon energy of ~3.1 eV. The negative SPV signals reached values of more than -100 mV in the photon energy range 3.4–4 eV for times shorter than 10 μs. At longer times and higher photon energies, the sign of the SPV signals became positive and reached values up to 20 eV. The films with a molar ratio of 1:4 had narrower regions of negative SPV signals in the photon energy range 3.2–3.7 eV for times up to 1 ms. At longer times, the SPV signals became positive in this spectral range and over the entire time range at higher photon energies. For the films with TTIP:AcacH 1:5, small negative SPV signals of up to -20 mV were observed in the photon energy range 3.2–3.6 eV at ~20 μs. The SPV signals became positive at longer times at photon energies below 3.6 eV. Positive SPV signals were measured at all times for photon energies above 3.6 eV. The film with a molar ratio of 1:8 exhibited a small negative SPV signal of up to -5 mV at a photon energy of 3.4 eV for times up to 20 μs. At longer times, an intense positive SPV signal was observed, reaching values of up to 100 mV. At molar ratios of 1:10 and 1:20, the response of the negative SPV signals was insignificant, similar to that observed for TTIP:AcacH 1:8 [III].

The changes in the SPV signals from negative to positive correlate with the increase in the amount of AcacH in the precursor solution. The intense negative and positive SPV signals signify the dominance of the separation of photogenerated electrons and holes towards the surface, respectively. The increase in the amount of AcacH in the spray solution leads to electron trap passivation and a reduction in electron back transfer.

For efficient photocatalysis, the photogenerated holes should be separated towards the surface, whereas the transfer of electrons towards the surface should be minimised. An increase in the AcacH molar ratio during the synthesis of TiO₂ thin films leads to electron trapping, thus facilitating the transfer of holes and formation of the reactive oxygen species (ROS) [III].

To summarise the changes in the material properties with an increase in the amount of AcacH in the precursor solution, the XRD analysis showed that an increase in the AcacH molar ratio in the precursor solution resulted in a shift in the (101) main peak of anatase TiO₂ to higher 2 theta values. The results of XPS demonstrated that the increase in the amount of AcacH in the precursor solution films resulted in more carbon on the film surface, which influenced the electronic structure of the film. The valence band edge shifted with an increase in the AcacH molar ratio. The SPV measurements inferred that, upon increasing the amount of AcacH in the precursor solution, the transition from preferential fast electron transfer to preferential fast hole transfer towards the surface occurs. Thus, films with a larger amount of AcacH in the precursor solution should have a lower recombination rate of the electron–hole pairs, more ROS, and higher PCO rates.

3.2 Photocatalytic activity of the TiO₂ thin films

The photocatalytic activities of all the obtained films were first estimated by the PCO of an 8.8 mM stearic acid (SA) layer deposited atop the TiO₂ film by spin coating [I]. Based on the results of SA PCO, two films with TTIP:AcacH molar ratios of 1:5 and 1:8 were selected for further study in gas-phase photocatalytic reactors for the PCO of the hazardous model air pollutants – acetone and acetaldehyde – which are small organic molecules [II]. The PCO of the films was compared to that of commercially available Pilkington Activ™ glass [II]. The film with the optimal TTIP:AcacH molar ratio of 1:8 was tested for the gas-phase PCO of refractory compounds – heptane and toluene [IV].

Moreover, the ability of the film to oxidise VOCs with different polarities and hydrophilicities in mixtures was tested [IV].

Finally, the antibacterial and antiviral properties of the film with the optimal TTIP:AcacH molar ratio of 1:8 were tested via the inactivation of *E.coli* [II] and H1N1, respectively.

3.2.1 Stearic acid photocatalytic oxidation

The PCO of the SA layer on the TiO₂ thin films with TTIP:AcacH molar ratios from 1:1 to 1:20 was investigated (Figure 3.8). The SA layer deposited onto the TiO₂ film provides a model solid organic film that pollutes surfaces, such as kitchen windows; thus, it is a fundamental method for assessing the self-cleaning properties of photocatalytic surfaces [161].

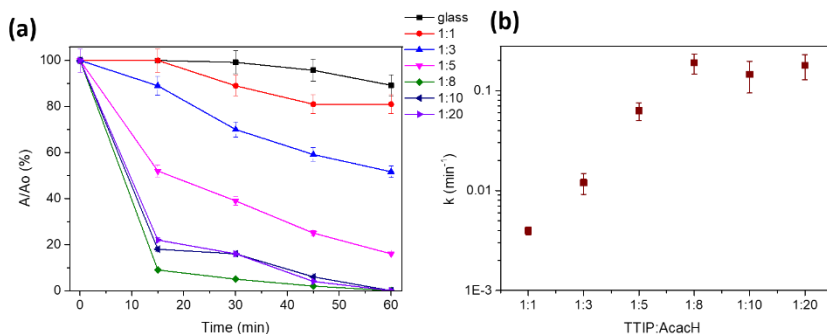


Figure 3.8. Photocatalytic oxidation (PCO) of stearic acid as a function of irradiation time (a) and reaction rate constants (b) for TiO₂ thin films at TTIP:AcacH molar ratios from 1:1 to 1:20, under UV-A irradiation.

Figure 3.8 shows that the reaction rate of stearic acid increased rapidly with an increase in the AcacH molar ratio in the precursor solution. After 60 min of UV-A irradiation, the conversion efficiencies of stearic acid were approximately 18%, 50%, and 90% on the films with TTIP:AcacH 1:1, 1:3, and 1:5, respectively, whereas the film with a molar ratio of 1:8 oxidised ~90% of the SA after 15 min of UV-A irradiation (Figure 3.8 a).

The PCO of SA follows first-order reaction kinetics [162]. Therefore, the reaction rate constant (k) was determined as the slope of the linear fit of the plot of $\ln(A/A_0)$ versus t [162]. Figure 3.8 b demonstrates that when the TTIP:AcacH molar ratio was increased from 1:1 to 1:8, k increased from 0.004 to 0.190 min⁻¹ under UV-A irradiation. The reaction rate of SA under VIS light irradiation was approximately five times lower than that under UV-A light irradiation; the results have been published in [I]. The TTIP:AcacH molar ratio of 1:8 can be considered optimal because a further increase in the amount of AcacH in the precursor solution did not result in an increase in k . Beyond the molar ratio of 1:8, the precursor solution was possibly saturated with AcacH. Thus, a plateau was formed, and the reaction rate did not increase further (Figure 3.8 b) [I].

The self-cleaning properties of TiO₂ films and coatings due to SA layer PCO have been studied by several researchers [39,161,162]. Liao et al. reported that TiO₂ coatings prepared from P 25 powder almost completely oxidised a 0.013 M stearic acid layer

after 15 min of UV radiation [163]. The performance of the thin film synthesised herein agrees with the activity of the coating prepared from powder under UV light by Liao et al. [163].

3.2.2 Gas-phase photocatalytic oxidation of VOCs

Gas-phase PCO was performed on four model air pollutants: acetaldehyde, acetone, heptane, and toluene. Acetaldehyde and acetone are relatively easily oxidised to hydrophilic and polar compounds. The PCO of these model pollutants on the TiO₂ films with TTIP:AcacH ratios of 1:5 (Figure 3.9 a) and 1:8 (Figure 3.9 b) was compared to the PCO of commercially available Pilkington Activ™ self-cleaning glass (Figure 3.9 c). The following operating parameters were used: an initial concentration of acetone and acetaldehyde of 10 ppm, an air flow rate of 0.5 L min⁻¹, an RH of 6%, and UV-A light as the irradiation source [II] (Table 2.2 Section 2.1.2).

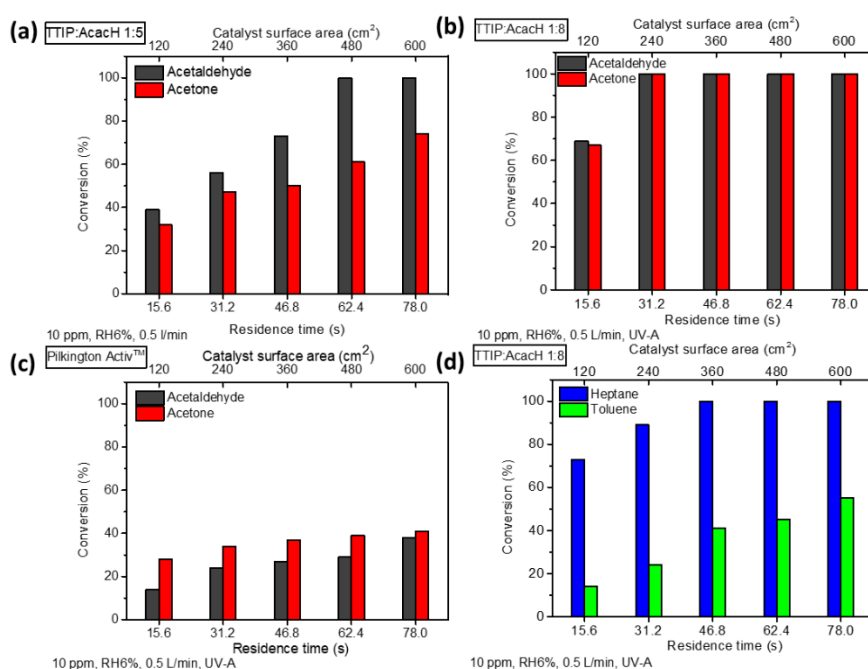


Figure 3.9. PCO of acetone and acetaldehyde (10 ppm) under ultraviolet (UV-A) irradiation on the films with TTIP:AcacH molar ratios 1:5 (a), 1:8 (b) and on Pilkington Activ™ glass (c) at different catalyst surface areas. PCO of heptane and toluene (10 ppm) under ultraviolet (UV-A) irradiation on the films with TTIP:AcacH molar ratios 1:8 (d).

Both the synthesised TiO₂ films with TTIP:AcacH 1:5 and 1:8 were significantly more active than the commercial Pilkington Activ™ glass (Figure 3.9). Acetaldehyde oxidised faster on the sprayed films than acetone. Acetaldehyde may be formed as an intermediate in acetone oxidation during full mineralisation, depending on the degradation pathway [163]. When there are sufficient surface-active sites in the catalyst, the PCO of acetaldehyde is expected to be faster than that of acetone. The same phenomenon was reported for P 25 powder by Bianchi et al. [137]. However, the opposite trend – a higher acetone conversion efficiency – was observed for the

Pilkington Activ™ glass. With an increase in the residence time from 15.6 to 78 s, the acetone conversion efficiency increased from 28% to 42%, whereas the acetaldehyde conversion efficiency increased from 14% to 38% (Figure 3.9 c). This could signify that the number of surface-active sites in Pilkington Activ™ is limited, given that the adsorption of the pollutants plays a key role in the PCO process. Acetone should be adsorbed faster on the surface-active sites because its molecular weight is higher and vapour pressure is lower, compared to those of acetaldehyde [165,166]. Dundar et al. [59] reported higher conversion efficiencies for acetone than those for acetaldehyde on sprayed TiO₂ thin films with a TTIP:AcacH molar ratio of 1:4 [59] (Appendix 2).

Acetone and acetaldehyde were completely oxidised on the TiO₂ film with TTIP:AcacH 1:8 and a catalyst surface area of 240 cm² (Figure 3.9 b); in the case of the TiO₂ film with a molar ratio of 1:5, two times larger catalyst surface area was required for the complete PCO of acetaldehyde (Figure 3.9 a). Acetone PCO on the film surface with a molar ratio of 1:5 was slower. Under the studied conditions, a maximum conversion efficiency of approximately 75% was achieved at a catalyst surface area of 600 cm² (Figure 3.9 a, [III]). Compared to the other films reported in the scientific literature, the TiO₂ thin films with a molar ratio of 1:8 exhibited higher acetone and acetaldehyde conversion efficiencies (Appendix 2). The photocatalytic activity of the TiO₂ thin film with a TTIP:AcacH molar ratio of 1:8 (Figure 3.9 b) was twice that of the film with a molar ratio of 1:5 (Figure 3.9 a) and more than four times that of the film with TTIP:AcacH 1:4 [59] (Appendix 2). In contrast, the coatings prepared from P 25 powder completely oxidised up to 20 ppm of acetone with a catalyst surface area of 120 cm² under the same experimental conditions [121]. However, the material loading of these coatings was more than ten times higher than that of the sprayed films.

The TiO₂ film with a molar ratio of 1:8 was tested for the PCO of two refractory compounds, namely, heptane and toluene (Figure 3.9 d) [IV]. These model pollutants are non-polar, hydrophobic, and have a more complex molecular structure than acetone and acetaldehyde. The heptane PCO occurred relatively quickly on the TiO₂ film with TTIP:AcacH 1:8. Heptane (10 ppm) was completely oxidised at a catalyst surface area of 360 cm², an air flow rate of 0.5 L min⁻¹, and an RH of 6%, under UV-A irradiation (Figure 3.9 d). Dundar et al. [59] achieved ~50% conversion of heptane (10 ppm) at a catalyst surface area of 600 cm² on a film with TTIP:AcacH 1:4 under the same experimental conditions [59]. Toluene PCO is more complicated because of the lower reactivity of the aromatic ring and the formation of intermediates, which can deactivate the photocatalyst [107]. The toluene conversion efficiency for an initial concentration of 10 ppm at a catalyst surface area of 600 cm² was ~55%, signifying the PCO of 5.5 ppm of toluene over a residence time of 78 s (Figure 3.9 d) [IV].

Effect of initial concentration of VOCs on photocatalytic oxidation

To study the effect of initial concentration of VOCs on their PCO, the initial concentration was changed from 5 to 40 ppm at an air flow rate of 0.5 L min⁻¹ and RH of 6%, under UV-A irradiation (Table 2.2 Section 2.1.2) [II, IV]. The reaction kinetics with respect to the increase in the initial concentration was estimated from the changes in the initial reaction rates (r_0) at a catalyst surface area of 120 cm². The initial reaction rate was calculated using Equation 3.

$$r_0 = -\frac{dC}{dt} \quad (3)$$

Figure 3.10 shows that the initial reaction rate increased with an increase in the concentration for all compounds, indicating that the PCO was not limited by the ROS. However, the increase in the initial reaction rate was non-linear; hence, at some point, the concentration would limit the efficiency of the process. The initial reaction rates for an initial concentration of 40 ppm were 1.7, 1.2, 1.1, and 0.9 ppm s⁻¹ for acetaldehyde, acetone, heptane, and toluene, respectively. Acetaldehyde is the smallest polar molecule and had the highest initial reaction rate. The toluene oxidation pathway involves many intermediate oxidation products, which can block the surface-active sites of the photocatalyst. Thus, toluene PCO is expected to have the lowest initial reaction rate (Figure 3.10).

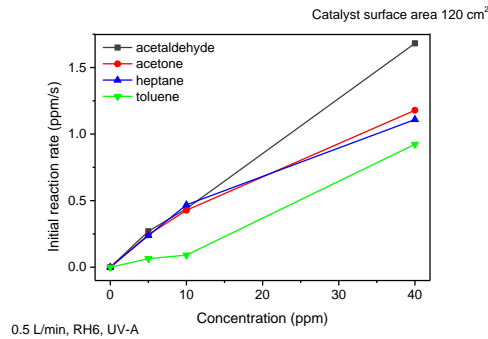


Figure 3.10. Initial reaction rate of VOCs PCO at different initial concentrations for a catalyst surface area of 120 cm².

Because the reaction rate is not diffusion-limited, the PCO reactions should determine the reaction rate, and the reaction kinetics can be investigated using the Langmuir–Hinshelwood model (Equation 4).

$$r_0 = \frac{k_r K C_0}{1 + K C_0} \quad (4)$$

The plot of 1/r₀ versus 1/C₀ yields a straight line, and the kinetic constants can be calculated using linear regression. The reaction rate constants and adsorption constants determined using the Langmuir–Hinshelwood model are listed in Table 3.3.

Table 3.3. Reaction rate and adsorption constants of VOCs PCO on the TiO₂ film under UV-A irradiation.

Pollutant	Reaction rate constant k _r (ppm s ⁻¹)	Adsorption constant K (ppm ⁻¹)
acetaldehyde	2.8	0.02
acetone	2.3	0.03
heptane	1.7	0.05
toluene	0.9	0.03

The reaction rate constants decreased in the following order: acetaldehyde > acetone > heptane > toluene. The decrease in the reaction rate constants correlated with the molecular structure of the pollutants. The reaction rate constant of acetaldehyde was more than three times higher than that of toluene. This indicates that toluene PCO occurred more slowly owing to the formation of complex intermediates, which can block the surface-active sites of the photocatalyst.

Effects of relative humidity and air flow rate on photocatalytic oxidation

To study the effect of water molecules on the PCO of VOCs, the RH was increased from 6% to 40% while maintaining the other parameters constant (an air flow rate of 0.5 L min⁻¹ and initial concentration of 10 ppm) (Figure 3.11, Table 2.2) [II, IV]. The presence of increased amount of water molecules inhibits the PCO of all pollutants. However, the increase in the RH affected the PCO of acetone and heptane more significantly; the conversion efficiencies of both the pollutants were two times lower at a catalyst surface area of 120 cm² and an RH of 40% (Figures 3.11 and 3.9 c) than those at an RH of 6%. The acetaldehyde and toluene conversion efficiencies changed only slightly upon increasing the RH at an air flow rate of 0.5 L min⁻¹.

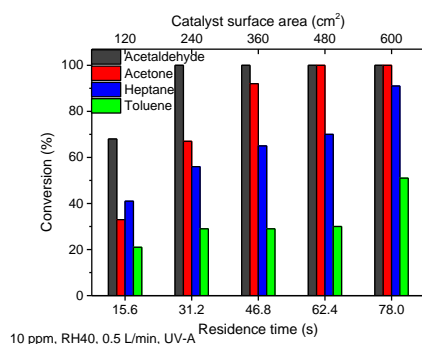


Figure 3.11. PCO of model air pollutants (10 ppm) on the film with TTIP:AcacH molar ratios 1:8 at different catalyst surface areas and an RH of 40%, under UV-A irradiation.

As per the literature, there is no consensus on the effects of water molecules on the PCO of VOCs. The impact depends on the ratio of water vapour in air, initial concentration, and pollutant type. A higher RH results in the production of more hydroxyl radicals ($\bullet\text{OH}$). Thus, it can increase the efficiency of PCO, especially at high initial concentrations of VOCs. However, a high RH could lead to competitive adsorption between the water molecules and VOCs on the surface-active sites of TiO₂ [7,167]. As demonstrated in Section 3.1.3 Table 3.2, the surface of the obtained TiO₂ film was superhydrophilic; thus, the adsorption rate of water was high. The adsorbed water formed a thin layer on the TiO₂ film surface. The adsorbed water layer can serve as a barrier to the diffusion of VOC molecules to the catalyst surface and decrease the PCO rate [168].

Next, the effect of high mass transfer on the PCO of pollutants was studied by increasing the air flow rate from 0.5 to 1 L min⁻¹ (Figures 3.9 and 3.12 a) [II, IV]. An increase in the air flow rate from 0.5 to 1 L min⁻¹ leads to a decrease in the residence time of the pollutants in the reactor section from 15.6 to 7.8 s. Because toluene has a lower reactivity than the other model pollutants (Figure 3.9 d) and its

PCO could deactivate the photocatalyst, its PCO at higher mass transfer was not considered in this study.

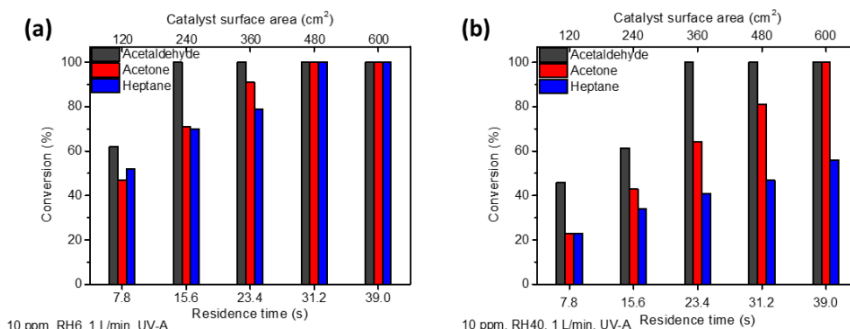


Figure 3.12. Effects of increase in the air flow rate (a) and RH (b) on the PCO of model air pollutants (10 ppm) on the film with TTIP:AcacH molar ratios 1:8 at different catalyst surface areas, under UV-A irradiation.

As shown in Figure 3.12, the air flow rate was increased to 1 L min^{-1} , which promoted the PCO of the pollutants. The acetaldehyde and acetone conversion efficiencies were higher at an air flow rate of 1 L min^{-1} than those at 0.5 L min^{-1} over the same residence time of 15.6 s, for the catalyst surface areas of 240 and 120 cm^2 , respectively (Figures 3.12 a and 3.9 c). The heptane conversion efficiency was approximately 70% at an air flow rate of 1 and 0.5 L min^{-1} for the catalyst surface areas of 240 and 120 cm^2 , respectively, over the same residence time of 15.6 s (Figures 3.12 a and 3.9 c). Moreover, an increase in the air flow rate up to 2.5 L min^{-1} [IV] results in the same heptane conversion efficiency of approximately 70% over the same residence time of 15.6 s for different air flow rates and catalyst surface areas. The construction of a multi-section reactor enables the purification of a larger volume of air at the same residence time by simultaneously increasing the air flow rate and catalyst surface area [IV].

The simultaneous increase in the RH to 40% and air flow rate to 1 L min^{-1} (Figure 3.12 b) intensified the negative effects of water molecules on pollutant adsorption on the catalyst surface. At an air flow rate of 0.5 L min^{-1} , an increase in the RH from 6% to 40% did not significantly influence acetaldehyde PCO (Figures 3.9 c and 3.11); however, when the air flow rate was increased to 1 L min^{-1} , the conversion efficiency decreased from 61% to 40% along with an increase in the RH, for a catalyst surface area of 120 cm^2 (Figure 3.12). Several authors have reported the decrease in the reaction rate of different VOCs with increasing RH, attributed to the competitive adsorption between the water molecules and pollutants on the catalyst surface [7,59].

The results obtained showed that operating parameters are instrumental in evaluating the photocatalytic activity. Thus, the effects of the operating parameters on the photocatalytic activity should be analysed with precision.

Photocatalytic oxidation of VOCs under visible light

The synthesised TiO_2 thin films showed promising photocatalytic activity in the PCO of VOCs under UV-A light irradiation. However, for practical indoor air treatment applications such as window glass coatings, the utilisation of VIS light is more beneficial.

To evaluate the photocatalytic activity of the obtained film under VIS light irradiation, the PCO of VOCs (initial concentration = 10 ppm) was studied at an air flow rate of 0.5 L min⁻¹ and RH of 6% (Figure 3.13, Table 2.2).

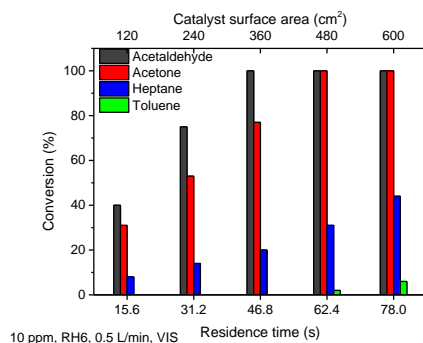


Figure 3.13. PCO of model air pollutants (10 ppm) on the film with TTIP:AcacH molar ratios 1:8 at different catalyst surface areas, under visible (VIS) light irradiation.

Figure 3.13 shows that the obtained TiO₂ film was active under VIS light irradiation. The conversion efficiencies of 10 ppm of the polar compounds – acetaldehyde and acetone – reached 100% at residence times of 46.8 and 62.4 s, respectively (air flow rate = 0.5 L min⁻¹, RH = 6%). Heptane PCO under VIS light irradiation occurred slower; 4.4 out of 10 ppm was degraded in 78 s. Toluene PCO was almost negligible; 0.6 ppm was degraded over a residence time of 78 s (Figure 3.13). The photocatalytic activity of the TiO₂ films under VIS light irradiation (Figure 3.13) was considerably lower than that under UV-A irradiation (Figure 3.9), for the same experimental conditions. The initial reaction rates of 10 ppm of acetaldehyde, acetone, and heptane under VIS light irradiation decreased 1.4, 1.9, and 8.7 times compared to those under UV-A irradiation, respectively (Table 3.4).

Table 3.4. Comparison of the initial reaction rates of VOCs PCO (initial concentrations = 10 ppm) on the TiO₂ film under UV-A and VIS light irradiation, for a catalyst surface area of 120 cm².

Pollutant	Initial reaction rate (ppm s ⁻¹)	
	UV-A	VIS
acetaldehyde	0.67	0.47
acetone	0.65	0.34
heptane	0.52	0.06
toluene	0.16	0.00

As discussed above in this section, under UV-A irradiation, the PCO was not limited by the amount of ROS; hence, the reaction rate increased as the initial concentration increased from 5 to 40 ppm. To study the effect of initial concentration on the reaction rate under VIS light irradiation, PCO of acetone (5 ppm) [II] and heptane (5 ppm) [IV] was performed at an air flow rate of 0.5 L min⁻¹ and RH of 6%. Under VIS light irradiation, the initial reaction rate for the degradation of pollutants with initial concentration of 10 ppm was lower than that of 5 ppm, unlike that corresponding to

the PCO under UV-A light irradiation. Thus, under VIS light irradiation, the photocatalytic activity is limited by the surface reactions.

The photocatalytic activity of the film under VIS light irradiation can be related to the carbon incorporated into the film surface (Section 3.1.2, Figure 3.3) [III]. Several authors have reported that the synergy between TiO₂ and carbon in TiO₂/C composites results in the high photocatalytic activity [148,169–171]. For example, Shayegan et al. [171] found out that upon modification with carbon P 25 powder, the conversion efficiency of methyl ethyl ketone increased from 77% to 94% and from 50% to 67% under UV-A and VIS light irradiation, respectively [171]. Yuan et al. [170] proposed that carbon absorbs VIS light and generates electrons that can be transferred directly to the conduction band of TiO₂ [170]. The formation of localised mid-gap energy states in carbon-modified TiO₂ was reported in another study [148]. The phenomenon explaining the results of the present study concurs with the changes in the electronic structure of the material due to carbon incorporation [III]. Further material modification can be implemented to enhance the photocatalytic activity of the TiO₂ films under VIS light. Some strategies involve the shift in the band gap to the VIS light region via doping or the use of sensitisers that can absorb VIS light. Moreover, heterojunction formation, semiconductor coupling, and co-catalyst loading can be implemented [172].

Photocatalytic oxidation of synthetic air mixtures of VOCs

Indoor air contains various mixtures of VOCs in low concentrations [115]. Thus, the PCO of two synthetic air mixtures was studied to mimic indoor air pollution, thereby inching closer to real applications. The first mixture consisted of 9 ppm of heptane–acetone–acetaldehyde (3 ppm of each component) (Figure 3.14, Table 2.2 in Section 2.1.2), and the second mixture consisted of 9 ppm of toluene–acetone–acetaldehyde (3 ppm of each component) (Figure 3.15, Table 2.2 in Section 2.1.2) [IV].

All the components in both mixtures were completely oxidised at a catalyst surface area of 360 cm² (residence time of 46.8 s), an RH of 6%, and an air flow rate 0.5 L min⁻¹, under UV-A irradiation (Figures 3.14 a and 3.15 a). The PCO of the compounds in the mixture containing heptane occurred faster. In the first mixture, the acetaldehyde, acetone, and heptane conversion efficiencies at a catalyst surface area of 120 cm² were 100%, 93%, and 77%, respectively (Figure 3.14 a). In the second mixture, the acetaldehyde, acetone, and toluene conversion efficiencies were 78%, 70%, and 71%, respectively, at a catalyst surface area of 120 cm² (Figure 3.15 a) [IV]. Thus, the initial reaction rates for acetaldehyde and acetone PCO in the second mixture decreased by 25% and 22%, respectively. The PCO of acetone and acetaldehyde in the mixture containing toluene was inhibited by the adsorption of highly stable intermediate by-products derived from toluene on the surface-active sites of TiO₂.

An increase in the air flow rate from 0.5 to 1 L min⁻¹ enhanced the initial reaction rates of all the pollutants in both mixtures (Figures 3.14 b and 3.15 b). However, the less polar compounds – heptane and toluene – were more affected by the high mass transfer. The complete PCO of 3 ppm of heptane and toluene was achieved in a residence time of 31.2 s (catalyst surface area = 480 cm²) at an air flow rate of 1 L min⁻¹, whereas a residence time of 46.8 s (catalyst surface area = 360 cm²) was required for an air flow rate of 0.5 L min⁻¹.

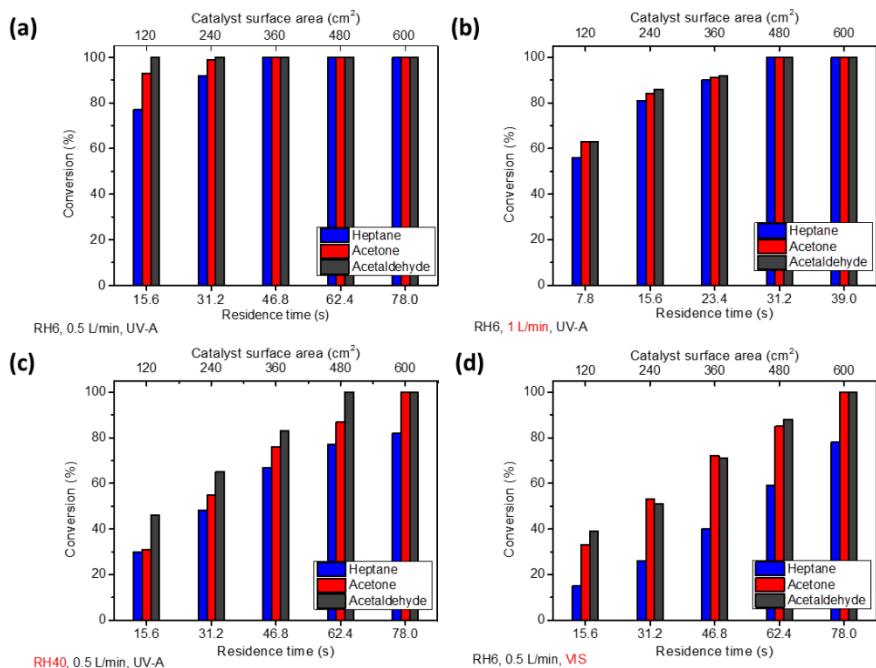


Figure 3.14. PCO of the heptane–acetone–acetaldehyde mixture on the TiO₂ film surface. PCO of the mixture (9 ppm) under UV-A light irradiation (a), the effect of increased air flow rate (b), the effect of increased relative humidity (RH) (c), and PCO under VIS light irradiation (d).

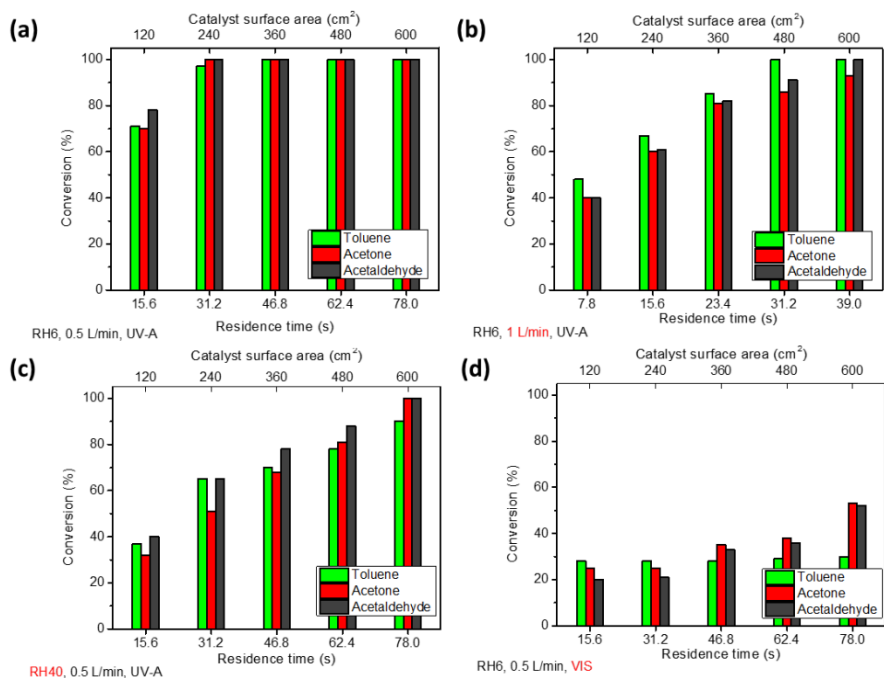


Figure 3.15. PCO of the toluene–acetone–acetaldehyde mixture on the TiO₂ film surface. PCO of the mixture (9 ppm) under UV-A light irradiation (a), the effect of increased air flow rate (b), the effect of increased RH (c), and PCO under VIS light irradiation (d).

The increase in the RH from 6% to 40% negatively impacted the PCO of all the compounds in both mixtures (Figures 3.14 c and 3.15 c). For the individual compounds (initial concentration = 10 ppm), at an air flow rate of 0.5 L min⁻¹, an increase in the RH predominantly inhibited the degradation of acetone and heptane (Section 3.2.2, Figure 3.11); in the mixtures, the conversion efficiencies of all the compounds decreased two times at a catalyst surface area of 120 cm². Thus, in the mixtures, competitive adsorption between the pollutant molecules and water molecules on the surface-active sites of the photocatalyst is dominant, inhibiting the PCO of all the pollutants.

Under VIS light irradiation, the initial reaction rates of the compounds in the mixture containing heptane or toluene decreased by 3 or 3.6 times on average, respectively, (Figures 3.14 d and 3.15 d) compared to those under UV-A irradiation. As inferred from Table 3.4, the PCO of VOCs as individual air pollutants under VIS light was limited by the amount of produced ROS. For the individual pollutants (initial concentration = 10 ppm), the initial reaction rates of acetone and acetaldehyde degradation decreased by approximately two times and that of heptane by more than eight times, under VIS light irradiation, compared to those under UV-A irradiation; toluene PCO was insignificant under VIS light. In the mixtures, the initial reaction rates of heptane and toluene degradation under VIS light irradiation decreased by five and four times, respectively, compared to those under UV-A irradiation.

Figure 3.16 summarises this section. When individual air pollutants were subjected to an air flow rate of 0.5 L min⁻¹ and RH of 6% under UV-A (irradiance = 3.5 mW cm⁻²), acetone and acetaldehyde (10 ppm each) completely oxidised at a catalyst surface area of 240 cm², heptane (10 ppm) at a catalyst surface area of 360 cm², and up to 5.5 out of 10 ppm of toluene oxidised at a catalyst surface area of 600 cm². When the same experimental conditions were applied under VIS light, acetaldehyde and acetone (10 ppm each) were oxidised at catalyst surface areas of 360 and 480 cm², respectively, and the heptane and toluene conversion efficiencies (10 ppm) at a catalyst surface area of 600 cm² reached 44% and 6%, respectively.

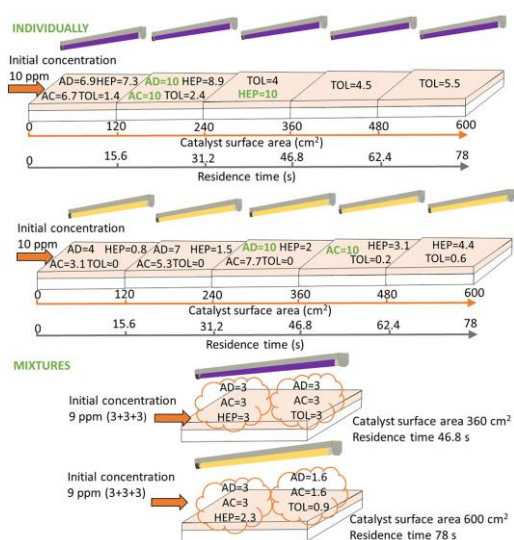


Figure 3.16. Quantity of oxidized VOCs (ppm) as individual pollutants and in the mixtures under UV-A (purple lamp) and VIS (yellow lamp) light irradiation at different catalyst surface areas. AD – acetaldehyde, AC – acetone, HEP – heptane, TOL – toluene.

In the 9 ppm mixtures, all the compounds were completely oxidised at a catalyst surface area of 360 cm² under UV-A irradiation at an air flow rate of 0.5 L min⁻¹ and RH of 6%. For the same experimental conditions under VIS light irradiation, at a catalyst surface area of 600 cm², 3, 3, and 2.3 ppm of acetaldehyde, acetone, and heptane were oxidised, respectively, in the first mixture, whereas 1.6, 1.6, and 0.9 ppm of acetaldehyde, acetone, and toluene were oxidised in the second mixture.

3.2.3 Photocatalytic inactivation of *E. coli* bacteria and H1N1 virus

The TiO₂ thin films were tested for their ability to inactivate *Escherichia coli* bacteria and H1N1 virus (Figure 3.17) [II]. The surface disinfection test was performed by dispersing the virus or bacteria in the liquid media because the bacteria and virus inactivate rapidly on dry surfaces, owing to which the results of the tests would be inconclusive. Moreover, bacteria and viruses can be killed by high-intensity UV-A light irradiation, even in the absence of a photocatalyst. Thus, the intensity of UV-A irradiation in the disinfection tests was set to 0.2–0.3 mW cm⁻², which is more than 10 times lower than the intensity used in the gas-phase experiments of VOC and SA layer PCO. The ROS produced during the irradiation of the photocatalysts are highly oxidising agents, stronger than chlorine, hydrogen peroxide, and ozone. Therefore, the viruses and bacteria attached to the photoinduced TiO₂ surface can be inactivated.

After 60 min of UV-A irradiation, more than 99% of the viable counts of *E. coli* bacteria were inactivated on the TiO₂ surface (Figure 3.17 a). Thus, approximately 5 × 10⁴ bacterial cells per cm² of TiO₂ film can be killed in 1 h, demonstrating the strong antibacterial activity of the thin film [II].

Rojviroon and Sirivithayapakorn [173] determined that the inactivation of *E. coli* bacteria on TiO₂ films follows pseudo-first-order reaction kinetics. The FE-SEM images showed that, after 180 min of UV-A irradiation, the outer cell membranes of the bacteria underwent deformation or even destruction [173]. Phuinthiang et al. [174] observed that over 97% of the *E. coli* bacteria was inactivated after 1 h of UV-A irradiation, and the bacteria were completely killed after 2 h of irradiation [174], the results obtained herein concur with their observations.

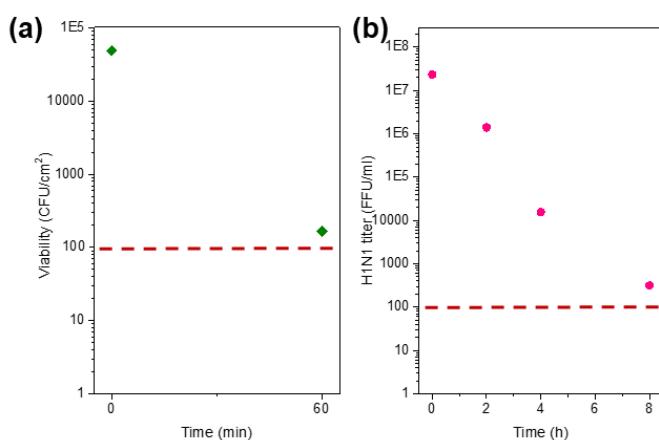


Figure 3.17. Antibacterial properties of the TiO₂ film against *E. coli* (a). Antiviral properties of the TiO₂ film against H1N1 virus (b). Red dashed line shows the limit of detection.

The inactivation of the H1N1 virus under UV-A irradiation was monitored for 8 h, with intermediate measurements being performed after 2 and 4 h (Figure 3.17 b). The decrease in the H1N1 virus titre was time-dependent, exhibiting first-order reaction kinetics. After 8 h of UV-A irradiation, more than 99% of the H1N1 virus was killed. TiO₂ film showed high virus inactivation capacity. The H1N1 virus belongs to a class of enveloped single-stranded RNA viruses. Because SARS-CoV-2 is a representative of the same class, it could be inactivated by photocatalytic treatment with TiO₂ films [104].

The TiO₂ thin film synthesised in this study can be used as an alternative for surface disinfection and continuous purification of high-touch surfaces from bacteria and viruses.

Conclusion

Low-material quantity ($< 0.2 \text{ mg cm}^{-2}$), transparent TiO_2 thin films were deposited by an easily scalable deposition technique – ultrasonic spray pyrolysis at $350 \text{ }^\circ\text{C}$ and annealed for 1 h at $500 \text{ }^\circ\text{C}$. The synthesis-dependent material properties of TiO_2 and the photocatalytic activity of the obtained films were studied comprehensively. The TiO_2 films were tested for their self-cleaning, gas-phase photocatalytic, antibacterial, and antiviral properties.

The novelty and the fundamental principle of this study are based on the modification of the precursor solution by increasing the amount of the organic stabilising agent – AcacH. The systematic study of TiO_2 spray-pyrolysis-synthesised films by changing the molar ratio of AcacH in the precursor and the comprehensive analysis of changes in the material properties and their effects on the photocatalytic performance of the films were performed. Moreover, the photocatalytic activity of the films was tested mimicking real indoor conditions in a multi-section gas flow reactor. This study showed that synthesised films with TTIP:AcacH molar ratios 1:8–1:20 demonstrated ca 10 times (under UV-A) and 5 times (under VIS light) higher photocatalytic performance compare to previously used TTIP:AcacH molar ratios of 1:2–1:4. AcacH increase leads to the incorporation of carbon and changes in charge carriers transfer. The photocatalytic activity of the obtained films was comparable to that of the coating prepared from the P 25 powder while reducing the material quantity of the films by more than ten times.

The main highlights of the thesis are as follows:

1. Irrespective of the TTIP:AcacH molar ratio in the precursor solution, all TiO_2 films deposited at $350 \text{ }^\circ\text{C}$ and annealed for 1 h at $500 \text{ }^\circ\text{C}$ consisted of the anatase phase with a mean crystallite size in the range 30–50 nm, were transparent in the VIS light region and had band gap $\sim 3.4 \text{ eV}$ and a smooth surface. The thickness of the films was $\sim 380 \text{ nm}$ (except film with TTIP:AcacH 1:1). An increase in the amount of AcacH in the precursor solution shifted the (101) main XRD peak of anatase TiO_2 to higher 2 theta values, which may indicate the incorporation of carbon impurities into the formed TiO_2 thin film. Moreover, the chemical composition revealed that upon increasing the TTIP:AcacH molar ratio from 1:5 to 1:8, the amount of adsorbed carbon on the film surface increased. The incorporation of carbon into the film influenced the electronic structure of the material; the valence band edge shifted down with an increase in the amount of AcacH enhancing the production of hydroxyl groups. The maximum signal of ΔCPD for the films with larger amount of AcacH was higher indicating stronger charge separation. The SPV measurements showed that with the changes in the TTIP:AcacH molar ratio from 1:1 to 1:20 the charge transfer toward the surface changed from preferential fast electron to preferential fast hole. Thus, the changes in the material properties with the increase in the amount of AcacH in the precursor solution should enhance the photocatalytic properties owing to facilitated faster hole transport to the photocatalyst surface, reduction in electron–hole pair recombination, and the production of more reactive oxygen species.
2. The self-cleaning properties of the TiO_2 films were studied by oxidising an 8.8 mM SA layer deposited atop the TiO_2 film by spin coating. The reaction rate

constant (k) of SA oxidation increased with increasing TTIP:AcacH molar ratio from 1:1 to 1:8 under both UV-A (k increased from 0.004 to 0.190 min^{-1}) and VIS (k increased from 0.002 to 0.032 min^{-1}) light irradiation. Starting from the molar ratio 1:8 the plateau is formed and no more increase in the reaction rate occurs. Thus, the optimal TTIP:AcacH molar ratio was determined to be 1:8.

3. The gas-phase photocatalytic activities of the films with TTIP:AcacH molar ratios of 1:5 and 1:8 were evaluated in a continuous-flow multi-section reactor. In the first step, the photocatalytic oxidation of acetone and acetaldehyde on films with TTIP:AcacH molar ratios of 1:5 and 1:8 was compared with that on commercially available Pilkington Activ™ glass. The initial reaction rates of both films synthesised with TTIP:AcacH 1:5 and 1:8 were several times higher than that of commercial glass. However, the photocatalytic activity of the film with TTIP:AcacH 1:8 was, on average, two times higher than that of the film with TTIP:AcacH 1:5. Subsequently, a more detailed study was conducted on the photocatalytic activity of the film with TTIP:AcacH 1:8 in oxidising VOCs as individual pollutants and in mixtures under different experimental conditions. Under UV-A (irradiance = 3.5 mW cm^{-2}) the deposited TiO_2 thin film with TTIP:AcacH 1:8 and a catalyst surface area ranging 120–600 cm^2 oxidised 9 ppm of VOCs in the mixtures (acetone-acetaldehyde-heptane/toluene) at a residence time of 46.8 s. As individual compounds (initial concentration of 10 ppm), 10 ppm of acetone and acetaldehyde were oxidised in 31.2 s, 10 ppm of heptane was oxidised in 46.8 s, and ~4 ppm of toluene was oxidised in 46.8 s. Under VIS light (irradiance = 3.3 mW cm^{-2}), 3, 3, and 2.3 ppm of acetaldehyde, acetone, and heptane were oxidised in 78 s, respectively, in the mixture containing acetone-acetaldehyde-heptane. For comparison, in the mixture containing acetone-acetaldehyde-toluene, 1.6, 1.6, and 0.9 ppm of acetaldehyde, acetone, and toluene were oxidised in 78 s, respectively. As individual pollutants (initial concentration of 10 ppm), 10, 10, 4.4, and 0.6 ppm of acetaldehyde, acetone, heptane, and toluene were oxidized in 46.8, 62.4, 78, and 78 s under VIS light irradiation, respectively. In general, an increase in air flow rate promotes the oxidation of all pollutants in the mixtures and individually, while an increase in relative humidity inhibits the oxidation.
4. The film with a TTIP:AcacH molar ratio of 1:8 was tested for its ability to inactivate surface-attached bacteria and virus in the liquid phase. A 99% reduction in *E. coli* bacteria with an initial concentration of 5×10^4 CFU cm^{-2} was achieved after 60 min under UV-A (irradiance = 0.26–0.33 mW cm^{-2}). A 99% reduction in H1N1 virus with an initial concentration of 10^7 – 10^8 FFU mL^{-1} was achieved after 8 h under UV-A (irradiance = 0.2–0.3 mW cm^{-2}).

This thesis presents an inexpensive, simple, and easily scalable method for synthesising TiO_2 thin films with a high photocatalytic activity under UV-A and VIS light irradiation by modifying the precursor solution. The results demonstrated the ability of the film to continuously oxidise different VOCs, which represent the common groups of indoor air pollutants. The VOCs were oxidised as individual pollutants and in 9 ppm mixtures under various operating conditions. The results of VOCs mixtures oxidation on the transparent TiO_2 films bring photocatalysis closer to real application. Owing to its excellent photocatalytic, antibacterial, and antiviral properties, the as-prepared film can be integrated with the surrounding environment as an innovative air-purifying and

surface-disinfecting material. Moreover, it can be applied to air-purifying devices as a non-replaceable module. Therefore, the data presented in this thesis provide a valuable basis for the practical incorporation of TiO₂ thin films into air treatment technologies.

The future outlook of this study includes several directions. First, theoretical study of photocatalytic oxidation on the TiO₂ thin films can be conducted. That is, the gas-phase photocatalytic activity in different carrier gases could be investigated to determine the reactive oxygen species (ROS) thus formed and identify the predominant ROS in the photocatalytic oxidation of various VOCs under ultraviolet and visible light irradiation. Next, a practical investigation of photocatalytic oxidation can be performed, for example, using larger reactors, applying higher air flow rates, and optimising for commercialisation. Finally, the development of thin films with an increased photocatalytic activity under visible light could be achieved through further modification of the material.

References

- [1] A. Fujishima, K. Honda, Electrochemical photolysis of water at a semiconductor electrode, *Nature*, **1972**, 238, 77-38, <https://doi.org/10.1038/238037a0>.
- [2] Q. Guo, C. Zhou, Z. Ma, X. Yang, Fundamentals of TiO₂ Photocatalysis: Concepts, Mechanisms, and Challenges, *Adv. Mater.*, **2019**, 32, 1901997, <https://doi.org/10.1002/adma.201901997>.
- [3] A.A. Assadi, B. Abdelkrim, W. Dominique, Kinetic Modeling of VOC Photocatalytic Degradation Using a Process at Different Reactor Configurations and Scales, *Int. J. Chem. React. Eng.*, **2016**, 14, 395-405, <https://doi.org/10.1515/ijcre-2015-0003>.
- [4] M. Schreck, M. Niederberger, Photocatalytic Gas Phase Reactions, *Chem. Mater.*, **2019**, 31, 597-618, <https://doi.org/10.1021/acs.chemmater.8b04444>.
- [5] J.M. Herrmann, Photocatalysis fundamentals revisited to avoid several misconceptions, *Appl. Catal. B Environ.*, **2010**, 99, 461-468, <https://doi.org/10.1016/j.apcatb.2010.05.012>.
- [6] D. V. Kozlov, Titanium Dioxide in gas-Phase Photocatalytic Oxidation of Aromatic and Heteroatom Organic Substances: Deactivation and Reactivation of Photocatalyst, *Theor. Exp. Chem.*, **2014**, 50, 133-154, <https://doi.org/10.1007/s11237-014-9358-6>.
- [7] K. Demeestere, J. Dewulf, H. Van Langenhove, Heterogeneous photocatalysis as an advanced oxidation process for the abatement of chlorinated, monocyclic aromatic and sulfurous volatile organic compounds in air: State of the art, *Crit. Rev. Environ. Sci. Technol.*, **2007**, 37, 489-538, <https://doi.org/10.1080/10643380600966467>.
- [8] F. Fresno, R. Portela, S. Suárez, J.M. Coronado, Photocatalytic materials: Recent achievements and near future trends, *J. Mater. Chem. A.*, **2014**, 2, 2863-2884, <https://doi.org/10.1039/c3ta13793g>.
- [9] Y. Oshida, *Bioscience and Bioengineering of Titanium Materials: Second Edition*, **2013**, <https://doi.org/10.1016/B978-0-444-62625-7.00001-7>.
- [10] Ş. Neaţu, J.A. Maciá-Agulló, H. Garcia, Solar light photocatalytic CO₂ reduction: General considerations and selected bench-mark photocatalysts, *Int. J. Mol. Sci.*, **2014**, 15, 5246-5262, <https://doi.org/10.3390/ijms15045246>.
- [11] T. Bak, W. Li, J. Nowotny, A.J. Atanacio, J. Davis, Photocatalytic Properties of TiO₂: Evidence of the Key Role of Surface Active Sites in Water Oxidation, *J. Phys. Chem. A.*, **2015**, 119, 9465-9473, <https://doi.org/10.1021/acs.jpca.5b05031>.
- [12] B. Liu, X. Zhao, C. Terashima, A. Fujishima, K. Nakata, Thermodynamic and kinetic analysis of heterogeneous photocatalysis for semiconductor systems, *Phys. Chem. Chem. Phys.*, **2014**, 16, 8751-8760, <https://doi.org/10.1039/c3cp55317e>.
- [13] M. Guo, Z. Zhou, S. Yan, P. Zhou, F. Miao, S. Liang, J. Wang, X. Cui, Bi₂WO₆-BiOCl heterostructure with enhanced photocatalytic activity for efficient degradation of oxytetracycline, *Sci. Rep.*, **2020**, 10, 18401, <https://doi.org/10.1038/s41598-020-75003-x>.

- [14] Y. Wangab, X. Ma, H. Li, B. Liu, H. Li, S. Yin, T. Sato, Recent Advances in Visible-Light Driven Photocatalysis, in: *Adv. Catal. Mater. - Photocatal. Other Curr. Trends*, **2016**, <https://doi.org/10.5772/61864>.
- [15] F. Chen, Y. Cao, D. Jia, A facile route for the synthesis of ZnS rods with excellent photocatalytic activity, *Chem. Eng. J.*, **2013**, 234, 223-231, <https://doi.org/10.1016/j.cej.2013.08.075>.
- [16] A. Al-Kattan, A. Wichser, R. Vonbank, S. Brunner, A. Ulrich, S. Zuin, B. Nowack, Release of TiO₂ from paints containing pigment-TiO₂ or nano-TiO₂ by weathering, *Environ. Sci. Process. Impacts.*, **2013**, 15, 2186-2193, <https://doi.org/10.1039/c3em00331k>.
- [17] U.S. Geological Survey, Mineral Commodity Summaries 2021 : Sand and Gravel (Industrial), **2021**.
- [18] M. Younes, G. Aquilina, L. Castle, K.H. Engel, P. Fowler, M.J. Frutos Fernandez, P. Fürst, U. Gundert-Remy, R. Gürtler, T. Husøy, M. Manco, W. Mennes, P. Moldeus, S. Passamonti, R. Shah, I. Waalkens-Berendsen, D. Wölfle, E. Corsini, F. Cubadda, D. De Groot, R. FitzGerald, S. Gunnare, A.C. Gutleb, J. Mast, A. Mortensen, A. Oomen, A. Piersma, V. Plichta, B. Ulbrich, H. Van Loveren, D. Benford, M. Bignami, C. Bolognesi, R. Crebelli, M. Dusinska, F. Marcon, E. Nielsen, J. Schlatter, C. Vleminckx, S. Barmaz, M. Carfí, C. Civitella, A. Giarola, A.M. Rincon, R. Serafimova, C. Smeraldi, J. Tarazona, A. Tard, M. Wright, Safety assessment of titanium dioxide (E171) as a food additive, *EFSA J.*, **2021**, 19, 6585, <https://doi.org/10.2903/j.efsa.2021.6585>.
- [19] Q. Deng, M. Wei, X. Ding, L. Jiang, B. Ye, K. Wei, Brookite-type TiO₂ nanotubes, *Chem. Commun*, **2008**, 3657-3659, <https://doi.org/10.1039/b802896f>.
- [20] C. Byrne, R. Fagan, S. Hinder, D.E. McCormack, S.C. Pillai, New approach of modifying the anatase to rutile transition temperature in TiO₂ photocatalysts, *RSC Adv.*, **2016**, 6, 95232-95238, <https://doi.org/10.1039/c6ra19759k>.
- [21] M. Sakar, R. Mithun Prakash, D. Trong-On, Insights into the TiO₂-based photocatalytic systems and their mechanisms, *Catalysts*, **2019**, 9, 680. <https://doi.org/10.3390/catal9080680>.
- [22] B. Ohtani, O.O. Prieto-Mahaney, D. Li, R. Abe, What is Degussa (Evonic) P25? Crystalline composition analysis, reconstruction from isolated pure particles and photocatalytic activity test, *J. Photochem. Photobiol. A Chem.*, **2010**, 216, 179–182. <https://doi.org/10.1016/j.jphotochem.2010.07.024>.
- [23] T. Ohno, K. Sarukawa, K. Tokieda, M. Matsumura, Morphology of a TiO₂ photocatalyst (Degussa, P-25) consisting of anatase and rutile crystalline phases, *J. Catal.*, **2001**, 203, 82-86. <https://doi.org/10.1006/jcat.2001.3316>.
- [24] S.W. Verbruggen, K. Masschaele, E. Moortgat, T.E. Korany, B. Hauchecorne, J.A. Martens, S. Lenaerts, Factors driving the activity of commercial titanium dioxide powders towards gas phase photocatalytic oxidation of acetaldehyde, *Catal. Sci. Technol.*, **2012**, 2, 2311-2318. <https://doi.org/10.1039/c2cy20123b>.
- [25] S.O. Hay, T. Obee, Z. Luo, T. Jiang, Y. Meng, J. He, S.C. Murphy, S. Suib, The viability of photocatalysis for air purification, *Molecules*, **2015**, 20, 1319-1356. <https://doi.org/10.3390/molecules20011319>.

- [26] K. Hashimoto, H. Irie, A. Fujishima, TiO₂ Photocatalysis: A Historical Overview and Future Prospects, *Jpn. J. Appl. Phys.*, **2005**, 44, 8269-8285, <https://doi.org/10.1143/JJAP.44.8269>.
- [27] D.L. Cunha, A. Kuznetsov, C.A. Achete, A.E. da H. Machado, M. Marques, Immobilized TiO₂ on glass spheres applied to heterogeneous photocatalysis: Photoactivity, leaching and regeneration process, *PeerJ.*, **2018**, 19, <https://doi.org/10.7717/peerj.4464>.
- [28] T.S. Le, T.H. Dao, D.C. Nguyen, H.C. Nguyen, I.L. Balikhin, Air purification equipment combining a filter coated by silver nanoparticles with a nano-TiO₂ photocatalyst for use in hospitals, *Adv. Nat. Sci. Nanosci. Nanotechnol.*, **2015**, 6, 015016, <https://doi.org/10.1088/2043-6262/6/1/015016>.
- [29] A. V. Vorontsov, E.E. Savinov, P.G. Smirniotis, Vibrofluidized- and fixed-bed photocatalytic reactors: Case of gaseous acetone photooxidation, *Chem. Eng. Sci.*, **2000**, 55, 5089-5098, [https://doi.org/10.1016/S0009-2509\(00\)00115-9](https://doi.org/10.1016/S0009-2509(00)00115-9).
- [30] M.J. Lima, A.M.T. Silva, C.G. Silva, J.L. Faria, N.M. Reis, Selective photocatalytic synthesis of benzaldehyde in microcapillaries with immobilized carbon nitride, *Chem. Eng. J.*, **2022**, 430, 132643, <https://doi.org/10.1016/j.cej.2021.132643>.
- [31] Air purifiers, *Eureka Forbes*, <https://www.eurekaforbes.com/air-purifiers> (accessed September 2, 2022).
- [32] Bhagat R.H, E.T. Bureau, *Eureka Forbes Aeroguard: Air purifiers that do a good job depending on your space*, *The Economic Times. Panache*, **2015**, https://economictimes.indiatimes.com//magazines/panache/eureka-forbes-aeroguard-air-purifiers-that-do-a-good-job-depending-on-your-space/articleshow/47812332.cms?utm_source=contentofinterest&utm_medium=text&utm_campaign=cppst (accessed May 2, 2022).
- [33] I.Oja Acik, Sol-Gel Deposition of Titanium Dioxide Films, doctoral thesis, Tallinn University of Tehnology, **2007**.
- [34] J.L. Rankinen, Microwave Characterization of Thin Film Titania, doctoral thesis, The Pennsylvania State University, **2005**.
- [35] W. Shimizu, S. Nakamura, T. Sato, Y. Murakami, Creation of high-refractive-index amorphous titanium oxide thin films from low-fractal-dimension polymeric precursors synthesized by a sol-gel technique with a hydrazine monohydrochloride catalyst, *Langmuir*, **2012**, 28, 12245-12255, <https://doi.org/10.1021/la3015139>.
- [36] I. Sta, M. Jlassi, M. Hajji, M.F. Boujmil, R. Jerbi, M. Kandyla, M. Kompitsas, H. Ezzaouia, Structural and optical properties of TiO₂ thin films prepared by spin coating, *J. Sol-Gel Sci. Technol.*, **2014**, 72, 421-427, <https://doi.org/10.1007/s10971-014-3452-z>.
- [37] B. Pant, M. Park, S.J. Park, Recent advances in TiO₂ films prepared by sol-gel methods for photocatalytic degradation of organic pollutants and antibacterial activities, *Coatings*, **2019**, 9, 613, <https://doi.org/10.3390/coatings9100613>.

- [38] S.C. Jung, S.J. Kim, N. Imaishi, Y.I. Cho, Effect of TiO₂ thin film thickness and specific surface area by low-pressure metal-organic chemical vapor deposition on photocatalytic activities, *Appl. Catal. B Environ.*, **2005**, 55, 253-257, <https://doi.org/10.1016/j.apcatb.2004.08.009>.
- [39] I. Dundar, A. Mere, V. Mikli, M. Krunks, I.Oja Acik, Thickness effect on photocatalytic activity of TiO₂ thin films fabricated by ultrasonic spray pyrolysis, *Catalysts*, **2020**, 10, 1058, <https://doi.org/10.3390/catal10091058>.
- [40] W. Ravisy, M. Richard-Plouet, B. Dey, S. Bulou, P. Choquet, A. Granier, A. Goullet, Unveiling a critical thickness in photocatalytic TiO₂ thin films grown by plasma-enhanced chemical vapor deposition using real time in situ spectroscopic ellipsometry, *J. Phys. D. Appl. Phys.*, **2021**, 54, 445303, <https://doi.org/10.1088/1361-6463/ac1ec1>.
- [41] I.N. Martyanov, K.J. Klabunde, Comparative study of TiO₂ particles in powder form and as a thin nanostructured film on quartz, *J. Catal.*, **2004**, 225, 408-416, <https://doi.org/10.1016/j.jcat.2004.04.019>.
- [42] K.L. Materna, L. Hammarström, Photoredox Catalysis Using Heterogenized Iridium Complexes, *Chem. - A Eur. J.*, **2021**, 27, 16966-16977, <https://doi.org/10.1002/chem.202101651>.
- [43] P. Lansaker, Gold-Based Nanoparticles and Thin Films, Uppsala Universitet, doctoral thesis, **2012**.
- [44] B. Dey, S. Bulou, T. Gaulain, W. Ravisy, M. Richard-Plouet, A. Goullet, A. Granier, P. Choquet, Anatase TiO₂ deposited at low temperature by pulsing an electron cyclotron wave resonance plasma source, *Sci. Rep.*, **2020**, 10, 21952, <https://doi.org/10.1038/s41598-020-78956-1>.
- [45] A. Jilani, M.S. Abdel-wahab, A.H. Hammad, Advance Deposition Techniques for Thin Film and Coating. In (Ed.), *Modern Technologies for Creating the Thin-film Systems and Coatings*. IntechOpen, **2017**, <https://doi.org/10.5772/65702>.
- [46] C. Garlisi, G. Palmisano, Radiation-free superhydrophilic and antifogging properties of e-beam evaporated TiO₂ films on glass, *Appl. Surf. Sci.*, **2017**, 420, 83-93, <https://doi.org/10.1016/j.apsusc.2017.05.077>.
- [47] A. Queffeuou, L. Geron, C. Archambeau, H. Le Gall, P.M. Marquaire, O. Zahraa, Kinetic study of acetaldehyde photocatalytic oxidation with a thin film of TiO₂ coated on stainless steel and CFD modeling approach, *Ind. Eng. Chem. Res.*, **2010**, 49, 6890-6897, <https://doi.org/10.1021/ie9017308>.
- [48] K. Eufinger, D. Poelman, H. Poelman, R. De Gryse, G.B. Marin, TiO₂ thin films for photocatalytic applications, *Thin Solid Films: Process and Applications*, **2008**, 189-227.
- [49] A. Vahl, S. Veziroglu, B. Henkel, T. Strunskus, O. Polonskyi, O.C. Aktas, F. Faupel, Pathways to tailor photocatalytic performance of TiO₂ thin films deposited by reactive magnetron sputtering, *Materials*, **2019**, 12, 2840, <https://doi.org/10.3390/ma12172840>.

- [50] S. Obregón, V. Rodríguez-González, Photocatalytic TiO₂ thin films and coatings prepared by sol-gel processing: a brief review, *J. Sol-Gel Sci. Technol.*, **2022**, 102, 125-141, <https://doi.org/10.1007/s10971-021-05628-5>.
- [51] T.K. Tseng, Y.S. Lin, Y.J. Chen, H. Chu, A review of photocatalysts prepared by sol-gel method for VOCs removal, *Int. J. Mol. Sci.*, **2010**, 11, 2336-2361, <https://doi.org/10.3390/ijms11062336>.
- [52] D. Wood, S. Shaw, T. Cawte, E. Shanen, B. Van Heyst, An overview of photocatalyst immobilization methods for air pollution remediation, *Chem. Eng. J.*, **2020**, 391, 123490, <https://doi.org/10.1016/j.cej.2019.123490>.
- [53] M.D. Hernández-Alonso, I. Tejedor-Tejedor, J.M. Coronado, M.A. Anderson, Operando FTIR study of the photocatalytic oxidation of methylcyclohexane and toluene in air over TiO₂-ZrO₂ thin films: Influence of the aromaticity of the target molecule on deactivation, *Appl. Catal. B Environ.*, **2011**, 101, 283-293, <https://doi.org/10.1016/j.apcatb.2010.09.029>.
- [54] N. Quici, M.L. Vera, H. Choi, G.L. Puma, D.D. Dionysiou, M.I. Litter, H. Destailats, Effect of key parameters on the photocatalytic oxidation of toluene at low concentrations in air under 254 + 185 nm UV irradiation, *Appl. Catal. B Environ.*, **2010**, 95, 312-319, <https://doi.org/10.1016/j.apcatb.2010.01.009>.
- [55] C. Sanchez, J. Livage, M. Henry, F. Babonneau, Chemical modification of alkoxide precursors, *J. Non. Cryst. Solids.*, **1988**, 100, 65-76, [https://doi.org/10.1016/0022-3093\(88\)90007-5](https://doi.org/10.1016/0022-3093(88)90007-5).
- [56] P. Dulian, J. Zajic, W. Zukowski, Effect of titanium source and sol-gel TiO₂ thin film formation parameters on its morphology and photocatalytic activity, *Mater. Sci. Pol.*, **2021**, 38, 424-433, <https://doi.org/10.2478/msp-2020-0056>.
- [57] U. Schubert, Chemical modification of titanium alkoxides for sol-gel processing, *J. Mater. Chem.*, **2005**, 15, 3701-3715, <https://doi.org/10.1039/b504269k>.
- [58] A.O. Juma, I.Oja Acik, V. Mikli, A. Mere, M. Krunk, Effect of solution composition on anatase to rutile transformation of sprayed TiO₂ thin films, *Thin Solid Films*, **2015**, 594, 287-292, <https://doi.org/10.1016/j.tsf.2015.03.036>.
- [69] I. Dundar, M. Krichevskaya, A. Katerski, M. Krunk, I.Oja Acik, Photocatalytic degradation of different VOCs in the gas-phase over TiO₂ thin films prepared by ultrasonic spray pyrolysis, *Catalysts*, **2019**, 9, 915, <https://doi.org/10.3390/catal9110915>.
- [60] Y. Djaoued, S. Badilescu, P. V. Ashrit, D. Bersani, P.P. Lottici, J. Robichaud, Study of anatase to rutile phase transition in nanocrystalline titania films, *J. Sol-Gel Sci. Technol.*, **2002**, 24, 255-264, <https://doi.org/10.1023/A:1015357313003>.
- [61] D. Vernardou, K. Vlachou, E. Spanakis, E. Stratakis, N. Katsarakis, E. Kymakis, E. Koudoumas, Influence of solution chemistry on the properties of hydrothermally grown TiO₂ for advanced applications, *Catal. Today.*, **2009**, 144, 172-176, <https://doi.org/10.1016/j.cattod.2009.02.009>.
- [62] S. Yamazaki, H. Uchiyama, H. Kozuka, Additive-free alkoxide-water-alcohol solutions as precursors for crystalline titania thin films, *J. Sol-Gel Sci. Technol.*, **2018**, 87, 537-543, <https://doi.org/10.1007/s10971-018-4715-x>.

- [63] T. Imao, N. Noma, S. Ito, Preparation of TiO₂ nanocrystalline films controlled by acetylacetone/polyethylene glycol and their photoelectric properties, *J. Sol-Gel Sci. Technol.*, **2006**, 38, 197-202, <https://doi.org/10.1007/s10971-006-6438-7>.
- [64] P. Kajitvichyanukul, S. Pongpom, Effect of Acetyl Acetone on Property of TiO₂ Thin Film for Photocatalytic Reduction of Chromium (VI) from Aqueous Solution, *CMU. Journal Special Issue on Nanotechnology*, **2005**, 4, 87-93.
- [65] J. Moon, T. Li, C.A. Randall, J.H. Adair, Low temperature synthesis of lead titanate by a hydrothermal method, *J. Mater. Res.*, **1997**, 12, 189-197, <https://doi.org/https://doi.org/10.1557/JMR.1997.0025>.
- [66] D. Marani, R.H. Silva, A. Dankeaw, M. Gudik-Sørensen, K. Norrman, K.K. Hansen, V. Esposito, Effect of the sol-gel conditions on the morphology and SCR performance of electrospun V-W-TiO₂ catalysts, *J. Phys. Chem. Solids.*, **2018**, 118, 255-261, <https://doi.org/10.1016/j.jpcs.2018.03.018>.
- [67] S. Majodina, Z.R. Tshentu, A.S. Ogunlaja, Effect of adding chelating ligands on the catalytic performance of rh-promoted mos₂ in the hydrodesulfurization of dibenzothiophene, *Catalysts*, **2021**, 11, 1398 <https://doi.org/10.3390/catal11111398>.
- [68] M. Yu, M. Liang, J. Liu, S. Li, B. Xue, H. Zhao, Effect of chelating agent acetylacetone on corrosion protection properties of silane-zirconium sol-gel coatings, *Appl. Surf. Sci.*, **2016**, 363, 229-239, <https://doi.org/10.1016/j.apsusc.2015.12.013>.
- [69] L.A. Almeida, A. Dosen, J. Viol, B.A. Marinkovic, TiO₂-Acetylacetone as an Efficient Source of Superoxide Radicals under Reduced Power Visible Light: Photocatalytic Degradation of Chlorophenol and Tetracycline, *Catalysts*, **2022**, 12, 116, <https://doi.org/10.3390/catal12020116>.
- [70] R.D.Y. Away, C. Takai-yamashita, T. Ban, Y. Ohya, Effect of Stabilizer on Structural, Optical and Photocatalytic Properties of Sol-Gel Dip-Coated TiO₂ Films, **2020**, 5, 46-51.
- [71] U. Kaltsum, A.F. Kurniawan, I. Nurhasanah, P. Priyono, The role of concentration ratio of TTiP: AcAc on the photocatalytic activity of TiO₂ thin film in reducing degradation products of used frying oil, *Bull. Chem. React. Eng. Catal.*, **2017**, 12, 430-436, <https://doi.org/10.9767/bcrec.12.3.951.430-436>.
- [72] Y. Chen, B. Wang, W. Huang, X. Zhang, G. Wang, M.J. Leonardi, Y. Huang, Z. Lu, T.J. Marks, A. Facchetti, Nitroacetylacetone as a Cofuel for the Combustion Synthesis of High-Performance Indium-Gallium-Zinc Oxide Transistors, *Chem. Mater.*, **2018**, 30, 3323-3329, <https://doi.org/10.1021/acs.chemmater.8b00663>.
- [73] B. Wang, M.J. Leonardi, W. Huang, Y. Chen, L. Zeng, B.J. Eckstein, T.J. Marks, A. Facchetti, Marked Cofuel Tuning of Combustion Synthesis Pathways for Metal Oxide Semiconductor Films, *Adv. Electron. Mater.*, **2019**, 5, 1900540, <https://doi.org/10.1002/aelm.201900540>.
- [74] I. Oja Acik, A. Junolainen, V. Mikli, M. Danilson, M. Krunk, Growth of ultra-thin TiO₂ films by spray pyrolysis on different substrates, *Appl. Surf. Sci.*, **2009**, 256, 1391-1394, <https://doi.org/10.1016/j.apsusc.2009.08.101>.

- [75] N.D. Sankir, E. Aydin, E. Ugur, M. Sankir, Spray Pyrolysis of Nano-Structured Optical and Electronic Materials, *Adv. Funct. Mater.*, **2015**, <https://doi.org/10.1002/9781118998977.ch3>.
- [76] A. Gowri manohari, S. Dhanapandian, K. Santhosh Kumar, T. Mahalingam, Optimization of Deposition Parameters on the Physical Properties of TiO₂ Thin Films by Spray Pyrolysis Technique, *Int. J. Thin Film. Sci. Technol.*, **2014**, *3*, 1-6, <https://doi.org/10.12785/ijtfst/030101>.
- [77] I. Dündar, M. Krichevskaya, A. Katerski, I.Oja Acik, TiO₂ thin films by ultrasonic spray pyrolysis as photocatalytic material for air purification, *R. Soc. Open Sci.*, **2019**, *6*, 181578, <https://doi.org/10.1098/rsos.181578>.
- [78] K. Yasuda, Y. Bando, S. Yamaguchi, M. Nakamura, A. Oda, Y. Kawase, Analysis of concentration characteristics in ultrasonic atomization by droplet diameter distribution, *Ultrason. Sonochem.*, **2005**, *12*, 37-41, <https://doi.org/10.1016/j.ultsonch.2004.05.008>.
- [79] I. Oja, A. Mere, M. Krunks, C.H. Solterbeck, M. Es-Souni, Properties of TiO₂ films prepared by the spray pyrolysis method, in: *Solid State Phenom.*, **2004**, 99-100, 254-264, <https://doi.org/10.4028/www.scientific.net/ssp.99-100.259>.
- [80] I. Oja, A. Mere, M. Krunks, R. Nisumaa, C.H. Solterbeck, M. Es-Souni, Structural and electrical characterization of TiO₂ films grown by spray pyrolysis, *Thin Solid Films*, **2006**, 515, 674-677, <https://doi.org/10.1016/j.tsf.2005.12.243>.
- [81] E. Arca, K. Fleischer, I. V. Shvets, Influence of the precursors and chemical composition of the solution on the properties of zno thin films grown by spray pyrolysis, *J. Phys. Chem. C.*, **2009**, *113*, 50, <https://doi.org/10.1021/jp907990z>.
- [82] F. Atay, I. Akyuz, M.S. Cergel, B. Erdogan, Production and Characterization of (004) Oriented Single Anatase TiO₂ Films, *J. Electron. Mater.*, **2018**, *47*, 1601-1610, <https://doi.org/10.1007/s11664-017-5988-5>.
- [83] Y. Cao, L. Huang, Y. Bai, K. Jermstipparsert, R. Hosseinzadeh, H. Rasoulnezhad, G. Hosseinzadeh, Synergic effect of oxygen vacancy defect and shape on the photocatalytic performance of nanostructured TiO₂ coating, *Polyhedron*, **2020**, *175*, 114214, <https://doi.org/10.1016/j.poly.2019.114214>.
- [84] I. Dündar, TiO₂ Thin Films by Ultrasonic Spray Pyrolysis for Photocatalytic Air-Cleaning Applications, doctoral thesis, Tallinn University of Tehnology, **2021**.
- [85] J. Moma, J. Baloyi, Modified Titanium Dioxide for Photocatalytic Applications, *Photocatal. - Appl. Attrib.*, **2019**, <https://doi.org/10.5772/intechopen.79374>.
- [86] C. Xu, J. Huang, X. Tan, T. Yu, Z. Cui, L. Zhao, Preparation, characteristics, and photocatalytic tests of fe-doped TiO₂ films prepared by a sol-gel drain coating via homemade devices, *J. Dispers. Sci. Technol.*, **2010**, *31*, 1732-1739, <https://doi.org/10.1080/01932690903543097>.
- [87] A.M. Alotaibi, P. Promdet, G.B. Hwang, J. Li, S.P. Nair, S. Sathasivam, A. Kafizas, C.J. Carmalt, I.P. Parkin, Zn and N Codoped TiO₂ Thin Films: Photocatalytic and Bactericidal Activity, *ACS Appl. Mater. Interfaces.*, **2021**, *13*, 10480-10489, <https://doi.org/10.1021/acsami.1c00304>.

- [88] Q. Jiang, C. Ding, Y. Liu, A type of novel glass for indoor air cleaning under visible-light, *Build. Environ.*, **2018**, 137, 226-234, <https://doi.org/10.1016/j.buildenv.2018.04.013>.
- [89] D. Zhang, X. Zhang, Q. Sun, S. Zheng, J. Hao, Y. Wang, Continuous Photocatalysis Based on Layer-by-Layer Assembly of Separation-Free TiO₂/Reduced Graphene Oxide Film Catalysts with Increased Charge Transfer and Active Site, *Eur. J. Inorg. Chem.*, **2019**, 5, 721-729, <https://doi.org/10.1002/ejic.201801282>.
- [90] S.A. Abdullah, M.Z. Sahdan, N. Nafarizal, H. Saim, A.S. Bakri, C.H. Cik Rohaida, F. Adriyanto, Y. Sari, Photoluminescence study of trap-state defect on TiO₂ thin films at different substrate temperature via RF magnetron sputtering, *J. Phys. Conf. Ser.*, **2018**, 995, 012067, <https://doi.org/10.1088/1742-6596/995/1/012067>.
- [91] J.J. Carey, K.P. McKenna, Screening Doping Strategies to Mitigate Electron Trapping at Anatase TiO₂ Surfaces, *J. Phys. Chem. C.*, **2019**, 123, 22358-22367, <https://doi.org/10.1021/acs.jpcc.9b05840>.
- [92] L. Zhou, S. Yan, B. Tian, J. Zhang, M. Anpo, Preparation of TiO₂-SiO₂ film with high photocatalytic activity on PET substrate, *Mater. Lett.*, **2006**, 60, 369-399, <https://doi.org/10.1016/j.matlet.2005.08.065>.
- [93] F. Pan, K. Wu, H. Li, G. Xu, W. Chen, Synthesis of {100} facet dominant anatase TiO₂ nanobelts and the origin of facet-dependent photoreactivity, *Chem. - A Eur. J.*, **2014**, 20, 15095-15101, <https://doi.org/10.1002/chem.201403866>.
- [94] B.I. Stefanov, G.A. Niklasson, C.G. Granqvist, L. Österlund, Gas-phase photocatalytic activity of sputter-deposited anatase TiO₂ films: Effect of (0 0 1) preferential orientation, surface temperature and humidity, *J. Catal.*, **2016**, 335, 187-196, <https://doi.org/10.1016/j.jcat.2015.12.002>.
- [95] K. Nakata, T. Ochiai, T. Murakami, A. Fujishima, Photoenergy conversion with TiO₂ photocatalysis: New materials and recent applications, *Electrochim. Acta.*, **2012**, 84, 103-111. <https://doi.org/10.1016/j.electacta.2012.03.035>.
- [96] S. Guo, Z. Wu, W. Zhao, TiO₂-based building materials: Above and beyond traditional applications, *Chinese Sci. Bull.*, **2009**, 54, 1137-1142, <https://doi.org/10.1007/s11434-009-0063-0>.
- [97] B. Ohtani, Preparing articles on photocatalysis - beyond the illusions, misconceptions, and speculation, *Chem. Lett.*, **2008**, 37, 216-229, <https://doi.org/10.1246/cl.2008.216>.
- [98] K. Nakata, A. Fujishima, TiO₂ photocatalysis: Design and applications, *J. Photochem. Photobiol. C Photochem. Rev.*, **2012**, 13, 169-189, <https://doi.org/10.1016/j.jphotochemrev.2012.06.001>.
- [99] H.A. Foster, I.B. Ditta, S. Varghese, A. Steele, Photocatalytic disinfection using titanium dioxide: Spectrum and mechanism of antimicrobial activity, *Appl. Microbiol. Biotechnol.*, **2011**, 90, 1847-1868, <https://doi.org/10.1007/s00253-011-3213-7>.

- [100] A. Habibi-Yangjeh, S. Asadzadeh-Khaneghah, S. Feizpoor, A. Rouhi, Review on heterogeneous photocatalytic disinfection of waterborne, airborne, and foodborne viruses: Can we win against pathogenic viruses?, *J. Colloid Interface Sci.*, **2020**, 580, 503-514, <https://doi.org/10.1016/j.jcis.2020.07.047>.
- [101] K. Sunada, T. Watanabe, K. Hashimoto, Studies on photokilling of bacteria on TiO₂ thin film, *J. Photochem. Photobiol. A Chem.*, **2003**, 156, 227-233, [https://doi.org/10.1016/S1010-6030\(02\)00434-3](https://doi.org/10.1016/S1010-6030(02)00434-3).
- [102] K. Ouyang, K. Dai, S.L. Walker, Q. Huang, X. Yin, P. Cai, Efficient photocatalytic disinfection of Escherichia coli O₁₅₇:H₇ using C₇₀-TiO₂ hybrid under visible light irradiation, *Sci. Rep.*, **2016**, 6, 25702, <https://doi.org/10.1038/srep25702>.
- [103] S.Y. Choi, B. Cho, Extermination of influenza virus H1N1 by a new visible-light-induced photocatalyst under fluorescent light, *Virus Res.*, **2018**, 248, 71-73, <https://doi.org/10.1016/j.virusres.2018.02.011>.
- [104] P. Micochova, A. Chadha, T. Hesseloj, F. Fraternali, J.J. Ramsden, R.K. Gupta, Rapid inactivation of SARS-CoV-2 by titanium dioxide surface coating, *Wellcome Open Res.*, **2021**, 6, 56 <https://doi.org/10.12688/wellcomeopenres.16577.1>.
- [105] R. Wang, K. Hashimoto, A. Fujishima, M. Chikuni, E. Kojima, A. Kitamura, M. Shimohigoshi, T. Watanabe, Light-induced amphiphilic surfaces, *Nature*, **1997**, 388, 431-432, <https://doi.org/10.1038/41233>.
- [106] H. Oladipo, C. Garlisi, K. Al-Ali, E. Azar, G. Palmisano, Combined photocatalytic properties and energy efficiency via multifunctional glass, *J. Environ. Chem. Eng.*, **2019**, 7, 102980, <https://doi.org/10.1016/j.jece.2019.102980>.
- [107] A. Mills, A. Lepre, N. Elliott, S. Bhopal, I.P. Parkin, S.A. O'Neill, Characterisation of the photocatalyst Pilkington Activ™: A reference film photocatalyst?, *J. Photochem. Photobiol. A Chem.*, **2003**, 160, 213-224, [https://doi.org/10.1016/S1010-6030\(03\)00205-3](https://doi.org/10.1016/S1010-6030(03)00205-3).
- [108] J. Chen, C. Poon, Photocatalytic construction and building materials: From fundamentals to applications, *Build. Environ.*, **2009**, 9, 1899-1906 <https://doi.org/10.1016/j.buildenv.2009.01.002>.
- [109] F. Hamidi, F. Aslani, TiO₂-based photocatalytic cementitious composites: Materials, properties, influential parameters, and assessment techniques, *Nanomaterials*, **2019**, 9, 1444, <https://doi.org/10.3390/nano9101444>.
- [110] E. Boonen, A. Beeldens, Recent photocatalytic applications for air purification in Belgium, *Coatings*, **2014**, 4, 553-573, <https://doi.org/10.3390/coatings4030553>.
- [111] Y. Boyjoo, H. Sun, J. Liu, V.K. Pareek, S. Wang, A review on photocatalysis for air treatment: From catalyst development to reactor design, *Chem. Eng. J.*, **2017**, 310, 537-559, <https://doi.org/10.1016/j.cej.2016.06.090>.
- [112] J. M. Formenti, P. Meriaudeau, S.J. Teichner, Heterogeneous photocatalysis for partial oxidation of paraffins, *Chem. Tech*, **1971**, 6, 680-686.
- [113] T. Maggos, V. Binas, V. Siaperas, A. Terzopoulos, P. Panagopoulos, G. Kiriakidis, A Promising technological approach to improve indoor air quality, *Appl. Sci.*, **2019**, 9, 4837, <https://doi.org/10.3390/app9224837>.

- [114] R.K. Nath, M.F.M. Zain, M. Jamil, An environment-friendly solution for indoor air purification by using renewable photocatalysts in concrete: A review, *Renew. Sustain. Energy Rev.*, **2016**, 62, 1184-1194, <https://doi.org/10.1016/j.rser.2016.05.018>.
- [115] S. Yang, V. Perret, C. Hager Jörin, H. Niculita-Hirzel, J. Goyette Pernot, D. Licina, Volatile organic compounds in 169 energy-efficient dwellings in Switzerland, *Indoor Air*, **2020**, 30, 481-491, <https://doi.org/10.1111/ina.12667>.
- [116] L. Du, V. Leivo, D. Martuzevicius, T. Prasauskas, M. Turunen, U. Haverinen-Shaughnessy, Improving energy efficiency of multifamily buildings, indoor environmental quality and occupant health - INSULAtE-project results, **2016**, 228. <http://urn.fi/URN:ISBN:978-952-302-772-5>.
- [117] E. Commission, J.R. Centre, European collaborative action 'Indoor air quality and its impact on man' : total volatile organic compounds (TVOC) in indoor air quality investigations, Publications Office, **1997**.
- [118] W.K. Jo, Y.J. Seo, Indoor and outdoor bioaerosol levels at recreation facilities, elementary schools, and homes, *Chemosphere*, **2005**, 61, 1570-1579, <https://doi.org/10.1016/j.chemosphere.2005.04.103>.
- [119] A. Poormohammadi, S. Bashirian, A.R. Rahmani, G. Azarian, F. Mehri, Are photocatalytic processes effective for removal of airborne viruses from indoor air? A narrative review, *Environ. Sci. Pollut. Res.*, **2021**, 28, 43007-43020, <https://doi.org/10.1007/s11356-021-14836-z>.
- [120] T. Kako, A. Nakajima, T. Watanabe, K. Hashimoto, Comparison of photocatalytic properties of a batch reactor with those of a flow reactor in a nearly controlled mass transport region, in: *Res. Chem., Intermed.*, **2005**, 31, 371-378, <https://doi.org/10.1163/1568567053956572>.
- [121] M. Kask, J. Bolobajev, M. Krichevskaya, Gas-phase photocatalytic degradation of acetone and toluene, and their mixture in the presence of ozone in continuous multi-section reactor as possible air post-treatment for exhaust from pulsed corona discharge, *Chem. Eng. J.*, **2020**, 399, 125815, <https://doi.org/10.1016/j.cej.2020.125815>.
- [122] J.M. Garcia Hernandez, Photocatalytic Reactors for Air Treatment: Energy Efficiencies and Kinetic Modeling, doctoral thesis, Western University, **2012**.
- [123] O. Tokode, R. Prabhu, L.A. Lawton, P.K.J. Robertson, A photocatalytic impeller reactor for gas phase heterogeneous photocatalysis, *J. Environ. Chem. Eng.*, **2017**, 5, 3942-3948. <https://doi.org/10.1016/j.jece.2017.07.068>.
- [124] Y.W. Li, W.L. Ma, Photocatalytic oxidation technology for indoor air pollutants elimination: A review, *Chemosphere*, **2021**, 280, 130667, <https://doi.org/10.1016/j.chemosphere.2021.130667>.
- [125] B.M. da Costa Filho, G. V. Silva, R.A.R. Boaventura, M.M. Dias, J.C.B. Lopes, V.J.P. Vilar, Ozonation and ozone-enhanced photocatalysis for VOC removal from air streams: Process optimization, synergy and mechanism assessment, *Sci. Total Environ.*, **2019**, 687, 1357-1368, <https://doi.org/10.1016/j.scitotenv.2019.05.365>.
- [126] C. Geankoplis, Transport processes and unit operations, 3rd ed., **1993**.

- [127] T.N. Obee, Photooxidation of sub-parts-per-million toluene and formaldehyde levels on titania using a glass-plate reactor, *Environ. Sci. Technol.*, **1996**, 30, 3578-3584, <https://doi.org/10.1021/es9602713>.
- [128] M. Sleiman, P. Conchon, C. Ferronato, J.M. Chovelon, Photocatalytic oxidation of toluene at indoor air levels (ppbv): Towards a better assessment of conversion, reaction intermediates and mineralization, *Appl. Catal. B Environ.*, **2009**, 86, 159-165, <https://doi.org/10.1016/j.apcatb.2008.08.003>.
- [129] W. Liang, J. Li, H. He, Photo-Catalytic Degradation of Volatile Organic Compounds (VOCs) over Titanium Dioxide Thin Film, *Adv. Asp. Spectrosc.*, **2012**, <https://doi.org/10.5772/48160>.
- [130] M.J. Sampaio, Z. Yu, J.C. Lopes, P.B. Tavares, C.G. Silva, L. Liu, J.L. Faria, Light-driven oxygen evolution from water oxidation with immobilised TiO₂ engineered for high performance, *Sci. Rep.*, **2021**, 11, 21306, <https://doi.org/10.1038/s41598-021-99841-5>.
- [131] Y. Li, F. Liu, M. Li, W. Li, X. Qi, M. Xue, Y. Wang, F. Han, Study on adsorption coupling photodegradation on hierarchical nanostructured g-C₃N₄/TiO₂/activated carbon fiber composites for toluene removal, *J. Sol-Gel Sci. Technol.*, **2020**, 93, 402-418, <https://doi.org/10.1007/s10971-019-05198-7>.
- [132] O. Debono, V. Hequet, L. Le Coq, N. Locoge, F. Thevenet, VOC ternary mixture effect on ppb level photocatalytic oxidation: Removal kinetic, reaction intermediates and mineralization, *Appl. Catal. B Environ.*, **2017**, 218, 359-369, <https://doi.org/10.1016/j.apcatb.2017.06.070>.
- [133] S.B. Kim, H.T. Hwang, S.C. Hong, Photocatalytic degradation of volatile organic compounds at the gas-solid interface of a TiO₂ photocatalyst, *Chemosphere*, **2002**, 48, 437-444, [https://doi.org/10.1016/S0045-6535\(02\)00101-7](https://doi.org/10.1016/S0045-6535(02)00101-7).
- [134] C. Raillard, V. Héquet, P. Le Cloirec, J. Legrand, TiO₂ coating types influencing the role of water vapor on the photocatalytic oxidation of methyl ethyl ketone in the gas phase, *Appl. Catal. B Environ.*, **2005**, 59, 213-220, <https://doi.org/10.1016/j.apcatb.2005.02.011>.
- [135] Z. Jiang, X. Yu, Kinetic studies on using photocatalytic coatings for removal of indoor volatile organic compounds, *Indoor Built Environ*, **2020**, 29, 689-700, <https://doi.org/10.1177/1420326X19861426>.
- [136] R. Dillert, A. Engel, J. Große, P. Lindner, D.W. Bahnemann, Light intensity dependence of the kinetics of the photocatalytic oxidation of nitrogen(ii) oxide at the surface of TiO₂, *Phys. Chem. Chem. Phys.*, **2013**, 48, 20876-20886, <https://doi.org/10.1039/c3cp54469a>.
- [137] M.G. Alalm, R. Djellabi, D. Meroni, C. Pirola, C.L. Bianchi, D.C. Boffito, Toward scaling-up photocatalytic process for multiphase environmental applications, *Catalysts*, **2021**, 11, 562, <https://doi.org/10.3390/catal11050562>.
- [138] R. Chen, J. Li, H. Wang, P. Chen, X. Dong, Y. Sun, Y. Zhou, F. Dong, Photocatalytic reaction mechanisms at a gas-solid interface for typical air pollutant decomposition, *J. Mater. Chem. A.*, **2021**, 9, 20184-20210, <https://doi.org/10.1039/d1ta03705f>.

- [139] W. Cui, J. Li, F. Dong, Optimizing the Gas-Solid Photocatalytic Reactions for Air Purification, *ACS ES T Engg.*, **2022**, 2, 1103-1115, <https://doi.org/10.1021/acsestengg.1c00503>.
- [140] S.W. Verbruggen, TiO₂ photocatalysis for the degradation of pollutants in gas phase: From morphological design to plasmonic enhancement, *J. Photochem. Photobiol. C Photochem. Rev.*, **2015**, 24, 64-82, <https://doi.org/10.1016/j.jphotochemrev.2015.07.001>.
- [141] W. Chen, J.S. Zhang, UV-PCO device for indoor VOCs removal: Investigation on multiple compounds effect, *Build. Environ.*, **2008**, 43, 246-252, <https://doi.org/10.1016/j.buildenv.2006.03.024>.
- [142] W.J. Liang, J. Li, Y.Q. Jin, Photocatalytic degradation of gaseous acetone, toluene, and p-xylene using a TiO₂ thin film, *J. Environ. Sci. Heal. - Part A Toxic/Hazardous Subst. Environ. Eng.*, 2010, 45, 1384-1390, <https://doi.org/10.1080/10934529.2010.500925>.
- [143] H. Einaga, S. Futamura, T. Ibusuki, Heterogeneous photocatalytic oxidation of benzene, toluene, cyclohexene and cyclohexane in humidified air: Comparison of decomposition behavior on photoirradiated TiO₂ catalyst, *Appl. Catal. B Environ.*, **2002**, 38, 215-225, [https://doi.org/10.1016/S0926-3373\(02\)00056-5](https://doi.org/10.1016/S0926-3373(02)00056-5).
- [144] M. Hegedüs, A. Dombi, Comparative study of heterogeneous photocatalytic decomposition of tetrachloroethene and trichloroethene in the gas phase, *Appl. Catal. A Gen.*, **2004**, 271, 177-184, <https://doi.org/10.1016/j.apcata.2004.02.057>.
- [145] W.J. Fisk, Health and productivity gains from better indoor environments and their relationship with building energy efficiency, *Annu. Rev. Energy Environ.*, **2000**, 25, 537-566, <https://doi.org/10.1146/annurev.energy.25.1.537>.
- [146] H. Rasoulnezhad, G. Hosseinzadeh, N. Ghasemian, R. Hosseinzadeh, A.H. Keihan, Transparent nanostructured Fe-doped TiO₂ thin films prepared by ultrasonic assisted spray pyrolysis technique, *Mater. Res. Express.*, **2018**, 5, 056401, <https://doi.org/10.1088/2053-1591/aabe5e>.
- [147] T. Olukan, J. Sydorenko, A. Katerski, M. Al Mahri, C-Y. Lai, A. Al-Hagri, M. Chiesa, S. Santos, Insights into TiO₂ thin film photodegradation from Kelvin Probe AFM maps, *Appl. Phys. Lett.*, **2022**, 121, 031901 <https://doi.org/10.1063/5.0098788>.
- [148] C. Di Valentin, G. Pacchioni, A. Selloni, Theory of carbon doping of titanium dioxide, *Chem. Mater.*, **2005**, 17, 6656-6665, <https://doi.org/10.1021/cm051921h>.
- [149] C. Parvathiraja, S. Katheria, M.R. Siddiqui, S.M. Wabaidur, M.A. Islam, W.C. Lai, Activated Carbon-Loaded Titanium Dioxide Nanoparticles and Their Photocatalytic and Antibacterial Investigations, *Catalysts*, **2022**, 12, 834, <https://doi.org/10.3390/catal12080834>.
- [150] H. Tang, F. Lévy, H. Berger, P.E. Schmid, Urbach tail of anatase TiO₂, *Phys. Rev. B.*, **1995**, 52, 7771, <https://doi.org/10.1103/PhysRevB.52.7771>.

- [151] V. Kumar, O.M. Ntwaeaborwa, J. Holsa, D.E. Motaung, H.C. Swart, The role of oxygen and titanium related defects on the emission of TiO₂:Tb³⁺ nanophosphor for blue lighting applications, *Opt. Mater.*, **2015**, 46, 510-516, <https://doi.org/10.1016/j.optmat.2015.05.011>.
- [152] I. Gromyko, M. Krunk, T. Dedova, A. Katerski, D. Klauson, I. Oja Acik, Surface properties of sprayed and electrodeposited ZnO rod layers, *Appl. Surf. Sci.*, **2017**, 405, 521-528, <https://doi.org/10.1016/j.apsusc.2017.02.065>.
- [153] R. Klaysri, M. Ratova, P. Praserttham, P.J. Kelly, Deposition of visible light-active C-doped titania films via magnetron sputtering using CO₂ as a source of carbon, *Nanomaterials*, **2017**, 7, 113, <https://doi.org/10.3390/nano7050113>.
- [154] S.M. El-Sheikh, T.M. Khedr, A. Hakki, A.A. Ismail, W.A. Badawy, D.W. Bahnemann, Visible light activated carbon and nitrogen co-doped mesoporous TiO₂ as efficient photocatalyst for degradation of ibuprofen, *Sep. Purif. Technol.*, **2017**, 173, 258-268, <https://doi.org/10.1016/j.seppur.2016.09.034>.
- [155] P.A.O. Rodríguez, T.B. Benzaquén, G.A. Pecchi, S.G. Casuscelli, V.R. Elías, G.A. Eimer, Novel route to obtain carbon self-doped TiO₂ mesoporous nanoparticles as efficient photocatalysts for environmental remediation processes under visible light, *Materials (Basel)*. (2019). <https://doi.org/10.3390/ma12203349>.
- [156] S.A. Ansari, M.H. Cho, Highly Visible Light Responsive, Narrow Band gap TiO₂ Nanoparticles Modified by Elemental Red Phosphorus for Photocatalysis and Photoelectrochemical Applications, *Sci. Rep.*, **2016**, 12, 3349, <https://doi.org/10.1038/srep25405>.
- [157] D.A. Armstronga, R.E. Huie, S. Lyman, W.H. Koppenol, G. Merényi, P. Neta, D.M. Stanbury, S. Steenken, P. Wardman, Standard electrode potentials involving radicals in aqueous solution: Inorganic radicals, *Bioinorg. React. Mech.*, **2013**, 9, <https://doi.org/10.1515/irm-2013-0005>.
- [158] T. Sano, E. Puzenat, C. Guillard, C. Geantet, S. Matsuzawa, N. Negishi, Improvement of photocatalytic degradation activity of visible-light-responsive TiO₂ by aid of ultraviolet-light pretreatment, *J. Phys. Chem. C.*, **2009**, 113, 5535-5540, <https://doi.org/10.1021/jp808032y>.
- [159] P.S. Mohamad Saad, H.B. Sutan, S.S. Shariffudin, H. Hashim, U. Mohd Noor, TiO₂ Thin Film via Sol-Gel Method: Investigation on Molarity Effect, *IOP Conf. Ser. Mater. Sci. Eng.*, **2015**, 99, 012006, <https://doi.org/10.1088/1757-899X/99/1/012006>.
- [160] W.N. Hansen, G.J. Hansen, Standard reference surfaces for work function measurements in air, *Surf. Sci.*, **2001**, 481, 172-184, [https://doi.org/10.1016/S0039-6028\(01\)01036-6](https://doi.org/10.1016/S0039-6028(01)01036-6).
- [161] N. Smirnova, T. Fesenko, M. Zhukovsky, J. Goworek, A. Eremenko, Photodegradation of Stearic Acid Adsorbed on Superhydrophilic TiO₂ Surface: In Situ FT-IR and LDI Study, *Nanoscale Res. Lett.*, **2015**, 10, 500, <https://doi.org/10.1186/s11671-015-1210-y>.
- [162] J. Montero, L. Österlund, Photodegradation of stearic acid adsorbed on copper oxide heterojunction thin films prepared by magnetron sputtering, *Chem. Engineering.*, **2018**, 2, 40. <https://doi.org/10.3390/chemengineering2030040>.

- [163] T.W. Liao, S.W. Verbruggen, N. Claes, A. Yadav, D. Grandjean, S. Bals, P. Lievens, TiO₂ films modified with au nanoclusters as self-cleaning surfaces under visible light, *Nanomaterials*, **2018**, 8, 30 <https://doi.org/10.3390/nano8010030>.
- [164] C.L. Bianchi, C. Pirola, M. Stucchi, B. Sacchi, G. Cerrato, S. Morandi, A. Di Michele, A. Carletti, V. Capucci, A New Frontier of Photocatalysis Employing Micro-Sized TiO₂: Air/Water Pollution Abatement and Self-Cleaning/ Antibacterial Applications, *Semicond. Photocatal. - Mater. Mech. Appl.*, **2016**. <https://doi.org/10.5772/62892>.
- [165] L. Li, Z. Sun, H. Li, T.C. Keener, Effects of activated carbon surface properties on the adsorption of volatile organic compounds, *J. Air Waste Manag. Assoc.*, **2012**, 62, 1196-1202. <https://doi.org/10.1080/10962247.2012.700633>.
- [166] C.P. Chang, J.N. Chen, M.C. Lu, Heterogeneous photocatalytic oxidation of acetone for air purification by near UV-irradiated titanium dioxide, *J. Environ. Sci. Heal. - Part A Toxic/Hazardous Subst. Environ. Eng.*, 2003, 38, 1131-1143, <https://doi.org/10.1081/ESE-120019869>.
- [167] S. Saqlain, B.J. Cha, S.Y. Kim, J.Y. Sung, M.C. Choi, H.O. Seo, Y.D. Kim, Impact of humidity on the removal of volatile organic compounds over Fe loaded TiO₂ under visible light irradiation: Insight into photocatalysis mechanism by operando DRIFTS, *Mater. Today Commun.*, **2021**, 26, 102119 <https://doi.org/10.1016/j.mtcomm.2021.102119>.
- [168] S.S. Latthe, S. Liu, C. Terashima, K. Nakata, A. Fujishima, Transparent, adherent, and photocatalytic SiO₂-TiO₂ coatings on polycarbonate for self-cleaning applications, *Coatings*, **2014**, 4, 497-507, <https://doi.org/10.3390/coatings4030497>.
- [169] M. Marszewski, J. Marszewska, S. Pylypenko, M. Jaroniec, Synthesis of Porous Crystalline Doped Titania Photocatalysts Using Modified Precursor Strategy, *Chem. Mater.*, **2016**, 28, 7878-7888, <https://doi.org/10.1021/acs.chemmater.6b03429>.
- [170] Y. Yuan, Z.H. Ruan, X. Huang, Y.Q. Jiang, H.P. Tan, Energy-absorption-based explanation of the TiO₂/C photocatalytic activity enhancement mechanism, *J. Catal.*, **2017**, 348, 246-255, <https://doi.org/10.1016/j.jcat.2016.12.022>.
- [171] Z. Shayegan, F. Haghghat, C.S. Lee, Carbon-doped TiO₂ film to enhance visible and UV light photocatalytic degradation of indoor environment volatile organic compounds, *J. Environ. Chem. Eng.*, **2020**, 8, 104162. <https://doi.org/10.1016/j.jece.2020.104162>.
- [172] I. Arora, H. Chawla, A. Chandra, S. Sagadevan, S. Garg, Advances in the strategies for enhancing the photocatalytic activity of TiO₂: Conversion from UV-light active to visible-light active photocatalyst, *Inorg. Chem. Commun.*, **2022**, 143, 109700. <https://doi.org/10.1016/j.inoche.2022.109700>.
- [173] T. Rojviroon, S. Sirivithayapakorn, E. Coli bacteriostatic action using TiO₂ photocatalytic reactions, *Int. J. Photoenergy.*, **2018**, <https://doi.org/10.1155/2018/8474017>.

- [174] P. Phuinthiang, D.T.T. Trinh, D. Channei, K. Ratananikom, S. Sirilak, W. Khanitchaidecha, A. Nakaruk, Novel strategy for the development of antibacterial TiO₂ thin film onto polymer substrate at room temperature, *Nanomaterials*, **2021**, 11, 1493, <https://doi.org/10.3390/nano11061493>.
- [175] N. Negishi, S. Matsuzawa, K. Takeuchi, P. Pichat, Transparent micrometer-thick TiO₂ films on SiO₂-coated glass prepared by repeated dip-coating/calcination: Characteristics and photocatalytic activities for removing acetaldehyde or toluene in air, *Chem. Mater.*, **2007**, 19, 3808-3814, <https://doi.org/10.1021/cm070320i>.
- [176] T. Watanabe, S. Fukayama, M. Miyauchi, A. Fujishima, K. Hashimoto, Photocatalytic activity and photo-induced wettability conversion of TiO₂ thin film prepared by sol-gel process on a soda-lime glass, *J. Sol-Gel Sci. Technol.*, **2000**, 19, 71–76. <https://doi.org/10.1023/A:1008762121743>.
- [177] S.W. Verbruggen, S. Deng, M. Kurttepli, D.J. Cott, P.M. Vereecken, S. Bals, J.A. Martens, C. Detavernier, S. Lenaerts, Photocatalytic acetaldehyde oxidation in air using spacious TiO₂ films prepared by atomic layer deposition on supported carbonaceous sacrificial templates, *Appl. Catal. B Environ.*, **2014**, 160-161, 204-210, <https://doi.org/10.1016/j.apcatb.2014.05.029>.
- [178] R.A. Aziz, I. Sopyan, Photocatalytic decomposition of acetaldehyde gas on TiO₂-SiO₂ thin film photocatalyst — A kinetic analysis, *Indian J. Chem. Tehnol.*, **2013**, 20, 137–144.
- [179] N. Yao, K. Lun Yeung, Investigation of the performance of TiO₂ photocatalytic coatings, *Chem. Eng. J.*, **2011**, 167, 13-21, <https://doi.org/10.1016/j.cej.2010.11.061>.
- [180] M.E. Zorn, D.T. Tompkins, W.A. Zeltner, M.A. Anderson, Photocatalytic oxidation of acetone vapor on TiO₂/ZrO₂ thin films, *Appl. Catal. B Environ.*, **1999**, 23, 1-8, [https://doi.org/10.1016/S0926-3373\(99\)00067-3](https://doi.org/10.1016/S0926-3373(99)00067-3).
- [181] T. Rojviroon, A. Laobuthee, S. Sirivithayapakorn, Photocatalytic activity of toluene under UV-LED light with TiO₂ thin films, *Int. J. Photoenergy.*, **2012**, <https://doi.org/10.1155/2012/898464>.
- [182] P.C. Yao, S.T. Hang, C.W. Lin, D.H. Hai, Photocatalytic destruction of gaseous toluene by porphyrin-sensitized TiO₂ thin films, *J. Taiwan Inst. Chem. Eng.*, **2011**, 42, 470-479, <https://doi.org/10.1016/j.jtice.2010.08.013>.

Acknowledgements

First, I would like to express my gratitude to my supervisors Prof. Ilona Oja Acik and Dr. Marina Kritševskaja for their guidance, advances, support, and motivation throughout my PhD study.

I would like to thank my co-authors and colleagues at the Department of Materials and Environmental Technology. I am thankful to Dr. Mati Danilson for the XPS measurements. I am grateful to Dr. Merilin Rosenberg and Prof. Anne Kahru from the Environmental Toxicology Laboratory for their assistance with the antibacterial measurements. I thank Dr. Marite Punapart from the University of Tartu for helping with the antiviral measurements.

Special thanks to Prof. Thomas Dittrich from Helmholtz Zentrum Berlin für Materialien und Energie GmbH for facilitating the surface photovoltage measurements and for pleasant collaboration. I would like to thank Prof. Matteo Chiesa and Dr. Sergio Santos from UiT, The Arctic University of Norway, for the atomic force microscopy measurements.

I am thankful to the members of the Laboratory of Thin Film Chemical Technologies for their discussions and support. I am very grateful to Dr. Arvo Mere and Prof. Malle Krunks for their valuable advices.

I would like to acknowledge the following funding sources for financial support during my doctoral research: the Estonian Ministry of Education and Research project IUT 19-4, the Estonian Research Council grant PRG627, the Estonian Centre of Excellence project TK141, and the European Commission's H2020 programme under the ERA Chair project 5GSOLAR grant agreement no. 952509. This research was also partially supported by ASTRA 'TUT Institutional Development Programme for 2016-2022' Graduate School of Functional Materials and Technologies (2014-2020.4.01.16-0032). The DoRa+ 1.1 travel scholarships for attendance at international conferences were financed by the Archimedes Foundation. The Raestipendium was financed by Tallinn City Council.

Finally, the deepest gratitude goes to my family, especially to my husband for being with me during these years with support and encouragement.

Abstract

Development of Spray-Pyrolysis-Synthesised TiO₂ Thin Films for Photocatalytic Degradation of Volatile Organic Compounds in Air

People typically spend most of their time indoors; however, this tendency has significantly increased since the spread of COVID-19. Indoor air contains various mixtures of volatile organic compounds (VOCs) in low concentrations, which are the main reason for poor indoor air quality. The continuous inhalation of polluted air can cause acute health problems, referred to as the sick building syndrome. However, not all technologies are suitable for indoor air purification. Therefore, there is growing scientific interest in photocatalytic oxidation as a cost-effective and efficient technology for VOCs removal from the indoor air.

The aim of the current study is to deposit TiO₂ thin films by chemical spray pyrolysis using different titanium isopropoxide (TTIP):acetylacetone (AcacH) molar ratios in a spray solution. The other objectives include determining the optimal TTIP:AcacH molar ratio for depositing photocatalytically active films, assessing the ability of the film to purify air from VOCs at different operating conditions, and testing the disinfectant properties of the film surfaces against bacteria and virus.

The TTIP:AcacH molar ratio in the spray solution was varied from 1:1 to 1:20. TiO₂ films were deposited onto the borosilicate glass substrates at 350 °C and heat-treated at 500 °C for 1 h. First, the photocatalytic activities of all the obtained films were estimated by the photocatalytic oxidation of an 8.8 mM stearic acid (SA) layer spin-coated onto the TiO₂ films. Second, some TiO₂ films were selected for the photocatalytic oxidation of VOCs (acetone, acetaldehyde, heptane, and toluene) as individual pollutants in the concentration range 5–40 ppm and as 9 ppm VOC mixtures. The photocatalytic oxidation of VOCs was analysed in a gas-phase multi-section reactor under ultraviolet (UV-A) and visible (VIS) light irradiation. Finally, the photocatalytic activity of the films in inactivating *E. coli* bacteria and H1N1 virus was estimated under UV-A irradiation.

Irrespective of the amount of AcacH in the solution, all the TiO₂ films consisted only of the anatase crystalline phase, exhibiting a transparency of ~80% in the visible spectral region and a band gap of ~3.4 eV. The X-ray photoelectron spectroscopy results revealed that the films with a larger amount of AcacH in the spray solution contained more adsorbed carbon on the surface. The Kelvin probe measurements showed that the contact potential differences maximum signals for the films with large AcacH molar ratios were higher than those of the films with small AcacH molar ratios indicating stronger charge separation with AcacH increase. The surface photovoltage measurements showed that an increase in the AcacH molar ratio led to preferential fast hole transfer towards the surface and electron passivation. The changes in the material properties was conducive to the production of more reactive oxygen species.

According to the results of the SA test, an increase in the amount of AcacH in the spray solution enhanced the photocatalytic oxidation of SA. The optimal TTIP:AcacH molar ratio was determined as 1:8, corresponding to a reaction rate constant of 0.243 min⁻¹, which was ten times higher than that of the 1:3 film. Therefore, the film with TTIP:AcacH 1:8 was selected for further comprehensive analyses in the gas-phase reactor for VOC photocatalytic oxidation. Primarily, the activity of the film in the gas phase was studied based on the photocatalytic oxidation of VOCs as individual model

pollutants under different operating conditions. A residence time of 31.2 s was sufficient for the complete oxidation of 10 ppm each of acetone and acetaldehyde, whereas heptane required a residence time of 46.8 s and up to 6 out of 10 ppm of toluene was oxidised at a residence time of 78 s, under UV-A irradiation. Under VIS light irradiation, the VOCs were oxidised slower owing to the limited amount of reactive oxygen species (ROS) on the surface. At a residence time of 46.8 and 62.4 s, 10 ppm each of acetaldehyde and acetone were completely oxidised, respectively; 4.5 out of 10 ppm of heptane was oxidised in 78 s, and the conversion efficiency of 10 ppm of toluene was less than 10% under VIS light irradiation. To mimic real indoor air pollution conditions, the photocatalytic oxidation of two VOCs mixtures (acetaldehyde, acetone, heptane/toluene) was studied. Under UV-A irradiation, the TiO₂ thin film degraded 9 ppm of VOCs in the mixtures at a residence time of 46.8 s. Under VIS light irradiation, 3 ppm each of acetaldehyde and acetone and 2.3 ppm of heptane in the mixture containing heptane were oxidised at a residence time of 78 s. In the mixture containing toluene, 1.6 ppm each of acetaldehyde and acetone and 0.9 ppm of toluene were oxidised, under VIS light irradiation. The presence of toluene inhibited the photocatalytic oxidation of other pollutants in the mixture owing to the adsorption of less reactive oxidation intermediates on the catalyst surface. Over 99% of *E. coli* bacteria was inactivated after 60 min of UV-A irradiation, and the film showed a high reduction factor of influenza virus inactivation after 8 h of UV-A irradiation.

The novelty and the fundamental principle of this study are based on the modification of the precursor solution by increasing the amount of the organic stabilising agent—AcacH. The systematic study of TiO₂ spray-pyrolysis-synthesised films by changing the molar ratio of AcacH in the precursor and the comprehensive analysis of changes in the material properties and their effects on the photocatalytic performance of the films were performed. Moreover, the photocatalytic activity of the films was tested mimicking real indoor conditions in a multi-section gas flow reactor. The results of VOCs mixtures oxidation on the transparent TiO₂ films bring photocatalysis closer to real application.

TiO₂ thin films with a TTIP:AcacH molar ratio of 1:8 exhibited excellent self-cleaning, antibacterial, and antiviral properties and a promising ability for indoor air purification from VOCs under UV-A and VIS light irradiation. The obtained film can be widely applied in the future as an innovative air-purifying material in buildings and devices.

Lühikokkuvõte

Pihustuspürolüüsiga sünteetitud TiO₂ õhukeste kilede väljatöötamine lenduvate orgaaniliste ühendite fotokatalüütiliseks lagundamiseks õhus

Siseruumide kliima on tänapäeval väga aktuaalne teema kogu maailmas. Nüüdisaegne inimene veedab suurema osa ajast siseruumides. Umbes 90% ajast viibime tööl, kodus, jõusaalis või kauplustes ja ainult 10% veedame väljas. Tänaases pandeemia ajastus veedavad mõned inimesed isegi terved päevad oma kodus, töötades kodukontoris ja ostes kõik kaubad interneti kaudu. Siseruumide õhukvaliteet mõjutab otseselt meie tervist. Siseruumi õhk võib sisaldada kuni 200 erinevat saasteainet, enamik neist on toksilised lenduvad orgaanilised ühendid (LOÜ). Need ühendid satuvad siseruumi õhku mitmetest toodetest, mida me igapäevaselt kasutame. Näiteks puhastuvahendid, kosmeetikatooted, mööbel, vaibad, ehitus- ja viimistlusmaterjalid. Isegi väikesed LOÜ kontsentratsioonid võivad tekitada niinimetatud “haige hoone” sündroomi. Ventilatsioonisüsteem vähendab saasteainete kontsentratsiooni õhus, kuid ei lagunda saasteaineid, seega ventilatsioonisüsteemide sidumine lisatehnoloogiatega oleks keskkonnasõbralikum lahendus siseruumide õhu puhastamiseks.

Seetõttu on hädavajalik leida täiendavaid efektiivseid tehnoloogiaid, mis hävitavad õhus olevad LOÜd ja on võimelised tagama siseruumides puhta õhu. Gaasifaasiline fotokatalüütiline oksüdatsioon on perspektiivne ja kuluefektiivne tehnoloogia siseruumide õhu puhastamiseks. Seda tehnoloogiat võib rakendada nii tavalistes elumajades kui ka haiglates, kauplustes, koolides ja muudes hoonetes. Selleks, et protsess toimiks on vaja ainult efektiivset katalüsaatorit ning valgusallikat.

Doktoritöö eesmärgiks oli sadestada TiO₂ õhukesed kiled ultraheli pihustuspürolüüsi meetodil erinevatel titaan(IV)isopropoksiid ja atsetüülatsetonni moolsuhetel pihustuslahuses; leida optimaalne moolsuhe fotokatalüütiliselt aktiivsete kilede valmistamiseks; uurida saadud kilede struktuuri, morfoloogiat, pinnaomadusi ja fotokatalüütilist võimekust LOÜ lagundamisel erinevatel katsetingimustel; hinnata kilede pinnavõimekust bakterite ja viiruste desaktiveerimisel.

TiO₂ õhukesed ja läbipaistvad kiled sadestati boorsilikaatklaasi pinnale kasutades ultraheli pihustuspürolüüsi meetodit temperatuuril 350 °C. Pärast sadestust kuumutati neid õhus ühe tunni jooksul temperatuuril 500 °C, et saada kristalliline anataasi struktuuriga TiO₂. Lähteainetena kasutati titaan(IV)isopropoksiidi, atsetüülatsetonni ja etanooli. Titaan(IV)isopropoksiid ja atsetüülatsetonni moolsuhet pihustuslahuses varieeriti vahemikus 1:1 kuni 1:20. TiO₂ kilede fotokatalüütilist aktiivsust hinnati steariinhappe lagundamisega. Selleks kanti 8,8 mM steariinhappe lahus ühtlaselt TiO₂ pinnale kasutades tsentrifugaalsadestuse meetodit ning uuriti steariinhappe lagunemist teatud ajaperioodi jooksul. Saadud tulemuste põhjal valiti kiled edasiseks fotokatalüütilise aktiivsuse uuringuteks pidevas gaasi-faasilises mitmesektsioonilises reaktoris. LOÜ (atsetaldehyüd, atsetoon, heptaan ja toluen) lagundati nii eraldi kui ka segudena nii ultraviolettkiirguse kui nähtava valguse toimel. Samuti testiti kilede võimekust desaktiveerida *E. coli* bakterit ja H1N1 viirust.

Sadestatud TiO₂ kilede optilised ja struktuursed omadused ei sõltu atsetüülatsetonni kogusest pihustuslahuses. TiO₂ kiled koosnevad anataasi faasist, nende paksus on ca 380 nm ja keelutsoon 3,4 eV ning nähtava valguse piirkonnas on nende optiline läbipaistvus ca. 80 %. Kõik TiO₂ kiled on superhüdrofiilsed pärast 15 min töötlust

ultraviolettkiirguse all. Kile keemilise koostise uuring XPS meetodil näitas, et atsetüülatssetooni koguse suurendamisega pihustuslahuses suurenes süsiniku kogus TiO₂ kile pinnal. Süsiniku inkorporeerimine TiO₂ materjali võib tekitada lisanivoosid materjali elektroonilises struktuuris, mis suurendab materjali fotokatalüütilist efektiivsust. Kile pinna fotopinge mõõtmised näitasid, et atsetüülatssetooni moolsuhte suurendamine pihustuslahuses viib elektronide passiveerimisele kile pinnal.

Steariinhappe lagundamise kiiruskonstandid kasvasid atsetüülatssetooni suhtelise koguse kasvamisega pihustuslahuses nii ultraviolettkiirguse kui ka nähtava valguse all. Titaan(IV)isopropoksiid ja atsetüülatssetooni moolsuhe 1 : 8 sadestuslahuses on optimaalne fotokatalüütiliselt aktiivse TiO₂ kile saamiseks. Kiiruskonstandi väärtus 1 : 8 kilel oli 0,243 min⁻¹, mis on kümme korda suurem kui 1 : 3 kilel. Seetõttu valiti 1 : 8 kile edasiseks LOÜ oksüdeerimise uuringuteks. Esimeses etapis uuriti kile aktiivsust lagundada individuaalseid LOÜ-sid. Leiti, et UV-A kiirguse all kulub 10 ppm atsetooni ja atseetaldehüüdi lagundamiseks TiO₂ pinnal 31,2 s, sama kogus heptaani laguneb 46,8 s jooksul ja 5.5 ppm tolueeni (algkontsentratsioon = 10 ppm) lagundamiseks kulub 78 s. Nähtava valguse all oksüdeerusid LOÜ-d aeglasemalt, sest reaktiivsete hapnikuosakeste hulk oli piiratud. Nimelt, 10 ppm atseetaldehüüdi ja atsetooni oksüdeerusid täielikult vastavalt 46,8 s ja 62,4 s jooksul; 4,5 ppm heptaani oksüdeerimiseks kuulus 78 s kusjuures 78 s jooksul lagunes vaid 0.6 ppm tolueeni.

Selleks et imiteerida siseruumide õhusaastet täpsemalt, valmistati erinevatest saasteainetest kaks sünteetilist segu. Esimese segu koostis oli 9 ppm atseetaldehüüd-atsetoon-heptaani ja teise segu koostis oli 9 ppm atseetaldehüüd-atsetoon-tolueeni (iga komponendi kontsentratsioon segus oli 3 ppm). Mõlemad segud olid täielikult oksüdeerunud 46,8 s jooksul ultraviolettkiirguse all. Nähtava valguse all oksüdeerus esimeses segus 78 s jooksul 3 ppm atseetaldehüüdi, 3 ppm atsetooni ja 2,3 ppm heptaani ning teises segus sama aja jooksul 1,6 ppm atseetaldehüüdi, 1,6 ppm atsetooni ja 0,9 ppm tolueeni. Ultraviolettkiirguse all oli TiO₂ kile pinnal *E. coli* hävimise efektiivsus üle 99% ning antud pinnakatted olid efektiivsed ka viiruste lagundamisel.

Doktoritöö uudsus seisneb kõrge fotokatalüütilise võimekusega TiO₂ õhukeste kilede sünteesi strateegias. Atsetüülatssetooni suhtelist kogust muudeti pihustuslahuses süstemaatiliselt ja selle mõju TiO₂ kilede omadustele s.h. fotokatalüütilisele LOÜ lagundamise võimekusele on igakülgelt uuritud. Kilede fotokatalüütilist võimekust hinnati tõelise siseruumi õhu tingimusi jäljendades, kasutades mõõtmisteks pidevat gaasi-faasilist mitmesektsioonilist reaktorit. Doktoritöö tulemused toovad fotokatalüüsi lähemale reaalsete rakenduste juurutamisele.

Saadud TiO₂ kilesid saab kasutada nii seadisintegreerituna õhupuhastusseadmetes ja ventilatsioonisüsteemides kui ka hoone aknaklaasile kantud pinnakattena, et tagada siseruumides puhas ja tervislik õhk.






Appendix 1

Publication I

J. Spiridonova, A. Katerski, M. Danilson, M. Krichevskaya, M. Krunks, I. Oja Acik. "Effect of the titanium isopropoxide:acetylacetonone molar ratio on the photocatalytic activity of TiO₂ thin films," *Molecules*, 24(23), 4326, 2019, doi.org/10.3390/molecules24234326.

Article

Effect of the Titanium Isopropoxide:Acetylacetonone Molar Ratio on the Photocatalytic Activity of TiO₂ Thin Films

Jekaterina Spiridonova ^{1,*}, Atanas Katerski ¹, Mati Danilson ², Marina Krichevskaya ^{3,*}, Malle Krunkis ¹ and Ilona Oja Acik ^{1,*}

¹ Laboratory of Thin Films Chemical Technologies, Department of Materials and Environmental Technology, Tallinn University of Technology, Ehitajate tee 5, 19086 Tallinn, Estonia; atanas.katerski@taltech.ee (A.K.); malle.krunkis@taltech.ee (M.K.)

² Laboratory of Optoelectronic Materials Physics, Department of Materials and Environmental Technology, Tallinn University of Technology, Ehitajate tee 5, 19086 Tallinn, Estonia; mati.danilson@taltech.ee

³ Laboratory of Environmental Technology, Department of Materials and Environmental Technology, Tallinn University of Technology, Ehitajate tee 5, 19086 Tallinn, Estonia

* Correspondence: jekaterina.spiridono@taltech.ee (J.S.); marina.kritsevskaja@taltech.ee (M.K.); ilona.oja@taltech.ee (I.O.A.); Tel.: +372-620-3369 (I.O.A.)

Academic Editors: Smagul Karazhanov, Ana Cremades and Cuong Ton-That

Received: 31 October 2019; Accepted: 25 November 2019; Published: 27 November 2019



Abstract: TiO₂ thin films with different titanium isopropoxide (TTIP):acetylacetonone (AcacH) molar ratios in solution were prepared by the chemical spray pyrolysis method. The TTIP:AcacH molar ratio in spray solution varied from 1:3 to 1:20. TiO₂ films were deposited onto the glass substrates at 350 °C and heat-treated at 500 °C. The morphology, structure, surface chemical composition, and photocatalytic activity of the obtained TiO₂ films were investigated. TiO₂ films showed a transparency of ca 80% in the visible spectral region and a band gap of ca 3.4 eV irrespective of the TTIP:AcacH molar ratio in the spray solution. TiO₂ films consist of the anatase crystalline phase with a mean crystallite size in the range of 30–40 nm. Self-cleaning properties of the films were estimated using the stearic acid (SA) test. A thin layer of 8.8-mM SA solution was spin-coated onto the TiO₂ film. The degradation rate of SA as a function of irradiation time was monitored by Fourier-transform infrared spectroscopy (FTIR). An increase in the TTIP:AcacH molar ratio from 1:4 to 1:8 resulted in a ten-fold increase in the photodegradation reaction rate constant (from 0.02 to the 0.2 min⁻¹) under ultraviolet light and in a four-fold increase under visible light.

Keywords: TiO₂; thin film; ultrasonic spray pyrolysis; acetylacetonone; photocatalysis; stearic acid

1. Introduction

The synthesis and optimization of TiO₂ thin films is a rapidly developing topic in the field of environmental engineering due to their great potential in pollution treatment and self-cleaning properties. Transparent glass has multiple applications. It is widely used in our homes (in windows, doors, and shower enclosures), in automobile windshields, in electronic device screens, and in construction materials for modern skyscrapers. Keeping the surface of the glass clean is not an easy task; due to its optical transparency, all the dirt particles, stains, and fingerprints which present on the surface are noticeable [1].

Today, more and more skyscrapers are built worldwide because they give us an opportunity to design a good deal of real estate using a relatively small ground area. However, skyscraper window cleaning is risky. According to the National Institute for Occupational Safety and Health (NIOSH) in

the United States there were 88 window cleaning accidents over a 15-year period; 70% of them ended in death [2]. Covering the surface of skyscrapers with a TiO₂ thin layer can substitute this risky job and save money (along with water and chemicals) on cleaning. TiO₂ has photocatalytic and hydrophilic properties when it is irradiated with light source that has an energy content equal to or higher than the band gap of the TiO₂. One of the first commercialized applications of TiO₂ as a photocatalytic material was a self-cleaning glass for tunnel light covers in Japan. Tunnel lamps in Japan emit ultraviolet (UV) light of about 3 mW cm⁻², which is enough to keep the glass cover surface clean of automobile exhaust when it is covered with the TiO₂ photocatalyst [3].

For commercial use, it is very important to find a cost-effective and efficient technology for thin film deposition. TiO₂ films have been prepared using a variety of deposition methods such as chemical vapor deposition [4], sputtering [5], hydrothermal [6], electrophoretic [7], sol-gel [8,9], and spray pyrolysis [10,11]. Among the above-mentioned methods, deposition of thin films with ultrasonic spray pyrolysis has the advantage of being a simple, inexpensive method that allows us to obtain transparent homogeneous films with high stability and quality. This method could be easily applied at the laboratory scale as well as in industry for film deposition on large surfaces [12,13]. Our research group is focused on gas-phase photocatalytic oxidation on TiO₂ thin films prepared by the spray pyrolysis technique. In our recent study, 350 °C was found as to be an optimal temperature for film deposition because this film has a greater number of surface defects [13].

Choosing a precursor solution for thin film preparation is the next essential step in the process of material synthesis. In solution preparation, mainly alkoxides are used as a titanium source, for example, titanium butoxide [12,14], titanium ethoxide [15], and titanium isopropoxide (TTIP) [8,13,16]. Since metal oxides are highly reactive with water, to stabilize the precursor solution and retard the hydrolysis rate, chemical additives are used. These can be acids (HCl) [17], bases (NaOH) [18], solvents (2-methoxyethanol) [9,19], or stabilizing agents (acetylacetone) [9,10,16]. The effects of organic additives such as benzoic acid [20], diethylene glycol [21], diethanolamine [22], humic acid [23], and glucose [24] on the properties of TiO₂ thin films and powder materials were studied. Byrne et al. (2016) have studied the effect of molar ratio TiO₂:benzoic acid on the phase transformation and carbon incorporation onto the surface of photocatalyst and found that benzoic acid enhances rutile phase formation [20]. Park and co-authors (2009) studied the carbon incorporation into the lattice of TiO₂ photocatalyst prepared by sol-gel by changing the calcination temperature without the addition of external carbon source. Lattice carbon incorporation enhances the photocatalytic oxidation of 4-chlorophenol and iodide under visible light [25].

In the current study, modifications in the precursor solution were done to prepare a more active material. Titanium isopropoxide (TTIP) was used as a precursor and acetylacetone (AcacH) as a stabilizing agent. The reaction of TTIP with AcacH has been well studied in the literature. Acetylacetone behaves as a nucleophilic reactant and replaces the alkoxy group; thus, a new molecular precursor is formed [26]. This reaction has been studied using Fourier-transform infrared spectroscopy (FTIR) [16,27]. However, it is known that the TTIP:AcacH molar ratio 1:1 is not sufficient for complete complex formation; the complex is formed at the molar ratio of 1:2 and starting from the ratio 1:3 an excess of acetylacetone can be seen in the solution [16]. Few studies have focused on the effect of the TTIP:AcacH molar ratio on the structural properties [16] and photocatalytic activity of the films [28] and powders [29]. No comprehensive studies about addition of a high AcacH molar ratio into the precursor solution and its effects on the material and photocatalytic properties of the films were found in the scientific literature. The aim of this study was to determine the optimal TTIP:AcacH molar ratio in the precursor solution for the deposition of photocatalytically active TiO₂ thin films by the ultrasonic spray pyrolysis method. The morphological and structural properties, surface chemical composition, and photocatalytic activity of TiO₂ thin films with different TTIP:AcacH molar ratios (from 1:3 to 1:20) were investigated. The photocatalytic activity in the current study was tested by the stearic acid test under ultraviolet (UV-A) and visible light (VIS).

2. Results and Discussion

2.1. Surface Morphology

Scanning electron microscopy (SEM) images of the TiO₂ thin films with TTIP:AcacH molar ratios of 1:4, 1:5, and 1:8 are presented in Figure 1. An increase in the amount of acetylacetone in the precursor solution makes the surface of the thin film flatter, smoother, and more uniform. Kajitvichyanukul et al. (2005) have studied the effect of acetylacetone on the morphology of TiO₂ thin films prepared by sol-gel dip coating. They found that with the increase in acetylacetone, smooth films, like TiO₂ sheets, were obtained [30].

Figure 1 shows that the surfaces of 1:4 and 1:5 TTIP:AcacH thin films have cracks, while the 1:8 film surface is crack-free. Addition of acetylacetone to titanium isopropoxide makes the process of gel formation slower. Therefore, the precursor solution is more stable and homogeneous, promoting the synthesis of thin films with a higher quality and better adhesion [26].

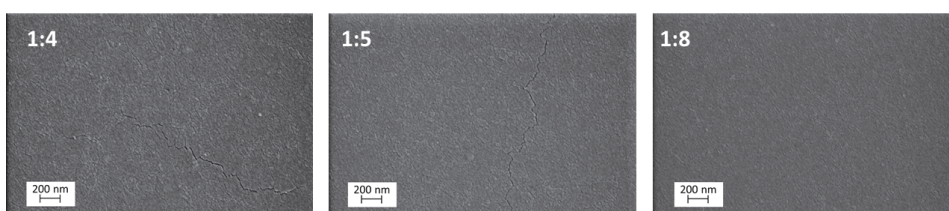


Figure 1. Scanning electron microscopy (SEM) surface images of TiO₂ thin films deposited on borosilicate glass at titanium isopropoxide (TTIP):acetylacetone (AcacH) molar ratios of 1:4, 1:5, and 1:8.

The thicknesses of the samples with the molar ratios 1:4 and 1:8 were determined from their SEM cross-sectional images and were 370 and 375 nm, respectively (Figure 2). It was observed that the thickness of the TiO₂ thin films was not affected by the increase in the acetylalacetone molar ratio in the starting solution.

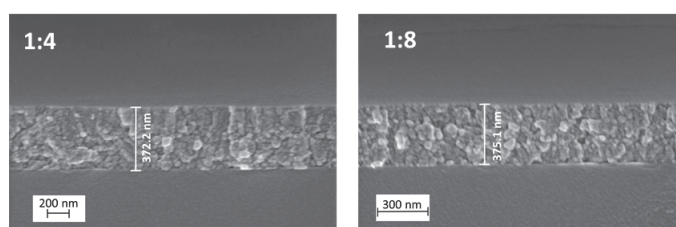


Figure 2. Cross-sectional SEM images of TiO₂ thin films deposited on borosilicate glass at TTIP:AcacH molar ratios of 1:4 and 1:8.

2.2. Structural Properties

X-ray diffraction (XRD) analysis was performed to investigate crystallinity, phase composition, and the mean crystallite size of TiO₂ thin films. All of the obtained films consist only of the anatase phase regardless of the acetylalacetone molar ratio in the precursor solution. Figure 3 reveals a diffractogram of TiO₂ films. The diffraction peaks at 2 theta of 25.3°, 37.0°, 37.8°, 38.6°, 48.1°, 53.9°, and 55° correspond to the reflection planes from (101), (103), (004), (112), (200), (105), and (211), respectively, of anatase TiO₂ [31]. No diffraction peaks belonging to the rutile or brookite phase were detected.

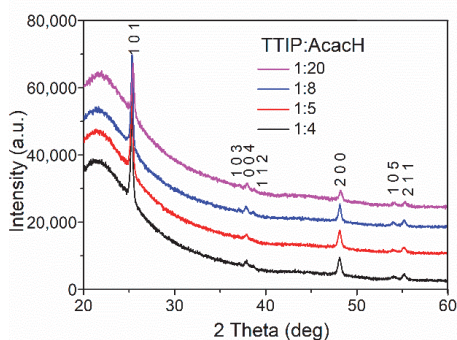


Figure 3. X-ray diffraction (XRD) patterns of TiO₂ thin films with different TTIP:AcacH molar ratios.

The mean crystallite size was calculated using the full width at half maximum (FWHM) of the most intense (101) peak of anatase phase by the Scherrer formula. The mean crystallite size of the films varies in the range of 30–40 nm. Slight changes in the values of crystallite size are not in correlation with the amount of acetylacetonate in the starting solution.

According to the literature, an increase of AcacH in the precursor solution affects the phase transformation process from anatase to rutile and enhances the crystallization process. The anatase to rutile phase transformation starts to occur at the annealing temperature about 800 °C when the precursor solution is not fully stabilized (in the case of a TTIP:AcacH molar ratio less than 1:3). Excess of AcacH in the starting solution lowers the transformation temperature by about 100 °C [16].

The results of this study demonstrate that an increase in the amount of the unchelated acetylacetonate in the precursor solution has no significant effect on the structural properties of TiO₂ thin films, since all the obtained films were annealed at the same temperature –500 °C.

2.3. Optical Properties

The optical transmittance spectra of TiO₂ thin films were measured in the wavelength range between 200 and 1200 nm (Figure 4). Obtained thin films are transparent in the visible light region. The transmittance is about 80% in the spectral region of 500–1200 nm for all obtained films irrespective of the TTIP:AcacH molar ratio in the spray solution.

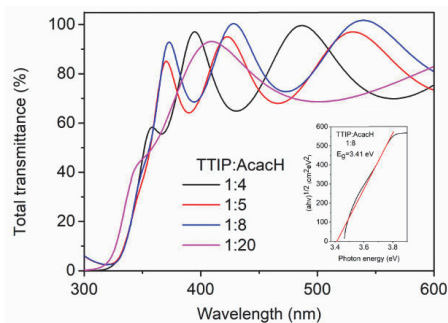


Figure 4. Total transmittance spectra for TiO₂ thin films deposited at different TTIP:AcacH molar ratios. The inset shows the band gap value of the sample deposited at the TTIP:AcacH molar ratio of 1:8.

Using maxima or/and minima of interference fringes of the optical spectrum, it is possible to investigate the thickness of the film by the so called Swanepoel's method. Thickness (d) can be found by the following equation:

$$d = \frac{\lambda_1 \lambda_2}{2(\lambda_1 n_2 - \lambda_2 n_1)}, \quad (1)$$

where n_1 and n_2 are reflective indexes at two adjacent maxima/minima, and $\lambda_1 \lambda_2$ is the wavelength of the maxima/minima [32].

The thickness calculated by Swanepoel's method corresponds to the thickness that was determined by SEM cross-sectional images (Figure 2, Section 2.1.) and is about 400 nm for all samples (Table 1), except for the sample with the TTIP:AcacH molar ratio of 1:20. This sample is about 100 nm thinner. This could be explained by a rise in the amount of free AcacH in precursor solution that increased the viscosity of the spray solution. Viscosity affects the transportation of aerosol produced by an ultrasonic generator. The aerosol flow rate decreases with the increase in the viscosity value. As a result, the growth of the thin film occurs more slowly [33].

The band gap was found using the Tauc plot. Since TiO₂ has an indirect band gap, a plot of the $\sqrt{\alpha E}$ function of photon energy, $E = h\nu$, was used [34]. Table 1 shows the band gaps of the obtained TiO₂ thin films, which are about 3.4 eV.

Table 1. Optical properties of TiO₂ thin films with different TTIP:AcacH ratios.

TTIP:AcacH Molar Ratio	Thickness, nm	Band Gap, eV
1:3	380	3.3
1:4	370	3.4
1:5	370	3.4
1:6	410	3.4
1:7	370	3.4
1:8	375	3.4
1:10	370	3.4
1:12	390	3.4
1:20	280	3.5

Overall, it was found that the optical properties of the TiO₂ films are not significantly affected by the acetylacetone amount in the precursor solution.

2.4. Chemical Composition and Wettability

X-ray photoelectron spectroscopy (XPS) study was performed to investigate the chemical composition and bonding structure of the obtained TiO₂ thin films. The XPS spectra of TiO₂ thin films after UV-A pre-treatment for O_{1s} and C_{1s} core levels are represented in Figure 5.

O_{1s} core level spectra consist of three peaks (Figure 5). The highest peak at the binding energy (BE) value 530.0 eV corresponds to the Ti-O bond. The peak at the BE value 531.0 eV indicates the O²⁻ ions in oxygen-deficient regions within the matrix of TiO₂ [35], which could be associated with oxygen vacancies (V_o), and the peak at the BE value 532.0 eV corresponds to hydroxyl groups adsorbed on the surface [36,37].

The carbon region consists of five singlets with maxima located at 285.0 eV, 285.9 eV, 286.9 eV, 288.5 eV, and 289.5 eV. The highest peak located at 285.0 eV originates from the C=C bond. The peak with the BE maxima at 285.9 eV corresponds to surface hydrocarbons. These forms of non-oxygenated carbons belong to contaminants adsorbed on the TiO₂ surface. Some studies propose that this carbon may exist in the grain boundaries of TiO₂ and it therefore acts as a photosensitizer [37,38]. Peaks with the BE values 286.9 eV and 288.5 eV represent the oxygen-bound species C-O and Ti-O-C bonds, respectively [39]. These peaks confirm the incorporation of carbon into the lattice in the place of the Ti atoms, i.e., interstitial carbon doping takes place [38].

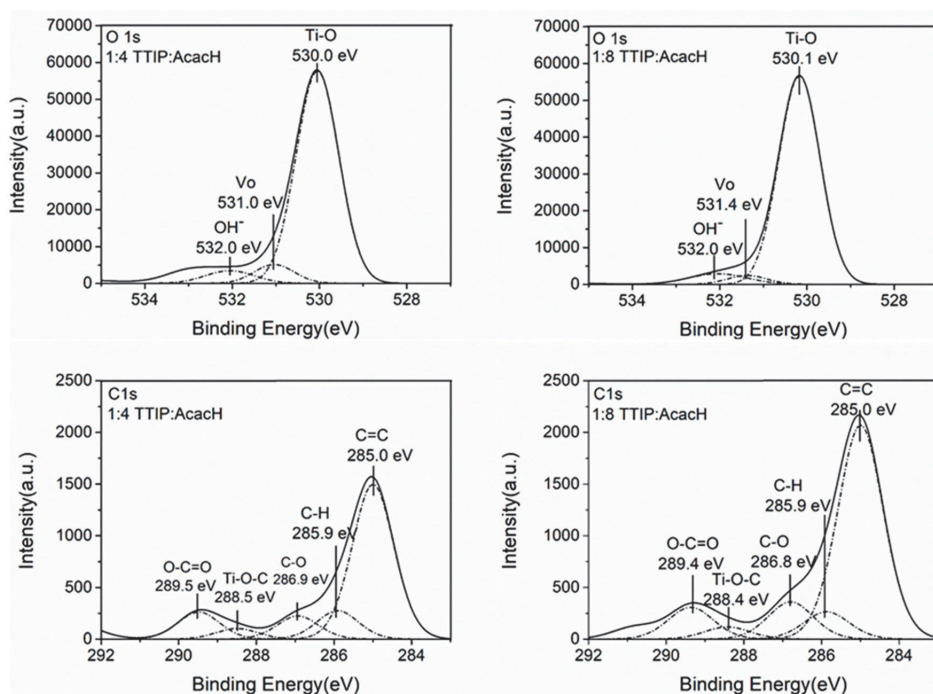


Figure 5. X-ray photoelectron spectroscopy (XPS) spectra of C_{1s} and O_{1s} core levels for 1:4 and 1:8 TTIP:AcacH molar ratios for TiO₂ thin films after ultraviolet (UV-A) pre-treatment.

The integrated areas of the peaks were used to calculate atomic concentrations of the chemical components. The atomic ratios of the components (OH⁻)/(Ti-O), (Vo)/(Ti-O), (C-O)/(C=O) and (C=C)/(C=O) ratios are presented in Table 2. There is no significant difference in the amount of oxygen vacancies and hydroxyl groups with the increase in AcacH, since the deposition parameters were the same. In their study, Dündar et al. (2019) showed that oxygen defects and the hydroxyl group amount on the surface depend on the temperature of the deposition [13].

Table 2. XPS data of the TiO₂ thin films after UV-A pre-treatment.

TTIP:AcacH Molar Ratio	(Vo)/(Ti-O) (at%/at%)	(OH ⁻)/(Ti-O) (at%/at%)	(C-O)/(C-H) (at%/at%)	(Ti-O-C)/(C-H) (at%/at%)	(C=C)/(C-H) (at%/at%)
1:4	0.08	0.07	0.8	0.38	5.43
1:8	0.06	0.07	1.35	0.44	7.80

XPS results showed that films with the higher AcacH molar ratio of 1:8 contained more adsorbed carbon on the surface of the film than films with TTIP:AcacH molar ratio of 1:4. It indicates that the surface of the 1:8 film could be more active since during the photocatalytic experiments, the oxidation of surface contaminant carbon takes place that leads to the increased number of active sites on the surface of the thin film [40]. The amount of C-O and Ti-O-C at the molar ratio 1:8 is also higher, which means that carbon from the unchelated acetylacetonate is transported to the TiO₂ lattice during the decomposition of organic matter. It is reported in the literature that carbon doping enhances photocatalytic activity since it results in localized states occupied in the band gap [41,42]. One carbon atom incorporation into the TiO₂ lattice in an interstitial position generates three strong covalent C-O bonds. These bonds in turn, create three bonding C-O states below the bottom of the O_{2p} valence band. Corresponding antibonding C-O states with high energy lie in the conduction band. The carbon

impurity in the interstitial position leads to the excess of electrons. Excess electrons moves from C-O state to the Ti_{3d} , not to corresponding C-O antibonding states, which creates two new occupied states in the band gap, Ti_{3d} and C_{2p} , below the bottom of the conduction band [43].

The wettability of the TiO_2 film surface was measured for as-deposited films after thermal treatment, one-month aged films, and for aged films after 15 min of UV-A pre-treatment. The average water contact angle (CA) values are shown in Table 3. There is no difference in wettability for as prepared samples with an increase of AcacH in precursor solution; both surfaces are hydrophilic with a CA of about 20° . After one month of storage in the plastic box hydrophilic properties of the films decreased while the sample with a lower AcacH molar ratio (1:4) had significantly higher CA. Contact angles increased to 55° and 30° for TTIP:AcacH molar ratios of 1:4 and 1:8, respectively. This means that the increase of acetylacetone in the precursor solution helps to keep the surface of the films photoinduced for a longer period of time, i.e., adsorption of water and contaminants from the ambient air on the surface of the TiO_2 film with a TTIP:AcacH molar ratio of 1:8 occurs more slowly than at a ratio of 1:4. [44–46]. However, after 15 min of UV-A pre-treatment, all samples became super-hydrophilic, with CA less than 5° .

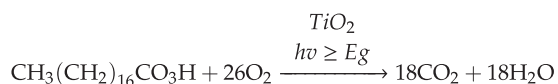
Table 3. Water contact angle values of as-deposited, one-month aged, and UV-A pre-treated films.

TTIP:AcacH Molar Ratio	Contact Angle $^\circ$		
	As-Deposited	One-month Aged	UV-A 15 min
1:4	20	55	4
1:8	20	30	0

During the UV-A pre-treatment water molecules desorb from TiO_2 surface and hydroxyl groups are formed, leading to a better wetting of the surface [46]. This is in accordance with the XPS results showing that after UV-A pre-treatment, the number of hydroxyl groups on the TiO_2 surface is the same for TTIP:AcacH molar ratios of 1:4 and 1:8 (Table 2). During the UV-A pre-treatment, besides hydroxyl groups, peroxy species (H_2O_2) are formed on the surface of the photocatalyst, which increases the photocatalytic activity of the material [47,48]. Organic substances on the surface of TiO_2 act as electron donors and enhance the production of H_2O_2 [47].

2.5. Photocatalytic Activity. Stearic Acid Test

The stearic acid (SA) test is a method for assessing the activity of self-cleaning photocatalyst films. The essence of this method is a deposition of a thin layer of SA onto the film of photocatalytic material and monitoring of the the destruction of SA as a function of irradiation time. The overall reaction can be summarized as follows:



The most commonly employed method of monitoring photodegradation of stearic acid is via the disappearance of the SA film using infrared absorption spectroscopy. SA absorbs strongly in the region $2700\text{--}3000\text{ cm}^{-1}$, with peaks at 2958 cm^{-1} , 2923 cm^{-1} , and 2853 cm^{-1} due to asymmetric in-plane C-H stretching in the CH_3 group and asymmetric and symmetric C-H stretching in the CH_2 groups, respectively (Figure 6a) [49–51].

A stearic acid layer was deposited after the TiO_2 film was pre-treated under UV-A to make the surface of the film photo-induced and super-hydrophilic. The decrease in stearic acid bond intensity was observed by FTIR measurements as a function of irradiation time. FTIR spectra were measured before the UV-A/VIS irradiation and every 15 min during an hour. The integrated area of the band was used to measure the degradation of stearic acid. It has been observed by several authors [52] that the surface structural and wettability properties of the films affect the growth of SA layer on the

surface of a photocatalytic material. Smirnova et al. (2015) detected a serious difference in the SA peaks intensities for TiO₂ thin films annealed at different temperatures [52]. In this study, films have similar structural and wettability properties (Sections 2.2 and 2.4); therefore, the initial integrated area of SA is almost the same.

Degradation of SA is known to follow first-order kinetics, i.e., the integrated band area (A) depends on time as follows:

$$A(t) = A_0 e^{-kt}, \quad (2)$$

where k is photodegradation rate constant. The photodegradation rate constant is the slope value of the linear fit of the plot $\ln(A/A_0)$ versus t [53]. The degradation of stearic acid by TiO₂ at the TTIP:AcacH molar ratio 1:4 and determination of the photodegradation rate constant are presented in Figure 6.

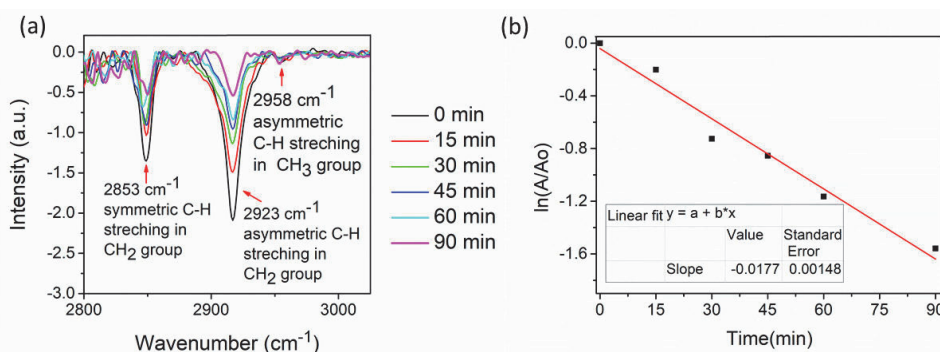


Figure 6. Fourier-transform infrared spectroscopy (FTIR) spectra of stearic acid on the surface of TiO₂ at the TTIP:AcacH molar ratio of 1:4 (a) and determination of the photodegradation rate constant (k) at the molar ratio of 1:4 (b).

The degradation of the stearic acid layer as a function of UV-A irradiation time and the photodegradation rate constants (k) at different TTIP:AcacH molar ratios under UV-A and VIS light for obtained TiO₂ thin films are illustrated in Figure 7.

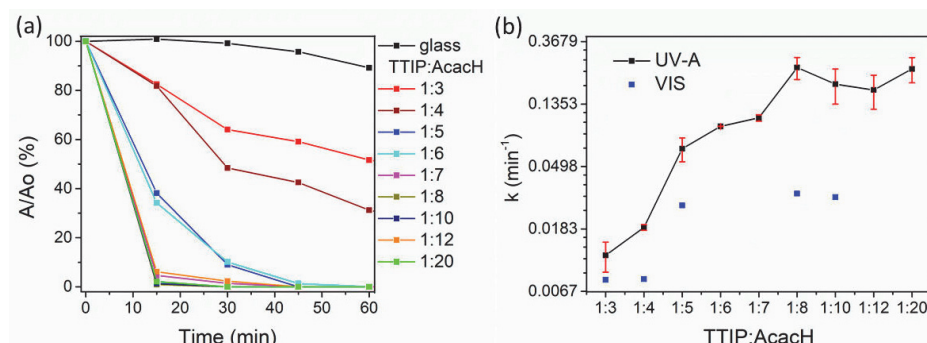


Figure 7. The degradation of stearic acid as a function of ultraviolet (UV-A) irradiation time (a) and photodegradation rate constants (k) under UV-A and visible (VIS) light (b) for TiO₂ thin films at different TTIP:AcacH molar ratios.

Figure 7 shows that the increase in acetylacetone in the precursor solution results in a rapid increase in the photodegradation rate of SA. As can be seen in Figure 7a, for the TTIP:AcacH molar ratios of 1:3 and 1:4, 60 min of UV-A irradiation were not sufficient for complete degradation of the 8.8-mM SA layer; the degradation values were 48% and 69%, respectively. For the molar ratios of

1:5 and 1:6, the degradation was about 90% after 30 min, while at the higher ratios 1:7–1:20, almost complete degradation was achieved after 15 min of UV-A irradiation.

Pore et al. (2006) achieved complete degradation of the 8.8-mM SA layer degradation for atomic layer-deposited TiO₂ thin films modified with H₂S after 60 min of UV-A irradiation, while an unmodified TiO₂ film was capable of degrading only half of SA at the same time of irradiation [51]. The optimal TTIP:AcacH molar ratio found was 1:8 at the reaction rate constant value 0.2427 min⁻¹. As Figure 7b shows, after the molar ratio 1:8, the precursor solution is saturated with AcacH. The plateau is formed and no more increase in the photodegradation rate occurs.

According to many authors, carbon doping enhances photocatalytic activity under visible light [25,54–59]. Therefore, some of the films were tested for the ability to degrade the stearic acid layer under VIS light (Figure 7b). Photodegradation rate constants under VIS light are on average five times lower than under UV-A light. However, the trend in the increase of k value with the increase in amount of AcacH is similar to the case of UV-A. Films were not capable of full mineralization of the SA layer after 60 min of VIS irradiation. However, the conversion of SA was about 90% for samples at 1:8 and 1:10. Ratova et al. (2018) found that interstitial carbon doping enhances the photocatalytic activity of the reactively co-sputtered TiO₂ films under UV and VIS light [55]. However, the red shift of the band gap to the visible spectra was not observed in the present study (Table 1). The enhanced photocatalytic activity of the films under UV-A caused by an increase of AcacH can be due to the formation of C-O bonds, which could form new occupied states in the band gap (Section 2.4) [43].

3. Materials and Methods

3.1. TiO₂ Thin Film Synthesis

TiO₂ thin films were deposited onto borosilicate glass substrates by the ultrasonic spray pyrolysis technique. Titanium (IV) isopropoxide (TTIP) was used as a titanium source, acetylacetone (AcacH) as a stabilizing agent, and ethanol as a solvent. All the deposition parameters were kept constant except the amount of acetylacetone in the precursor solution. The molar ratio of TTIP:AcacH in the precursor solution varied from 1:3 to 1:20. The TTIP concentration in the precursor solution was 0.2 M. To prepare the precursor solutions different amounts of acetylacetone were added to the 3.5 mL TTIP and after some minutes of mixing, the solution was adjusted to the 60 mL by ethanol. Prepared solutions were stirred for one hour. Aerosol produced by an ultrasonic generator was transported by compressed air with a flow rate of 5 L/min. The deposition temperature was set up to 350 °C. As-deposited samples were annealed at 500 °C for 1 h in air.

3.2. Characterization of Films

Scanning electron microscope (SEM, Carl Zeiss, Jena, Germany) was used to investigate the surface morphology of the samples and cross-section images were used to determine the thickness of the films. X-ray diffraction (XRD) was used to study structural properties of the obtained TiO₂ thin films. The XRD diffractograms were obtained from the Rigaku Ultima IV diffractometer (Tokyo, Japan) with Cu K α radiation of $\lambda = 1.5406 \text{ \AA}$, 40 kV, at 40 mA, using a silicon strip detector. The measurements were performed in 2 theta configurations with the scan range 20–60°, with a scanning speed rate of 5° min⁻¹ and a step of 0.02°. The mean crystallite size was calculated using the Scherrer formula from the full width at half maximum (FWHM) of the most intense peak (101) reflection of TiO₂ anatase phase. Optical properties were measured with Jasco V-670 UV-VIS-NIR spectrophotometer (Tokyo, Japan) equipped with an integrating sphere in the spectral range 250–1500 nm. X-ray photoelectron spectroscopy (XPS) with use of a Kratos Analytical AXIS ULTRA DLD spectrometer (Manchester, England) in conjunction with a 165-mm hemispherical electron energy analyzer (Kratos Analytical, Manchester, England) and delay-line detector (Kratos Analytical, Manchester, England) was used to investigate the chemical composition of the surface of TiO₂ thin films. The analysis was carried out with monochromatic Al K α X-rays (1486.6 eV) operating at 15 kV and 150 W. All XPS spectra were

recorded using an aperture slot of 300–700 nm and pass energy of 20 eV. Binding energy (BE) values were calculated based on the C1s core level peak at 285.0 eV. Wettability of the films was studied with water contact angle (CA) measurements.

3.3. Evaluation of Photocatalytic Activity

Photocatalytic activity of the thin films was studied using a stearic acid (SA) test. A thin layer of 8.8-mM SA solution was deposited onto the TiO₂ thin film by the spin coating technique. For this, 100 µL of SA solution in methanol was dropped onto the center of the film (dimensions of the sample ≈ 2 × 2 cm). The rotation speed was 1000 rpm and the rotation time was 30 s. After the deposition, samples with stearic acid layer were dried at 80 °C in air for 10 min. The degradation of SA as a function of UV-A or VIS irradiation time was monitored by Fourier-transform infrared spectroscopy (FTIR, PerkinElmer, Beaconsfield, England) in the wavenumber region 3200–2500 cm⁻¹ in a transmission mode [46,47]. The instrument parameters for the measurements were as follows: wavenumber region 3200–2500 cm⁻¹, number of scans 32, resolution 4 cm⁻¹. The UV Philips Actinic BL 15 W (Philips, Poland), irradiance 3.5 mW cm⁻² with reflector (integrated in the range of 180–400 nm, with maximum emission at 365 nm, UV-B/UV-A ratio < 0.2%) or the VIS Philips TL-D 15 W (Philips, Poland), irradiance 3.3 mW cm⁻² with reflector lamps (integrated in the range of 180–700 nm, UV/UV-VIS ratio < 5%) were used as an irradiation source. The sample of the TiO₂ thin film without a stearic acid layer on it was used as a background during all the measurements. The integrated area of the bands was used to measure the degradation of stearic acid.

4. Conclusions

TiO₂ thin films with TTIP:AcacH molar ratios from 1:3 to 1:20 were deposited on a borosilicate glass substrate. The quantity of acetylacetone in the precursor solution had no significant effect on the optical and structural properties of the TiO₂ thin films. Films consisted of the anatase phase, with a band gap in the range of 3.3–3.5 eV and thickness in the range of 280–410 nm. However, the morphological study of the TiO₂ films showed that an increase in AcacH quantity in the precursor solution made the surface of the thin film more uniform.

Photocatalytic activity of the TiO₂ thin films with different TTIP:AcacH molar ratios was studied by the stearic acid test under UV-A and VIS light. It was found that with the increase in AcacH in the precursor solution, the photodegradation rate of stearic acid increased rapidly under both irradiations. However, as expected, the photocatalytic activity of the films was much higher under UV-A. The film with TTIP:AcacH molar ratio 1:8 had the highest activity in SA degradation under UV-A with the reaction rate constant $k = 0.2427 \text{ min}^{-1}$, which is 10 times higher compared to the molar ratio 1:4. The film with the molar ratio of 1:8 also showed maximum activity under VIS with $k = 0.0323 \text{ min}^{-1}$, which is four times higher than for the molar ratio 1:4. The optimal molar ratio of TTIP:AcacH 1:8 for ultrasonically sprayed TiO₂ thin films, which was found in this study, could be also applied for other chemical solution deposition techniques to produce photocatalytically efficient films.

The photodegradation rate of SA is enhanced with an increase in the AcacH amount in the precursor solution due to changes in the morphological and wettability properties and due to the incorporation of carbon into the TiO₂ lattice. XPS results showed that the film with a higher AcacH molar ratio contains more adsorbed carbon (BE = 285 eV) on the surface of the film and more carbon incorporated into the lattice of TiO₂, which presumably improves the photocatalytic activity of the films.

Author Contributions: J.S. performed the deposition and characterization (XRD, optical properties, wettability, stearic acid test) of the films, participated in data collection and formal analysis, and participated in writing of the original draft; A.K. participated in material synthesis, data curation, and software; M.D. carried out the XPS measurements and XPS data formal analysis; M.K. (Marina Krichevskaya) participated in writing of the manuscript and formal analysis; M.K. (Malle Krunk) participated in formal analysis, project administration, and acquisition; I.O.A. supervised the study and participated in formal analysis, writing of manuscript, and project administration. All authors participated in manuscript review and editing and gave final approval for publication.

Funding: This research was funded by the Estonian Ministry of Education and Research, Estonian Research Council projects IUT19-4 and IUT19-28, and the Estonian Centre of Excellence project TK141. This work has been partially supported by the ASTRA TUT Institutional Development Programme for the 2016–2022 Graduate School of Functional Materials and Technologies (2014–2020.4.01.16-0032).

Acknowledgments: The authors acknowledge Olga Volobujeva for SEM measurements.

Conflicts of Interest: The authors declare no conflict of interest.

References

1. Adachi, T.; Latthe, S.S.; Gosavi, S.W.; Roy, N.; Suzuki, N.; Ikari, H.; Kato, K.; Katsumata, K.; Nakata, K.; Furudate, M.; et al. Photocatalytic, superhydrophilic, self-cleaning TiO₂ coating on cheap, lightweight, flexible polycarbonate substrates. *Appl. Surf. Sci.* **2018**, *458*, 917–923. [CrossRef]
2. Falling is Every Window Cleaner’s Nightmare. When His Scaffolding Broke Five Stories up, Jim Willingham Had to Think Fast. Available online: <https://consumer.healthday.com/encyclopedia/work-and-health-41/occupational-health-news-507/window-washers-646930.html> (accessed on 2 October 2019).
3. Hashimiti, K.; Irie, H.; Fujishima, A. TiO₂ Photocatalysis: A Historical Overview and Future Prospects. *Jpn. J. Appl. Phys.* **2005**, *44*, 8269–8285. [CrossRef]
4. Mauchauffé, R.; Kang, S.; Kim, J.; Kim, J.H.; Moon, S.Y. Spectroscopic study of an atmospheric pressure plasma generated for the deposition of titanium dioxide thin films. *Curr. Appl. Phys.* **2019**, *19*, 1296–1304. [CrossRef]
5. Wei, B.; Xue, J.L.; Cao, H.T.; Li, H.G.; Wen, F.; Pei, Y.T. Effects of annealing on the composition, structure and photocatalytic properties of C-doped titania films deposited by reactive magnetron sputtering using CO₂ as carbon source. *Surf. Rev. Lett.* **2019**, *26*. [CrossRef]
6. Rahman, K.H.; Kumar, A.K. Effect of precursor concentration of microstructured titanium-di-oxide (TiO₂) thin films and their photocatalytic activity. *Mater. Res. Express* **2019**, *6*. [CrossRef]
7. Sayahi, H.; Mohsenzadeh, F.; Hamadian, M. Cost-effective fabrication of perdurable electrodeposited TiO₂ nano-layers on stainless steel electrodes applicable to photocatalytic degradation of methylene blue. *Res. Chem. Intermed.* **2019**, *45*, 4275–4286. [CrossRef]
8. Tariq, M.K.; Riaz, A.; Khan, R.; Wajid, A.; Haq, H.; Javed, S.; Akram, M.A.; Islam, M. Comparative study of Ag, Sn or Zn doped TiO₂ thin films for photocatalytic degradation of methylene blue and methyl orange. *Mater. Res. Express* **2019**, *6*. [CrossRef]
9. Es-Souni, M.; Oja, I.; Krunk, M. Chemical solution deposition of thin TiO₂-anatase films for dielectric applications. *J. Mater. Sci.-Mater. El.* **2014**, *15*, 341–344. [CrossRef]
10. Acik, I.O.; Katerski, A.; Mere, A.; Aarik, J.; Aidla, A.; Dedova, T.; Krunk, M. Nanostructured solar cell by spray pyrolysis: Effect of titania barrier layer on the cell performance. *Thin Solid Film.* **2009**, *517*, 2443–2447. [CrossRef]
11. Cergel, M.S.; Menir, E.; Atay, F. The effect of the structural, optical, and surface properties of anatase - TiO₂ film on photocatalytic degradation of methylene blue organic contaminant. *Ionic* **2019**, *25*, 4481–4492. [CrossRef]
12. Rasoulnezhad, H.; Hosseinzadeh, G.; Ghasemian, N.; Hosseinzadeh, R.; Keihan, A.H. Transparent nanostructured Fe-doped TiO₂ thin films prepared by ultrasonic assisted spray pyrolysis technique. *Mater. Res. Express* **2018**, *5*. [CrossRef]
13. Dündar, I.; Krichevskaya, M.; Katerski, A.; Oja-Acik, I. TiO₂ thin films by ultrasonic spray pyrolysis as photocatalytic material for air purification. *R. Soc. Open Sci.* **2019**, *6*, 1–12. [CrossRef]
14. Muniz-Serrato, O.; Serrato-Rodriguez, J. Formation of flow coated high catalytic activity thin films from the low temperature sol-gel titanium butoxide precursor. *J. Ceram. Res.* **2018**, *19*, 306–310.
15. With, P.C.; Helmstedt, U.; Naumov, S.; Sobottka, A.; Prager, A.; Decker, U.; Heller, R.; Abel, B.; Prager, L. Low-Temperature Photochemical Conversion of Organometallic Precursor Layers to Titanium(IV) Oxide Thin Films. *Chem. Mater.* **2016**, *28*, 7715–7724. [CrossRef]
16. Juma, A.O.; Oja Acik, I.; Mikli, V.; Mere, A.; Krunk, M. Effect of solution composition on anatase to rutile transformation of sprayed TiO₂ thin films. *Thin Solid Films* **2015**, *594*, 287–292. [CrossRef]
17. Lourduraj, S.; Williams, V. Effect of molarity on sol-gel routed nano TiO₂ thin films. *J. Adv. Dielectr.* **2017**, *7*, 7. [CrossRef]

18. Vernardou, D.; Vlachou, K.; Spanakis, E.; Stratakis, E.; Katsarakis, N.; Kymakis, E.; Koudoumas, E. Influence of solution chemistry on the properties of hydrothermally grown TiO₂ for advanced applications. *Catal. Today* **2009**, *144*, 172–176. [CrossRef]
19. Yamazaki, S.; Uchiyama, H.; Kozuka, H. Additive-free alkoxide–water–alcohol solutions as precursors for crystalline titania thin films. *J. Sol.-Gel Sci. Techn.* **2018**, *87*, 537–543. [CrossRef]
20. Byrne, C.; Fagan, R.; Hinder, S.; McCormack, D.E.; Pillai, S.C. New approach of modifying the anatase to rutile transition temperature in TiO₂ photocatalysts. *R. Soc. Chem.* **2016**, *6*, 95232–95238. [CrossRef]
21. Kajitvichyanukul, P.; Amornchat, P. Effects of diethylene glycol on TiO₂ thin film properties prepared by sol–gel process. *Sci. Techn. Adv. Mater.* **2005**, *6*, 344–347. [CrossRef]
22. Arjan, W.A.; Hector, A.L.; Levason, W. Speciation in diethanolamine-moderated TiO₂ precursor sols and their use in film formation. *J. Sol.-Gel Sci. Technol.* **2016**, *79*, 22. [CrossRef]
23. Wu, W.; Shan, G.; Xiang, Q.; Zhang, Y.; Yi, S.; Zhu, L. Effects of humic acids with different polarities on the photocatalytic activity of nano-TiO₂ at environment relevant concentration. *Water Res.* **2017**, *122*, 78–85. [CrossRef]
24. Maletic, M.; Vukcevic, M.; Kalijadis, A.; Jankovic–Castvan, I.; Dapcevic, A.; Lausevic, Z.; Lausevic, M. Hydrothermal synthesis of TiO₂/carbon composites and their application for removal of organic pollutants. (in press)
25. Park, Y.; Kim, W.; Park, H.; Tachikawa, T.; Majima, T.; Choi, W. Carbon-doped TiO₂ photocatalyst synthesized without using an external carbon precursor and the visible light activity. *Appl. Catal. B-Environ.* **2009**, *91*, 355–361. [CrossRef]
26. Moon, J.; Li, T.; Randall, C.A.; Adair, J.H. Low temperature synthesis of lead titanate by a hydrothermal method. *J. Mater. Res.* **1997**, *12*, 189–197. [CrossRef]
27. Leautic, A.; Babonneau, F.; Livage, J. Structural Investigation of the Hydrolysis–Condensation Process of Titanium Alkoxides Ti(OR)₄ (OR = OPr₁, OEt) Modified by Acetylacetone. 1. Study of the Alkoxide Modification. *Chem. Mater.* **1989**, *1*, 240–247. [CrossRef]
28. Kaltsum, U.; Kurniawan, A.F.; Nurhasanah, I.; Priyono, P. The Role of Concentration Ratio of TTiP:AcAc on the Photocatalytic Activity of TiO₂ Thin Film in Reducing Degradation Products of Used Frying Oil. *Bull. React. Eng. Catal.* **2017**, *12*, 430–436.
29. Siwinska-Stefanska, K.; Zdarta, J.; Paukszta, D.; Jesionowski, T. The influence of addition of a catalyst and chelating agent on the properties of titanium dioxide synthesized via the sol–gel method. *J. Sol.-Gel Sci. Technol.* **2015**, *75*, 264–278. [CrossRef]
30. Kajitvichyanukul, P.; Pongpom, S.; Watcharenwong, A.; Ananpattarachai, J. Effect of Acetyl Acetone on Property of TiO₂ Thin Film for Photocatalytic Reduction of Chromium(VI) from Aqueous Solution. *J. Spec. Issue Nanotech.* **2005**, *4*, 87–93.
31. RRUFF – Database. Available online: <http://rruff.info/Anatase/R060277> (accessed on 8 October 2019).
32. Pimpabute, N.; Burinprakhon, T.; Somkunthot, W. Determination of optical constants and thickness of amorphous GaP thin film. *Opt. Appl.* **2011**, *1*.
33. Duminica, F.D.; Maury, F.; Abisset, S. Pyrosol deposition of anatase TiO₂ thin films starting from Ti(OiPr)₄/acetylacetone solutions. *Thin Solid Films* **2007**, *515*, 7732–7739. [CrossRef]
34. Stefanov, B.; Österlund, L. Tuning the Photocatalytic Activity of Anatase TiO₂ Thin Films by Modifying the Preferred <001> Grain Orientation with Reactive DC Magnetron Sputtering. *Coatings* **2014**, *4*, 587–601. [CrossRef]
35. Kumar, K.; Ntwaeaborwa, O.M.; Holsa, J.; Motaung, D.E.; Swart, H.C. The role of oxygen and titanium related defects on the emission of TiO₂:Tb³⁺ nano-phosphor for blue lighting applications. *Opt. Mater.* **2015**, *46*, 510–516. [CrossRef]
36. Naeem, M.; Hasanain, S.K.; Kobayashi, M.; Ishida, Y.; Fujimori, A.; Buzby, S.; Shah, I. Effect of reducing atmosphere on the magnetism of Zn_{1-x}CoxO (0 ≤ x ≤ 0.10) nanoparticles. *Nanotechnology* **2006**, *17*, 2675–2680. [CrossRef] [PubMed]
37. Gromyko, I.; Krunks, M.; Dedova, T.; Katerski, A.; Klauson, D.; Oja Acik, I. Surface properties of sprayed and electrodeposited ZnO rod layers. *Appl. Surf. Sci.* **2017**, *405*, 521–528. [CrossRef]

38. Klaysri, R.; Ratova, M.; Prasertthdam, P.; Kelly, P.J. Deposition of Visible Light-Active C-Doped Titania Films via Magnetron Sputtering Using CO₂ as a Source of Carbon. *Nanomaterials* **2017**, *7*, 113. [[CrossRef](#)] [[PubMed](#)]
39. Zhang, Y.; Zhao, Z.; Chen, J.; Chenga, L.; Changa, J.; Shenga, W.; Huc, C.; Cao, S. C-doped hollow TiO₂ spheres: In situ synthesis, controlled shell thickness, and superior visible-light photocatalytic activity. *Appl. Catal. B-Environ.* **2015**, *165*, 715–722. [[CrossRef](#)]
40. Seo, H.O.; Woo, T.G.; Park, E.J.; Cha, B.J.; Kim, I.H.; Han, S.W.; Kim, Y.D. Enhanced photo-catalytic activity of TiO₂ films by removal of surface carbon impurities; the role of water vapor. *Appl. Surf. Sci.* **2017**, *420*, 808–816. [[CrossRef](#)]
41. Rajkumar, R.; Nisha, S. To Study the Effect of the Concentration of Carbon on Ultraviolet and Visible Light Photo Catalytic Activity and Characterization of Carbon Doped TiO₂. *J. Nanomed. Nanotechnol.* **2015**, *6*, 7.
42. Shi, Z.J.; Ma, M.G.; Zhu, J.F. Recent Development of Photocatalysts Containing Carbon Species: A Review. *Catalysts* **2019**, *9*, 20. [[CrossRef](#)]
43. Valentin, C.D.; Pacchioni, D.; Selloni, A. Theory of Carbon Doping of Titanium Dioxide. *Chem. Mater.* **2005**, *172*, 66656–66665. [[CrossRef](#)]
44. Banerjee, S.; Dionysiou, D.D.; Pillai, S.C. Self-cleaning applications of TiO₂ by photo-induced hydrophilicity and photocatalysis. *Appl. Catal. B-Environ.* **2015**, *176–177*, 396–428. [[CrossRef](#)]
45. Zheng, J.Y.; Bao, S.H.; Gou, Y.; Jin, P. Natural Hydrophobicity and Reversible Wettability Conversion of Flat Anatase TiO₂ Thin Film. *Appl. Mater. Inter.* **2014**, *6*, 1351–1355. [[CrossRef](#)] [[PubMed](#)]
46. Schneider, J.; Matsuoka, M.; Takeuchi, M.; Zhang, J.; Horiuchi, Y.; Anpo, M.; Bahnemann, D.W. Understanding TiO₂ Photocatalysis: Mechanisms and Materials. *Chem. Rev.* **2014**, *114*, 9919–9986. [[CrossRef](#)] [[PubMed](#)]
47. Sano, T.; Puzenat, E.; Guillard, G.; Geantet, C.; Matsuzawa, S.; Negishi, N. Improvement of Photocatalytic Degradation Activity of Visible-Light-Responsive TiO₂ by Aid of Ultraviolet-Light Pretreatment. *J. Phys. Chem. C* **2009**, *113*, 5535–5540. [[CrossRef](#)]
48. Higashimoto, S.; Katsuura, K.; Yamamoto, M.; Takahashi, M. Photocatalytic activity for decomposition of volatile organic compound on Pt-WO₃ enhanced by simple physical mixing with TiO₂. *Catal. Commun.* **2020**, *133*, 1566–7367. [[CrossRef](#)]
49. Mills, A.; Lepre, A.; Elliott, N.; Bhopal, S.; Parkin, I.P.; O'Neill, S.A. Characterisation of the photocatalyst Pilkington Activ™: A reference film photocatalyst? *J. Photoch. Photobio. A* **2003**, *160*, 213–224. [[CrossRef](#)]
50. Mills, A.; Wang, J. Simultaneous monitoring of the destruction of stearic acid and generation of carbon dioxide by self-cleaning semiconductor photocatalytic films. *J. Photoch. Photobio. A* **2006**, *182*, 181–186. [[CrossRef](#)]
51. Pore, V.; Ritala, M.; Lekelä, M.; Areva, S.; Järn, M.; Järnström, J. H₂S modified atomic layer deposition process for photocatalytic TiO₂ thin films. *J. Mater. Chem.* **2007**, *17*, 1361–1371. [[CrossRef](#)]
52. Smirnova, N.; Fesenko, T.; Zhukovsky, M.; Goworek, J.; Eremenko, A. Photodegradation of Stearic Acid Adsorbed on Superhydrophilic TiO₂ Surface: In Situ FTIR and LDI Study. *Nanoscale Res. Lett.* **2015**, *10*, 7. [[CrossRef](#)]
53. Montero, J.; Österlund, L. Photodegradation of Stearic Acid Adsorbed on Copper Oxide Heterojunction Thin Films Prepared by Magnetron Sputtering. *ChemEngineering* **2018**, *2*, 40. [[CrossRef](#)]
54. Wang, S.-H.; Chen, T.-K.; Rao, K.K.; Wong, M.-S. Nanocolumnar titania thin films uniquely incorporated with carbon for visible light photocatalysis. *Appl. Catal. B-Environ.* **2007**, *76*, 328–334. [[CrossRef](#)]
55. Ratova, M.; Klaysri, R.; Prasertthdam, P.; Kelly, P.J. Visible light active photocatalytic C-doped titanium dioxide films deposited via reactive pulsed DC magnetron co-sputtering: Properties and photocatalytic activity. *Vacuum* **2018**, *149*, 214–224. [[CrossRef](#)]
56. Varnagir, S.; Medvids, A.; Lelis, M.; Milcius, D.; Antuzevics, A. Black carbon-doped TiO₂ films: Synthesis, characterization and photocatalysis. *J. Photochem. Photobio. A-Chem.* **2019**, *382*, 9. [[CrossRef](#)]
57. Aiyng, B.; Wei, L.; Gengle, Z.; Jinbo, X. Preparation and Enhanced Daylight-Induced Photo-Catalytic Activity of Transparent C-Doped TiO₂ Thin Films. *J. Wuhan Univ. Tehnol.-Mater. Sci. Ed.* **2010**, *25*, 738–742.

58. Klauson, D.; Poljakova, A.; Pronina, N.; Krichevskaya, M.; Moiseev, A.; Dedova, T.; Preis, S. Aqueous Photocatalytic Oxidation of Doxycycline. *Adv. Oxid. Technol.* **2013**, *16*, 234–243. [[CrossRef](#)]
59. Klauson, D.; Budarnaja, O.; Stepanova, K.; Krichevskaya, M.; Dedova, T.; Käkinen, A.; Preis, S. Selective Performance of Sol–Gel Synthesised Titanium Dioxide Photocatalysts in Aqueous Oxidation of Various-Type Organic Pollutants. *Kinet. Cata.* **2014**, *55*, 47–55. [[CrossRef](#)]

Sample Availability: Samples of the compounds are available from the authors.



© 2019 by the authors. Licensee MDPI, Basel, Switzerland. This article is an open access article distributed under the terms and conditions of the Creative Commons Attribution (CC BY) license (<http://creativecommons.org/licenses/by/4.0/>).

Publication II

J. Spiridonova, A. Mere, M. Krunk, M. Rosenberg, A. Kahru, M. Danilson, M. Krichevskaya, I. Oja Acik. "Enhanced visible and ultraviolet light-Induced gas-phase photocatalytic activity of TiO₂ thin films modified by increased amount of acetylacetone in precursor solution for spray pyrolysis," *Catalysts*, 10(9), 1011, 2020, doi.org/10.3390/catal10091011.

Article

Enhanced Visible and Ultraviolet Light-Induced Gas-Phase Photocatalytic Activity of TiO₂ Thin Films Modified by Increased Amount of Acetylacetone in Precursor Solution for Spray Pyrolysis

Jekaterina Spiridonova ^{1,*}, Arvo Mere ¹, Malle Krunks ¹, Merilin Rosenberg ^{2,3},
Anne Kahru ^{2,4}, Mati Danilson ⁵, Marina Krichevskaya ⁶ and Ilona Oja Acik ^{1,*}

¹ Laboratory of Thin Films Chemical Technologies, Department of Materials and Environmental Technology, Tallinn University of Technology, Ehitajate tee 5, 19086 Tallinn, Estonia; arvo.mere@taltech.ee (A.M.); malle.krunks@taltech.ee (M.K.)

² Laboratory of Environmental Toxicology, National Institute of Chemical Physics and Biophysics, Akadeemia tee 23, 12618 Tallinn, Estonia; merilin.rosenberg@kbfi.ee (M.R.); anne.kahru@kbfi.ee (A.K.)

³ Department of Chemistry and Biotechnology, Tallinn University of Technology, Akadeemia tee 15, 12618 Tallinn, Estonia

⁴ Estonian Academy of Sciences, Kohtu 6, 10130 Tallinn, Estonia

⁵ Laboratory of Optoelectronic Materials Physics, Department of Materials and Environmental Technology, Tallinn University of Technology, Ehitajate tee 5, 19086 Tallinn, Estonia; mati.danilson@taltech.ee

⁶ Laboratory of Environmental Technology, Department of Materials and Environmental Technology, Tallinn University of Technology, Ehitajate tee 5, 19086 Tallinn, Estonia; marina.krichevskaja@taltech.ee

* Correspondence: jekaterina.spiridono@taltech.ee (J.S.); ilona.oja@taltech.ee (I.O.A.);
Tel.: +372-620-3369 (I.O.A.)

Received: 23 July 2020; Accepted: 1 September 2020; Published: 3 September 2020



Abstract: TiO₂ thin films, modified by acetylacetone (AcacH) in solution, were deposited on glass substrate by ultrasonic spray pyrolysis and tested for photocatalytic activity in a multi-section continuous flow reactor by degradation of acetone and acetaldehyde under ultraviolet and visible light. The increase in molar ratio of AcacH in respect of titanium (IV) isopropoxide (TTIP) from 1:5 to 1:8 modified the electronic structure of the films, favoring enhanced photocatalytic activity. The photocatalytic activity was enhanced approximately twofold on the film with molar ratio 1:8 under both irradiations; the film completely oxidized 10 ppm of acetone and acetaldehyde. The photocatalytic efficacy of TiO₂ films in oxidation of air pollutants was three times higher compared to the industrial glass Pilkington Activ™. Moreover, all the synthesized films indicate antibacterial efficiency against *E. coli* of over 99% under ultraviolet. TiO₂ film, with TTIP:AcacH molar ratio 1:8 having great possibility for its commercial use as a material for indoor air purification.

Keywords: TiO₂ thin film; spray pyrolysis; indoor air purification; VOC elimination; antimicrobial activity

1. Introduction

The modern lifestyle implies spending about 90% of time indoors (office, home, shops, recreation centres, etc.). Therefore, the quality of indoor air is a vital parameter for humans to sustain life [1]. Studies show that indoor air contains a variety of gases, chemicals and other substances. Common indoor air contains about 200 different gaseous components, most of them volatile organic compounds (VOCs) with the individual concentrations ≤10 ppb [2].

Concentrations of VOCs in the indoor air are up to 10 times higher than in the outdoor air since many products that are constantly used in daily life, for instance, air fresheners, cosmetics, some furniture or building materials and indoor activities like cooking release VOCs [3]. Modern homes built after 1970s are better insulated in order to obtain greater energy efficiency, which has minimized natural ventilation. According to the recommendations of the American Society of Heating, Refrigerating and Air-Conditioning Engineers (ASHREA) natural ventilation of living buildings should be able to replace 35% of the entire air by fresh outdoor air every hour. However, the value of the air exchange rate in modern buildings may be as low as 20% per hour [4]. Therefore, due to insufficient natural ventilation, air pollutants may exist in indoor air for a longer time leading to long-term exposure of humans to these chemicals. In 1983, the term “Sick Building Syndrome” was introduced to describe the situations when people experience acute health problems or feel discomfort due to staying in the building [1].

The World Health Organization (WHO) has reported that around 3.8 million people die from indoor air pollution each year [5]. Acetone and acetaldehyde are typical indoor air pollutants, the oxidative degradation pathways of which are well-studied in the literature [6–10]. In the United States, the average concentration of acetone in an office building’s indoor air is 27.1 ppb and that of acetaldehyde 4.2 ppb [2]. European Chemicals Agency (ECHA) legislation attributes acetaldehyde (EC/List no.: 200-836-8) to carcinogenic substances, which can cause genetic defects, and serious eye and respiratory irritation [11]. Moreover, in some European countries, the occupational exposure limit values for acetaldehyde have been set e.g., the limit of 8-h for workers’ exposure is 25 ppm [12].

Air-cleaning devices based on several technologies (filtration, ionising etc.) can be used to improve the poor quality of indoor air. One of the promising technologies for indoor air purification is heterogeneous photocatalytic oxidation (PCO). The main advantages of PCO are that the catalyst is relatively inexpensive and chemically inert. In the market there are several air purifiers based on the PCO principle and using TiO₂ nanoparticles supported on the plates as photocatalytic modules. Most of the photocatalytic air-purifiers available in the market contain an ultraviolet (UV-C) lamp and a photocatalytic module, consisting of a thick coating of TiO₂ nanoparticles (usually a mixture of anatase and rutile TiO₂ nanopowder, type P25). It has been reported that these purifiers are effective in decomposing VOCs such as formaldehyde, acetone, diethyl ether, benzene, butanol etc. and could kill bacteria and fungi in the air and on surfaces [13–15].

However, the application of these air-cleaning devices with supported TiO₂ nanoparticles is limited due to several factors such as further separation requirements of the powder, periodic maintenance and replacement of the photocatalyst module in the purifiers due to the low adhesion strength of nanoparticles in the layer [2,16].

To overcome these disadvantages, the nanoparticle coating with a thickness of more than couple of micrometres and specific material quantity of more than 10 mg/cm² [15] can be replaced by an economically feasible and resource-saving TiO₂ thin film with approximately 100 times lower material amount. In general TiO₂ thin films have lower photocatalytic activity compared to TiO₂ nanopowders. However, the deposition of transparent films onto a large surface, e.g., windows, can overcome this problem. The main advantage of TiO₂ thin films are transparency in the visible spectral range, good mechanical stability and adhesion [16–24], thus allowing uniform coverage of large areas and long-term stability.

TiO₂ coatings possess multifunctional properties when exposed to the light. In addition to the oxidation of organic pollutants, due to the super hydrophilicity the surface coated with TiO₂ film also has self-cleaning properties, i.e., keeping the surface free from dirt [25,26]. Moreover, hydroxyl radicals produced during the photo irradiation of TiO₂ can also inactivate airborne and surface-associated bacteria [27–30], fungi [28] and viruses [29]. Nakano et al. [29] used TiO₂ spin-coated glass to test the disinfection ability against Gram-positive bacteria (*Staphylococcus aureus*, *Enterococcus faecalis*, *Streptococcus pneumonia*), Gram-negative bacteria (*Escherichia coli*, *Pseudomonas aeruginosa*) and viruses (human influenza virus and feline calicivirus). They found that TiO₂ can be used as an effective

functional surface coating with broad-spectrum antimicrobial activity. Inactivation efficiency of infectious agents depended on the structure of their surface layers and followed this order: Gram-positive bacteria > enveloped viruses > Gram-negative bacteria > non-enveloped viruses [29].

In the last few decades, in addition to the application of TiO₂ in air purifiers, there has been a growing interest in the development of visible light active TiO₂ thin films to be used as indoor air purifying window coatings [13,31,32]. To improve the photocatalytic efficiency in visible light region TiO₂ films could be modified by metal doping e.g., Cu, Au, Pt, Sr and non-metal doping e.g., C, S, N [32–35] or composite material could be synthesized like TiO₂/SiO₂, TiO₂/WO₃, TiO₂/GO [32,33]. Several experimental and theoretical studies have reported that carbon impurities in the TiO₂ lattice can act as a photosensitizer, narrow the band gap, favour the formation of oxygen vacancies and create midgap states, and thereby enhance the photocatalytic activity of TiO₂ under UV-A and visible (VIS) light [34,36–38].

The most common methods for deposition of TiO₂ thin films for degradation of acetone and acetaldehyde are sputtering, sol-gel spin-coating and electrochemically assisted procedures [17–24]. Recently we have demonstrated that TiO₂ thin films deposited by ultrasonic spray pyrolysis with specific material quantity of 0.2 mg/cm² are effective in the decomposition of several VOCs such as acetone, acetaldehyde and heptane [6]. The interest in the fabrication of thin films by ultrasonic spray pyrolysis method is rapidly increasing due to its simplicity and the possibility to cost-effectively deposit coatings on the large surface area [6,17,26].

Chemical solution-based methods have the advantage of carbon impurities in the fabricated films, as carbon-containing precursors are used. Several strategies have been employed; to engineer the synthesis-accompanying carbon contamination in thin films fabricated by the chemical solution methods, such as varying the deposition temperature [17,39,40], post-deposition heat treatment temperature [6,17,26,38–41], amount of complexing agent [26,41–43]. The most common precursor system for solution synthesized TiO₂ thin films consists of titanium isopropoxide (TTIP) as a Ti-source and acetylacetone (AcacH) as a complexing agent [6,17,26,39,41–43], indicating decomposition of organic fraction in the temperature region between 100 and 550 °C, according to the thermoanalytical studies [44,45] and the presence of carbon containing species on the film surface deposited and/or annealed at temperatures of ca 500 °C [6,17,26,41].

A limited number of prior studies have shown that changing titanium isopropoxide (TTIP) and acetylacetone (AcacH) molar ratio in the solution from 1:0.7 to 1:2 affects photocatalytic activity of the TiO₂ films [42,43]. However, the first systematic study on the effect of TTIP:AcacH molar ratio on the TiO₂ thin films' structural, optical properties, surface chemical composition and photocatalytic self-cleaning activity was recently published by our research group. In this study we showed that by increasing the AcacH molar ratio in the spray solution from TTIP:AcacH 1:3 to 1:20 exhibits the highest photocatalytic self-cleaning activity at optimal molar ratio of 1:8 under UV-A and VIS light [26].

The current study is a logical continuation of our previous research and provides systematic study on the effect of titanium isopropoxide and acetylacetone molar ratio in the spray solution on the photocatalytic degradation of VOCs under UV-A and VIS light, and gives insights on the effect of antibacterial activity.

The specific aims of the current study were to: (i) test the photocatalytic activity of TiO₂ thin films, modified by an increased molar ratio of acetylacetone to titanium isopropoxide in the spray solution, in a multi-section continuous gas flow reactor for photodegradation of acetone and acetaldehyde under ultraviolet and visible light; (ii) compare the photocatalytic efficiency of TiO₂ thin films with the commercial Pilkington Activ™ glass; (iii) study the effect of operating parameters such as the initial concentration of the model pollutants (acetone and acetaldehyde), air flow rate and relative humidity on the reaction kinetics; and (iv) evaluate the antimicrobial properties of the synthesized films against *Escherichia coli* according to the modified ISO 27,447 and 22,196 standards.

The results of this study demonstrate great industrial significance for the obtained TiO₂ thin film considering its practical application for indoor air treatment in photocatalytic degradation of

the VOCs and killing bacteria under UV-A as a photocatalytic module. Additionally, the TiO₂ thin film showed enhanced visible light photocatalytic activity, which allows the use of these films for indoor surface coatings, thus providing a photoactive alternative for the thick coatings fabricated from commercial powders.

2. Results and Discussion

2.1. Material Characterization

The detailed characterization of the morphological, optical, structural, chemical composition and wettability properties of the TiO₂ thin films with different titanium isopropoxide: acetylacetonate (TTIP:AcacH) molar ratios has been reported in our previous paper [26].

The thickness of the T-1:5 film was 370 nm and that of the T-1:8 film 375 nm (Figure S1) and they were not affected by the amount of acetylacetonate in precursor solution [26]. The morphology of the films surface was studied by atomic force microscopy (AFM) (Figure S2). According to AFM analysis, increasing TTIP:AcacH molar ratio from 1:4 (Figure S2a) to 1:8 (Figure S2c) in the spray solution resulted in the formation of finer grains and loss in periodic surface structure of the films. Moreover, with the increase in AcacH amount in precursor solution the variations in height across the thin film are less pronounced. Thus, an increased amount of AcacH in the spray solutions promoted the growth of TiO₂ films with more uniform surface.

According to X-ray photoelectron spectroscopy (XPS) results, the increased amount of AcacH in precursor solution resulted in higher amount of carbon adsorbed on the surface of the film (Figure S3). In our recent paper [26], we showed that the photocatalytic degradation of stearic acid layer by TiO₂ thin films rapidly increased in parallel with the increase in the AcacH molar ratio. The photodegradation rate constant changed from 0.08 to 0.24 min⁻¹ for the films with TTIP:AcacH molar ratios 1:5 and 1:8, respectively [26].

However, to better understand the enhanced photocatalytic activity of the film T-1:8, the density of states (DOS) was evaluated from the valence band (VB) XPS spectra (Figure 1b) [46]. The band gap of TiO₂ films was calculated from the Tauc plot (Figure 1a) obtained from UV-VIS total transmittance spectra. Obtained band gaps of the T-1:4, T-1:5 and T-1:8 films were 3.32, 3.33 and 3.36 eV, respectively.

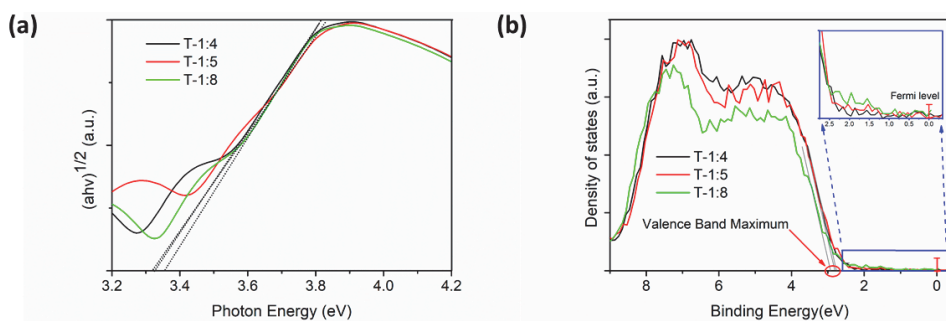


Figure 1. (a) Tauc plot for band gap determination and (b) X-ray photoelectron spectroscopy (XPS) valence band spectra of the TiO₂ thin films with different titanium isopropoxide:acetylacetonate (TTIP:AcacH) molar ratios. The inset on panel b shows zoomed Fermi level region of the TiO₂ films.

Figure 1b shows the valence band (VB) spectra of the T-1:4, T-1:5 and T-1:8 films. The T-1:4 and T-1:5 films showed VB with the edge of the maximum energy at ca. 2.65 eV, while the T-1:8 film VB top edge was at ca. 2.82 eV (Figure 1b). This means that with the increase in the AcacH amount the VB of the T-1:8 film shifted down. The down-shift in the VB top edge can be related with carbon incorporation [26,34]. Moreover, as could be seen from the plot of density of states at zero energy, which is equal to the Fermi level (Figure 1b), midgap states above VB in the band structure of the T-1:8

film were formed. These states could provide the major pathway for electron transfer between the catalyst material and acceptor species [47].

Figure 2 represents a schematic diagram of the TiO₂ films band gap structure obtained by combining the results of the UV-VIS and VB XPS.

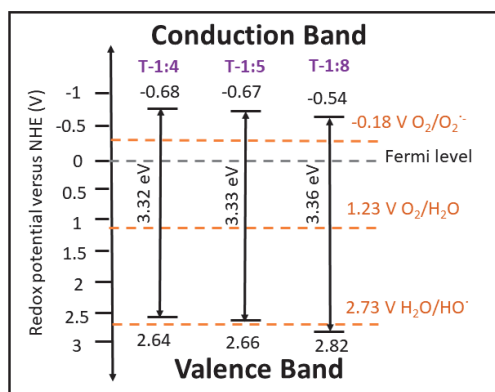


Figure 2. Valence and conduction band edges of the TiO₂ films with different TTIP:AcacH molar ratios and standard redox potentials of the (O₂/O₂^{•-}), (O₂/H₂O) and (H₂O/HO[•]) versus normal hydrogen electrode (NHE).

From the thermodynamics point of view, VB positive holes may oxidize the compounds that are adsorbed on the surface of the catalyst if the top of VB edge has a more positive redox potential than that of the adsorbed species. Analogically, CB electrons reduce compounds if their redox potential is more negative than that of the adsorbed species. In the absence of suitable adsorbents, recombination of electron-hole pairs occurs [48,49]. Figure 2 shows that due to the downshift of VB edge the redox potential of the T-1:8 film is more positive than the redox potential of the H₂O/HO[•] couple [50]. According to Equation (1), film with TTIP:AcacH molar ratio 1:8 can produce extra hydroxyl radicals by oxidizing water, which increases its ability to mineralize VOCs and reduces the recombination of electron-hole pairs [47].



In our previous study we demonstrated that an increase in the amount of AcacH in precursor solution had no significant impact on structural and optical properties of the films [26]. However, increasing AcacH amount in TTIP:AcacH molar ratio from 1:4 to 1:8 influenced the surface morphology and chemical composition of the TiO₂ films [26]. In the current study, we showed that in addition to morphological changes, increasing the AcacH molar ratio also affected the electronic structure of the TiO₂ thin films. Based on the obtained results, TiO₂ films with TTIP:AcacH molar ratios 1:5 and 1:8 were selected for the study of their photocatalytic activity in the gas-phase since these films demonstrated the observable difference in material properties and photocatalytic degradation of stearic acid [26].

2.2. Gas-Phase Photocatalytic Activity of the TiO₂ Thin Films

2.2.1. Photocatalytic Oxidation of Acetone and Acetaldehyde under Ultraviolet (UV-A) Light

In this study, acetone and acetaldehyde were chosen as model volatile organic air pollutants for the estimation of the gas-phase activity of the photocatalytic material. The application of acetone and acetaldehyde as model volatile organic air pollutants for the estimation of the gas-phase activity of photocatalytic material or performance of the reactor has been previously studied by several authors [6–10,27]. Both pollutants are hydrophilic and polar, and their oxidation occurs relatively

fast without forming long-lived intermediates. Moreover, acetaldehyde may also be one potential intermediate of acetone oxidation, depending on the degradation pathway [10].

In the current study, the oxidation of acetone and acetaldehyde was initially evaluated on the sprayed TiO₂ films with TTIP:AcAcH molar ratios of 1:5, 1:8 in the spray solution, and commercially available Pilkington Activ™ glass applying to all five sections of the modular reactor. The obtained results for the degradation of 10 ppm of acetone and 10 ppm of acetaldehyde at air flow rate of 0.5 L/min and relative humidity (RH) 6% are presented in Figure 3. No gaseous by-products except CO₂ and H₂O were detected during the experiments. Adsorption of acetone and acetaldehyde on the films at initial concentration of 10 ppm (air flow rate 0.5 L/min and RH 6%) was studied in the dark. The difference between the reactor inlet and outlet concentrations of VOCs was not registered by Fourier transform infrared (FTIR) spectroscopy, which means the adsorption was negligible and below the detection limit of used analytical apparatus (0.5 ppm).

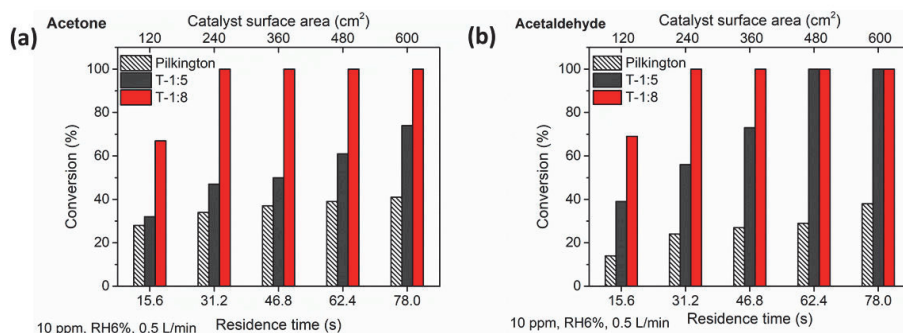


Figure 3. Photocatalytic oxidation of (a) 10 ppm acetone and (b) 10 ppm of acetaldehyde under ultraviolet (UV-A) irradiation on the films with TTIP:AcAcH molar ratios 1:5 (T-1:5), 1:8 (T-1:8) in precursor solution and on Pilkington Activ™ glass at different catalyst surface areas.

Figure 3 shows that T-1:8 film was on average two times more photocatalytically active than T-1:5. Complete degradation of both pollutants on the T-1:8 film surface occurred at the catalyst surface area of 240 cm², while twice the catalyst surface area (480 cm²) was needed for complete degradation of 10 ppm acetaldehyde on the T-1:5 film. It was not possible, however, to achieve complete oxidation of 10 ppm of acetone on the T-1:5 film under described experimental conditions. The enhanced oxidation ability of the T-1:8 film with increase in molar ratio of AcAcH in spray solution could be explained by the increase in the amount of carbon on the surface of the film [26] and changes in the electronic structure of the band gap, allowing to produce a larger number of hydroxyl radicals (Section 2.1). Dundar et al. [6] obtained the conversion of ca. 25 and 20% of 10 ppm of acetone and 10 ppm of acetaldehyde, respectively, on the sprayed TiO₂ film (thickness 190 nm) with TTIP:AcAcH molar ratio 1:4 with catalyst surface area of 240 cm² [6]. However, on the T-1:8 film used in the current study 100% conversion of 10 ppm of acetone and 10 ppm of acetaldehyde was reached at this catalyst surface area (Figure 3).

As mentioned above, acetaldehyde is one of the oxidation by-products of acetone, thus oxidation of acetaldehyde overall should proceed faster than that of acetone. However, on the T-1:8 film for the degradation of 10 ppm of acetone and 10 ppm of acetaldehyde residence time of approximately 30 s was needed (Figure 3). The hypothesis that acetaldehyde is more easily oxidizable compound was proven in the current study since the oxidation of acetaldehyde took less time than acetone, especially on the T-1:5 film surface (Figure 3). Similar tendency has been observed by Bianchi et al. [10] on the P25 surface for the complete oxidation of 400 ppm of acetone 70 min was needed, while for complete mineralization of 400 ppm of acetaldehyde 60 min was enough [10].

TiO₂ films synthesized with TTIP:AcAcH molar ratios 1:5 and 1:8 were generally both more active in photocatalytic degradation of 10 ppm of acetone and acetaldehyde compared to commercial

self-cleaning Pilkington Activ™ glass (Figure 3). Contrary to the T-1:5 and T-1:8 films obtained by the spray pyrolysis, on the commercial Pilkington Activ™ glass the oxidation of acetone occurred slightly faster than that of acetaldehyde. On the Pilkington Activ™ glass the change in the conversion value of acetone with the increase in residence time was very small, from 28% to 42% (Figure 3). Acetaldehyde conversion increased from 14% to 38% with residence time increasing from 15.5 to 78 s, indicating that the acetaldehyde might need more time to adsorb on the active sites of catalyst surface. This phenomenon could indicate that the oxidation process was limited by the amount of active sites on the surface of the catalyst resulting in an increase in the time needed for adsorption. Yao et al. [51] have reported that adsorption of acetone and acetaldehyde on the TiO₂ surface occurred preferably between the carbonyl group and Ti sites. Acetaldehyde has a bare carbonyl group in the molecular structure, while in acetone structure it is surrounded by methyl groups. Therefore, acetaldehyde has stronger adsorption energy and is more stable on the surface [52]. However, since acetone has higher molecular weight and lower vapour pressure compared to acetaldehyde, acetone adsorption on the active sites of the photocatalyst surface is supposed to occur faster [53]. Dundar et al. [6] also observed that the degradation of 5 ppm of acetone occurred faster than that of 5 ppm of acetaldehyde on the sprayed TiO₂ thin film, achieving 100% conversion for acetone and ca. 80% conversion for acetaldehyde at residence time ca. 60 s. [6].

2.2.2. Effect of Pollutant's Initial Concentration on Its Photocatalytic Oxidation

The effect of the initial concentration of acetone on its photocatalytic oxidation on the films with TTIP:AcacH 1:5 and 1:8 was studied using three concentrations of acetone, 5, 10 and 40 ppm, at relative humidity (RH) 6% air flow rate of 0.5 L/min (Figures 3a and 4). Moreover, the effect of acetone initial concentration on the initial reaction rate was investigated (Figure 5). Acetone was chosen as a model pollutant since acetone's reaction rate on the T-1:5 and T-1:8 films was lower if compared to acetaldehyde.

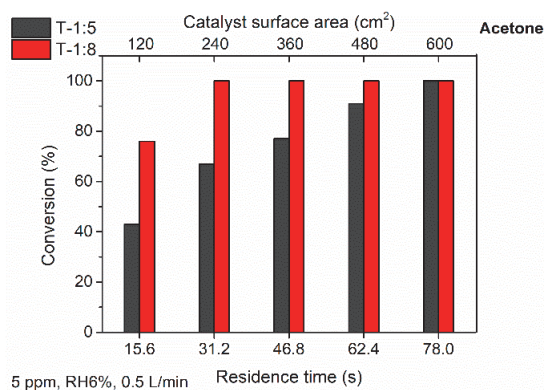


Figure 4. Photocatalytic oxidation of 5 ppm of acetone under UV-Airradiation on the TiO₂ thin films with TTIP:AcacH molar ratios 1:5 (T-1:5), 1:8 (T-1:8) in precursor solution depending on the catalyst surface area.

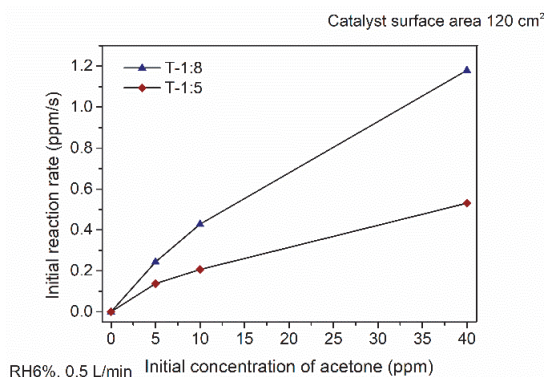


Figure 5. Initial reaction rate of acetone degradation under UV-A irradiation at different initial concentrations on the TiO₂ films with TTIP:AcacH molar ratios 1:5 (T-1:5), 1:8 (T-1:8) in precursor solution.

In the case of the T-1:5 film, the decrease in the concentration of acetone from 10 ppm to 5 ppm led to complete mineralization of acetone at catalyst surface area of 600 cm² (Figure 4), while at initial concentration of 10 ppm conversion was only 74% (Figure 3a). In the case of the T-1:8 film, the increase in the initial concentration of acetone from 5 ppm (Figure 4) to 10 ppm (Figure 3a) did not affect the photocatalytic oxidation; for complete oxidation the same catalyst surface area of 240 cm² was needed. However, a further increase in concentration of acetone up to 40 ppm required catalyst surface area of 360 cm² for acetone degradation on the T-1:8 film (Figure 6a).

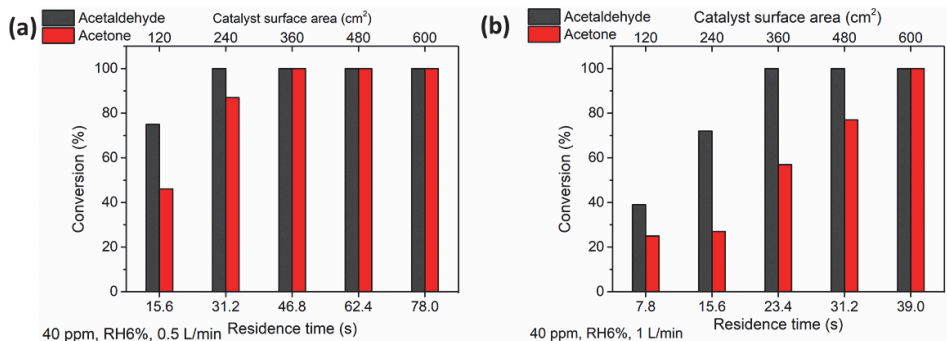


Figure 6. Effect of air flow rate on photocatalytic oxidation of 40 ppm of acetone and 40 ppm of acetaldehyde under UV-A irradiation on the films with TTIP:AcacH molar ratio 1:8 in precursor solution at air flow rate (a) 0.5 L/min and (b) 1 L/min depending on catalyst surface area.

The initial concentration of VOCs strongly affects the photocatalytic reaction kinetics [51–53]. To study the effect of the initial concentration of acetone on the reaction kinetics, the initial reaction rates (r_0) at initial concentrations of 5, 10 and 40 ppm at residence time of 15.6 s (catalyst surface area 120 cm²) were calculated according to the Equation (2) [53].

$$r_0 = -\frac{dC}{dt} \quad (2)$$

Figure 5 demonstrates the dependence of initial reaction rate on the initial concentration of acetone on the films with TTIP:AcacH molar ratios of 1:5 and 1:8.

The degradation of acetone on the T-1:8 film had substantially higher initial reaction rate compared to T-1:5 whereas in case of both films the initial reaction rate depended on initial concentration of acetone (Figure 5). However, dependence of the reaction rate on concentration was not linear, indicating that the reaction rate was not diffusion-limited; oxidation reactions on the surface of thin films were supposed to be a rate-determining step. Therefore, it could be assumed that the reaction kinetics was consistent with the Langmuir–Hinshelwood model (Equation (3)) [7,23,47].

$$r_0 = \frac{k_r K C_0}{1 + K C_0} \quad (3)$$

where r_0 is initial reaction rate (ppm/s), C_0 is initial concentration of acetone (ppm), k_r is reaction rate constant (ppm/s) and K is adsorption constant (1/ppm).

The linearized form of Equation (3) gives the following (Equation (4)).

$$\frac{1}{r_0} = \frac{1}{k_r K} \cdot \frac{1}{C_0} + \frac{1}{k_r} \quad (4)$$

The kinetics constants of photocatalytic oxidation reaction of acetone can be found from the plot $1/r_0$ versus $1/C_0$, which gives a straight line (Figure S4) [54]. The kinetic parameters such as reaction rate constant and adsorption constant that were found from the Langmuir–Hinshelwood kinetic plots are listed in the Table 1.

Table 1. Reaction rate constant and adsorption constant of the TiO₂ films with TTIP:AcacH 1:5 and 1:8 for the degradation of acetone under UV-A irradiation.

TTIP:AcacH in Precursor Solution	k_r ppm/s	K 1/ppm
1:5	0.728	0.0452
1:8	2.395	0.0225

Reaction rate constant (k_r) on the T-1:8 film was more than three times higher compared to T-1:5 (Table 1). This implies that T-1:8 film surface was very active and oxidation of pollutants occurred very fast. However, the adsorption coefficient (K) was two times lower on T-1:8 film (Table 1). Lower adsorption of acetone on the T-1:8 film was probably due to the smoother morphology of the surface (Section 2.1, Figure S2). However, due to the increased amount of active sites on the T-1:8 film, adsorption of the pollutant apparently did not limit the process.

Chang et al. [53] studied the reaction kinetics of acetone degradation in the batch annular reactor using the Langmuir–Hinshelwood model at acetone initial concentrations from 0.36 to 3.5 ppb using as a TiO₂ photocatalyst P25 powder with catalyst surface area of 52 cm². In their study, a reaction rate constant of 0.0153 ppb/s was obtained [53]. Maudhuit et al. [55] in their study of photocatalytic oxidation of 5–10 ppm of acetone in a dynamic reactor on supported P25 powder with specific quantity of material 1.6 mg/cm² obtained the reaction rate constant of 0.110 ppm/s (air flow rate 2.5 L/min, RH 50%) [55]. It implies that design of the multi-section reactor used in the current study due to the high catalyst surface area of photocatalytically active TiO₂ thin film allowed us to operate in the continuous flow regime at the concentrations measured in ppm. Due to the enhanced photocatalytic activity (Table 1), T-1:8 film was selected for further studies of the effects of operating parameters such as air flow rate and relative humidity on the photocatalytic degradation of acetone and acetaldehyde.

2.2.3. Effect of Air Flow Rate and Relative Humidity

The effect of air flow rate on the degradation of acetone and acetaldehyde at initial concentration of 40 ppm (Figure 6) and 10 ppm (Figure 7a,b) at RH 6% was studied on the film with TTIP:AcacH 1:8. The air flow rate was increased from 0.5 to 1 L/min, which reduced the residence time twofold respectively from 15.6 to 7.8 s in one section of the modular reactor.

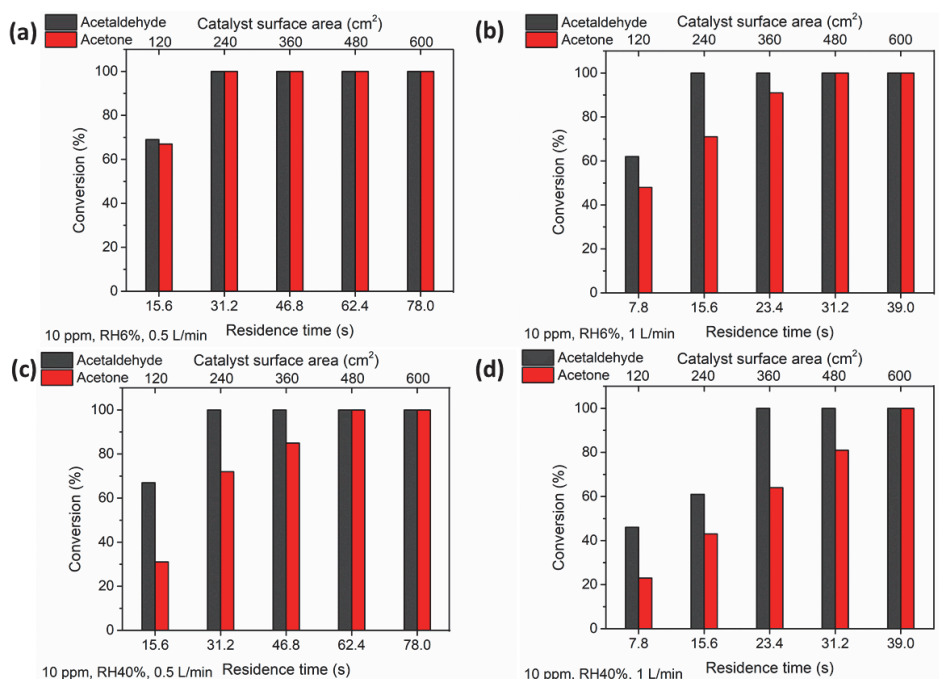


Figure 7. Effect of air flow rate and relative humidity (RH) on photocatalytic oxidation of 10 ppm acetone and 10 ppm of acetaldehyde under UV-A irradiation on the films with TTIP:AcacH molar ratio 1:8 in precursor solution at RH 6% air flow rates (a) 0.5 and (b) 1 L/min and at RH 40% air flow rates (c) 0.5 and (d) 1 L/min depending on catalyst surface area.

Figure 6 shows the oxidation of 40 ppm of acetone and 40 ppm of acetaldehyde at air flow rates 0.5 L/min (Figure 6a) and 1 L/min (Figure 6b) at RH 6%. The conversions of acetone and acetaldehyde at the same residence time (15.5 and 31.2 s), but doubled catalyst surface area are compared in the Table 2.

Table 2. Comparison of conversions of acetone and acetaldehyde at the residence time of 15.6 and 31.2 s at air flow rates 0.5 and 1 L/min on the film with TTIP:AcacH 1:8 in precursor solution.

Residence Time, s	Catalyst Surface Area, cm ²	Air Flow, L/min	Conversion, %			
			Acetone		Acetaldehyde	
			40 ppm	10 ppm	40 ppm	10 ppm
15.6	120	0.5	46	67	75	68
	240	1	27	71	79	100
31.2	240	0.5	87	100	100	100
	420	1	77	100	100	100

According to the results shown in Figure 6, an increase in air flow rate from 0.5 to 1 L/min had a negative effect on the oxidation of 40 ppm of acetone since at the same residence time (15.6 s) conversion was about 19% lower at air flow rate of 1 L/min (Table 2). The conversion of 40 ppm of acetaldehyde at the same residence time of 15.6 s is not affected by the air flow rate (Table 2). The oxidation of acetaldehyde occurred on the T-1:5 and T-1:8 films faster as discussed above (Section 2.2.2.). Therefore, it was not substantially affected by mass transfer unlike acetone oxidation. However, at initial

concentration of the pollutants of 10 ppm (Figure 7a,b) increased air flow rate had a positive effect on degradation of acetaldehyde (the conversions were 68% and 100% at the residence time of 15.6 s, at the air flow rates 0.5 and 1 L/min, respectively) and no changes in the conversion of acetone were observed (Table 2).

The increase in air flow rate resulted in the decrease in residence time of the pollutant's molecule in the reactor and in the intensification of mass transfer of polluted air. This means that changes in fluid dynamics can either promote or inhibit the photocatalytic oxidation. However, air flow is laminar at both rates (0.5 and 1 L/min), i.e., Reynolds numbers [56] were under 40 (the calculations are not shown for the sake of brevity). In a laminar flow regime, theoretically air is moving through each reactor section layer by layer without or with minimal mixing [56]. Thus, mixing of the air takes place only after each section of the reactor due to the passing through sections connecting tubing, where air velocity drastically increases. It could be assumed that the more laminar regime at air flow rate of 0.5 L/min promoted the adsorption of acetone and, thus, the higher degree of its degradation. In the case of acetaldehyde, adsorption is supposed to be not such a pronounced prerequisite for the degradation and it was not influenced by mass transfer at higher acetaldehyde inlet concentration (40 ppm). At lower inlet concentration of acetaldehyde (10 ppm), however, the additional mixing (application of two sections of the reactor instead of one) gave its positive effect. As for the acetone at its lower inlet concentration (10 ppm), the effect of intensified mass transfer was negligible.

To estimate the effect of increased air flow rate on the reaction kinetics, the initial reaction rate (r_0) was calculated according to the Equation (2). The results are presented in Table 3. At increased air flow rate the initial reaction rate of degradation of VOCs at inlet concentration of 40 ppm was 7% lower for acetone, while for acetaldehyde the initial reaction rate was 16% higher (Table 3). At an initial concentration of 10 ppm the initial reaction rate of both model pollutants was higher at air flow rate of 1 L/min; 18% and 35% for acetone and acetaldehyde, respectively (Table 3). These results demonstrate that differences in air flow regime affected the reaction kinetics; the effect was more pronounced at lower inlet concentrations of pollutants and depended on the type of pollutant. The differences in the character of oxidation of pollutants could be easily monitored using a continuous multi-section reactor.

Table 3. Initial reaction rates of acetone and acetaldehyde photocatalytic degradation at different air flow rates and relative humidity on the film with TTIP:AcAcH 1:8 in precursor solution.

Air Flow Rate, L/min	Concentration, ppm	Relative Humidity (RH), %	Acetone		Acetaldehyde	
			Initial Reaction Rate		Initial Reaction Rate	
			ppm/s	ppm/(s cm ²)	ppm/s	ppm/(s cm ²)
0.5	40	6	1.70	0.0142	2.01	0.0167
1	40	6	1.59	0.0132	2.38	0.0199
0.5	10	6	0.74	0.0061	0.66	0.0055
1	10	6	0.86	0.0074	1.17	0.0084
0.5	10	40	0.20	0.0016	0.60	0.0050
1	10	40	0.37	0.0031	0.72	0.0060

Liang et al. [23] studied the effect of air flow rate on the oxidation of acetone in a cylindrical reactor whereas sol-gel-synthesized 0.2 mm thick anatase TiO₂ film attached to glass spring was used as a catalyst. They showed that for 2445 ppm of acetone the intensification of mass transfer promoted the oxidation despite the decrease in residence time. The efficiency of photocatalytic oxidation increased from 18 to 78% with the increase in air flow rate from 1 to 3 L/min; however, a further increase in air flow up to 9 L/min resulted in drastic drop in photocatalytic efficiency to approximately 5% [23], which confirms that ascertaining the optimal air flow rate is an important step in technology development.

The effect of an increase in RH from 6 to 40% on the photocatalytic (UV-A light) degradation of acetone and acetaldehyde at initial concentration of 10 ppm was studied on the TiO₂ film with TTIP:AcAcH 1:8 at air flow rate 0.5 (Figure 7a,c) and 1 L/min (Figure 7b,d).

Complete oxidation of 10 ppm of acetone and acetaldehyde at an air flow rate of 0.5 L/min was achieved at a catalyst surface area of 240 cm², when relative humidity was 6% (Figure 7a). At relative humidity of 40%, for the complete degradation of acetone the catalyst surface area was increased two times (480 cm²), while for acetaldehyde it remained the same at 240 cm² (Figure 7c). Table 3 demonstrates, that at lower air flow rate (0.5 L/min) water molecules inhibited the degradation of acetone, the initial reaction rate was 74% lower at RH 40%. For 10 ppm of acetaldehyde at lower air flow rate, an increased amount of water molecules had no specific effect on photocatalytic degradation of pollutant. However, when the air flow rate of 1 L/min was used the initial reaction rate was decreased for both model pollutants at RH 40%.

The increased amount of water molecules can influence the performance of the photocatalytic oxidation process in different ways; this effect strongly depends on the water vapour concentration and the type of pollutant. The photocatalytic reaction rate can be enhanced since water molecules act as hole traps and form hydroxyl radicals participating in the oxidation of pollutants. On the other hand, water molecules can inhibit the adsorption of some pollutants on the surface of the catalyst, which may lead to a decrease in the degradation efficiency [6,26,47]. In this study, the increase in the RH from 6 to 40% deteriorated the performance of photocatalytic oxidation of VOCs despite the probable formation of higher number of hydroxyl radicals. Supposedly, water adsorbed on the active sites of TiO₂ thin films and inhibited the adsorption of the pollutants, thus the prolonged residence time may contribute to complete degradation of VOCs at higher water vapour content.

The same observations on the negative effects of an increased water vapour amount on oxidation of acetone and acetaldehyde have been reported by other authors [56–58]. Kim et al. [57] showed that on dip-coated TiO₂ thin film with thickness of 65 nm the increase in the amount of water vapour from 0 to 0.766 mol/m³ decreased the photodegradation rate of 274 ppm of acetone from 0.71 ppm/s to 0.21 ppm/s [57]. Seo et al. [58] studied the degradation of acetaldehyde at different RH on the 7 μm thick P25 layer and observed the decrease of 16% in the photodegradation rate with an increase in RH from 0% to 33.6% [58].

2.2.4. Photocatalytic Oxidation of Acetone and Acetaldehyde under Visible Light

Sprayed TiO₂ thin films were tested for photocatalytic oxidation of 10 ppm of acetone and 10 ppm of acetaldehyde under VIS light (Figure 8). The effect of air flow rate and relative humidity on the photocatalytic oxidation of acetone and acetaldehyde under VIS light was also studied. (Figure 8). Figure 8a demonstrates that TiO₂ film with molar ratio 1:8 was capable of oxidizing 10 ppm of acetaldehyde and 10 ppm of acetone under VIS light at catalyst surface area of 360 and 480 cm², respectively (air flow rate 0.5 L/min, RH 6%). For the comparison under UV-A light the photocatalytic activity of the films was substantially higher; both model compounds were fully degraded at a catalyst surface area of 240 cm² on the T-1:8 film (Section 2.2.1, Figure 3). The initial reaction rates on the T-1:8 film at air flow rate of 0.5 L/min and RH 6% under VIS were 0.35 ppm/s for 10 ppm of acetone and 0.52 ppm/s for 10 ppm of acetaldehyde which is, respectively, 53 and 21% lower compared to results obtained under UV-A (Table 3).

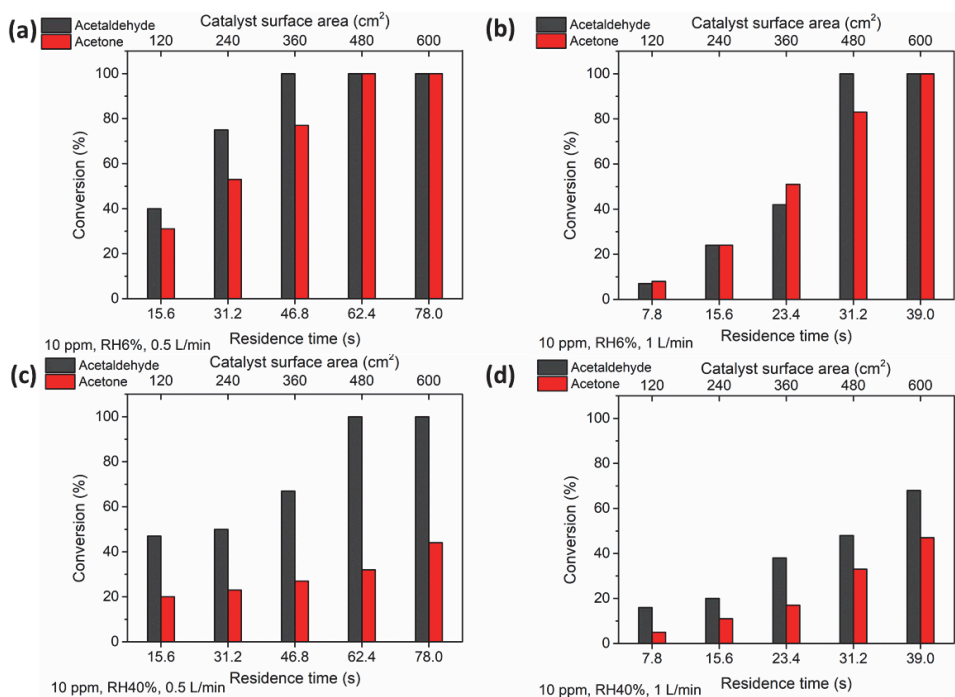


Figure 8. Effect of air flow rate and relative humidity (RH) on photocatalytic oxidation of 10 ppm acetone and 10 ppm of acetaldehyde under visible (VIS) light on the films with TTIP:AcacH molar ratio 1:8 in precursor solution at RH 6% air flow rates (a) 0.5 and (b) 1 L/min and at RH 40% air flow rates (c) 0.5 and (d) 1 L/min depending on catalyst surface area.

The photocatalytic activity of the film with TTIP:AcacH molar ratio 1:5 under VIS light was very low, ca. 20% conversion of pollutants was achieved at residence time of 78 s (Figure S5). However, the increase in the content of organic matter by changing the AcacH molar ratio in precursor solution enhanced the photocatalytic activity of the T-1:8 film (Figure 8a). Previous studies have clearly demonstrated that carbon incorporation in TiO₂ photocatalyst enhanced the photocatalytic activity for the degradation of stearic acid, 4-chlorfenol, paroxon and methylene blue under VIS light [26,34,56–58], while the current study showed also profound improvement in the photocatalytic oxidation of VOCs.

The increase in the air flow rate from 0.5 (Figure 8a) to 1 L/min (Figure 8b) under VIS light inhibited the degradation of model pollutants at lower residence time (15.6 s) and promoted the degradation at higher residence time (31.2 s). In Figure 8a,b, at the same residence time of 15.6 s (air flow rates 0.5 and 1 L/min, catalyst surface areas 120 and 240 cm², respectively) the conversion was higher at lower air flow rate of 0.5 L/min (catalyst surface area 120 cm² on the Figure 8a). However, at residence time of 31.2 s (air flow rates 0.5 and 1 L/min, catalyst surface areas 240 and 480 cm², respectively) conversion was higher at an air flow rate of 1 L/min (catalyst surface area 480 cm² on the Figure 8b). Increased mass transfer at residence time 15.6 s had negative effect on the photocatalytic oxidation. However, at the residence time 31.2 s additional mixings (application of four sections of reactor instead of two) had a positive effect on the degradation of model pollutants. The oxidation of pollutants under VIS light needed more residence time in the reactor since the photocatalytic activity of the film was lower compared to UV-A.

The increase in RH from 6 to 40% strongly inhibited the degradation of acetone and acetaldehyde under VIS light (Figure 8a,c). However, if under UV-A at a lower air flow rate (0.5 L/min) the effect of water vapour on photocatalytic oxidation of acetaldehyde was almost imperceptible (Section 2.2.3,

Figure 7c); then, under VIS light the conversion of acetaldehyde at RH 40% was deteriorated, but the complete degradation of pollutant was nevertheless achieved at an air flow rate of 0.5 L/min (Figure 8c). A similar tendency as under UV-A irradiation was observed, acetone oxidation is more affected by the increase in air RH compared to acetaldehyde.

2.2.5. Reusability of the Film

The reusability of the photocatalytic materials is an important factor to consider since it shows the practical application of the material for air purification from VOCs [28]. In order to estimate the lifetime of the sprayed TiO₂ thin film the reusability of the film with TTIP:AcacH molar ratio 1:8 under UV-A irradiation was studied. No deactivation of the photocatalyst was observed after more than three months of daily work with a short regeneration (approximately 30 min) of the TiO₂ films with UV-A light after each experimental run. Moreover, a long-term experiment on the photocatalytic oxidation of 40 ppm of acetone on the T-1:8 film under UV-A irradiation was carried out (Figure 9). The results confirmed that the film had extreme stability and high photoactivity for at least 120 min of continuous use.

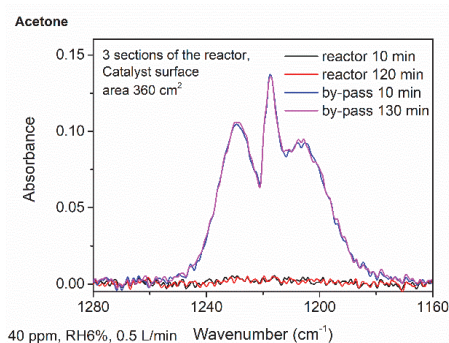


Figure 9. Fourier transform infrared (FTIR) spectra of characteristic acetone C–CO–C stretching at different times of experimental run under UV-A irradiation on the TiO₂ film with TTIP:AcacH molar ratio 1:8 in precursor solution.

Some experiments with acetaldehyde on the film with TTIP:AcacH 1:8 were repeated after at least one month of daily experiments to check the repeatability of the results. The average difference in the initial reaction rates between I and II experimental runs was 3.0% and did not exceed 5.3% for an individual series of experiments (Figure 10).

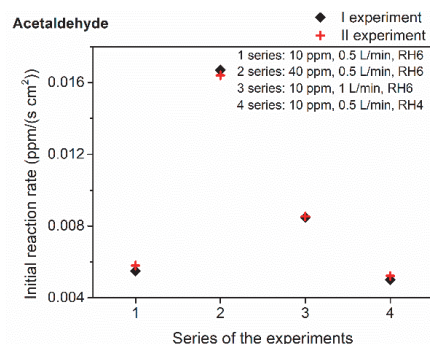


Figure 10. The repeatability of initial reaction rate values for some series of experiments on acetaldehyde oxidation under UV-A irradiation on the TiO₂ film with TTIP:AcacH molar ratio 1:8 in precursor solution.

Thus, an applied 30-min regeneration of the film with UV-A light allows continuous long-term application of this type of TiO₂ thin films for the degradation of acetone and acetaldehyde without any loss in films' photocatalytic activity. The study on the optimal time for the regeneration of the film with TTIP:AcacH 1:8 will be of great interest in the future; however, this was not under the scope of present research.

2.3. Antibacterial Activity

An antibacterial test was performed in the liquid phase since drying of the system leads to inactivation of the most used laboratory strains of bacteria and renders test results inconclusive. The well-established protocol was used; it allows us to compare the results with preceding literature and commercial products [59]. Antibacterial activity of the photocatalytic TiO₂ films with TTIP:AcacH molar ratios 1:4, 1:5 and 1:8 towards the Gram-negative model organism *Escherichia coli* MG1655 is shown in Figure 11.

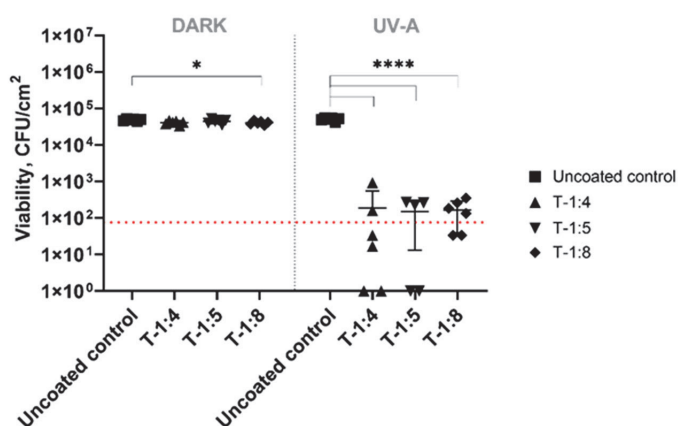


Figure 11. Viability of *Escherichia coli* after 60 min exposure to the TiO₂ thin films with TTIP:AcacH molar ratios 1:4, 1:5 and 1:8 in precursor solution with and without UV-A irradiation. Limit of quantification is marked in red (76 CFU/cm²). Statistically significant differences ($p < 0.05$) are marked on the graph (* < 0.05 ; **** < 0.0001).

All the TiO₂ films irrespective of TTIP:AcacH molar ratios demonstrated strong antibacterial activity of over 99% reduction in viable counts compared to the control surface during 60 min exposure with UV-A illumination ($p < 0.0001$). Despite very small statistically significant difference (16% reduction in viable count compared to the control in case of T-1:8 film, $P = 0.04$) no biologically relevant antimicrobial activity was observed in dark conditions. The antibacterial activity was not enhanced with the increase in AcacH amount. Less variable results on the T-1:8 film under UV-A illumination could partly be obtained due to the superior surface morphology. Indeed, the surface of the film with TTIP:AcacH 1:8 is smoother and more uniform (Section 2.1, Figure S3).

Many authors have reported that the reactive oxygen species (ROS) generated by TiO₂ have antibacterial activity. However, it should be mentioned that the bactericidal mechanism is more complex compared to VOCs oxidation since bacteria are complex unicellular organisms separated from the surrounding environment by a membrane and cell wall [60,61]. Thus, the mechanism of degradation of bacterial cells includes, first, damage to the cell wall, peroxidation of membrane lipids and further leakage of the cytoplasm due to the membrane damage [16]. Our results are comparable with those obtained by Kim and Kwak [62], who obtained 99% degradation of 1×10^6 cells/mL *E. coli* for the mesoporous P25 films after 60 min of UV-A irradiation [62].

All TiO₂ thin films obtained in the current study indicate antibacterial activity, in addition to gas-phase photocatalytic oxidation of VOCs. However, to compare the results of the film's gas-phase photocatalytic efficiency with antibacterial activity further tests with airborne microorganisms are needed, which is of great interest and will be under the scope of future studies.

3. Materials and Methods

3.1. Preparation and Characterization of TiO₂ Thin Films

Anatase phase TiO₂ thin films with thickness of ca. 400 nm were deposited on borosilicate glass substrate at temperature of 350 °C by ultrasonic spray pyrolysis technique. The details of the film preparation have been published elsewhere [26]. The as-deposited films were annealed for one hour at 500 °C in air. Titanium (IV) isopropoxide (TTIP): acetylacetonate (AcacH) molar ratios 1:4, 1:5 and 1:8 were used for precursor solution preparation, the samples obtained were further designated T-1:4, T-1:5 and T-1:8, respectively. The concentration of TTIP was 0.2 M.

The band gap of TiO₂ thin films was calculated from the Tauc plot using total transmittance spectra measured with a Jasco V-670 UV-VIS-NIR (near infrared) spectrophotometer (Jasco, Tokyo, Japan) equipped with an integrating sphere in the spectral range 250–1500 nm. X-ray photoelectron spectroscopy (XPS) with a Kratos Analytical AXIS ULTRA DLD spectrometer (Kratos Analytical, Manchester, England) in conjunction with a 165-mm hemispherical electron energy analyzer and delay-line detector was used to analyse the location of the valence band.

3.2. Evaluation of Gas-Phase Photocatalytic Activity of the TiO₂ Thin Films

Photocatalytic oxidation of acetone and acetaldehyde (both Sigma-Aldrich, ≥ 99.5% purity) over TiO₂ thin films was studied in a continuous multi-section plug flow reactor. A detailed description of the set up for photocatalytic experiments was published elsewhere [63]. The reactor consists of five sections with the volume of 130 mL each. Four pieces of TiO₂ thin film with dimensions 4 cm × 7.5 cm were placed inside each section, giving the catalyst surface area 120 cm² per section and 600 cm² for five sections. UV Philips Actinic BL 15 W, irradiance 3.5 mW/cm² with reflector (integrated in the range of 180–400 nm, with maximum emission at 365 nm, UV-B/UV-A ratio <0.2%) lamps were used as an UV-A irradiation source and VIS Philips TL-D 15 W, irradiance 3.3 mW/cm² with reflector (integrated in the range of 180–700 nm, UV/UV-VIS ratio <5%) lamps as VIS irradiation source over each section of the reactor with the distance of 6 cm. The construction of this modular reactor allows an increase in the residence time in the reactor by increasing the catalyst surface area without changing the mass transfer in the reactor. Polluted (spiked with acetone and acetaldehyde) air was prepared in a 50 L tank using regular ambient air. Two air flow rates 0.5 and 1 L/min were used during the experiments, which yielded the residence time in the reactor 15.6 and 7.8 s per section, respectively. The air flow rate was measured by two gas flow controllers, one for measuring the diluent and one for the polluted gas flow rates. Gas humidifier was used to change the air humidity. INTERSPEC 200-X FTIR infrared spectrometer (Interspectrum OÜ, Tõravere, Estonia) with the 8 m gas cell (Specac) was used for measuring the concentration of VOCs. Spectra were acquired in the absorbance mode, with the number of scans 5 and resolution 1 cm⁻¹. The spectra of filtered and dried ambient air were used as a reference. The characteristic C–C stretching of acetone was measured at the IR bands from 1270 to 1240 cm⁻¹ [64] and C–H aldehyde stretching of acetaldehyde at the IR bands from 2900 to 2600 cm⁻¹ [65] and were quantified with the limit of detection of about 0.5 ppm and the limit of quantification of 1.0 ppm. All spectra were measured at least twice and the difference between the experiments did not exceed 5%. The air spectra were acquired using an Interspec version 3.40 Pro (Interspectrum OÜ, Estonia, 2012) and processed by the Essential FTIR software (Version 3.50.075, Operant LLC, Madison, WI, USA, 2016).

3.3. Study of Antibacterial Activity of the TiO₂ Thin Films

The surfaces of TiO₂ thin films were pre-treated by rinsing with 70% ethanol and 3 mW/cm² UV-A irradiation (24 h) in aseptic conditions. Antibacterial testing was carried out using in-house protocol based on modified ISO 27,447 and ISO 22,196 protocols [59]. Bacterial suspension was prepared in 500-fold diluted nutrient broth (NB: 3 g/L meat extract, 10 g/L peptone, 5 g/L NaCl in deionized water), optimized to optical density (600 nm) of 0.01 resulting in 5×10^4 cells per cm². To determine the antibacterial properties of test surfaces, 15 μ L of bacterial suspension was applied to test surface and covered with $20 \times 20 \times 0.05$ mm polyethylene film to attain an even, thin coverage of bacterial suspension with good contact between bacterial cells and the surface and even UV-A exposure. Samples were kept either in the dark or exposed to 0.26–0.33 mW/cm² UV-A irradiation measured in the 315–400 nm spectral range. Surfaces with bacterial suspension were incubated in a humid environment on a bent glass U-rod over sterile wet filter paper covered by Petri dish cover in dark conditions or 1.1 mm thick UV-A-transmissive borosilicate moisture preservation glass under UV-A illumination. UV-A intensity was measured at a test surface height with a light meter detector covered by both polyethylene film and borosilicate moisture preservation glass. Media, solutions and glass rods were autoclaved at 121 °C for 15 min prior to each experiment. Polyethylene cover films and control surfaces were rinsed with 70% ethanol and air-dried under UV-C irradiation. After exposure, each sample was washed with 2 mL of toxicity neutralizing soybean casein digest broth with lecithin and polysorbate medium (SCDLP: 17 g/L casein peptone, 3 g/L soybean peptone, 5 g/L sodium chloride, 2.5 g/L disodium hydrogen phosphate, 2.5 g/L glucose, 1 g/L lecithin and 7 g/L polysorbate 80 in deionized water) by pipetting, serially diluted in phosphate buffered physiological saline (PBS) and drop-plated for counting. Nutrient agar (NA: 5 g/L meat extract, 10 g/L peptone, 5 g/L sodium chloride, 15 g/L agar powder in deionized water) was used for plating and colony forming units were counted after 24 h incubation at 30 °C. Statistical analysis to detect statistically significant differences in viable counts was performed by one-way analysis of variance (ANOVA) followed by Tukey's HSD (honestly significant difference) using the program GraphPad Prism version 8.3.0 (GraphPad Software, LLC, San Diego, CA, USA, 2019)

4. Conclusions

TiO₂ thin films with an increased amount of AcacH in precursor solution were deposited on borosilicate glass substrate by the ultrasonic spray pyrolysis technique. The increased molar ratio of AcacH changed the position of valence band, leading to the higher production of hydroxyl radicals on the catalyst surface and thus enhanced the photocatalytic activity of the TiO₂ thin films under ultraviolet (UV-A) and visible (VIS) lights. Indeed, the efficiency of photocatalytic oxidation of 10 ppm of acetone and 10 ppm of acetaldehyde on the film T-1:8 was about two times higher compared to film T-1:5 under UV-A and VIS irradiation. The reaction kinetics was studied using the Langmuir–Hinshelwood model. The initial reaction rate of acetone oxidation increased as expected, with an increase in its concentration on both films. However, the reaction rate constant on film T-1:8 was more than three times higher compared to T-1:5. The increase in air flow rate had different effects on the oxidation of pollutants depending on their initial concentration. Higher air humidity had negative effect on the degradation of acetone and acetaldehyde, but for acetaldehyde the effect was less pronounced, especially under UV-A irradiation. TiO₂ thin films demonstrated strong antibacterial activity towards Gram-negative *E. coli* under UV-A irradiation irrespective of TTIP:AcacH molar ratio in precursor solution.

Thus, the results of this study demonstrate that TiO₂ films with TTIP:AcacH molar ratio 1:8 could be successfully applied for indoor air purification in photocatalytic air cleaners instead of powder modules since their efficiency under UV-A is substantially higher than that of commercial Pilkington Activ™ glass and comparable with thick coatings of P25 nanopowder used in the literature. The results of visible light photocatalytic activity showed that film deposited on a large surface area could be applied as an indoor air purifying coating. Moreover, the antimicrobial properties including the

antiviral properties need further investigation under visible light as obtained films may have the potential for the purification of microbial-polluted indoor air.

Supplementary Materials: The following are available online at <http://www.mdpi.com/2073-4344/10/9/1011/s1>. Figure S1: Cross-sectional scanning electron microscopy (SEM) image of TiO₂ thin film on borosilicate glass substrate at TTIP:AcacH molar ratio 1:8 (T-1:8), Figure S2: Atomic force microscope (AFM) images of the TiO₂ films (a) T-1:4, (b) T-1:5 and (c) T-1:8, Figure S3: X-ray photoelectron spectroscopy (XPS) spectra of C1s core level for (a) 1:5 and (b) 1:8 TTIP:AcacH molar ratios in precursor solution for TiO₂ thin films, Figure S4: Langmuir-Hinshelwood kinetic plot for the determination of acetone degradation reaction rate constant and adsorption constants on TiO₂ films with TTIP:AcacH molar ratios (a) 1:5 and (b) 1:8 in precursor solution, Figure S5: Photocatalytic oxidation of 10 ppm of acetone and 10 ppm of acetaldehyde under VIS light on the T-1:5 film depending on the catalyst surface area.

Author Contributions: J.S.: Conceptualization, Investigation, Formal analysis, Writing—Original Draft, Visualization. A.M.: Investigation, Formal analysis. M.K. (Malle Krunks): Formal analysis, Funding acquisition, Writing—Review and Editing. M.R.: Antibacterial activity Investigation, Formal analysis, Validation, Writing—Review and Editing. A.K.: Writing—Review & Editing. M.D.: XPS Investigation, Formal analysis. M.K. (Marina Krichevskaya): Conceptualization, Methodology, Writing—Review and Editing, Supervision. I.O.A.: Conceptualization, Methodology, Writing—Review and Editing, Supervision, Resources, Funding acquisition. All authors have read and agreed to the published version of the manuscript.

Funding: This research was funded by the Estonian Ministry of Education and Research, Estonian Research Council projects IUT19-4, PRG627 and PRG776, and the Estonian Centre of Excellence project TK141. Estonian Research Agency grant EAG20 and European Regional Development Fund grants NAMUR+ 2014-2020.4.01.16-0123 and TK134 are acknowledged.

Acknowledgments: The authors acknowledge Georgiy Shevelev for AFM measurements.

Conflicts of Interest: The authors declare no conflict of interest.

References

1. Jafari, M.J.; Khajevandi, A.A.; Najarkola, S.A.M.; Yekaninejad, M.S.; Pourhoseingholi, M.A.; Omidi, L.; Kalantary, S. Association of sick building syndrome with indoor air parameters. *Tanaffos* **2015**, *14*, 55–62.
2. Hay, S.O.; Obee, T.; Luo, Z.; Jiang, T.; Meng, Y.; He, J.; Murphy, S.C.; Suib, S. The Viability of Photocatalysis for Air Purification. *Molecules* **2015**, *20*, 1319–1356. [[CrossRef](#)] [[PubMed](#)]
3. Nath, R.K.; Zain, M.F.M.; Jamil, M. An environment-friendly solution for indoor air purification by using renewable photocatalysts in concrete: A review. *Renew. Sust. Energ. Rev.* **2016**, *62*, 1184–1194. [[CrossRef](#)]
4. Franklin, P.J. Indoor air quality and respiratory health of children. *Paediatr. Respir. Rev.* **2007**, *8*, 281–286. [[CrossRef](#)] [[PubMed](#)]
5. World Health Organization (WHO). Air pollution, Household Air Pollution: Pollutants. Available online: <https://www.who.int/airpollution/household/pollutants/en/> (accessed on 10 December 2019).
6. Dundar, I.; Krichevskaya, M.; Katerski, A.; Krunks, M.; Oja Acik, I. Photocatalytic degradation of different vocs in the gas-phase over tio₂ thin films prepared by ultrasonic spray pyrolysis. *Catalyst* **2019**, *9*, 915. [[CrossRef](#)]
7. Luga-Vega, C.S.; Moreira, J.; Serrano-Roseles, B.; de Lasa, H. Kinetics of the pollutant photocatalytic conversion in a Photo-CREC-Air Reactor. *Chem. Eng. J.* **2017**, *317*, 1069–1082. [[CrossRef](#)]
8. Bianchi, C.L.; Gatto, S.; Pirola, C.; Naldoni, A.; Di Michele, A.; Cerrato, G.; Crocellà, V.; Capucci, V. Photocatalytic degradation of acetone, acetaldehyde and toluene in gas-phase: Comparison between nano and micro-sized TiO₂. *Appl. Catal. B-Environ.* **2014**, *146*, 123–130. [[CrossRef](#)]
9. Tomida, T.; Okada, N.; Katoh, M. Adsorption and photocatalytic decomposition of volatile organic compounds on photocatalyst of TiO₂—Silica beads. *Adsorption* **2005**, *11*, 865–869. [[CrossRef](#)]
10. Bianchi, C.L.; Pirola, C.; Stucchi, M.; Sacchi, B.; Cerrato, G.; Morandi, S.; Di Michele, A.; Carletti, A.; Capucci, V. A New Frontier of Photocatalysis Employing Micro-Sized Tio₂: Air/Water Pollution Abatement and Self-Cleaning/Antibacterial Applications. In *Semiconductor Photocatalysis—Materials, Mechanisms and Applications*; Cao, W., Ed.; IntechOpen: London, UK, 2015.
11. European Chemical Agency (ECHA), Substance Infocard, Acetaldehyde. Available online: <https://echa.europa.eu> (accessed on 20 April 2020).

12. Exploratory Survey of Occupational Exposure Limits for Carcinogens, Mutagens and Reprotoxic Substances at EU Member States Level. In European Agency for Safety and Health at Work; European Risk Observatory Report. 2007. Available online: <https://osha.europa.eu/en/publications> (accessed on 2 September 2020).
13. Augugliaro, V.; Loddo, V.; Pagliaro, M.; Giovanni, P.; Palmisano, L. Clean by Light Irradiation: Practical Applications of Supported TiO₂. In *Royal Society of Chemistry*; RSC publishing: Cambridge, UK, 2010.
14. Airscience Technology Co., Ltd., Air Steril. Available online: <http://www.airpurifier.com.hk/product-en.htm> (accessed on 13 March 2020).
15. Son Le, T.; Hien Dao, T.; Cuong Nguyen, D.; Chau Nguyen, H.; Balikhin, I.L. Air purification equipment combining a filter coated by silver nanoparticles with a nano-TiO₂ photocatalyst for use in hospitals. *Adv. Nat. Sci. Nanosci. Nanotechnol.* **2015**, *6*, 8. [[CrossRef](#)]
16. Pant, B.; Park, M.; Park, S.J. Recent advances in tio₂ films prepared by sol-gel methods for photocatalytic degradation of organic pollutants and antibacterial activities. *Coatings* **2019**, *9*, 613. [[CrossRef](#)]
17. Dundar, I.; Krichevskaya, M.; Katerski, A.; Oja Acik, I. TiO₂ thin films by ultrasonic spray pyrolysis as photocatalytic material for air purification. *R. Soc. Open Sci.* **2019**, *6*, 181578. [[CrossRef](#)] [[PubMed](#)]
18. Saad, P.S.M.; Sutan, H.B.; Shariffudin, S.S.; Hashim, H.; Noor, U.M. TiO₂ thin film via sol-gel method: Investigation on molarity effect. *IOP Conf. Ser. Mater. Sci. Eng.* **2015**, *99*, 012006. [[CrossRef](#)]
19. Stefanov, B.I.; Niklasson, G.A.; Granqvist, G.G.; Österlund, L. Gas-phase photocatalytic activity of sputter-deposited anatase TiO₂ films: Effect of <001> preferential orientation, surface temperature and humidity. *J. Catal.* **2016**, *335*, 187–196. [[CrossRef](#)]
20. Al-Hajji, L.A.; Ismail, A.A. Photooxidation of acetaldehyde over TiO₂ film: Impact of the substrate glassy structure on the photonic efficiency. *Superlatt. Microst.* **2019**, *129*, 259–267. [[CrossRef](#)]
21. Antonello, A.; Soliveri, G.; Meroni, D.; Cappelletti, G.; Ardizzone, S. Photocatalytic remediation of indoor pollution by transparent TiO₂ films. *Catal. Today* **2014**, *230*, 35–40. [[CrossRef](#)]
22. Kim, S.H.; Kim, S.B.; Kim, G.S.; Jang, H.T.; Hong, S.C. Kinetic study on degradation of gaseous acetone over thin-film TiO₂ photocatalyst in a continuous flow system. *React. Kinet. Catal. Lett.* **2007**, *90*, 85–91. [[CrossRef](#)]
23. Liang, W.; Li, J.; He, H. *Photo-Catalytic Degradation of Volatile Organic Compounds (VOCs) over Titanium Dioxide Thin Film, Advanced Aspects of Spectroscopy*; IntechOpen: London, UK, 2012. [[CrossRef](#)]
24. Simonsen, M.E.; Sorensen, M.B.; Sogaard, E.G. Comparison of methods for evaluation of activity of photocatalytic films. *Environ. Sci. Pollut. Res.* **2012**, *19*, 3772–3781. [[CrossRef](#)]
25. Adachi, T.; Latthe, S.S.; Gosavi, S.W.; Roy, N.; Suzuki, N.; Ikari, H.; Kato, K.; Katsumata, L.; Nakata, K.; Furudate, M.; et al. Photocatalytic, superhydrophilic, self-cleaning TiO₂ coating on cheap, light-weight, flexible polycarbonate substrates. *Appl. Surf. Sci.* **2018**, *458*, 917–923. [[CrossRef](#)]
26. Spiridonova, J.; Katerski, A.; Danilson, M.; Krichevskaya, M.; Krunks, M.; Oja Acik, I. Effect of the titanium isopropoxide:acetylacetone molar ratio on the photocatalytic activity of TiO₂ thin films. *Molecules* **2019**, *24*, 4326. [[CrossRef](#)]
27. Yao, N.; Yeung, K.L. Investigation of the performance of TiO₂ photocatalytic coatings. *Chem. Eng. J.* **2011**, *167*, 13–21. [[CrossRef](#)]
28. Abidi, M.; Assadi, A.A.; Bouzaza, A.; Hajjaji, A.; Bessais, B.; Rtimi, S. Photocatalytic indoor/outdoor air treatment and bacterial inactivation on Cu_xO/TiO₂ prepared by HiPIMS on polyester cloth under low intensity visible light. *Appl. Catal. B-Environ.* **2019**, *259*, 118074. [[CrossRef](#)]
29. Nakano, R.; Hara, M.; Ishiguri, H.; Yao, Y.; Ochiai, T.; Nakata, K.; Murakami, T.; Kajioka, J.; Sunada, K.; Hashimoto, K.; et al. Broad spectrum microbicidal activity of photocatalysis by TiO₂. *Catalyst* **2013**, *3*, 310–323. [[CrossRef](#)]
30. De Falco, G.; Porta, A.; Petrone, A.M.; Del Gaudio, P.; El Hassanin, A.; Commodo, M.; Minutolo, P.; Squillaceband, A.; D’Anna, A. Antimicrobial activity of flame-synthesized nano-TiO₂ coatings. *Environ. Sci. Nano* **2017**, *4*, 1095. [[CrossRef](#)]
31. Peerakiatkhajorn, P.; Chawengkijwanich, C.; Onreabroy, W.; Chiarakorn, S. Novel Photocatalytic Ag/TiO₂ Thin Film on Polyvinyl Chloride for gaseous BTEX Treatment. *Mater. Sci. Forum* **2012**, *712*, 133–145. [[CrossRef](#)]
32. Garlisi, C.; Scandura, G.; Alabi, A.; Aderemi, A.; Palmosano, G. Self-Cleaning Coatings Activated by Solar and Visible Radiation. *J. Adv. Chem. Eng.* **2015**, *5*, 3. [[CrossRef](#)]

33. Raza, N.; Kim, K.-H.; Agbe, H.; Kailase, S.K.; Szulejko, J.E.; Brown, R.J.C. Recent advances in titania-based composites for photocatalytic degradation of indoor volatile organic compounds. *Asian J. Atmos. Environ.* **2017**, *11*, 217–234. [[CrossRef](#)]
34. Di Valentin, C.; Pacchioni, G.; Selloni, A. Theory of carbon doping of titanium dioxide. *Chem. Mater.* **2015**, *17*, 6656–6665. [[CrossRef](#)]
35. Klauseon, D.; Portjanskaya, E.; Budarnaja, O.; Krichevskaya, M.; Preis, S. The synthesis of sulphur and boron-containing titania photocatalysts and the evaluation of their photocatalytic activity. *Catal. Commun.* **2010**, *11*, 715–720. [[CrossRef](#)]
36. Ratova, M.; Klaysri, R.; Praserttham, P.; Kelly, P.J. Visible light active photocatalytic C-doped titanium dioxide films deposited via reactive pulsed DC magnetron co-sputtering: Properties and photocatalytic activity. *Vacuum* **2018**, *149*, 214–224. [[CrossRef](#)]
37. Rasoulnezhad, H.; Kavei, G.; Ahmadi, K.; Rahimpour, M.R. Visible light photocatalytic degradation of paraoxon and parathion pesticides on carbon-doped TiO₂ nanorod thin films. *J. Mater. Sci. Mater. Electron.* **2017**, *28*, 18337–18347. [[CrossRef](#)]
38. Park, Y.; Kim, W.; Park, H.; Tachikawa, T.; Majima, T.; Choi, W. Carbon-doped TiO₂ photocatalyst synthesized without using an external carbon precursor and the visible light activity. *Appl. Catal. B Environ.* **2009**, *91*, 355–361. [[CrossRef](#)]
39. Oja, I.; Mere, A.; Krunks, M.; Solterbeck, C.-H.; Es-Souni, M. Properties of TiO₂ films prepared by the spray pyrolysis method. *Solid State Phenom.* **2004**, *99–100*, 259–262. [[CrossRef](#)]
40. Krunks, M.; Dedova, T.; Oja Acik, I. Spray pyrolysis deposition of zinc oxide nanostructured layers. *Thin Solid Film.* **2006**, *515*, 1157–1160. [[CrossRef](#)]
41. Juma, A.O.; Acik, O.I.; Mikli, V.; Mere, A.; Krunks, M. Effect of solution composition on anatase to rutile transformation of sprayed TiO₂ thin films. *Thin Solid Film.* **2015**, *594*, 287–292. [[CrossRef](#)]
42. Kaltsum, U.; Kurniawan, A.F.; Nurhasanah, I.; Priyono, P. The role of concentration ratio of ttip:acac on the photocatalytic activity of TiO₂ thin film in reducing degradation products of used frying oil. *Bull. Chem. React. Eng. Catal.* **2017**, *12*, 430–436. [[CrossRef](#)]
43. Duminica, F.D.; Mauray, F.; Abisset, S. Pyrosol deposition of anatase TiO₂ thin films starting from Ti(OiPr)₄/acetylacetone solutions. *Thin Solid Film.* **2007**, *515*, 7732–7739. [[CrossRef](#)]
44. Krunks, M.; Oja, I.; Tonsuaadu, K.; Es-Souni, M.; Gruselle, M.; Niinisto, L. Thermoanalytical study of acetylacetonate-modified titanium(IV) isopropoxide as a precursor for TiO₂ films. *J. Therm. Anal. Calorim.* **2005**, *80*, 483–488. [[CrossRef](#)]
45. Oja Acik, I.; Madarasz, J.; Krunks, M.; Tõnsuaadu, K.; Janke, D.; Pokol, G.; Niinistö, L. Thermoanalytical studies of titanium(IV) acetylacetonate xerogels with emphasis on evolved gas analysis. *J. Therm. Anal. Calorim.* **2007**, *88*, 557–563. [[CrossRef](#)]
46. Ansari, S.A.; Cho, M.H. Highly visible light responsive, narrow band gap TiO₂ nanoparticles modified by elemental red phosphorus for photocatalysis and photoelectrochemical applications. *Sci. Rep.* **2016**, *6*, 25405. [[CrossRef](#)]
47. Yaghoubi, H.; Li, Z.; Chen, Y.; Ngo, H.T.; Bhethanabotla, V.R.; Joseph, B.; Ma, S.; Schlaf, R.; Takshi, A. Toward a visible light-driven photocatalyst: The effect of midgap-states-induced energy gap of undoped TiO₂ nanoparticles. *Am. Chem. Soc.* **2015**, *5*, 327–335. [[CrossRef](#)]
48. Demeestere, K.; Dewulf, J.; Van Langenhove, H. Heterogeneous photocatalysis as an advanced oxidation process for the abatement of chlorinated, monocyclic aromatic and sulfurous volatile organic compounds in air: State of the art. *Crit. Rev. Environ. Sci. Tec.* **2007**, *37*, 489–538. [[CrossRef](#)]
49. Liu, B.; Zhao, X.; Terashima, C.; Fujishima, A.; Nakata, K. Thermodynamic and kinetic analysis of heterogeneous photocatalysis for semiconductor systems. *Phys. Chem. Chem. Phys.* **2014**, *16*, 8751–8760. [[CrossRef](#)] [[PubMed](#)]
50. Armstrong, D.A.; Huie, R.E.; Koppenol, W.H.; Lymar, S.V.; Merenyi, G.; Neta, P.; Ruscic, B.; Stanbury, D.M.; Steenken, S.; Wardman, P. Standard electrode potentials involving radicals in aqueous solution: Inorganic radicals. *IUPAC Tech. Rep.* **2016**, *87*, 1365–3075. [[CrossRef](#)]
51. Yao, M.; Ji, Y.; Wang, H.; Ao, Z.; Li, G.; An, T. Adsorption mechanisms of typical carbonyl-containing volatile organic compounds on anatase TiO₂ (001) surface: A DFT investigation. *J. Phys. Chem. C* **2017**, *121*, 13717–13722. [[CrossRef](#)]

52. Li, L.; Sun, Z.; Li, H.; Keener, T.C. Effects of activated carbon surface properties on the adsorption of volatile organic compounds. *J. Air Waste Manag.* **2012**, *62*, 1196–1202. [[CrossRef](#)] [[PubMed](#)]
53. Chang, C.P.; Chen, J.N.; Lu, M.C. Heterogeneous photocatalytic oxidation of acetone for air purification by near uv-irradiated titanium dioxide. *J. Environ. Sci. Health* **2003**, *38*, 1131–1143. [[CrossRef](#)]
54. Aisien, F.A.; Amenaghawon, N.A.; Urhobotie, O.I. Potential application of a locally sourced photocatalyst for the photocatalytic decolourisation of methyl orange in aqueous solution. *J. Eng. Sci. Technol.* **2015**, *10*, 1641–1653.
55. Maudhuit, A.; Raillard, C.; Hequet, V.; Le Coq, L.; Sablayrolles, J.; Molins, L. Adsorption phenomena in photocatalytic reactions: The case of toluene, acetone and heptane. *Chem. Eng. J.* **2011**, *170*, 464–470. [[CrossRef](#)]
56. Han, Y.; Kanno, H.; Ahn, Y.J.; Shikazono, N. Measurement of liquid film thickness in micro tube annular flow. *Int. J. Multiph. Flow* **2015**, *72*, 264–274. [[CrossRef](#)]
57. Kim, S.B.; Hwang, H.T.; Hong, S.C. Photocatalytic degradation of volatile organic compounds at the gas–solid interface of a TiO₂ photocatalyst. *Chemosphere* **2002**, *48*, 437–444. [[CrossRef](#)]
58. Seo, H.O.; Park, E.J.; Kim, I.H.; Han, S.W.; Cha, B.J.; Wo, T.G.; Kim, Y.D. Influence of humidity on the photo-catalytic degradation of acetaldehyde over TiO₂ surface under UV light irradiation. *Catal. Today* **2017**, *295*, 102–109. [[CrossRef](#)]
59. Visnapuu, M.; Rosenberg, M.; Truska, E.; Nömmiste, E.; Šutka, A.; Kahru, A.; Rähn, M.; Vija, H.; Orupöld, K.; Kisand, V.; et al. UVA-induced antimicrobial activity of ZnO/Ag nanocomposite covered surfaces. *Colloids Surf. B* **2018**, *169*, 222–232. [[CrossRef](#)] [[PubMed](#)]
60. Huang, Z.; Maness, P.C.; Blake, D.M.; Wolfrum, E.J.; Smolinski, S.L.; Jacoby, W.A. Bactericidal mode of titanium dioxide photocatalysis. *J. Photochem. Photobiol. A* **2000**, *130*, 16–170. [[CrossRef](#)]
61. Jacoby, W.A.; Maness, P.C.; Wolfrum, E.J.; Blake, D.M.; Fennell, J.A. Mineralization of bacterial cell mass on a photocatalytic surface in air. *Environ. Sci. Technol.* **1998**, *32*, 2650–2653. [[CrossRef](#)]
62. Kim, D.S.; Kwak, S.J. Photocatalytic inactivation of *E. coli* with a mesoporous TiO₂ coated film using the film adhesion method. *Environ. Sci. Technol.* **2009**, *43*, 148–151. [[CrossRef](#)] [[PubMed](#)]
63. Kask, M.; Bolobajev, J.; Krichevskaya, M. Gas-phase photocatalytic degradation of acetone and toluene, and their mixture in the presence of ozone in continuous multi-section reactor as possible air post-treatment for exhaust from pulsed corona discharge. *Chem. Eng. J.* **2020**, *399*, 125815. [[CrossRef](#)]
64. Hu, Z.; Tan, K.; Lustig, W.P.; Wang, H.; Zhao, Y.; Zheng, C.; Banerjee, D.J.; Emge, T.J.; Chabal, V.; Li, J. Effective sensing of RDX via instant and selective detection of ketone vapors. *Chem. Sci.* **2014**, *5*, 4873. [[CrossRef](#)]
65. Tsuji, M.; Miyano, M.; Kamo, N.; Kawahara, T.; Uto, K.; Hayashi, J.; Tsuji, T. Photochemical removal of acetaldehyde using 172 nm vacuum ultraviolet excimer lamp in N₂ or air at atmospheric pressure. *Environ. Sci. Pollut. Res.* **2019**, *26*, 11324–11325. [[CrossRef](#)]



Publication III

T. Dittrich, J. Sydorenko, N. Spalatu, H. N. Nickel, A. Mere, M. Krunks, I. Oja Acik. "Synthesis Control of Charge Separation at Anatase TiO₂ Thin Films Studied by Transient Surface Photovoltage Spectroscopy", ACS Applied Materials & Interfaces journal, 14(38), 43163-43170, 2022, doi.org/10.1021/acscami.2c09032.

Synthesis Control of Charge Separation at Anatase TiO₂ Thin Films Studied by Transient Surface Photovoltage Spectroscopy

Thomas Dittrich,* Jekaterina Sydorenko, Nicolae Spalatu,* Norbert H. Nickel, Arvo Mere, Malle Krunk, and Ilona Oja Acik

Cite This: <https://doi.org/10.1021/acsami.2c09032>

Read Online

ACCESS |

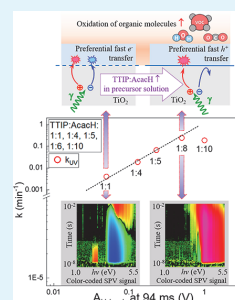
Metrics & More

Article Recommendations

Supporting Information

ABSTRACT: For the efficient photocatalytic oxidation of organic pollutants at surfaces of semiconductors, photogenerated holes shall be separated toward the surface and transferred to reactive surface sites, whereas the transfer of photogenerated electrons toward the surface shall be minimized. In this Research Article, the identification of suitable synthesis control of charge separation combined with an in-depth understanding of charge kinetics and trapping passivation mechanisms at the related surfaces can provide tremendous opportunities for boosting the photocatalytic performance. In this work, a comprehensive transient surface photovoltage spectroscopy study of charge separation at anatase TiO₂ thin films, synthesized by ultrasonic spray pyrolysis from titanium(IV) isopropoxide (TTIP)–acetylacetonate (AcacH) based precursor is reported. By varying the amount of AcacH in the precursor solution, an experimental approach of synthesis control of the charge transfer toward TiO₂ surface is provided for the first time. An increased amount of AcacH in the precursor promotes transition from preferential fast electron to preferential fast hole transfer toward anatase surface, correlating with a strong increase of the photocatalytic decomposition rate of organic pollutants. Suitable mechanisms of AcacH-induced passivation of electron traps at TiO₂ surfaces are analyzed, providing a new degree of freedom for tailoring the properties of photocatalytic systems.

KEYWORDS: TiO₂, charge separation, photocatalytic activity, surface photovoltage, transient spectroscopy



1. INTRODUCTION

For the initiation of photocatalytic reactions at surfaces of semiconductors, for example at TiO₂, photogenerated electrons and holes shall be separated toward the external surface and transferred to reactive surface sites. Photogenerated electrons and holes transferred toward reactive surface sites are responsible for photocatalytic reduction (or inhibition of oxidation) or oxidation (or inhibition of reduction), respectively. The investigation of limiting processes is important for a deeper understanding of photocatalytic reactions at semiconductor surfaces and for the further development and optimization of photocatalytic systems.

The discovery by Fujishima and Honda in 1972 of water splitting with a photoirradiated titania electrode opened a new field in photocatalysis and highly stimulated the research interest in this field.¹ Some of the most important applications of photocatalysis are in the area of environmental remediation. Hydroxyl radicals produced during illumination of photocatalytic materials can be used for decomposition of organic molecules adsorbed on so-called self-cleaning surfaces. Organic pollutants dispersed in water, air, or soil can also be destroyed by photocatalytic oxidation.

TiO₂ is a wide band gap photocatalyst, and thus, it needs ultraviolet (UV) light for excitation of photogenerated charge carriers and high photocatalytic activity.² There are innumerable permutations of research aimed to increase the absorption

of visible (VIS) light and the corresponding photocatalytic performance of TiO₂, for example, by doping/codoping, dye sensitization, or implementation of heterojunctions. However, the VIS light sensitization of photocatalysts remains a major challenge in the field.^{3,4} Therefore, further steps in material synthesis, understanding and process optimization are needed to broaden applications of photocatalytic systems, also from an economic point of view.

Different properties of materials can play a significant role in determining their photocatalytic activity. For example, surface states and facet orientations play an important role for adsorption of reactants and charge transfer during photo-reactions.^{5,6} In turn, diffusion and recombination of photogenerated charge carriers depend on the average size of nanoparticles or grains and grain boundaries.⁷ Photoinduced surface defects, such as oxygen vacancies, can act as trapping sites for charge carriers, which reduce the mobility, and reactivity of photogenerated holes.⁸ Moreover, pretreatment of TiO₂ surfaces with UV light enhances the production of active

Received: May 30, 2022

Accepted: September 2, 2022

sites even for photocatalytic purification processes driven by VIS light. The surface of TiO₂ is modified during absorption of UV light and a metastable surface structure is formed, which is closely related to the reverse superhydrophilic properties.⁹

The influence of organic additives for the formation of anatase TiO₂ has been studied for many years, especially in relation to the preparation of nanoporous anatase matrices for dye-sensitized solar cells¹⁰ and to photocatalysis.¹¹ Stabilization of titanium(IV) isopropoxide (TTIP) with acetylacetone (AcacH) and effects of AcacH on the film properties have been studied by several authors.^{12–14} Recently, it has been shown that the increase of the AcacH molar ratio in precursor solutions can increase the photocatalytic activity of the TiO₂ films.¹⁵ For example, a change of the TTIP: AcacH molar ratio from 1:4 to 1:8 resulted in an increase of the photodegradation reaction-rate constant under UV light by about a factor of 10.¹⁵ At the same time, an increase of the concentration of carbon species was observed at the TiO₂ surfaces by X-ray photoelectron emission spectroscopy (XPS).¹⁵ Therefore, the enhanced photocatalytic performance was tentatively explained by the effect of carbon species on the surface of TiO₂ films. However, the cause of the influence of AcacH in the precursor solution on the photocatalytic activity of anatase TiO₂ films remains unclear.

Surface photovoltage (SPV) signals arise due to separation of photogenerated charge carriers in space (see, for example, the review¹⁶). In contrast to other techniques, SPV gives specific information about the direction of charge separation. Usually, positive or negative signs of SPV signals are related to preferential separation of positive or negative charge toward the external surface. Charge separation can be driven by different processes, such as drift in built-in electrical fields or asymmetric trapping (see for details also ref 19). Furthermore, a sign can change during an SPV transient, for example, if electrons and holes are trapped both at the surface whereas the charge carriers with the highest trap density relax faster than the charge carriers with the lowest trap density. Transient SPV spectroscopy^{17–19} is based on the measurement of SPV signals as functions of photon energy and relaxation time. This allows to select contributions to SPV signals with opposite sign and, therefore, gives the opportunity to distinguish between the relaxation in certain time domains of electrons or holes which have been preferentially transferred toward the external surface. In this work, the spectral range of transient SPV spectroscopy was extended to 5.5 eV. The measurements were performed with a perforated electrode and a charge amplifier.²⁰

By applying transient surface photovoltage spectroscopy, we showed for the first time that trapping of electrons at anatase TiO₂ thin films can be minimized by increasing the amount of acetylacetone (AcacH) in the titanium(IV) isopropoxide (TTIP) precursor solution—a widely used precursor by many research groups for synthesis of TiO₂. The passivation of electron traps at the surface of anatase TiO₂ films correlated with a strong increase of photodegradation rate constants. These results open a new way to unravel limiting electronic processes not only at photocatalytic surfaces but also at other kinds of surfaces and buried interfaces.

2. EXPERIMENTAL SECTION

Anatase TiO₂ thin films were synthesized by ultrasonic spray pyrolysis from mixtures of titanium(IV)isopropoxide (TTIP, Sigma-Aldrich) as a titanium source, acetylacetone (AcacH, Sigma-Aldrich) as a stabilizing agent, and ethanol as a solvent (see for details also ref

15). After deposition on glass substrates at 350 °C, the layers were annealed at 500 °C in air for 1 h. The TTIP: AcacH molar ratio ratio was changed between 1:1 and 1:20. The mean crystallite size of anatase TiO₂ was on the order of 40 nm for all layers and the layers had a thickness of 300 to 400 nm.¹⁵ All films irrespective of the amount of AcacH in the precursor solution showed reversed photoinduced superhydrophilic properties after 15 min of UV-A irradiation (Table S1). Moreover, photoinduction of TiO₂ surface with UV-A treatment before experiments strongly enhanced the photocatalytic activity under VIS light (Figure S1). Secondary-ion-mass spectrometry (SIMS) measurements showed a correlation of the carbon distribution with the spray cycles whereas the absolute concentrations of carbon atoms is independent of the TTIP: AcacH ratio (Figure S2).

Before performing transient SPV spectroscopy measurements, the samples were compared by the measurements of the light induced change of the contact potential difference (Δ CPD) with a Kelvin probe (Besocke delta phi) in air. For illumination, a Xe lamp with a quartz prism monochromator (SPM2, Carl Zeiss Jena) was used.

A preparation of charge-selective contacts is not necessary for obtaining SPV signals on a thin film. In the study at hand, for the TiO₂/glass system, there are two interfaces: (i) the interface between glass and TiO₂ layer and (ii) the interface between TiO₂ and environment (free surface of TiO₂ films). The interface between glass and the TiO₂ layer has much lower trap density than the free surface, making the asymmetry for getting the SPV signal. The free surface is exposed to molecules and the defect density/trap density at the free surface is much higher so that it allows to probe the changes at the external free surface.

SPV transients were excited with laser pulses from a tunable Nd:YAG laser (NT230-50, $\lambda = 216\text{--}2600$ nm) that is equipped with a spectral cleaning unit, EKSPLA. The laser pulses had a width of 3–5 ns, and the photon flux was nearly constant between about 2.4 and 4 eV (see Figure S3 and for more details see ref 18).

SPV transients were measured with a fixed perforated electrode, a charge amplifier (Elektronik Manufaktur Mahlsdorf, resolution time 7 ns) and an oscilloscope card (Gage, CSE 1622-4GS). The SPV signal height was calibrated with a periodic square wave signal ($1 V_{pp}$) applied at the back side of the sample (for more details see ref 20). The repetition rate of the laser pulses was 1 Hz and 10 transients were averaged. SPV signals were analyzed as the difference to signals of a bare substrate to discriminate parasitic background.

3. RESULTS AND DISCUSSION

3.1. DC (Kelvin Probe) SPV Spectroscopy. Figure 1 shows the spectra of Δ CPD for layers of anatase TiO₂

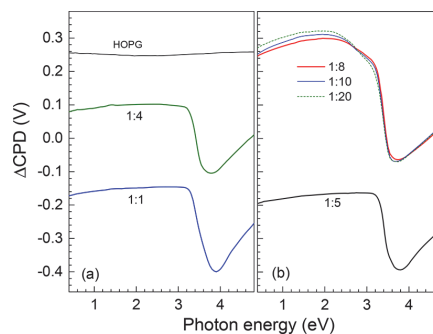


Figure 1. Spectra of the contact potential difference for layers of anatase TiO₂ thin films synthesized with TTIP: AcacH = 1:1 and 1:4 (a, green and blue lines, respectively) and 1:5, 1:8, 1:10, and 1:20 (b, black, red, blue, and dashed green lines, respectively). HOPG is shown for comparison.

synthesized with TTIP: AcacH = 1:1, 1:4, 1:5, 1:8, 1:10, and 1:20. Highly oriented pyrolytic graphite (HOPG) is shown for comparison. The Δ CPD of HOPG did not show an influence of illumination. For HOPG, the value of Δ CPD was about 0.26 V, which corresponds to the work function (WF) of HOPG. At low photon energies, the values of Δ CPD were about -0.17 , 0.08 , -0.19 , 0.247 , 0.254 , and 0.273 V for TTIP: AcacH of 1:1, 1:4, 1:5, 1:8, 1:10, and 1:20, respectively. In air, the WF of HOPG can be used as a reference (WF of HOPG in air: 4.475 eV).²¹ Therefore, the values of WF were 4.045 , 4.295 , 4.025 , 4.462 , 4.469 , and 4.488 eV for TiO₂ thin films prepared at TTIP: AcacH of 1:1, 1:4, 1:5, 1:8, 1:10, and 1:20, respectively. The changes of the WF of anatase TiO₂ thin films is in qualitative agreement with the shift of the valence band in X-ray photoelectron spectroscopy (XPS) measurements.²² The values of WF for TiO₂ thin films prepared at TTIP: AcacH of 1:8, 1:10, and 1:20 were larger than for the other films and very similar. In contrast, the values of WF for TiO₂ thin films prepared at TTIP: AcacH of 1:1, 1:4, and 1:5 scattered significantly. Therefore, the surface dipole formed on TiO₂ thin films prepared at TTIP: AcacH of 1:8, 1:10, and 1:20 was practically constant, whereas the negative surface charge was larger than for the other films.

Strong changes of the slopes of the Δ CPD spectra of anatase (Figure 1) set on at about 3.2 eV, which usually referred to the band gap of anatase TiO₂. The change of the slope of the Δ CPD is related to the evolution of SPV signals, whereas the signs of the light induced Δ CPD and SPV are opposite. The corresponding maximum SPV signals were reached at photon energies between about 3.7 and 3.9 eV and amounted, with respect to Δ CPD at the lowest photon energies, to 0.23 , 0.185 , 0.202 , 0.309 , 0.323 , 0.342 V for TTIP: AcacH = 1:1, 1:4, 1:5, 1:8, 1:10, and 1:20, respectively. Therefore, photogenerated electrons and holes were preferentially separated toward the bulk and external surface of the layers of anatase, respectively, whereas charge separation was stronger for TTIP: AcacH of 1:8, 1:10, and 1:20 than for 1:1, 1:4, and 1:5. However, this overall charge separation does not give specific information about fast and local processes of charge separation, which are most important for photocatalysis.

3.2. Contour Plots of Transient SPV Spectroscopy.

Figure 2 shows the contour plots of transient SPV spectroscopy, that is, the color-coded SPV signals as a map in photon energy and time, for TTIP: AcacH of 1:1, 1:4, 1:5, 1:8, 1:10, and 1:20. For TTIP: AcacH of 1:1, negative SPV signals set at around 3.1 eV and reached values up to more than -100 mV in the spectral range between about 3.4 and 4 eV for times shorter than 10 μ s. At longer times (from about 10 ms at 3.3 eV to about 100 μ s at 4.8 eV), the sign of the SPV signals changed to positive and positive signals were measured up to the order of 20 mV at longer times and higher photon energies. Below the band gap, positive SPV signals appeared between 2 and 2.5 eV at times up to about 1 μ s.

For TTIP: AcacH = 1:4, negative SPV signals appeared as well but in a narrower spectral range between about 3.2 and 3.7 eV and for times up to about 1 ms. At longer times, positive SPV signals were observed in this spectral range and over the whole time domain at higher photon energies. For TTIP: AcacH = 1:5, small negative signals up to about -20 mV appeared in a range between about 3.2 and 3.6 eV for times up to about 20 μ s and positive SPV signals were measured at longer times and in the whole domain for photon energies

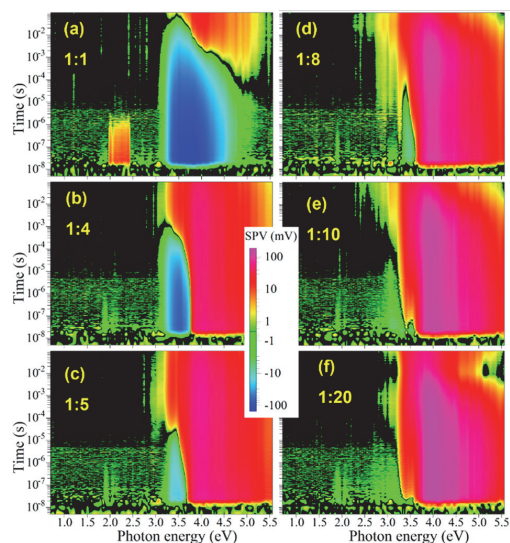


Figure 2. Contour plots of transient SPV spectroscopy for layers of anatase TiO₂ thin films synthesized with TTIP: AcacH = 1:1, 1:4, 1:5, 1:8, 1:10, and 1:20 (a–f, respectively). Remark: A contour plot shows the color-coded SPV signals as a map in photon energy and time. Note the logarithmic color scale for the SPV signals.

above 3.6 eV, whereas positive SPV signals set on at longer times at photon energies of about 2.8 eV.

For TTIP: AcacH = 1:8, very small negative signals up to about -5 mV still appeared for times up to about 20 μ s at 3.4 eV. At longer times, positive SPV signals set on at photon energies of about 2.4 eV and the positive SPV signals reached values up to about 100 mV. Only a tiny rest of negative SPV signals appeared in the contour plot for TTIP: AcacH = 1:10 whereas it was very similar to that for TTIP: AcacH = 1:8 in the other parts. Incidentally, regarding the reproducibility of preparation and measurements, Figure S4 compares the contour plots of transient SPV spectroscopy for the first and second series of the films with TTIP:AcacH 1:8 synthesized in the same way in the different times. A comparison between panels a and b shows the excellent reproducibility of the preparation. After annealing, the amount of electron traps as well as of electronic states in the band gap of anatase increased. For TTIP: AcacH = 1:20, negative SPV signals of up to about 1 – 2 mV were observed only between 3.3 and 3.6 eV for times shorter than about 30 ns. Furthermore, the highest positive SPV signals of up to about 170 mV were measured for TTIP: AcacH = 1:20. In addition, the positive SPV signals decreased drastically for TTIP: AcacH = 1:20 at photon energies above 5 eV and times longer than 2 – 3 ms.

3.3. Spectral Analysis and Correlation of Urbach Tails with Decomposition Rates. SPV spectra were extracted from the contour plots at times of 30 ns, 10 μ s, 1 ms, and 94 ms after switching on the laser pulses (see Figure 3) and are given for layers of anatase TiO₂ synthesized with TTIP: AcacH = 1:1, 1:4, 1:5, 1:8, and 1:20 (a–e, respectively). At the shortest times for TTIP: AcacH = 1:1 and at the longest times for TTIP: AcacH = 1:20, the negative and positive SPV signals increased exponentially at the onsets and were fitted with a characteristic tail energy of $E_t = 60$ meV. This tail energy is

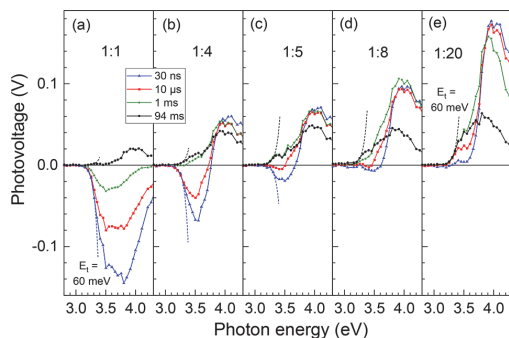


Figure 3. SPV spectra for layers of anatase TiO₂ thin films synthesized with TTIP: AcAcH = 1:1, 1:4, 1:5, 1:8, and 1:20 (a–e, respectively) obtained at times of 30 ns, 10 μs, 1 ms, and 94 ms after switching on the laser pulses (black, red, blue, and green lines, respectively). The dotted blue and dashed black lines correspond to exponential tails with $E_t = 60$ meV at 30 ns and 94 ms, respectively. The value of E_t was obtained by fitting for TTIP:AcAcH = 1.1 (at 30 ns) and 1:20 (at 94 ms).

close to that of anatase single crystals, depending also on polarization,²³ what gives evidence for one dominating mechanism of charge separation. Furthermore, other onsets of the SPV signals can also be treated by an exponential increase with $E_t = 60$ meV (see the dashed and dotted lines in Figure 3).

Most of the onset regions of SPV signals are characterized by the low signals case with one dominating mechanism of charge separation, i.e., the SPV signals are proportional to the generation rate or absorption coefficient. Closer to the indirect or optical band gap ($E_{ig} = 3.46$ eV²⁴ or $E_{og} = 3.42$ or 3.46 eV depending on polarization,²³ respectively), the low signal case is no longer valid and dominating mechanisms of charge separation can change. For example, a change from negative toward positive SPV signals set on slightly above E_{ig} at 30 ns and 10 μs for TTIP: AcAcH = 1:4, 1:5, 1:8, and 1:20 and at 1 ms for TTIP: AcAcH = 1:1, whereas even the sign did change for TTIP: AcAcH = 1:4, 1:5, and 1:8. Furthermore, a change from negative toward positive SPV signals set on above 3.8 eV at 30 ns and 10 μs for TTIP: AcAcH = 1:1. For the other samples and times, a steep increase toward more positive SPV signals was observed above 3.8 eV what is close to the direct band gap of anatase (3.97 eV).²⁴

For photocatalytic oxidation reactions, photogenerated holes shall be separated toward the external surface, i.e., corresponding SPV signals shall be positive. Positive SPV signals were observed for all samples at 94 ms. As a parameter, the amplitude of the exponential onset of positive SPV signals (A_{Urbach}) measured at 94 ms was correlated with the degradation rates of stearic acid under illumination in UV-A and visible light (k_{UV} and k_{VIS} , red circles and blue triangles, respectively) in Figure 4 (values were taken from ref 15). A square dependence of k_{UV} and k_{VIS} on A_{Urbach} was found for TTIP: AcAcH = 1:1, 1:4, 1:5, and 1:8 and for TTIP: AcAcH = 1:1, 1:4, and 1:5. Therefore, k_{UV} and k_{VIS} were limited by photogeneration in these regions. At higher values of TTIP: AcAcH, the degradation rates saturated, i.e., limitation by photogeneration changed to limitation by another process as, for example, charge transfer rates into reactive species adsorbed at the surface of anatase nanoparticles.

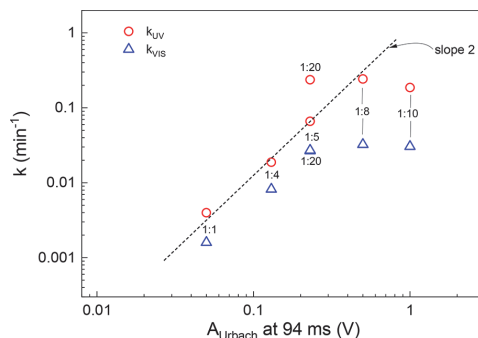


Figure 4. Correlation plots between A_{Urbach} measured at 94 ms and the photocatalytic degradation rates of stearic acid under illumination in UV-A and visible light (k_{UV} and k_{VIS} , red circles and blue triangles, respectively). The values of k_{UV} and k_{VIS} were reproduced from ref 15. Copyright 2019, MDPI open access Creative Commons CC BY 4.0 license. The numbers correspond to the TTIP: AcAcH ratios.

3.4. Transient Analysis and Correlation of Back Transfer Rates with Decomposition Rates.

For getting a deeper insight into processes of charge separation and relaxation, SPV transients were selected at characteristic energies of 2.4, 3.3, 3.6, and 4.0 eV. The absorption lengths in anatase are about 10 μm,²³ 300 nm, and 30 nm²⁵ at the photon energies of 3.3, 3.6, and 4.0 eV, respectively. Therefore, excitation at the photon energies of 3.3, 3.6, and 4.0 eV corresponded to homogeneous absorption across the whole anatase layer, to homogeneous absorption across the first monolayers of anatase TiO₂ crystallites and to preferential absorption within the first monolayer of crystallites in the thin films, respectively.

Figure 5 shows the SPV transients excited at characteristic energies of 2.4, 3.3, 3.6, and 4.0 eV for layers of anatase nanoparticles synthesized with TTIP: AcAcH = 1:1, 1:4, 1:5, 1:8, and 1:20 (a–e, respectively). For excitation at 2.4 eV, a transient appeared only for TTIP: AcAcH = 1:1. For excitation at 3.3 eV, the amplitudes at about 20 ns after the onsets of the

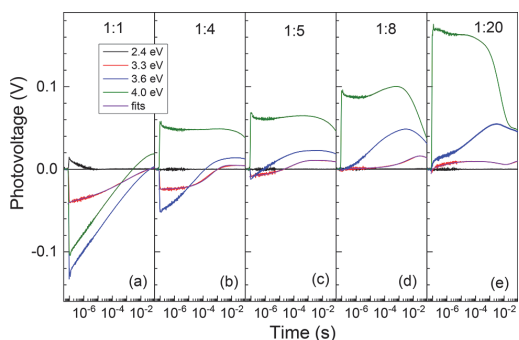


Figure 5. SPV transients for layers of anatase TiO₂ thin films synthesized with TTIP: AcAcH = 1:1, 1:4, 1:5, 1:8, and 1:20 (a–e, respectively) excited at photon energies of 2.4, 3.3, 3.6, and 4.0 eV (black, red, blue, and green lines, respectively). The onsets of the laser pulses were shifted to 80 ns in order to show the baseline on the logarithmic time scale. The solid pink lines are fits for excitation at 3.3 eV according to eq 1.

laser pulses decreased from -40 to -24 , -8 , and about -1 and -2 mV and the time at which the sign of the SPV signals changed to positive from 40 to 1 ms, 20 μ s, and about 30 and 30 ns (after switching on the laser pulses) for TTIP: AcacH = 1:1, 1:4, 1:5, 1:8, and 1:20, respectively. For excitation at 3.6 eV, the amplitudes at about 20 ns after the onsets of the laser pulses changed from -130 to -51 , -12 , and about -1 and 0 mV for TTIP: AcacH = 1:1, 1:4, 1:5, 1:8, and 1:20, respectively, whereas the time at which the sign changed from negative to positive became shorter for TTIP: AcacH = 1:4 and 1:5. For excitation at 4.0 eV, the amplitudes at about 20 ns after the onsets of the laser pulses changed strongly from -104 to $+57$, $+68$, $+95$, and $+175$ mV for TTIP: AcacH = 1:1, 1:4, 1:5, 1:8, and 1:20, respectively.

With respect to the facts of homogeneous absorption and small signals case for excitation at 3.3 eV, it is reasonable to fit the related SPV transients. SPV transients with only one component can often be fitted by stretched exponentials, for example, when relaxation is dominated by tunneling steps from localized states (see, for example ref 26). Fitting of SPV transients with a minimum number of components gives information about limiting processes involved in charge separation and relaxation. The transients excited at 3.3 eV could be well fitted with one positive and one negative stretched exponentials for TTIP: AcacH = 1:4, 1:5, and 1:8 (amplitudes, time constants, and stretching parameters for negative and positive components are denoted by A_e and A_h , τ_e and τ_h , and β_e and β_h in equation 1, respectively). An additional logarithmic decay factor ($C_1(t)$) was needed for fitting the negative stretched exponential component for TTIP: AcacH = 1:1. A logarithmic decay is close to relaxation limited by distant dependent tunneling recombination.²⁷ Furthermore, an additional positive component increasing in time by a (stretched) logistic growth ($C_2(t)$) was needed for fitting the SPV transient for TTIP: AcacH = 1:20. In general, SPV signals can grow in time, for example, due to diffusion.²⁸ Here, the slow increase of SPV of positive signals for TTIP: AcacH = 1:20 can be assigned to diffusion of electrons toward the bulk of the layer of anatase nanoparticles (interparticle transport limited by trapping).

$$\text{SPV}(t) = -C_1(t) \cdot A_e \cdot \exp\left[-\left(\frac{t}{\tau_e}\right)^{\beta_e}\right] + A_h \cdot \exp\left[-\left(\frac{t}{\tau_h}\right)^{\beta_h}\right] + C_2(t) \quad (1)$$

with

$$C_1(t) = 1 - b \cdot \ln^2\left(1 + \frac{t}{\tau_c}\right) \text{ for TTIP: AcacH} = 1:1 \quad (1')$$

and

$$C_2(t) = A_L \cdot \left(\frac{1}{1 + \exp\left[-\left(\frac{t}{\tau_L}\right)^{\beta_L}\right]} - \frac{1}{2} \right) \text{ for TTIP: AcacH} = 1:20 \quad (1'')$$

Additionally, a sum of two negative stretched exponentials was needed for obtaining reasonably well fits of the SPV transients for TTIP: AcacH = 1:8 and 1:10. Fitted transients

are shown in Figure 5 for TTIP: AcacH = 1:1, 1:4, 1:5, 1:8, and 1:20. The parameters b , τ_c , A_L , τ_L , and β_L amounted to 0.002 , 0.5 ns, 21 mV, 0.2 s, and 0.8 , respectively.

The trends of the fitting parameters for the positive and negative stretched exponentials are summarized in Figure 6 for

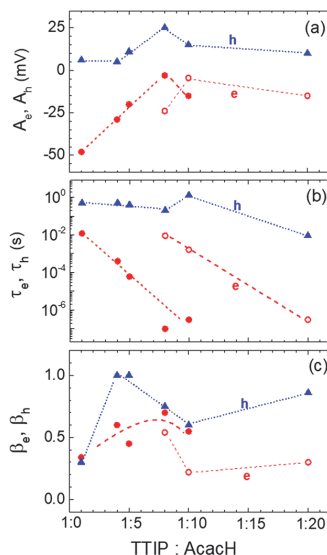


Figure 6. Dependencies of the fit parameters A_e and A_h (a), τ_e and τ_h (b), and β_e and β_h (c) on TTIP:AcacH for the transients measured at 3.3 eV. The red circles and blue triangles in panels a–c are related to the electron and hole components, respectively. The filled and open red circles represent the two components of the negative stretched exponentials regarding to the trends of τ_e . The dotted and dashed lines in panels a–c are guides for the eye.

A_e and A_h (a), τ_e and τ_h (b), and β_e and β_h (c). The most striking difference appeared in the trends of τ_e , which strongly decreased from about 10 ms at TTIP: AcacH = 1:1 to about 0.1 – 0.3 μ s for the fast component at TTIP: AcacH = 1:8 and 1:10 and from about 10 ms for the slow component at TTIP: AcacH = 1:8 to about 0.3 μ s at TTIP: AcacH = 1:20. Therefore, the dominating relaxation mechanism of electrons separated in space changed around TTIP: AcacH = 1:8. The values of τ_h were mainly limited by the repetition rate of the laser pulses and ranged, therefore, between about 0.2 to 1 s for TTIP: AcacH = 1:1–1:10, depending also on the stretching parameters and additional slow processes. For TTIP: AcacH = 1:20, τ_h was on the order of 10 ms so that an additional slow process could be observed. It can be supposed that similar additional slow processes were present but masked by the dominating slow relaxation of holes separated toward the external surface for lower values of TTIP: AcacH.

A_e decreased from about -48 mV to -3 mV between TTIP: AcacH = 1:1 and 1:8 which correlates with an increase of the photocatalytic degradation rates of stearic acid in this range.¹⁵ A_h or A_e show a maximum or a local maximum at TTIP: AcacH = 1:8 if considering the sum of the amplitudes of both negative stretched exponentials for TTIP: AcacH = 1:8 and 1:10. In contrast to τ_e , the values of β_e did not show very clear trends. The lowest values of β_e were found for TTIP: AcacH = 1:1, 1:10 (slow component), and 1:20. The highest value of β_e

was obtained for TTIP: AcacH = 1:8 (fast component). Interestingly, β_h showed a strong increase from about 0.3 at TTIP: AcacH = 1:1 to 1 at TTIP: AcacH = 1:4 and 1:5 and a decrease to 0.6 at TTIP: AcacH = 1:10, followed by an increase to 0.86 at TTIP: AcacH = 1:20.

The values of k_{UV} and k_{VIS} are correlated with τ_e in Figure 7. An anticorrelation with a square dependence, i.e., $k_{UV(VIS)} \propto$

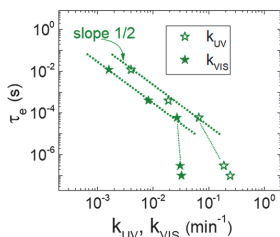


Figure 7. Correlation between k_{UV} and k_{VIS} (open and filled stars, respectively) and τ_e . The values of k_{UV} and k_{VIS} were taken after.¹⁵

τ_e^{-2} (corresponds to the electron back transfer rate), has been found for TTIP: AcacH = 1:1, 1:4, and 1:5. For TTIP: AcacH = 1:8 and 1:10, the correlation was much weaker. The correlation of the electron back transfer rates with the photocatalytic degradation rates is also similar to the correlation between increasing $k_{UV(VIS)}$ at decreasing A_e (not shown).

As remark, in principle, fits can also be performed for excitation at higher photon energies. However, components cannot be so obviously assigned to given processes since charge transport shall be considered due to gradients in photogeneration. Furthermore, saturation phenomena can dominate at higher photon energies due to (very) high absorption so that the interpretation of fitting parameters is less straightforward in relation to the photocatalytic activity.

3.5. Suitable Mechanism of AcacH-Induced Passivation of Electron Traps at TiO₂ Surfaces. The experimental results presented above show that the sign of the transient SPV signal changes from negative to positive with increasing TTIP:AcacH ratio. This is directly related to the electron concentration at the surface of the specimens, which is vastly reduced with an increase of the AcacH concentration in the precursor solution. The source of electrons is widely believed to be oxygen vacancies (V_O) that can act as double donors. For rutile and anatase TiO₂, the ionization energies of the (0/+) and (+/2+) adiabatic transitions amount to $E_I = 0.1$ and 0.4 eV and <0.1 and 0.3 eV, respectively.²⁹ The question is which mechanisms are behind the processes leading to a reduction of electron concentration at the TiO₂ anatase surfaces. Considering the conditions of the experiments, a decrease of the electron concentration can occur when (i) the concentration of oxygen vacancies decreases, (ii) electrons are trapped at localized states, induced by incorporation of carbon species in the TiO₂ lattice, and (iii) absorption of O–H complexes at the sample surface inducing capture of charge carriers from the TiO₂ surface. With respect to mechanism (i), an increased amount of AcacH in the precursor solution leads to more fuel for the combustion process, first, at the stage of the TiO₂ film deposition by USP at 350 °C in air, and second, during crystallization of the layers in the subsequent air treatment at 500 °C. The latest process is more intensive, in which the

oxygen partial pressure $P(O_2)$ practically remains constant (considering the open atmospheric conditions), whereas the partial pressures of CO₂ and H₂O can significantly increase by increased temperature of AcacH-assisted combustion process. It is likely that a higher temperature and higher CO₂ partial pressures can raise oxygen chemical potentials that could lead to a reduction of the V_O concentration, thereby causing a decrease of the free electron concentration. (ii) On the other hand, within the same process, the carbon impurity incorporates into the lattice and probably also accumulates at the grain boundaries of TiO₂, as suggested by cumulative results of XRD peak shift and XPS and SIMS analysis (Figures S5, S6, and S2). Incorporation of carbon atoms into the lattice of anatase TiO₂ can occur through a substitutional mechanism at the oxygen sites³⁰ or by taking an interstitial site.^{31,32} Thus, the carbon impurity may introduce localized states³³ through which the electrons are trapped and thereby, decreasing the overall electron concentration. (iii) While the former mechanisms can occur at the surface and in the bulk of the samples, transient SPV measurements are surface sensitive, and a change of the surface composition or surface chemistry could also result in the observed decreased electron concentration. Since the SPV measurements are performed in air, it is conceivable that the adsorption of O–H groups could be responsible for the decrease of the electron concentration. Initially, neutral O–H complexes could adsorb on the sample surface, and subsequently, they could capture charge carriers from the TiO₂ surface region thereby effectively reduce the surface electron concentration. However, to elucidate the exact microscopic mechanism responsible for the reduction of electrons at the sample surface additional measurements are required.

4. CONCLUSIONS

Due to transport limitation across grain boundaries and symmetry of charge selectivity embedded by neighbored grains in anatase TiO₂, fast charge separation was related to charge transfer within the anatase TiO₂ crystallites closest to the external surface (first monolayer). The negative and positive stretched exponentials belonged to relaxation of photogenerated electrons and holes separated in space within the duration time of the laser pulse (fast charge separation). The correlation between the amplitudes of the Urbach tails (positive component at long times) and the photocatalytic activity gave evidence that fast separation of photogenerated holes was caused by hole transfer toward the external surface. Furthermore, the correlation of the decreasing τ_e with an increasing photocatalytic degradation rate under both ultraviolet and visible light gave evidence that electrons separated toward the external surface strongly limited the photocatalytic activity for oxidation of organic molecules with anatase nanoparticles. It was demonstrated that an increased amount of AcacH in the TTIP solution led to a passivation of electron traps at the anatase surface and to a reduction of the electron back transfer rate. Suitable mechanisms of AcacH-induced passivation of electron traps at TiO₂ surfaces were analyzed and discussed, providing new and complementary insights in understanding the electronic processes in photocatalytic systems and related buried interfaces.

■ ASSOCIATED CONTENT

SI Supporting Information

The Supporting Information is available free of charge at <https://pubs.acs.org/doi/10.1021/acsami.2c09032>.

Contact angles of anatase TiO₂ thin films, reversible activation of anatase TiO₂ thin films under illumination with UV light, carbon content in anatase TiO₂ thin films, photon flux spectrum in transient SPV spectroscopy, the structural properties of TiO₂ thin films, and the C 1s core level of TiO₂ thin films (PDF)

■ AUTHOR INFORMATION

Corresponding Authors

Thomas Dittrich – Helmholtz Zentrum Berlin für Materialien und Energie GmbH, Institut für Silizium-Photovoltaik, D-12489 Berlin, Germany; orcid.org/0000-0002-2698-9481; Email: dittrich@helmholtz-berlin.de

Nicolae Spalatu – Tallinn University of Technology, Department of Materials and Environmental Technology, 19086 Tallinn, Estonia; orcid.org/0000-0003-0234-2170; Email: nicolae.spalatu@taltech.ee

Authors

Jekaterina Sydorenko – Tallinn University of Technology, Department of Materials and Environmental Technology, 19086 Tallinn, Estonia; orcid.org/0000-0001-7675-0471

Norbert H. Nickel – Helmholtz Zentrum Berlin für Materialien und Energie GmbH, Institut für Silizium-Photovoltaik, D-12489 Berlin, Germany

Arvo Mere – Tallinn University of Technology, Department of Materials and Environmental Technology, 19086 Tallinn, Estonia

Malle Krunks – Tallinn University of Technology, Department of Materials and Environmental Technology, 19086 Tallinn, Estonia; orcid.org/0000-0003-4658-4403

Ilona Oja Acik – Tallinn University of Technology, Department of Materials and Environmental Technology, 19086 Tallinn, Estonia

Complete contact information is available at: <https://pubs.acs.org/doi/10.1021/acsami.2c09032>

Author Contributions

The manuscript was written through contributions of all authors. All authors have given approval to the final version of the manuscript.

Funding

This study was funded by the Estonian Research Council project PRG627 and PSG689. The Estonian Centre of Excellence project TK141 (TAR16016EK). The European Union's Horizon2020 program under the ERA Chair project SGSOLAR, grant agreement No 952509.

Notes

The authors declare no competing financial interest.

■ ABBREVIATIONS

SPV, surface photovoltage; AcAcH, acetylacetone; TTIP, titanium(IV)isopropoxide; CPD, contact potential difference

■ REFERENCES

- (1) Fujishima, A.; Honda, K. Electrochemical Photolysis of Water at a Semiconductor Electrode. *Nature* **1972**, *238*, 37.
- (2) Etacheri, V.; Di Valentin, C.; Schneider, J.; Bahnemann, D.; Pillai, S. C. Visible-Light Activation of TiO₂ Photocatalysts: Advances in Theory and Experiments. *Journal of Photochemistry and Photobiology C: Photochemistry Reviews*. **2015**, *25*, 1.
- (3) Navidpour, A. H.; Hosseinzadeh, A.; Zhou, J. L.; Huang, Z. Progress in the Application of Surface Engineering Methods in Immobilizing TiO₂ and ZnO Coatings for Environmental Photocatalysis. *Catal. Rev. - Sci. Eng.* **2021**, *1*.
- (4) Banerjee, S.; Dionysiou, D. D.; Pillai, S. C. Self-Cleaning Applications of TiO₂ by Photo-Induced Hydrophilicity and Photocatalysis. *Appl. Catal. B: Environmental*. **2015**, *176-177*, 396.
- (5) Pan, F.; Wu, K.; Li, H.; Xu, G.; Chen, W. Synthesis of {100} Facet Dominant Anatase TiO₂ Nanobelts and the Origin of Facet-Dependent Photoreactivity. *Chem. - A Eur. J.* **2014**, *20* (46), 15095–15101.
- (6) Stefanov, B. I.; Niklasson, G. A.; Granqvist, C. G.; Österlund, L. Gas-Phase Photocatalytic Activity of Sputter-Deposited Anatase TiO₂ Films: Effect of (0 0 1) Preferential Orientation, Surface Temperature and Humidity. *J. Catal.* **2016**, *335*, 187.
- (7) Quirk, J. A.; Miao, B.; Feng, B.; Kim, G.; Ohta, H.; Ikuhara, Y.; McKenna, K. P. Unveiling the Electronic Structure of Grain Boundaries in Anatase with Electron Microscopy and First-Principles Modeling. *Nano Lett.* **2021**, *21*, 9217.
- (8) Dagdeviren, O. E.; Glass, D.; Sapienza, R.; Cortés, E.; Maier, S. A.; Parkin, I. P.; Grütter, P.; Quesada-Cabrera, R. The Effect of Photoinduced Surface Oxygen Vacancies on the Charge Carrier Dynamics in TiO₂ Films. *Nano Lett.* **2021**, *21*, 8348.
- (9) Sano, T.; Puzenat, E.; Guillard, C.; Geantet, C.; Matsuzawa, S.; Negishi, N. Improvement of Photocatalytic Degradation Activity of Visible-Light-Responsive TiO₂ by Aid of Ultraviolet-Light Pretreatment. *J. Phys. Chem. C* **2009**, *113*, 5535.
- (10) Chang, C. H.; Chuang, C. H.; Zhong, D. Y.; Lin, J. C.; Sung, C. C.; Hsu, C. Y. Synthesized TiO₂ Mesoporous by Addition of Acetylacetone and Graphene for Dye Sensitized Solar Cells. *Coatings* **2021**, *11*, 796.
- (11) Byrne, C.; Fagan, R.; Hinder, S.; McCormack, D. E.; Pillai, S. C. New Approach of Modifying the Anatase to Rutile Transition Temperature in TiO₂ Photocatalysts. *RSC Adv.* **2016**, *6* (97), 95232–95238.
- (12) Juma, A. O.; Acik, I. O.; Mikki, V.; Mere, A.; Krunks, M. Effect of Solution Composition on Anatase to Rutile Transformation of Sprayed TiO₂ Thin Films. *Thin Solid Films* **2015**, *594*, 287.
- (13) Kaltsum, U.; Kurniawan, A. F.; Nurhasanah, I.; Priyono, P. The Role of Concentration Ratio of TTiP: AcAc on the Photocatalytic Activity of TiO₂ Thin Film in Reducing Degradation Products of Used Frying Oil. *Bull. Chem. React. Eng. & Catal.* **2017**, *12* (3), 430–436.
- (14) Siwińska-Stefańska, K.; Zdzarta, J.; Paukszta, D.; Jesionowski, T. The Influence of Addition of a Catalyst and Chelating Agent on the Properties of Titanium Dioxide Synthesized via the Sol–Gel Method. *J. Sol-Gel Sci. Technol.* **2015**, *75*, 264–278.
- (15) Spiridonova, J.; Katerski, A.; Danilson, M.; Krichevskaya, M.; Krunks, M.; Oja Acik, I. Effect of the Titanium Isopropoxide:Acetylacetone Molar Ratio on the Photocatalytic Activity of TiO₂ Thin Films. *Molecules* **2019**, *24*, 4326.
- (16) Kronik, L.; Shapira, Y. Surface Photovoltage Phenomena: Theory, Experiment, and Applications. *Surf. Sci. Rep.* **1999**, *37*, 1.
- (17) Dittrich, T.; Valle Rios, L. E.; Kapil, S.; Gurieva, G.; Rujisamphan, N.; Schorr, S. Temperature Dependent Transient Surface Photovoltage Spectroscopy of a Cu_{1.95}Zn_{1.1}Sn_{0.96}Se₄ Kesterite Single Phase Powder. *Appl. Phys. Lett.* **2017**, *110*, 023901.
- (18) Fengler, S.; Kriegel, H.; Schieda, M.; Gutzmann, H.; Klassen, T.; Wollgarten, M.; Dittrich, T. Charge Transfer in C-Si(N²⁺)/TiO₂(ALD) at the Amorphous/Anatase Transition: A Transient Surface Photovoltage Spectroscopy Study. *ACS Appl. Mater. Interfaces* **2020**, *12*, 3140.

- (19) Dittrich, T.; Fengler, S. *Surface Photovoltage Analysis of Photoactive Materials* **2020**, DOI: [10.1142/q0227](https://doi.org/10.1142/q0227).
- (20) Dittrich, T.; Fengler, S.; Nickel, N. Surface Photovoltage Spectroscopy over Wide Time Domains for Semiconductors with Ultrawide Bandgap: Example of Gallium Oxide. *Phys. Status Solidi Appl. Mater. Sci.* **2021**, *218*, 2100167.
- (21) Hansen, W. N.; Hansen, G. J. Standard Reference Surfaces for Work Function Measurements in Air. *Surf. Sci.* **2001**, *481*, 172.
- (22) Spiridonova, J.; Mere, A.; Krunks, M.; Rosenberg, M.; Kahru, A.; Danilson, M.; Krichevskaya, M.; Oja Acik, I. Enhanced Visible and Ultraviolet Light-Induced Gas-Phase Photocatalytic Activity of TiO₂ Thin Films Modified by Increased Amount of Acetylacetone in Precursor Solution for Spray Pyrolysis. *Catalysts* **2020**, *10*, 1011.
- (23) Tang, H.; Lévy, F.; Berger, H.; Schmid, P. E. Urbach Tail of Anatase TiO₂. *Phys. Rev. B* **1995**, *52*, 7771.
- (24) Baldini, E.; Chiodo, L.; Dominguez, A.; Palumbo, M.; Moser, S.; Yazdi-Rizi, M.; Auböck, G.; Mallett, B. P. P.; Berger, H.; Magrez, A.; Bernhard, C.; Grioni, M.; Rubio, A.; Chergui, M. Strongly Bound Excitons in Anatase TiO₂ Single Crystals and Nanoparticles. *Nat. Commun.* **2017**, DOI: [10.1038/s41467-017-00016-6](https://doi.org/10.1038/s41467-017-00016-6).
- (25) Jellison, G. E.; Boatner, L. A.; Budai, J. D.; Jeong, B. S.; Norton, D. P. Spectroscopic Ellipsometry of Thin Film and Bulk Anatase (TiO₂). *J. Appl. Phys.* **2003**, *93*, 9537.
- (26) Fengler, S.; Zillner, E.; Dittrich, T. Density of Surface States at CdSe Quantum Dots by Fitting of Temperature-Dependent Surface Photovoltage Transients with Random Walk Simulations. *J. Phys. Chem. C* **2013**, *117*, 6462.
- (27) Kytin, V.; Duzhko, V.; Timoshenko, V. Y.; Rappich, J.; Dittrich, T. Injection Photovoltage in Thin Anodic TiO₂ Layers. *Phys. Status Solidi Appl. Res.* **2001**, *185*, R1.
- (28) Timoshenko, V. Y.; Duzhko, V.; Dittrich, T. Diffusion Photovoltage in Porous Semiconductors and Dielectrics. *Phys. Status Solidi Appl. Res.* **2000**, *182*, 227.
- (29) Deák, P.; Aradi, B.; Frauenheim, T. Quantitative Theory of the Oxygen Vacancy and Carrier Self-Trapping in Bulk TiO₂. *Phys. Rev. B* **2012**, DOI: [10.1103/PhysRevB.86.195206](https://doi.org/10.1103/PhysRevB.86.195206).
- (30) Lee, J. C.; Gopalan, A. I.; Saianand, G.; Lee, K. P.; Kim, W. J. Manganese and Graphene Included Titanium Dioxide Composite Nanowires: Fabrication, Characterization and Enhanced Photocatalytic Activities. *Nanomaterials* **2020**, *10*, 456.
- (31) Matsyina, Z. A.; Zaginaichenko, S. Y.; Schur, D. V. Hydrogen Solubility in Alloys under Pressure. *Int. J. Hydrogen Energy* **1996**, *21*, 1085.
- (32) Zhao, H.; Pan, F.; Li, Y. A Review on the Effects of TiO₂ Surface Point Defects on CO₂ Photoreduction with H₂O. *Journal of Materiomics*. **2017**, *3*, 17.
- (33) Di Valentin, C.; Pacchioni, G.; Selloni, A. Theory of Carbon Doping of Titanium Dioxide. *Chem. Mater.* **2005**, *17*, 6656.

Publication IV

J. Sydorenko, A. Mere, M. Krunk, M. Krichevskaya, I. Oja Acik. "Transparent TiO₂ thin films with high photocatalytic activity for indoor air purification", RSC Advances, 2022 (under review).


 Cite this: *RSC Adv.*, 2022, 12, 35531

Transparent TiO₂ thin films with high photocatalytic activity for indoor air purification†

 Jekaterina Sydorenko,^{id}*^a Arvo Mere,^{id}^a Malle Krunks,^{id}^a Marina Krichevskaya^{id}*^b and Ilona Oja Acik^{id}*^a

The development of low-material-quantity, transparent, anatase TiO₂ nanoparticle free thin films as photocatalytic materials together with a profound understanding of their photocatalytic activity under ultraviolet (UV-A) and visible (VIS) light is crucial for environmentally friendly indoor air photocatalytic coatings. In this work, a TiO₂ thin film modified by an increased amount of acetylacetone in the precursor solution with a material quantity of 0.2 mg cm⁻² was successfully deposited on a borosilicate glass substrate by ultrasonic spray pyrolysis. VOC degradation as a single model pollutant and in mixtures under different operating conditions was studied in a multi-section continuous flow reactor. Under UV-A the reaction rate constants for heptane and toluene oxidation as individual pollutants were 1.7 and 0.9 ppm s⁻¹, respectively. In 9 ppm VOC mixtures of acetaldehyde, acetone, heptane and toluene all the compounds were completely oxidized in a reaction time of less than 50 s. The TiO₂ film showed moderately high photocatalytic activity under VIS light. The conversions of acetaldehyde, acetone, heptane and toluene in 9 ppm VOC mixtures under VIS light reached 100, 100, 78 and 31%, respectively. The synthesized TiO₂ film shows promising ability in indoor air purification from VOCs. The results of this study give an extensive estimation of the thin film's photocatalytic efficiency and provide valuable data for future applications in environmental remediation.

 Received 14th October 2022
 Accepted 26th November 2022

DOI: 10.1039/d2ra06488j

rsc.li/rsc-advances

1. Introduction

People used to spend most of their time indoors. The COVID-19 pandemic forced people to stay in their homes for months and to take more care about disinfection and cleaning. Detergents and antiseptics release volatile organic compounds (VOCs) into the air, which are the primary source of poor indoor air quality and sick building syndrome.^{1,2} Such syndromes as allergies, rhinitis, asthma and conjunctivitis could appear.³ Not all technologies are suitable for indoor air purification at home. Photocatalytic oxidation is an ideal technology for air treatment that mimics nature's photochemical process, which is capable of completely mineralizing almost all types of organic pollutant while being both energy and cost-efficient.^{1,4,5}

TiO₂ is considered the most widely used photocatalyst. However, it must be mentioned that 99% of the TiO₂ studies (according to the Web of Science database only 285 papers were found with the keywords 'transparent film' out of 30 910 entries

with the keywords 'TiO₂ photocatalysis') focus on pre-fabricated nanopowders such as P25, PC500, and UV100. Nanopowder-based coatings with a thickness of several micrometres have a milky non-transparent surface.⁶ Despite this, several studies have been conducted on TiO₂ thin films and coatings,³⁻¹³ and still higher photocatalytic activity has been achieved using thick coatings prepared from TiO₂ nanopowders.⁷⁻⁹ In particular, Zou and co-authors obtained 55% conversion of 100 ppm of toluene after 60 min of ultraviolet (UV-A) irradiation on a 7 μm-thick TiO₂ coating prepared from P25 powder.⁹ However, the thin films with a thickness less than 1 μm needed up to 30 hours for the degradation of a couple of ppm of the same pollutant.^{10,11}

In the case of any photocatalytic application, special care should be taken over the material design so as not to be the source of extra pollution. The use of powders is not amenable since it leads to serious drawbacks related to the recovery and recycling of the photocatalyst. These are extremely significant issues, considering the risk of the release of nanosized particles of the material into the environment.¹² Thus, the deposition of well-adhered photocatalysts in the form of thick or thin films onto a substrate, such as glass or stainless steel depending on its destined application, is the most viable strategy for the technological application of photocatalytic nanomaterials in any field, and especially in the environmental sector.^{12,13} Polycrystalline TiO₂ thin films synthesized from a Ti-alkoxide precursor solution deposited by sol-gel spin/dip coating or

^aLaboratory of Thin Films Chemical Technologies, Department of Materials and Environmental Technology, Tallinn University of Technology, Ehitajate tee 5, 19086 Tallinn, Estonia. E-mail: jekaterina.spiridono@taltech.ee; ilona.oja@taltech.ee

^bLaboratory of Environmental Technology, Department of Materials and Environmental Technology, Tallinn University of Technology, Ehitajate tee 5, 19086 Tallinn, Estonia. E-mail: marina.krichevskaja@taltech.ee

† Electronic supplementary information (ESI) available. See DOI: <https://doi.org/10.1039/d2ra06488j>



spray pyrolysis methods is an old established route¹⁴ and it profits from lower quantities of materials ($<1 \text{ mg cm}^{-2}$), good adhesion properties and optical transparency in the visible range.^{10,13,15} Photocatalysts in the form of thin or thick films possess another advantage over nanopowders, making them applicable as multifunctional surfaces for photocatalytic VOC degradation: antimicrobial and self-cleaning properties.¹³ Thus, they are also applicable in medicine, *e.g.* to deactivate viruses.¹

However, there is still a technological gap in the development of thin transparent films with high photocatalytic activity under both UV-A and VIS light, which can be applied as a windowpane coating for indoor air treatment.^{13,16} The loss in photocatalytic performance in the case of thin films compared to nanopowders can be effectively compensated for by using a convenient deposition technique, selecting suitable substrates and properly tuning preparative conditions.¹² In order to increase the VIS light activity of a TiO_2 photocatalyst, several strategies, such as doping with vanadium,¹⁷ silver,¹⁸ nitrogen¹⁹ or composite materials such as $\text{TiO}_2/\text{ZrO}_2$ ²⁰ and $\text{TiO}_2/\text{carbon}$,^{21–23} have been applied. It has been found that with modification of TiO_2 the conversion of toluene under VIS light was in the range 35–80%, while for pure TiO_2 the conversion was below 10%.^{17–24} The incorporation of doping components into the TiO_2 lattice results in the formation of new mid-gap energy states, promoting the absorption of VIS light.^{17–22}

Moreover, when designing the photocatalyst, it must be taken into account that indoor air is a challenging source of pollution, as air in total could contain a wide range of VOCs in small concentrations (ppb). Many VOCs have similar structures, which makes it difficult to distinguish them in a gas mixture. Therefore, it is important to have a non-selective photocatalyst and to study the synergistic effects of VOC photocatalytic oxidation in the mixtures. There are only a few studies where photocatalytic oxidation of VOC mixtures in air was investigated, and most of these studies still consider nanopowders or nanopowder-based coatings.^{7,8,11,17,18,25} The use of transparent thin films is rather limited due to their lower activity. It should be highlighted that in this paper the term ‘thin film’ means a transparent layer of TiO_2 less than 500 nm thick synthesized from chemicals, while ‘coating’ refers to a TiO_2 layer prepared from pre-fabricated nanopowders. Peerakiathajorn *et al.* studied the oxidation of a 25 ppm VOC mixture (toluene, benzene, ethylbenzene, xylene) on Ag-doped TiO_2 film with a thickness of 87 nm in a batch reactor under VIS light.¹⁸ After 300 min of irradiation they achieved *ca.* 80% VOC degradation.¹⁸ Pham and Lee studied the oxidation of hexane and butyl acetate individually and in a mixture in a continuous flow reactor on an Ag/V-co-doped TiO_2 photocatalyst immobilized on polyurethane. They found that in the mixture stream, oxidation of butyl acetate was higher because of the higher polarity of the compound.¹⁷ Most studies are carried out in laboratory-scale batch reactors, which do not have the potential for practical application.^{7,18,25} However, the main problem in a continuous flow device design is the low contact time between the photocatalyst surface and pollutants.^{9,26} Therefore, in this paper we used a continuous flow multi-section reactor that allowed us to increase the reaction time by increasing the photocatalytic

surface area. The area coated by photocatalytic thin film was increased five times, from 120 to 600 cm^2 , to follow the effects of reaction time and specific surface area. Additional sections of the reactor can be easily added to amplify the air purification. The specific construction of the reactor gives an opportunity to estimate the effectiveness of the performance of the obtained films in a real application to indoor air purification.

This paper builds on our previous research on the development of UV-A and VIS light active TiO_2 thin films by systematically changing the precursor's molar ratio in the solution. In particular, experimental studies have shown that changing the titanium(IV) isopropoxide (TTIP) and acetylacetone (AcacH) molar ratio from 1 : 1 to 1 : 20 in the precursor solution results in a higher amount of adsorbed carbon on the film surface²⁷ and enhanced photocatalytic activity of the obtained TiO_2 films under UV-A and VIS light. For example, a ten-fold increase in the degradation rate constant of stearic acid was observed with a change of TTIP : AcacH molar ratio in the precursor solution from 1 : 3 to 1 : 8.²⁷ TiO_2 film with a molar ratio of 1 : 8 showed twice-as much activity compared to a film with a molar ratio of 1 : 5 in the gas-phase photodegradation of acetone and acetaldehyde under UV-A and VIS light.²⁸ In the present study, TiO_2 films deposited from a solution with a TTIP and AcacH molar ratio of 1 : 8 were further investigated by the photocatalytic degradation of refractory VOCs—heptane and toluene and their mixtures with relatively easily oxidized VOCs such as acetone and acetaldehyde—under UV-A and VIS light. A multi-section gas flow reactor was used to conduct VOC degradation. The quantum efficiency, by-product formation and synergistic effects of compounds with different polarities and hydrophobicities in a synthetic air mixture during photocatalytic oxidation under different operating conditions, such as air flow rate, humidity and light source, were studied and are discussed in this study.

Our focus is to add substantial data on photocatalytic oxidation, namely to examine a UV-A and VIS light active transparent TiO_2 thin film fabricated in one step without any additional doping agents. Moreover, a multi-section gas flow reactor design allows mimicking of real indoor conditions and tests the performance of the obtained films. The results of this study bring photocatalysis closer to real application.

2. Experimental data

2.1 TiO_2 thin film preparation

TiO_2 thin films were prepared by an ultrasonic spray pyrolysis technique in ambient atmosphere (Fig. SI-1 in ESI†); more detailed information of film preparation has been published elsewhere.²⁷ Borosilicate glass heated up to 350 °C was used as a substrate. Then, 0.2 M titanium(IV) isopropoxide (TTIP) ($\text{C}_{12}\text{H}_{28}\text{O}_4\text{Ti}$ 98+%, Acros Organics) was used as a titanium source for solution preparation, and acetylacetone (AcacH) ($\text{C}_5\text{H}_8\text{O}_2 > 99\%$, Sigma-Aldrich) was added as a stabilizing agent. A molar ratio of TTIP : AcacH of 1 : 8 was used for solution preparation as it was found to be an optimal molar ratio to obtain photocatalytically active film.^{27,28} The as-deposited films were annealed at 500 °C for one hour in air atmosphere. The



films possess good adhesion properties and cannot be washed away by solvents e.g. water or ethanol.

2.2 Gas-phase photocatalytic activity measurements

A continuous multi-section plug flow photocatalytic reactor was used to study the gas-phase oxidation of VOCs over TiO₂ film. A detailed description of the set-up used for the experiments (Fig. SI-2 in ESI†) was published elsewhere.⁸ The multi-section reactor has five sections connected in series with a volume of 130 mL each. The TiO₂ catalyst in the form of a thin film on the glass substrate was located in each section of the reactor. Simplification was undertaken—the photocatalytic surface is the same as the glass substrate. The surface coated with photocatalytic thin film in one section of the reactor was 120 cm², which gave 600 cm² for all five sections. However, the surface of catalyst per reactor volume did not change during the experiments and was 0.92 cm² cm⁻³. Ultraviolet²⁹ (UV Philips Actinic BL 15 W, irradiance 3.5 mW cm⁻² with reflector integrated in the range of 180–400 nm, with maximum emission at 365 nm, UV-B/UV-A ratio < 0.2%) or visible³⁰ (VIS Philips TL-D 15 W, irradiance 3.3 mW cm⁻² with reflector integrated in the range of 180–700 nm, UV/UV-VIS ratio < 5%) lights were located over each section of the reactor at a distance of 6 cm.

The photocatalytic oxidation of heptane (C₇H₁₆ ≥ 99%, Honeywell) and toluene (C₇H₈ ≥ 99%, Sigma-Aldrich) in the reactor was studied separately in conjunction with their oxidation in a mixture with acetone (C₃H₆O ≥ 99.5%, Sigma-Aldrich) and acetaldehyde (C₃H₈O₂ ≥ 99.5%, Sigma-Aldrich). The inlet concentrations of heptane and toluene in the polluted air varied from 5 to 40 ppm, when their oxidation was studied separately. The concentration in the polluted air mixtures was set to 9 ppm (3 ppm acetone, 3 ppm acetaldehyde and 3 ppm heptane or toluene). To simulate the air polluted with VOCs, a pre-calculated amount of the pollutants was injected into the feed tank under vacuum and after the evaporation of compounds, the tank was filled with compressed air. The temperature in the reactor was measured using a temperature controller with a thermocouple (Omega, CN9000A) and was 40 ± 2 °C. Two mass flow controllers were used: one for regulation of the flow rate of polluted air and one for that of diluent air. The gas flow rates varied from 0.5 to 2.5 L min⁻¹, which resulted in a change in the reaction time in the reactor from 15.6 to 3.12 s. The reaction time was calculated as the residence time for an ideal plug flow reactor under steady-state conditions (not taking into account the residence time distribution) and does not reproduce the real contact time between the pollutant and the catalyst surface. Air was moving in the reactors in a laminar way; however, due to it passing through narrow piping between sections, the air flow was changed to turbulent and intensive mixing took place before reaching the new section of the reactor (Fig. SI and S2 in ESI†). Intensive mixing provided a uniform concentration of the polluted air after passing each section. Relative humidities of the air of 6 ± 1% and 40 ± 5% (measured at 20 °C) were used. In the experiments with toluene, ozone was generated by a UV-C lamp (LSE Lighting, GPH287T5VH/4) emitting at 254 and 185 nm.

An Interspec 200-X FTIR infrared spectrometer with an 8 m gas cell (Specac Tornado) was used to measure the concentration of heptane and toluene; a 20 m gas cell (Specac Atmos) was used to measure the concentration of VOCs in the mixtures. The air spectra were collected in-line using an Interspec version 3.40 Pro and processed with Essential FTIR software. For quantitative analysis, the heptane bond was measured at the IR bands 3020–2790 cm⁻¹, toluene at the IR bands 2975–2850 cm⁻¹, acetone at the IR bands 1250–1780 cm⁻¹ and acetaldehyde at the IR bands 1170–1060 cm⁻¹. The concentration was calculated based on one typical FTIR band for each organic pollutant. The limits of detection were 0.5 ppm and 0.2 ppm for Tornado and Atmos gas cells, respectively. The limits of quantification were 1 ppm and 0.4 ppm for the Tornado and Atmos gas cells, respectively. Control experiments for photochemical degradation and adsorption were carried out. No degradation of pollutants was detected in the presence of UV-A without a catalyst. No adsorption of the pollutants on the catalyst was detected in the dark where the limit of detection was 0.5 ppm. All spectra were recorded at least three times with a standard deviation lower than 5%, indicating good reproducibility of the results. The same TiO₂ film was used in all photocatalytic experiments. The film showed high stability and repeatability of the results after a short 30 min period of regeneration with UV-A light.

3. Results and discussion

3.1 TiO₂ thin film properties

TiO₂ thin film prepared by ultrasonic spray pyrolysis on a borosilicate glass substrate from 0.2 M titanium(IV) isopropoxide (TTIP) solution with the addition of acetylacetone (AcacH) in a molar ratio TTIP:AcacH of 1 : 8 was used in this paper for VOC degradation. The reaction between TTIP and AcacH has been well studied in the literature.^{31–33} However, the effect of an increased amount of AcacH in the precursor on the photocatalytic properties of the film needs further investigation.²⁷

The obtained TiO₂ thin film with a thickness *ca.* 370 nm and a material quantity of *ca.* 0.2 mg cm⁻² consists of crystalline anatase TiO₂ (Fig. 1a), with a mean crystallite size in the range 30–40 nm. Optical transparency in the visible spectral range is *ca.* 80% and the bandgap is 3.4 eV (Fig. 1b). Surface morphology was studied using scanning electron microscopy²⁷ and atomic force microscopy³⁴ (Fig. SI-3 in ESI†). Studies showed that the synthesized film had a homogeneous, smooth non-porous surface with a root mean square roughness of 1.4 nm.

It was found by XPS studies that an increased AcacH molar ratio in the precursor solution promoted a larger number of carbon species on the surface of the film.^{21,27} Di Valentin *et al.*,³⁵ in their study found the formation of localized midgap states for carbon-modified TiO₂, in agreement with the findings of our previous study.²⁸ Moreover, surface photovoltage (SPV) measurements showed that passivation of electron traps at the surface takes place with an increase in organic additive, which means preferential separation of photogenerated holes. The SPV signal changed from negative to positive with an increase in AcacH molar ratio, which allows us to control the charge



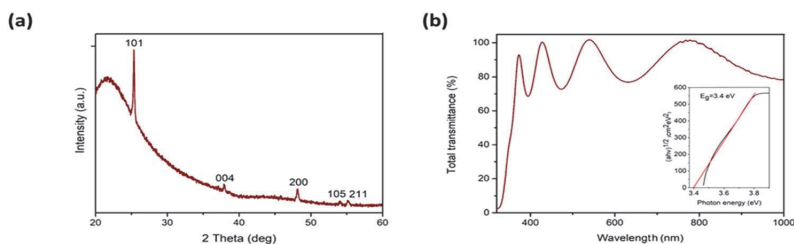


Fig. 1 X-ray diffraction pattern (a) and total transmittance spectrum (b) of TiO_2 thin film. The inset in the Fig. 1b shows the band gap value of TiO_2 thin film.

transfer toward the TiO_2 surface during the synthesis of the film.³⁶ The recombination of the electron–hole pairs is reduced and more reactive oxygen species (ROS) are produced, which enhance the photocatalytic activity.^{27,28,35,36} The generation of ROS plays an essential role in photocatalytic reactions since ROS can degrade a wide range of organic pollutants.^{37–39}

The film obtained in the current study shows super-hydrophilic properties after 15 min of UV-A irradiation;²⁷ thus a short *ca.* 30 min pre-treatment of the catalyst with UV-A was used before the photocatalytic experiments to restore the surface. The film oxidized gas-phase pollutants such as acetone and acetaldehyde with reaction rate constants of 2.3 and 2.4 ppm s^{-1} , respectively. It was found that the films show high photocatalytic activity and stability. The same photocatalytic films were used for several months of study with no decrease in efficiency. Repeatability tests showed that the difference between the parallel series did not exceed 5%.²⁸ More detailed analysis of the material and its properties is given in the ref. 27 and 28.

In this paper we present a systematic study of the synthesized TiO_2 film with an optimized TTIP:AcAcH molar ratio applied for the degradation of refractory compounds such as heptane and toluene. In addition to their more complex structures, these pollutants are both nonpolar and hydrophobic compounds compared to previously studied model pollutants such as acetone and acetaldehyde. Moreover, to mimic real indoor air pollution, the degradation of mixtures of VOCs with different polarities and hydrophilicities on TiO_2 thin films was monitored.

3.2 Photocatalytic oxidation of heptane

The photocatalytic oxidation of heptane at different initial concentrations, air flow rates, relative humidity (RH) and irradiation on the TiO_2 thin film was studied.

First, in order to estimate the initial concentration effect on heptane degradation on the TiO_2 film under ultraviolet (UV-A) light, the photocatalytic oxidation of heptane at initial concentrations of 5, 10 and 40 ppm was studied (air flow rate 0.5 L min^{-1} and RH 6%) (Fig. 2a). At an initial concentration of 5 ppm complete oxidation of heptane occurred with a catalyst surface of 240 cm^2 , but an additional section of the reactor (catalyst surface of 360 cm^2) was needed for the degradation of 10 ppm and a catalyst surface of 600 cm^2 coped with the

oxidation of 40 ppm of heptane (Fig. 2a). For comparison, in the case of sprayed TiO_2 films from TTIP:AcAcH 1:4 solution, only 20% conversion for 10 ppm of heptane was achieved at a catalyst surface of 360 cm^2 under the same experimental conditions, indicating 5 times greater photocatalytic activity of TiO_2 1:8 film.⁴⁰ The effect of an increase in initial concentration on reaction performance was studied by calculating the quantum efficiency (QE) at initial heptane concentrations of 5, 10 and 40 ppm at a catalyst surface of 120 cm^2 (reaction time 15.6 s) (eqn (1) and Fig. 2b).⁴¹

$$\text{QE} = \frac{\text{Number of degraded molecules}}{\text{Number of incident photons}} \quad (1)$$

At a wavelength 365 nm in the case of UV-A, the measured incident photon energy in one section of the reactor at 1 s corresponded to 7.717×10^{17} J. The illuminated surface of the film in one section was 120 cm^2 and in the calculations it was assumed that all photons impinge on the catalyst surface (the calculations are shown in ESI†).

Fig. 2b shows that under the studied conditions, QE increased from 9.74×10^{-5} to 1.5×10^{-4} molecules per photons when the concentration increased from 5 to 10 ppm. The increase is not linear, indicating that at some initial concentration the amount of ROS will start to limit the efficiency of the process. In contrast, TiO_2 films deposited from TTIP:AcAcH 1:4 solution showed a decrease in QE from 1.73×10^{-5} to 5.78×10^{-6} molecules per photons when the concentration of heptane increased from 5 to 10 ppm under similar experimental conditions.⁴⁰ This demonstrates that the concentration of ROS produced on the surface of TiO_2 thin film from the TTIP:AcAcH 1:8 solution used in the current study does not limit oxidation under the studied conditions, unlike the case of TiO_2 films deposited from 1:4 solution.

Gas-phase photocatalytic reactions take place primarily at the interface between adsorbed molecules of pollutants and the surface of the photocatalyst. Thus, both the adsorption and activation of reactants play a significant role in the process.³⁸ To determine the reaction rate constants of heptane oxidation on TiO_2 film the reaction kinetics were studied. The Langmuir–Hinshelwood kinetic model was assumed (eqn (2)).⁷

$$r_o = \frac{k_r K C_o}{1 + K C_o} \quad (2)$$



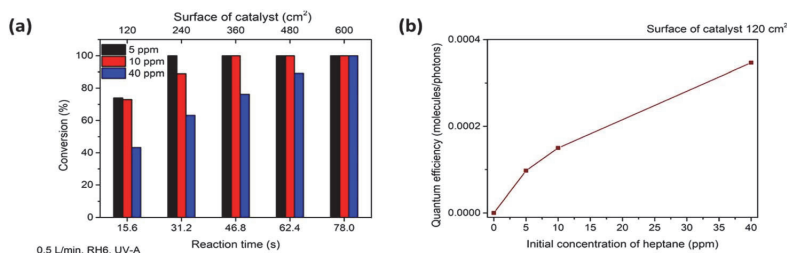


Fig. 2 The effect of initial concentration of heptane on photocatalytic oxidation for different photocatalyst surface areas (a) and quantum efficiency (QE) of heptane degradation at different initial concentrations with a photocatalyst surface of 120 cm² (b). The average values of heptane conversion are shown. The standard deviation was <5%.

The reaction rate constant (k_r) and adsorption constant (K) were found using the Langmuir–Hinshelwood kinetic plot $1/r_o$ versus $1/C_o$, which showed linear dependence (Fig. SI-4 in ESI†).²⁸ In Table 1, the kinetic constants of heptane oxidation are compared to those of acetone, which were obtained in our previous study for the same sprayed TiO₂ film (TTIP: AcacH 1 : 8).²⁸

The reaction rate constant of heptane decreased by about 30% compared to acetone, when the same film and operating parameters of the reactor were used. This can be explained by the more complex molecular structure of heptane, so it needs more time for oxidation. At the same time, the adsorption constant for heptane oxidation increased almost two times. This could be because the molecular weight of heptane is almost twice as high and the vapour pressure at 20 °C is almost five times lower than that of acetone. Moreover, the surface affinity of the photocatalyst could play a certain role in the adsorption process; pollutants prefer to interact with a photocatalyst of similar polarity. Carbon-species-containing TiO₂ film was found to have a nonpolar structure.⁴² Acetone is a polar compound, while heptane is nonpolar. Adsorption of the pollutant molecules is an important step in the photocatalysis process since the molecule should reach the surface for oxidation. However, for a continuous flow reactor with a high surface area a high amount of ROS is beneficial for process efficiency. In gas-phase photocatalytic reactions, species such as $\cdot\text{OH}$ and $\cdot\text{O}_2^-$ play a dominant role. Air contains enough molecular oxygen and water, which can be converted to ROS on the surface of photoinduced TiO₂.^{38,39}

Heptane degradation with initial concentrations of 4.15–16.6 ppm in a 300 mL batch reactor was studied for TiO₂

powders prepared *via* sol–gel by Shang *et al.*⁷ At a TiO₂ load of 0.1 g, they obtained a reaction rate constant of 0.005 ppm s⁻¹. Due to the high specific surface area of TiO₂ particles, the adsorption constant in their study was 0.3 ppm⁻¹; nevertheless, 360 min of irradiation was needed to achieve 99.7% mineralization.⁷ In the current study, 40 ppm of heptane was completely oxidized on the transparent TiO₂ film with a material quantity of 0.2 mg cm⁻² in a time of less than 2 minutes (Fig. 2a). A detailed comparison of the thin film prepared in this study with other thin films to oxidize heptane is given in ESI Table SI-I.† The construction of the reactor used in the present study allows the pollutant to continuously meet fresh catalyst, slowing down the deactivation. The results demonstrate that the effective continuous purification of polluted air by the obtained thin film in a multi-section reactor is more practical than that with powder in periodic mode reactors. Next, the effect of reaction time and mass transfer on heptane oxidation under UV-A was studied. The gas flow rate was changed from 0.5 to 2.5 L min⁻¹, while the concentration of heptane was set to 10 ppm and the RH of the air was 6% (Fig. 3a).

An increase in air flow rate resulted in faster oxidation of heptane (Fig. 3a and Table 2). As can be seen in the last row in Table 2, complete oxidation of 10 ppm of heptane at an air flow rate of 2 L min⁻¹ occurred in twice as short a time interval (reaction time between 15.6 and 19.5 s) compared to the air flow rate of 0.5 L min⁻¹ (reaction time between 31.2 and 46.8 s) (Fig. 3a and Table 2). Although it should be taken into account that the applied photocatalytic surface area is higher at an air flow rate of 2.0 L min⁻¹ and air passed more sections of the reactors, which means more frequent mixing took place at the same reaction time. A decrease in reaction time means less time for adsorption and oxidation on the catalyst surface. However, on the other hand, if the amount of ROS does not limit the surface reaction, then increased mass transfer could promote the photocatalytic oxidation.⁴³ As mentioned above, heptane degradation at an air flow rate of 0.5 L min⁻¹ was not limited by the concentration of ROS, which proves that a higher air flow rate should enhance the overall reaction rate.

An increase in the air flow rate from 0.5 to 2.5 L min⁻¹ decreased the reaction time of the pollutant in the reactor from 15.6 to 3.12 s (Table 2), while it intensified the mass transfer. For the current reactor design, with an increase in air flow rate

Table 1 Comparison of reaction rate and adsorption constants of TiO₂ films for the degradation of heptane and acetone with initial concentrations of 5–40 ppm studied at an air flow rate of 0.5 L min⁻¹ and relative humidity 6% under UV-A light

Pollutant	k_r (ppm s ⁻¹)	K (ppm ⁻¹)	Ref.
Heptane	1.7	0.05	This study
Acetone	2.3	0.03	28



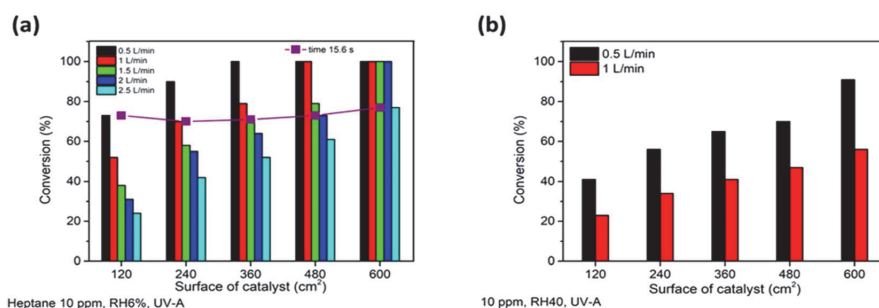


Fig. 3 The effect of air flow rate on photocatalytic oxidation of heptane at different photocatalyst surface areas of TiO₂ thin film at RH 6% (a) and the effect of increased relative humidity (RH 40%) on heptane oxidation at different photocatalyst surfaces. The average values of heptane conversion are shown. The standard deviation was < 5%.

from 0.5 to 2.5 L min⁻¹ air was still flowing in a laminar way: *i.e.* air layers slide in parallel with no swirls or currents normal to the catalyst surface (the Reynolds number changed from 19 to 97; calculations are shown in ESI†). Laminar air flow results in non-optimal mass transfer of pollutants to the catalyst surface. However, this represents a real indoor application in the form of windowpanes, when air is moving in the room by natural convection with periodic mixing by a fan, for example.

Moreover, the design of the multi-section reactor used in the current study allows us to obtain the same reaction time of 15.6 seconds by increasing the air flow rate by 0.5 L min⁻¹ and the surface of the catalyst by 120 cm² simultaneously (adding one more section to the reactor) (Table 2). This means that the reaction time of a pollutant molecule per unit of catalyst, *i.e.* the specific reaction time (Table 2), decreases, while the reaction time stays the same. In Fig. 3a it can be seen that at the same reaction time of 15.6 seconds (the purple line in Fig. 3a) at different air flow rates the conversion of 10 ppm of heptane was about 70%. This suggests that a higher volume of air could be purified by increasing the surface of the catalyst and by mass transfer. Applying a higher catalyst surface helps to overcome the challenge of the low contact time between the pollutants and the catalyst surface in continuous flow reactors and gives a good representation of TiO₂ film application in indoor air purification.

The effect of water vapour was studied by increasing the relative humidity (RH) of air from 6 to 40% at an initial heptane concentration of 10 ppm at air flow rates of 0.5 and 1 L min⁻¹ under UV-A (Fig. 3b). Fig. 3 implies that an increase in water vapour content in air from 6 (Fig. 3a) to 40% (Fig. 3b) inhibited the oxidation of heptane. The initial QE of heptane decreased by 35 and 57% at air flow rates of 0.5 and 1 L min⁻¹, respectively, with an RH increase from 6 to 40%. The negative impact of an RH increase was intensified 1.6 times with an air flow rate increase from 0.5 to 1 L min⁻¹; thus the oxidation of heptane by active sites of the photocatalyst is limited because of the adsorption of water molecules. A similar tendency of a negative water vapour effect on heptane photooxidation due to competitive adsorption on the surface was observed in other studies.^{7,40}

The obtained TiO₂ film showed promising performance in heptane photocatalytic oxidation under different operating conditions under UV-A light. However, for real applications in indoor conditions, oxidation under visible (VIS) light is more essential. To study TiO₂ film activity under VIS light, heptane oxidation at concentrations of 5 and 10 ppm at an air flow rate 0.5 L min⁻¹ and RH 6% was studied (Fig. 4).

Fig. 4 shows that TiO₂ film could completely oxidize 5 ppm of heptane at a catalyst surface of 480 cm² (reaction time 62.4 s) under VIS light. An increase in heptane initial concentration from 5 to 10 ppm led to 45% conversion of the pollutant at

Table 2 Residence time of pollutants in the reactor at different air flow rates with different numbers of applied reactor sections and residence time needed for complete oxidation of 10 ppm of heptane at different air flow rates at RH 6%

Number of reactor sections	Surface of catalyst (cm ²)	Reaction time of pollutant (s) at different air flow rates				
		0.5 L min ⁻¹	1 L min ⁻¹	1.5 L min ⁻¹	2 L min ⁻¹	2.5 L min ⁻¹
1	120	15.6	7.8	5.2	3.9	3.12
2	240	31.2	15.6	10.4	7.8	6.24
3	360	46.8	23.4	15.6	11.7	9.36
4	480	62.4	31.2	20.8	15.6	12.48
5	600	78	39	26	19.5	15.6
Specific reaction time (s cm ⁻²)		0.13	0.065	0.043	0.033	0.026
Reaction time for complete degradation of 10 ppm of heptane (s)		31.2–46.8	23.4–31.2	20.8–26	15.6–19.5	Not achieved



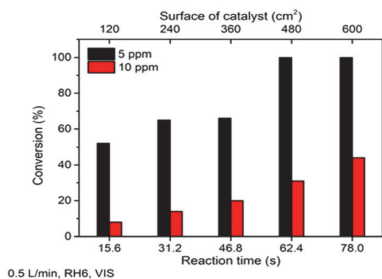


Fig. 4 The effect of initial concentration on photocatalytic oxidation of heptane under visible light at different photocatalyst surfaces. The average values of heptane conversion are shown. The standard deviation was <5%.

a catalyst surface of 600 cm² (reaction time 78 s), which means oxidation of *ca.* 4.5 ppm of heptane (Fig. 4). These results indicate that the prepared TiO₂ film is active under VIS light. The VIS light photocatalytic activity of the TiO₂ film could be explained by a synergistic effect between carbon species and TiO₂. That is, carbon absorbs VIS light and generates electrons, which are then transferred to the valence band of TiO₂.^{20–22}

As expected, the activity under VIS was lower than that under UV-A. QE for 5 ppm of heptane were 9.74×10^{-5} and 3.44×10^{-5} molecules per photons under UV-A and VIS light, respectively. At a concentration of 10 ppm under UV-A, QE increased to 1.50×10^{-4} molecules per photons, while under VIS light it decreased to 1.60×10^{-5} molecules per photons. If in the case of UV-A the oxidation process was not limited by the concentration of ROS, then under VIS light not enough ROS are produced and thus, the process is surface reaction limited. However, the results demonstrate that the film completely oxidized heptane at an initial concentration of 5 ppm under VIS light, which makes its application suitable for indoor air treatment for VOCs.

According to the literature, the formation of propanal, butanal, 3-heptanone, 4-heptanone and CO could follow the oxidation of heptane by TiO₂.⁷ However, in the current study no gaseous by-products except CO₂ and H₂O were detected on the FTIR spectra of purified air during the performed experiments. Moreover, long-term experiments with 40 ppm of heptane at a catalyst surface of 120 cm² (air flow rate 0.5 L min⁻¹, RH 6%, UV-A) were performed to study the deactivation of the photocatalyst. The conversion of heptane was *ca.* 43% and did not change during 180 min of continuous use. This means that at a residence time of 15.6 s and catalyst surface of 120 cm², TiO₂ film can continuously oxidize 17 ppm of heptane out of 40 ppm with no deactivation during the experimental run time up to 180 min.

To summarise this section, TiO₂ film synthesized in the current study can continuously oxidize such model pollutants as heptane under both UV-A and VIS light under different experimental conditions without forming any toxic by-products.

3.3 Photocatalytic oxidation of toluene

The photocatalytic oxidation of toluene at different initial concentrations and RH and with the addition of ozone on the TiO₂ thin film was studied. Similar to heptane oxidation, no by-products except CO₂ and H₂O were detected on the FTIR spectra of purified air during the experiments with toluene.

The photocatalytic oxidation of toluene at initial concentrations of 5, 10, 20 and 40 ppm at an air flow rate of 0.5 L min⁻¹ and RH 6% was studied under UV-A (Fig. 5). Fig. 5a reveals that it was possible to partially oxidize toluene at initial concentrations in the range 5–40 ppm on the TiO₂ thin film. 3.5 ppm out of 5 ppm was converted after 78 s in the reactor; 16.8 ppm was oxidized at the same time when the initial concentration was increased to 40 ppm (Fig. 5a). The maximum conversion of *ca.* 70% was achieved at a catalyst surface of 600 cm² at an initial toluene concentration of 20 ppm (Fig. 5a). Toluene photocatalytic oxidation is more complicated compared to straight-chain compounds such as heptane. Moreover, the toluene oxidation pathway contains intermediates, which can block the active site of the photocatalyst and deactivate it.^{8,44} During photocatalytic toluene decomposition, gas-phase oxidation by-products are generated. Furthermore, during the toluene gas-phase oxidation, solid-phase partial oxidation products can form and adsorb on the surface of the photocatalyst causing its deactivation. The by-products of toluene monitored in the gas phase are benzaldehyde, methanol, acetaldehyde, acetone, acetic acid, butyraldehyde, benzene. Benzoic acid, benzene, acrylaldehyde, butyraldehyde and pentanal could adsorb on the surface of TiO₂ during the oxidation of toluene.⁴⁴

The increase in conversion with an increase in the surface of the catalyst (reaction time) was negligible (Fig. 5); most of the toluene was converted after the first section of the reactor (reaction time 15.6 s). At the highest initial concentration (40 ppm), the conversion at all sections of the reactor was almost the same at *ca.* 40% (Fig. 5a). This could indicate that toluene and its intermediate products are adsorbed on the surface of TiO₂, blocking the active sites. Hence, no intermediate products of toluene were detected in the FTIR spectra of treated air during all the experimental runs, so it could be assumed that the formation of mostly solid-phase partial oxidation products takes place.

The QE at the first section of the reactor increased with the growth in the initial concentration (Fig. 5b). Thus, the film is capable of oxidizing some amount of toluene at a catalyst surface of 120 cm². Then ROS produced by additional surface of the catalyst mostly compensate for the number of ROS which were involved in the oxidation of toluene and blocked by solid intermediate products in the previous section of the reactor.

The possible deactivation of a catalyst surface by toluene by-products has been reported in the literature.^{8,20,45,46} For example it was found by M. D. Hernández-Alonso *et al.* in the case of TiO₂ films deposited by the sol-gel method that the adsorption of a toluene by-product benzoic acid decreased the initial reaction rate from 0.14 to 0.01 ppm s⁻¹ after 180 min of measurements.²⁰

Several studies on powdered materials with high material quantity have reported a color change of the photocatalyst and



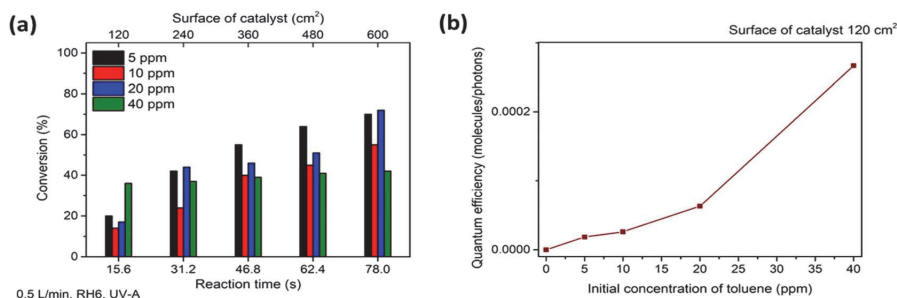


Fig. 5 The effect of initial concentration on the photocatalytic oxidation of toluene at different catalyst surfaces (a) and QE of toluene degradation at different initial concentrations at a photocatalyst surface of 120 cm² (b). The average values of toluene conversion are shown. The standard deviation was <5%.

a decrease in toluene conversion.^{8,45,46} Kask *et al.*, in their study achieved complete degradation of 20 ppm of toluene at a catalyst surface of 240 cm² under similar experimental conditions to those in the current study for 1 μm P25 TiO₂-covered glass. They observed the yellowish surface of the catalyst after a 190 min experimental run, which probably indicates the deactivation of the catalyst by intermediates of toluene oxidation.⁸ Einaga *et al.* observed a decrease in toluene conversion from 66 to 9% after 120 min of continuous use with P25 powder applied to the wall of a flow-type reactor. They suggested that deactivation takes place due to the formation of less reactive intermediates, which can be detected as carbon deposits on the surface of the catalyst.⁴⁵

In the current study, no changes in film color were observed, which could be due to the low material quantity and transparency of the synthesized material. However, no decrease in photocatalytic activity could mean that the intermediates of toluene oxidation adsorbed on the film surface are degradable. The toluene oxidation rate was lower than that of heptane (Section 3.2, Fig. 2). The reaction rate ($k = 0.895 \text{ ppm s}^{-1}$) and adsorption ($K = 0.028 \text{ ppm}^{-1}$) constants of toluene decreased by almost two times compared to heptane. However, this is still higher than other kinetic constants reported in the literature for toluene. For example, Sleiman *et al.* reported a reaction rate constant of 3.55 ppb s^{-1} for toluene and an adsorption constant of 0.0025 ppb^{-1} for an annular-flow-through reactor with PC500 TiO₂ immobilized on fiber paper.⁴⁷ In another study by Garlisi and Palmisano of TiO₂ thin film with a thickness of 20 nm, the photocatalytic oxidation of toluene with an initial concentration of 0.5 ppm obtained an initial reaction rate of $3.6 \times 10^{-6} \text{ ppm s}^{-1}$.¹⁰ Ku and co-authors obtained 26% conversion of toluene with an initial concentration of 41.13 ppm on P25 TiO₂ powder spin coated onto Pyrex glass with a material quantity of 1.3 mg cm⁻² at an air flow rate of 0.4 L min⁻¹ (reaction time ca. 2 min) and RH 5%.⁴⁸ A detailed comparison of the thin film prepared in this study with other thin films to oxidize toluene is presented in ESI Table SI-I.†

The film synthesized in the current study has a material quantity of about 0.2 mg cm⁻², whereas the initial reaction rate for 40 ppm of toluene oxidation is more than 10 times higher

compared to the study by Ku and co-authors, who obtained an initial reaction rate of 0.1 ppm s⁻¹. This confirms that the activity of the thin film under study is competitive with coatings prepared by powder immobilization.

It is generally known that toluene photocatalytic oxidation could be limited due to the low reactivity of the aromatic ring and deactivation of the catalyst by toluene intermediate products.^{8,45-48} Several studies claim that water molecules could help to protect the photocatalyst from deactivation since they prevent the adsorption of intermediate products.^{44,47}

To increase the efficiency of toluene degradation, initially the RH of polluted air was increased from 6 to 40%; the study was carried out with an initial toluene concentration of 10 ppm and air flow rate of 0.5 L min⁻¹ (Fig. 6).

Fig. 6 shows that an increase in RH from 6 to 40% resulted in slight changes in toluene conversion (not more than 15%). If in the first two sections of the reactor (reaction times 15.6 and 31.2 s) conversion was increased at RH 40%, then starting from a reaction time of 46.8 s the conversion was higher in drier air. It can be concluded that no significant effect of an increase in water vapour content in air on toluene oxidation was detected in the current study. However, it was reported by Sleiman *et al.* that for toluene with a high initial concentration (499 ppm) an

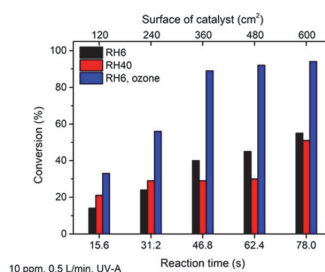
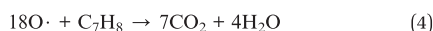
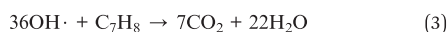


Fig. 6 The effect of an increase in RH and addition of ozone on the photocatalytic oxidation of toluene at different photocatalyst surface areas. The average values of toluene conversion are shown. The standard deviation was <5%.



increase in RH from 0 to 70% enhanced the decomposition rate.⁴⁷

Another common additive to promote photocatalytic toluene degradation is a strong oxidant like ozone. The positive effect of ozone on the photocatalytic degradation of toluene for a P25 TiO₂ photocatalyst has been studied by several authors.^{8,26} Therefore, the ozone was generated by a UV-C lamp and mixed with polluted air, giving an initial concentration of ozone in the polluted air of ca. 50 ppm. The results showed that addition of small amount of ozone as a strong oxidant in combination with TiO₂ photocatalysis increased the conversion of 10 ppm of toluene from 51 to 94% at a catalyst surface of 600 cm² (Fig. 6). Applying only 50 ppm of ozone or ozone combined with UV-A without a TiO₂ photocatalyst did not result in toluene decomposition. Thus, it could be concluded that the photocatalytic oxidation of toluene by ROS on the TiO₂ surface is the main degradation mechanism. Ozone is depleted on the surface of TiO₂ film and forms additional radicals (O[•]) to protect the catalytic surface from fast deactivation. Probably ozone helps to avoid rapid blocking of the active sites by toluene degradation intermediates, thus enhancing the oxidation ability of the catalyst. According to eqn (3) and (4) for toluene oxidation, 36 OH[•] are needed, while the number of O[•] molecules needed for toluene oxidation is 18.



Prepared by spray pyrolysis, the TiO₂ thin film used in the current study is able to significantly reduce the amount of toluene in air with an initial concentration up to 40 ppm without forming any detectable gas-phase intermediate products, which makes it a suitable candidate for indoor air purification.

3.4 Photocatalytic oxidation of air mixtures

Indoor air could contain hundreds of different organic pollutants in very small concentrations. To mimic the real conditions of indoor air pollution, the degradation of two synthetic air mixtures of 9 ppm of heptane–acetone–acetaldehyde (Fig. 7a)

and 9 ppm of toluene–acetone–acetaldehyde (Fig. 7b) were studied. The multicomponent mixtures of synthetic air were analysed to investigate how components interfere with each other. Moreover, how compounds in a multicomponent mixture with different polarities and hydrophilicities affect the photocatalytic performance was studied under different operating conditions.

All pollutants in both studied mixtures were completely oxidized at RH 6% and an air flow rate of 0.5 L min⁻¹ under UV-A, if three sections of the reactor were applied (catalyst surface of 360 cm²) (Fig. 7 and ESI Tables SI-2 and SI-3†). Complete oxidation of acetaldehyde had already been achieved after the polluted air had passed through the first section of the reactor (catalyst surface of 120 cm²), when it was in the mixture with heptane, while the conversion of acetone and heptane were 93 and 77%, respectively (Fig. 7a and Table SI-2†). The conversions of acetaldehyde, acetone and toluene in the mixture with toluene at the same catalyst surface (120 cm²) were 78, 70 and 71%, respectively (Fig. 7b and Table SI-3†). The degradation rate of compounds in the mixture with heptane followed the order: acetaldehyde, acetone, heptane with QE of 5.6, 5.2, 4.3 × 10⁻⁵ molecules per photons, respectively (Table 3). Acetaldehyde and acetone having simpler molecular structures are expected to be oxidized faster in the mixture. However, the QE of acetone and acetaldehyde degradation decreased 25 and 22%, respectively, when these compounds were in the mixture with toluene (Tables 3 and 4). The degradation of acetone and acetaldehyde molecules in the mixture with toluene probably decreased due

Table 3 Quantum efficiencies of 9 ppm of a mixture of heptane, acetone and acetaldehyde with different experimental parameters after the first section of the reactor (catalyst surface of 120 cm²)

Operating parameters (air flow rate, RH, irradiation source)	Quantum efficiency, × 10 ⁻⁵ molecules per photons		
	Heptane	Acetone	Acetaldehyde
0.5 L min ⁻¹ , RH6, UV-A	4.282	5.170	5.560
1 L min ⁻¹ , RH6, UV-A	12.46	14.01	14.01
0.5 L min ⁻¹ , RH40, UV-A	1.683	1.703	2.568
0.5 L min ⁻¹ , RH6, VIS	0.797	1.791	2.085

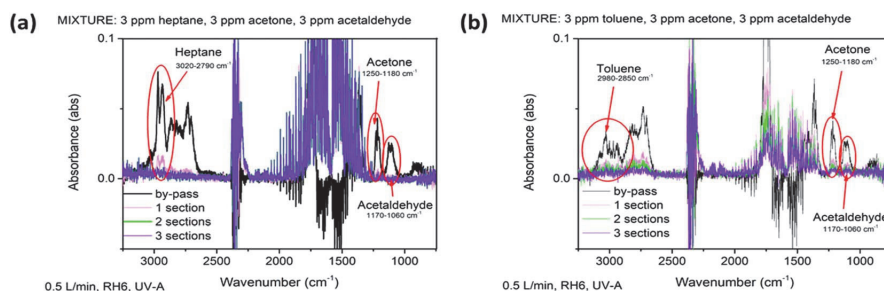


Fig. 7 FTIR spectra of heptane–acetone–acetaldehyde (a) and toluene–acetone–acetaldehyde (b) mixtures passing through the by-pass line and through the reactors under UV-A irradiation on the TiO₂ film.



Table 4 Quantum efficiencies of 9 ppm of a mixture of toluene, acetone and acetaldehyde with different experimental parameters after the first section of the reactor (catalyst surface of 120 cm²)

Operating parameters (air flow rate, RH, irradiation source)	Quantum efficiency, $\times 10^{-5}$ molecules per photons		
	Toluene	Acetone	Acetaldehyde
0.5 L min ⁻¹ , RH6, UV-A	3.970	3.895	2.232
1 L min ⁻¹ , RH6, UV-A	10.59	8.934	8.946
0.5 L min ⁻¹ , RH40, UV-A	2.056	1.790	2.322
0.5 L min ⁻¹ , RH6, VIS	1.514	1.318	1.077

to competitive adsorption on the surface of the photocatalyst. Toluene by-products oxidize more slowly than the initial compound, so these could adsorb on the surface of the photocatalyst inhibiting the adsorption of acetone and acetaldehyde.

To study the synergistic effect of the VOC mixtures on photocatalytic oxidation in more detail, the decomposition of VOC mixtures under different experimental conditions was studied. The effects of air flow rate, water vapour and irradiation source on the QE and conversions of VOCs in the mixtures are presented in Tables 3 and 4 and in ESI Tables SI-2 and SI-3.† In the heptane–acetone–acetaldehyde mixture, the degradation reaction rate under all operating conditions followed the order (from the highest to lowest): acetaldehyde, acetone, heptane (Tables 3 and SI-2†). In the toluene–acetone–acetaldehyde mixture, toluene affected the degradation rates of acetone and acetaldehyde and the values of the QE of the components were very close (Tables 4 and SI-3†).

An increase in the air flow rate from 0.5 to 1 L min⁻¹ resulted in higher QE for all compounds in both mixtures (Tables 3 and 4). However, the increase in QE of heptane and toluene degradation with increased mass transfer was higher than for acetone and acetaldehyde. At an air flow rate of 1 L min⁻¹, RH 6%, under UV-A, the QE of toluene was even higher than that of acetone and acetaldehyde (Table 4). This indicates that for less polar compounds, such as heptane and toluene, compared to oxygen-containing compounds, the intensification of mass transfer favors their oxidation. The same was found for individual pollutants as RH increases from 6 to 40%: the QE of all compounds in the mixtures decreased by about twice (Tables 3 and 4). This also confirms the competitive adsorption of compounds on the surface of TiO₂ with water vapor. The QE of all compounds decreased drastically under VIS light (Tables 3 and 4), showing that the amount of ROS produced is limited under VIS light. However, with increased residence time in the reactor (catalyst surface of 600 cm²) the average conversion of the pollutants in the mixture with heptane and toluene under VIS light reached 92 and 45%, respectively (Tables SI-2 and SI-3†). That is, 3 ppm of acetaldehyde, 3 ppm of acetone and 2.3 ppm of heptane were oxidized in the first mixture at a catalyst surface of 600 cm² (air flow rate 0.5 L min⁻¹, RH6%) (Table SI-2†). In the second mixture, 1.6 ppm of acetaldehyde, 1.6 ppm of acetone and 0.9 ppm of toluene were oxidized under the same conditions (Table SI-3†).

There are only a few studies, where photocatalytic oxidation of VOCs in air mixtures is investigated and most use modified TiO₂ powders under UV-A.^{7,8,11,25} For example, the photocatalytic oxidation of toluene, decane and trichloroethylene separately and in mixtures was studied by Debono *et al.* in a batch reactor with 100 mg of P25 TiO₂ powder load. In general, the oxidation of pollutants in the mixture was up to twice as slow as its degradation as a single compound. As in the current study, they observed sequential degradation of VOCs, which related to the competitive adsorption of different compounds on the surface of the photocatalyst.²⁵ Liang *et al.* studied the degradation of 11 ppb of acetone, toluene and *p*-xylene in a mixture and separately on sol-gel TiO₂ film. They found that degradation of *p*-xylene and acetone occurred at lower rates in the mixture, and the conversion of acetone and *p*-xylene decreased more than 15% in the mixtures. The opposite trend was observed for toluene, where the conversion increased by ca. 20%.^{8,11} Chen and Zhang studied the oxidation of a VOC mixture, which consisted of 16 different compounds, in a honeycomb reactor coated with a TiO₂-based catalyst. The oxidation efficiency for all components in the mixture was lower compared to the single compounds. It was found that the interference effect is obvious and the molecules with higher affinity to the catalyst are more easily adsorbed on its active sites and oxidize faster.²⁶

The TiO₂ thin film prepared in this study degraded 9 ppm of VOCs in the mixture at a reaction time of 46.8 s (catalyst surface of 360 cm², RH 6%, UV-A). A reaction time of 31.2 s was needed to oxidize 10 ppm of acetone or acetaldehyde, when these compounds were studied separately under the same experimental conditions.²⁸ A reaction time of 46.8 s was needed for 10 ppm of heptane oxidation as a separate compound (Section 3.2, Fig. 2a) and ca. 4 ppm of toluene (initial concentration 10 ppm, Section 3.3, Fig. 5a) was oxidized at a reaction time of 46.8 s. The results of the current study demonstrate that TiO₂ films could significantly decrease or completely photocatalytically oxidize the variety of VOCs under different operating conditions.

4 Conclusions

A sprayed TiO₂ thin film prepared from a solution with a TTIP : AcAcH molar ratio of 1 : 8 was thoroughly studied for its photocatalytic activity in the continuous flow gas-phase degradation of heptane and toluene as single compounds and in mixtures with acetone and acetaldehyde. Under UV-A light, heptane degradation was not hindered by an increase in its initial concentration up to 40 ppm and air flow rate up to 2.5 L min⁻¹; only an increased content of water molecules in the air decreased the reaction rate. Under VIS light, 5 ppm of heptane were completely oxidized at a reaction time of 62.4 s; however in the case of 10 ppm, the photocatalytic oxidation was limited by the number of ROS produced. In the case of toluene, 70% of its 5 ppm initial concentration was degraded at a reaction time of 78 s under UV-A light. Toluene oxidation was hindered by the insufficient amount of ROS and the adsorption of less reactive degradation intermediates on the catalyst surface. The



performance of the photocatalytic air treatment device could be augmented by decreasing the reaction time with a simultaneous increase in the surface area of the film. Variations in relative humidity from 6 to 40% were found not to have an effect on toluene degradation. However, the addition of 50 ppm of ozone increased the conversion of 10 ppm of toluene from 51 to 94%.

The degradation rate of compounds in mixtures with heptane followed the order (from the highest to lowest): acetaldehyde, acetone, heptane. However, in a mixture with toluene, the degradation of acetone and acetaldehyde was affected by toluene. The presence of aromatic compounds in the VOC mixture retards the degradation of otherwise easily degraded aliphatic compounds. An increase in air flow rate promotes the degradation of all compounds in both mixtures. The degradation rate of less polar poorly adsorbed VOCs could be enhanced by intensifying the mass transfer in the reactor. Higher humidity and visible light decreased the initial reaction rate of all compounds in both mixtures. This indicates the formation of a limiting amount of reactive species and competitive adsorption between the pollutants and their intermediate products on the surface of the catalyst.

Under UV-A (irradiance 3.5 mW cm^{-2}), the synthesized TiO_2 thin film at catalyst surfaces of $120\text{--}600 \text{ cm}^2$ degrades 9 ppm of VOCs in the mixtures at a reaction time of 46.8 s. As individual compounds 10 ppm of acetone and acetaldehyde degrade at a reaction time of 31.2 s, 10 ppm of heptane at a reaction time of 46.8 s and ca. 4 ppm of toluene out of 10 ppm was oxidized at a reaction time of 46.8 s. Under VIS light in a mixture with heptane, 3 ppm of acetaldehyde, 3 ppm of acetone and 2.3 ppm of heptane were oxidized at a reaction time of 78 s. In a mixture with toluene under VIS light, oxidation of 1.6 ppm of acetaldehyde, 1.6 ppm of acetone and 0.9 ppm of toluene oxidation was achieved. TiO_2 film prepared in the current study demonstrated excellent capability for successful application for the treatment of indoor air from low concentrations of VOC mixtures causing sick building syndrome.

This study confirms that TiO_2 thin films obtained by a simple and cost-effective method of chemical spray pyrolysis are highly effective for indoor air purification from VOCs. Transparent TiO_2 film with a material quantity of ca. 0.2 mg cm^{-2} shows competitive photocatalytic activity compared with a coating prepared from P25 powder and could continuously oxidize 9 ppm of VOC mixture. The obtained film can be widely applied as an innovative air purifying material in buildings or devices.

Author contributions

Jekaterina Sydorenko: formal analysis, investigation, writing—original draft, visualization. Arvo Mere: writing – review & editing. Malle Krunks: writing – review & editing. Marina Krichevskaya: conceptualization, methodology, writing – review & editing, supervision. Ilona Oja Acik: conceptualization, methodology, writing – review & editing, supervision, project administration, funding acquisition.

Conflicts of interest

There are no conflicts to declare.

Acknowledgements

This research was funded by the Estonian Ministry of Education and Research, Estonian Research Council project PRG627 “Antimony chalcogenide thin films for next-generation semi-transparent solar cells applicable in electricity producing windows”, European Union's Horizon 2020 programme under the ERA Chair project 5GSOLAR, grant agreement No. 952509 and the Estonian Centre of Excellence project TK141 (TAR16016EK) “Advanced materials and high-technology devices for energy recuperation systems”.

Notes and references

- 1 W. Abou Saoud, A. Kane, P. Le Cann, A. Gerard, L. Lamaa, L. Peruchon, C. Brochier, A. Bouzaza, D. Wolbert and A. A. Assadi, *Chem. Eng. J.*, 2021, **411**, 128622, DOI: [10.1016/j.cej.2021.128622](https://doi.org/10.1016/j.cej.2021.128622).
- 2 S. Domínguez-amarillo, J. Fernández-agüera, S. Cesteros-garcía and R. A. González-lezcano, *Int. J. Environ. Res. Public Health*, 2020, **17**, 7183, DOI: [10.3390/ijerph17197183](https://doi.org/10.3390/ijerph17197183).
- 3 Y. Huang, S. S. H. Ho, R. Niu, L. Xu, Y. Lu, J. Cao and S. Lee, *Molecules*, 2016, **21**, 56, DOI: [10.3390/ijerph17197183](https://doi.org/10.3390/ijerph17197183).
- 4 A. Maudhuit, C. Raillard, V. Héquet, L. Le Coq, J. Sablayrolles and L. Molins, *Chem. Eng. J.*, 2011, **170**, 464–470, DOI: [10.1016/j.cej.2011.02.040](https://doi.org/10.1016/j.cej.2011.02.040).
- 5 Y. Ji, A. Mattsson, G. A. Niklasson, C. G. Granqvist and L. Österlund, *Joule*, 2019, **3**, 2457–2471, DOI: [10.1016/j.joule.2019.06.024](https://doi.org/10.1016/j.joule.2019.06.024).
- 6 S. Obregón and V. Rodríguez-González, *J. Sol-Gel Sci. Technol.*, 2022, **102**, 125–141, DOI: [10.1007/s10971-021-05628-5](https://doi.org/10.1007/s10971-021-05628-5).
- 7 J. Shang, Y. Du and Z. Xu, *Chemosphere*, 2002, **46**, 93–99, DOI: [10.1016/S0045-6535\(01\)00115-1](https://doi.org/10.1016/S0045-6535(01)00115-1).
- 8 M. Kask, J. Bolobajev and M. Krichevskaya, *Chem. Eng. J.*, 2020, **399**, 125815, DOI: [10.1016/j.cej.2020.125815](https://doi.org/10.1016/j.cej.2020.125815).
- 9 T. Zou, C. Xie, Y. Liu, S. Zhang, Z. Zou and S. Zhang, *J. Alloys Compd.*, 2013, **552**, 504–510, DOI: [10.1016/j.jallcom.2012.11.061](https://doi.org/10.1016/j.jallcom.2012.11.061).
- 10 C. Garlisi and G. Palmisano, *Appl. Surf. Sci.*, 2017, **420**, 83–93, DOI: [10.1016/j.apsusc.2017.05.077](https://doi.org/10.1016/j.apsusc.2017.05.077).
- 11 W. J. Liang, J. Li and Y. Q. Jin, *J. Environ. Sci. Health, Part A: Toxic/Hazard. Subst. Environ. Eng.*, 2010, **45**, 1384–1390, DOI: [10.1080/10934529.2010.500925](https://doi.org/10.1080/10934529.2010.500925).
- 12 M. Dell'Edera, C. Lo Porto, I. De Pasquale, F. Petronella, M. L. Curri, A. Agostiano and R. Comparelli, *Catal. Today*, 2021, **380**, 62–83, DOI: [10.1016/j.cattod.2021.04.023](https://doi.org/10.1016/j.cattod.2021.04.023).
- 13 A. H. Navidpour, A. Hosseinzadeh, J. L. Zhou and Z. Huang, *Catal. Rev.-Sci. Eng.*, 2021, 1–52, DOI: [10.1080/01614940.2021.1983066](https://doi.org/10.1080/01614940.2021.1983066).



- 14 S. D. Burnside, V. Shklover, C. Barbé, P. Comte, F. Arendse, K. Brooks and M. Grätzel, *Chem. Mater.*, 1998, **10**, 2419–2425, DOI: [10.1021/cm980702b](https://doi.org/10.1021/cm980702b).
- 15 V. Rodríguez-González, M. Sasaki, J. Ishii, S. Khan, C. Terashima, N. Suzuki and A. Fujishima, *Chemosphere*, 2021, **275**, 129992, DOI: [10.1016/j.chemosphere.2021.129992](https://doi.org/10.1016/j.chemosphere.2021.129992).
- 16 F. He, W. Jeon and W. Choi, *Nat. Commun.*, 2021, **12**, 6259, DOI: [10.1038/s41467-021-26541-z](https://doi.org/10.1038/s41467-021-26541-z).
- 17 T. D. Pham and B. K. Lee, *Chem. Eng. J.*, 2017, **307**, 53–73, DOI: [10.1016/j.cej.2016.08.068](https://doi.org/10.1016/j.cej.2016.08.068).
- 18 P. Peerakiathajorn, C. Chawengkijwanich, W. Onreabroy and S. Chiarakorn, *Mater. Sci. Forum*, 2012, **712**, 133–145, DOI: [10.4028/www.scientific.net/MSF.712.133](https://doi.org/10.4028/www.scientific.net/MSF.712.133).
- 19 Y. Y. Kannangara, R. Wijesena, R. M. G. Rajapakse and K. M. N. de Silva, *Int. Nano Lett.*, 2018, **8**, 31–39, DOI: [10.1007/s40089-018-0230-x](https://doi.org/10.1007/s40089-018-0230-x).
- 20 M. D. Hernández-Alonso, I. Tejedor-Tejedor, J. M. Coronado and M. A. Anderson, *Appl. Catal., B*, 2011, **101**, 283–293, DOI: [10.1016/j.apcatb.2010.09.029](https://doi.org/10.1016/j.apcatb.2010.09.029).
- 21 M. Marszewski, J. Marszewska, S. Pylypenko and M. Jaroniec, *Chem. Mater.*, 2016, **28**, 7878–7888, DOI: [10.1021/acs.chemmater.6b03429](https://doi.org/10.1021/acs.chemmater.6b03429).
- 22 Y. Yuan, Z. H. Ruan, X. Huang, Y. Q. Jiang and H. P. Tan, *J. Catal.*, 2017, **348**, 246–255, DOI: [10.1016/j.jcat.2016.12.022](https://doi.org/10.1016/j.jcat.2016.12.022).
- 23 L. Hua, Z. Yin and S. Cao, *Catalysts*, 2020, **10**, 1431, DOI: [10.3390/catal10121431](https://doi.org/10.3390/catal10121431).
- 24 D. M. Tobaldi, D. Dvoranová, L. Lajaunie, N. Rozman, B. Figueiredo, M. P. Seabra, A. S. Škapin, J. J. Calvino, V. Brezová and J. A. Labrincha, *Chem. Eng. J.*, 2021, **405**, 126651, DOI: [10.1016/j.cej.2020.126651](https://doi.org/10.1016/j.cej.2020.126651).
- 25 O. Debono, V. Hequet, L. Le Coq, N. Locoge and F. Thevenet, *Appl. Catal., B*, 2017, **218**, 359–369, DOI: [10.1016/j.apcatb.2017.06.070](https://doi.org/10.1016/j.apcatb.2017.06.070).
- 26 W. Chen and J. S. Zhang, *Build. Environ.*, 2008, **43**, 246–252, DOI: [10.1016/j.buildenv.2006.03.024](https://doi.org/10.1016/j.buildenv.2006.03.024).
- 27 J. Spiridonova, A. Katerski, M. Danilson, M. Krichevskaya, M. Krunk and I. Oja Acik, *Molecules*, 2019, **24**, 4326, DOI: [10.3390/molecules24234326](https://doi.org/10.3390/molecules24234326).
- 28 J. Spiridonova, A. Mere, M. Krunk, M. Rosenberg, A. Kahru, M. Danilson, M. Krichevskaya and I. O. Acik, *Catalysts*, 2020, **10**, 1011, DOI: [10.3390/catal10091011](https://doi.org/10.3390/catal10091011).
- 29 Philips, conventional lamps and tubes, special lamps, insect trap, actinic BL, Actinic BL TL(-K)/TL-D(-K) spec sheet. https://www.lighting.philips.com/api/assets/v1/file/PhilipsLighting/content/fp928024801029-pss-global/ADAM-2015121113552500%40en_AA.pdf. (accessed on 12 October 2022).
- 30 Philips, conventional lamps and tubes, fluorescent lamps and starters, TL-D, TL-D 15W/827 1PP/10 spec sheet, https://www.lighting.philips.com/api/assets/v1/file/PhilipsLighting/content/fp927922282766-pss-global/ADAM-201512111035306769%40en_AA.pdf. (accessed on 12 October 2022).
- 31 J. Moon, T. Li, C. A. Randall and J. H. Adair, *J. Mater. Res.*, 1997, **12**, 189–197, DOI: [10.1016/j.cej.2021.132766](https://doi.org/10.1016/j.cej.2021.132766).
- 32 A. O. Juma, I. O. Acik, V. Mikli, A. Mere and M. Krunk, *Thin Solid Films*, 2015, **594**, 287–292, DOI: [10.1016/j.tsf.2015.03.036](https://doi.org/10.1016/j.tsf.2015.03.036).
- 33 A. Léaustic, F. Babonneau and J. Livage, *Chem. Mater.*, 1989, **1**, 240–247, DOI: [10.1021/cm00002a015](https://doi.org/10.1021/cm00002a015).
- 34 T. Olukan, J. Sydorenko, A. Katerski, M. Al Mahri, C.-Y. Lai, A. Al-Hagri, M. Chiesa and S. Santos, *Appl. Phys. Lett.*, 2022, **121**, 031901, DOI: [10.1063/5.0098788](https://doi.org/10.1063/5.0098788).
- 35 C. Di Valentin, G. Pacchioni and A. Selloni, *Chem. Mater.*, 2015, **17**, 6656–6665, DOI: [10.1021/cm051921h](https://doi.org/10.1021/cm051921h).
- 36 T. Dittrich, J. Sydorenko, N. Spalatu, N. H. Nickel, A. Mere, M. Krunk and I. Oja Acik, *ACS Appl. Mater. Interfaces*, 2022, **14**, 43163–43170, DOI: [10.1021/acsami.2c09032](https://doi.org/10.1021/acsami.2c09032).
- 37 R. Wang, M. Shi, F. Xu, Y. Qiu, P. Zhang, K. Shen, Q. Zhao, J. Yu and Y. Zhang, *Nat. Commun.*, 2020, **11**, 4465, DOI: [10.1038/s41467-020-18267-1](https://doi.org/10.1038/s41467-020-18267-1).
- 38 R. Chen, J. Li, H. Wang, P. Chen, X. Dong, Y. Sun, Y. Zhou and F. Dong, *J. Mater. Chem. A*, 2021, **9**, 20184, DOI: [10.1039/d1ta03705f](https://doi.org/10.1039/d1ta03705f).
- 39 Z. Rao, G. Lu, L. Chen, A. Mahmood, G. Shi, Z. Tang, X. Xie and J. Sun, *Chem. Eng. J.*, 2022, **430**, 132766, DOI: [10.1016/j.cej.2021.132766](https://doi.org/10.1016/j.cej.2021.132766).
- 40 I. Dundar, M. Krichevskaya, A. Katerski, M. Krunk and I. O. Acik, *Catalysts*, 2019, **9**, 915, DOI: [10.3390/catal9110915](https://doi.org/10.3390/catal9110915).
- 41 N. Serpone, *J. Photochem. Photobiol., A*, 1997, **104**, 1–12, DOI: [10.1016/S1010-6030\(96\)04538-8](https://doi.org/10.1016/S1010-6030(96)04538-8).
- 42 X. Dai, Y. Wang, X. Wang, S. Tong and X. Xie, *Appl. Surf. Sci.*, 2019, **485**, 255–265, DOI: [10.1016/j.apsusc.2019.04.221](https://doi.org/10.1016/j.apsusc.2019.04.221).
- 43 L. Zhong and F. Haghight, *Build. Environ.*, 2015, **91**, 191–203, DOI: [10.1016/j.buildenv.2015.01.033](https://doi.org/10.1016/j.buildenv.2015.01.033).
- 44 J. Mo, Y. Zhang, Q. Xu, Y. Zhu, J. J. Lamson and R. Zhao, *Appl. Catal., B*, 2009, **89**, 570–576, DOI: [10.1016/j.apcatb.2009.01.015](https://doi.org/10.1016/j.apcatb.2009.01.015).
- 45 H. Einaga, S. Futamura and T. Ibusuki, *Appl. Catal., B*, 2002, **38**, 215–225, DOI: [10.1016/S0926-3373\(02\)00056-5](https://doi.org/10.1016/S0926-3373(02)00056-5).
- 46 S. Jöks, D. Klauson, M. Krichevskaya, S. Preis, F. Qi, A. Weber, A. Moiseev and J. Deubener, *Appl. Catal., B*, 2012, **111–112**, 1–9, DOI: [10.1016/j.apcatb.2011.09.007](https://doi.org/10.1016/j.apcatb.2011.09.007).
- 47 M. Sleiman, P. Conchon, C. Ferronato and J. M. Chovelon, *Appl. Catal., B*, 2009, **86**, 159–165, DOI: [10.1016/j.apcatb.2008.08.003](https://doi.org/10.1016/j.apcatb.2008.08.003).
- 48 Y. Ku, J. S. Chen and H. W. Chen, *J. Air Waste Manage. Assoc.*, 2007, **57**, 279–285, DOI: [10.1080/10473289.2007.10465335](https://doi.org/10.1080/10473289.2007.10465335).



Appendix 2

Table 1.1. Comparative table of photocatalytic oxidation of VOCs on the TiO₂ thin films.

Photocatalyst	Thick-ness	Pollutant	Initial concen-tration	Reactor	Catalyst surface area	Light source	Oxidation conditions	Conversion/ degradation rate	Reac-tion time	Ref
Sol-gel dip-coated TiO ₂ thin film	0.9 μm	Acetaldehyde	3 ppm	Continuous flow reactor	50 cm ²	UV-A, 1 mW cm ⁻²	RH 50%, Air flow rate 0.5 L min ⁻¹	80%	0.2 s	[175]
Spray pyrolysis-synthesized TiO ₂ thin film	2.1 μm	Acetaldehyde	1350 ppm	Batch 1.5 L reactor	50 cm ²	UV-A, 1.2 mW cm ⁻²	Dry air	48%	60 min	[176]
Atomic layer deposited TiO ₂ thin film	1 μm	Acetaldehyde	50 ppm	Continuous flow reactor	7.5 cm ²	UV-A, 2.6 mW cm ⁻²	RH 5%, Air flow rate 0.4 L min ⁻¹	72%	1.2 s	[177]

TiO ₂ thin film deposited by evaporation technique	100 nm	Acetaldehyde	40 ppm	Continuous flow reactor	594 cm ²	UV-A, 39.5 mW cm ⁻²	RH 5%, Air flow rate 0.5 L min ⁻¹	80.5%	20 s	[47]
Spin-coated TiO ₂ -SiO ₂ thin film	Not reported	Acetaldehyde	2500 ppm	Batch reactor	131 cm ²	UV-A, 3.5 mW cm ⁻²	Dry air	70%	300 min	[178]
Spray pyrolysis-synthesized TiO ₂ thin film	200 nm	Acetaldehyde	10 ppm	Continuous flow reactor	600 cm ²	UV-A, 3.5 mW cm ⁻²	RH 6%, Air flow rate 0.5 L min ⁻¹	75%	78 s	[59]
Spray pyrolysis-synthesized TiO ₂ thin film	200 nm	Acetaldehyde	10 ppm	Continuous flow reactor	600 cm ²	UV-A, 3.5 mW cm ⁻²	RH 40%, Air flow rate 0.5 L min ⁻¹	75%	78 s	[59]
Magnetron sputtered TiO ₂ thin film	900 nm	Acetaldehyde	10 ppm	Continuous flow reactor	25 cm ²	UV LEDs, 70 mW	RH 0%, Air flow rate 0.15 L min ⁻¹	1.831 mmol cm ⁻² min ⁻¹	11 s	[94]
Magnetron sputtered TiO ₂ thin film	900 nm	Acetaldehyde	10 ppm	Continuous flow reactor	25 cm ²	UV LEDs, 70 mW	RH 40%, Air flow rate 0.15 L min ⁻¹	1.542 mmol cm ⁻² min ⁻¹	11 s	[94]

Spray pyrolysis-synthesized TiO ₂ thin film	200 nm	Acetone	10 ppm	Continuous flow reactor	600 cm ²	UV-A, 3.5 mW cm ⁻²	RH 6%, Air flow rate 0.5 L min ⁻¹	93%	78 s	[59]
Spray pyrolysis-synthesized TiO ₂ thin film	200 nm	Acetone	10 ppm	Continuous flow reactor	600 cm ²	UV-A, 3.5 mW cm ⁻²	RH 40%, Air flow rate 0.5 L min ⁻¹	30%	78 s	[59]
Spray pyrolysis-synthesized TiO ₂ thin film	200 nm	Acetone	10 ppm	Continuous flow reactor	600 cm ²	VIS, 3.3 mW cm ⁻²	RH 40% Air flow rate 0.5 L min ⁻¹	33%	78 s	[59]
Sol-gel wash-coated TiO ₂ thin film	Not reported	Acetone	10 ppm	Continuous flow reactor	6.25 cm ²	Fluorescent lamp 6W	Dry air, Air flow rate 2 L min ⁻¹	70%	0.2 s	[179]
Sol-gel dip coated TiO ₂ /ZrO ₂ thin film	Not reported	Acetone	1652 ppm	Continuous flow reactor	81.6 cm ²	UV-A, 3.1 mW cm ⁻²	Air flow rate 0.015 L min ⁻¹	60%	1.8 s	[180]
Spray pyrolysis-synthesized TiO ₂ thin film	200 nm	Heptane	10 ppm	Continuous flow reactor	600 cm ²	UV-A, 3.5 mW cm ⁻²	RH 6%, Air flow rate 0.5 L min ⁻¹	48%	78 s	[59]
Spray pyrolysis-	200 nm	Heptane	10 ppm	Continuous flow reactor	600 cm ²	UV-A, 3.5	RH 40%, Air flow	20%	78 s	[59]

synthesized TiO ₂ thin film						mW cm ⁻²	rate 0.5 L min ⁻¹			
TiO ₂ thin film prepared by electron beam evaporation	20 nm	Toluene	5 ppm	Batch 0.314 L reactor	18.75 cm ²	UV-A, 30.4 mW cm ⁻²	Water vapour atmosphere	40%	30 min	[46]
Sol-gel dip-coated TiO ₂ thin film	470 nm	Toluene	192 ppm	Batch 0.55 L recirculating reactor	20 cm ²	UV-A, 4W	Dry air, Recirculation flow rate 0.075 L min ⁻¹	60%	2 h	[53]
Sol-gel dip-coated Ti _{0.90} Zr _{0.10} O ₂ thin film	540 nm	Toluene	192 ppm	Batch 0.55 L recirculating reactor	20 cm ²	UV-A, 4W	Dry air, Recirculation flow rate 0.075 L min ⁻¹	70%	2 h	[53]
Sol-gel dip-coated 10% ZrO ₂ /TiO ₂ thin film	410 nm	Toluene	192 ppm	Batch 0.55 L recirculating reactor	20 cm ²	UV-A, 4W	Dry air, Recirculation flow rate 0.075 L min ⁻¹	50%	2 h	[53]
Sol-gel dip-coated TiO ₂ thin film	Not reported	Toluene	50-180 ppm	Batch 1.1 L reactor	68 cm ²	UV-LED, 10 mW cm ⁻²	Dry air	1.83 x 10 ⁻⁴ mol m ⁻³ min ⁻¹	1 h	[181]
Sol-gel dip-coated 0.7% Fe-TiO ₂ thin film	Not reported	Toluene	50-180 ppm	Batch 1.1 L reactor	68 cm ²	UV-LED, 10 mW cm ⁻²	Dry air	2.57 x 10 ⁻⁴ mol m ⁻³ min ⁻¹	1 h	[181]

Sol-gel dip-coated TiO ₂ thin film	0.9 μm	Toluene	1 ppm	Continuous flow reactor	50 cm ²	UV-A, 1 mW cm ⁻²	RH 50%, Air flow rate 0.5 L min ⁻¹	46%	0.2 s	[175]
Sol-gel dip coated TiO ₂ thin film	350 nm	Toluene	155 ppb	Benchtop continuous flow reactor	1.2 cm ²	UV-C, 3.0 mW cm ⁻²	Air flow rate 0.5 L min ⁻¹ , dry air	78%	1 s	[54]
Sol-gel dip coated TiO ₂	1.3 μm	Toluene	0.5 ppm	Continuous flow tubular reactor	184 cm ²	UV-A, 10W	Air flow rate 0.2 L min ⁻¹ , dry air	95%	25 s	[182]
Sol-gel dip coated porphyrin-sensitized TiO ₂ thin films	1.3 μm	Toluene	0.5 ppm	Continuous flow tubular reactor	184 cm ²	VIS, 10W	Air flow rate 0.2 L min ⁻¹ , dry air	15%	25 s	[182]

Curriculum vitae

Personal data

Name: Jekaterina Sydorenko (née Spiridonova)
Date of birth: 24.12.1991
Place of birth: Narva, Estonia
Citizenship: Estonian

Contact data

E-mail: jekaterina.spiridono@taltech.ee

Education

2018–2022 Tallinn University of Technology, Materials and Environmental Technology – PhD
2014–2016 Tallinn University of Technology, Chemical and Environmental Technology – MSC (cum laude)
2011–2014 Tallinn University of Technology, Chemical and Environmental Technology – BSC
1999–2011 Narva Pähklikmäe Gümnaasium

Language competence

Russian native speaker
Estonian fluent
English fluent

Professional employment

2018–2022 Tallinn University of Technology, School of Engineering, Department of Materials and Environmental Technology, Junior Researcher
2016–2018 PharmaEstica Manufacturing OÜ, Quality Control Analyst

Defended dissertations

Master's Degree, 2016, Gas-phase photocatalytic reactor for the study of thin films' activity, Tallinn University of Technology, Department of Chemical and Environmental Technology. Supervisor: Marina Kritševskaja.

Involvement in research projects

IUT19-4 "Thin films and nanomaterials by wet-chemical methods for next-generation photovoltaics (1.01.2014–31.12.2019)"

PRG627 "Antimony chalcogenide thin films for next-generation semi-transparent solar cells applicable in electricity producing windows (1.01.2020–31.12.2024)"

TAR16016EK "Advanced materials and high-technology devices for energy recuperation systems (1.01.2015–1.03.2023)"

Awards

2022 Tallinn city Rae scholarship
2022 Dora Plus program (activity 1.1) scholarship

Participation in conferences

- 2022 Attendance with an oral presentation at “11th European Conference on Solar Chemistry and Photocatalysis: Environmental Applications (SPEA)”;
- 2022–2018 Attendance with oral and poster presentations at Graduate School of Functional Materials and Technologies (GSFMT) scientific conferences
- 2019 Attendance with an oral presentation at “European Materials Research Society (E-MRS)”;
- Fall meeting, September 16-19, Poland, Warsaw

Supervised dissertations

Dmitri Ivanov, Master’s Degree, 2020, (sup) Marina Kritševskaja; **Jekaterina Spiridonova**, Gas-phase photocatalytic activity of spray-pyrolysis-synthesized TiO₂ thin films modified by increased amount of acetylacetone in precursor solution, Tallinn University of Technology School of Engineering, Department of Materials and Environmental Technology

Julia Komljuk, Bachelor’s Degree, 2022, (sup) **Jekaterina Sydorenko**, Optimal temperature determination of sprayed TiO₂ thin films prepared for photocatalytic applications, Tallinn University of Technology School of Engineering, Department of Materials and Environmental Technology

Rasmus Tõniste, Bachelor’s Degree, 2022, (sup) **Jekaterina Sydorenko**; Ilona Oja Acik, Development of self-cleaning surface coatings, Tallinn University of Technology School of Engineering, Department of Materials and Environmental Technology

List of publications

T. Dittrich, **J. Sydorenko**, N. Spalatu, N. H. Nickel, A. Mere, M. Krunks, I. Oja Acik. “Synthesis control of charge separation at anatase TiO₂ thin films studied by transient surface photovoltage spectroscopy”, ACS Applied Materials & Interfaces journal, 14(38), 43163-43170, 2022, doi.org/10.1021/acsami.2c09032.

T. Olukan, **J. Sydorenko**, A. Katerski, M. Al Mahri, C-Y. Lai, A. Al-Hagri, S. Santos, M. Chiesa. “Insights into TiO₂ thin film photodegradation from Kelvin Probe AFM maps”, Applied Physics Letters, 121(3), 031901, 2022, dx.doi.org/10.1063/5.0098788.

J. Sydorenko, A. Mere, M. Krunks, M. Krichevskaya, I. Oja Acik. “Transparent TiO₂ thin films with high photocatalytic activity for indoor air purification”, RSC Advances, 12(55), 35531-35542, 2022, https://doi.org/10.1039/D2RA06488J.

J. Spiridonova, A. Mere, M. Krunks, M. Rosenberg, A. Kahru, M. Danilson, M. Krichevskaya, I. Oja Acik. “Enhanced visible and ultraviolet light-Induced gas-phase photocatalytic activity of TiO₂ thin films modified by increased amount of acetylacetone in precursor solution for spray pyrolysis,” Catalysts, 10(9), 1011, 2020, doi.org/10.3390/catal10091011.

J. Spiridonova, A. Katerski, M. Danilson, M. Krichevskaya, M. Krunks, I. Oja Acik. “Effect of the titanium isopropoxide:acetylacetone molar ratio on the photocatalytic activity of TiO₂ thin films”, Molecules, 24(23), 4326, 2019, doi.org/10.3390/molecules24234326.

Popular science publications

- 2021, April “Innovative coatings for air purification from harmful viruses and bacteria”, article in portal Novaator, ERR, in Estonian language.
<https://novaator.err.ee/1608169126/uudsed-pinnakatted-puhastavad-ohu-kahjulikest-viirustest-ja-bakteritest>
- 2021, April “Innovative coatings for air purification from harmful viruses and bacteria”, article in portal Research in Estonia, English translation of article in portal Novaator, ERR,
<https://researchinestonia.eu/2021/04/27/innovative-coatings-clean-the-air-of-harmful-viruses-and-bacteria/>
- 2021, Aprill “Tallinna teadlased leiutasid õhku puhastavad pinnakatted”, interview in portal Forte Delfi, in Estonian language.
<https://forte.delfi.ee/artikkel/93199975/tallinna-teadlased-leiutasid-ohku-puhastavad-pinnakatted>
- 2021, April “TalTech develops self-cleaning titanium dioxide coating”, interview in morning show ETV+ Кофе+, in Russian language.
<https://etvpluss.err.ee/1608192499/v-taltech-razrabotali-samoochiwajuweesja-pokrytie-na-osnove-dioksida-titana>

Elulookirjeldus

Isikuandmed

Nimi: Jekaterina Sydorenko (endine Spiridonova)
Sünniaeg: 24.12.1991
Sünnikoht: Narva, Eesti
Kodakondsus: Eesti

Kontaktandmed

E-post: jekaterina.spiridono@taltech.ee

Hariduskäik

2018–2022 Tallinna Tehnikaülikool, Inseneriteaduskond, Materjali- ja keskkonnatehnoloogia instituut – PhD
2014–2016 Tallinna Tehnikaülikool, Keemia- ja keskkonnakaitse tehnoloogia instituut – magistrikraad (cum laude)
2011–2014 Tallinna Tehnikaülikool, Keemia- ja keskkonnakaitse tehnoloogia instituut – bakalaureusekraad
1999–2011 Narva Pähklmäe Gümnaasium

Keelteoskus

Vene keel emakeel
Eesti keel kõrgtase
Inglise keel kõrgtase

Teenistuskäik

2018–2022 Tallinna Tehnikaülikool, Inseneriteaduskond, Materjali- ja keskkonnatehnoloogia instituut, doktorant-nooremteadur
2016–2018 PharmaEstica Manufacturing OÜ, Kvaliteedikontrolli osakonna analüütik

Kaitstud väitekirjad

Magistrikraad, 2016, Gaasifaasiline fotokatalüütiline reaktor õhukeste kiledede aktiivsuse uurimiseks, Tallinna Tehnikaülikool, Keemia ja materjalitehnoloogia teaduskond, Keemiatehnika instituut, Keskkonnakaitse ja keemiatehnoloogia õppetool, Juhendaja: Marina Kritševskaja

Teadusprojektid

IUT19-4 "Õhukesed kiled ja nanomaterjalid keemilistel vedeliksadestusmeetoditel uue põlvkonna fotovoltseadistele (1.01.2014–31.12.2019)"

PRG627 "Antimon-kalkogeniid õhukesed kiled järgmise põlvkonna pool-läbipaistvatele päikeseelementidele kasutamiseks elektrit tootvates akendes (1.01.2020–31.12.2024)"

TAR16016EK "Uudsed materjalid ja kõrgtehnoloogilised seadmed energia salvestamise ja muundamise süsteemidele (1.01.2015–1.03.2023)"

Tunnustused

2022	Tallinna linna Raestipendium
2022	Dora Pluss programmi (tegevus 1.1) stipendium

Osalemise konverentsidel

2022	Suulise ettekandega esinemine konverentsil "11th European Conference on Solar Chemistry and Photocatalysis: Environmental Applications (SPEA)"; 6-10.06.2022, Torino, Itaalia
2022–2018	Suulise ja posterettekannetega esinemine Funktsionaalsete materjalide ja tehnoloogiate doktorikooli (FMTDK) teaduskonverentsidel
2019	Suulise ettekandega esinemine konverentsil "European Materials Research Society (E-MRS)"; Fall meeting, 16-19.09.2019, Poola, Varssavi

Juhendatud lõputööd

Dmitri Ivanov, magistrikraad 2020, (juh) Marina Kritševskaja; **Jekaterina Spiridonova**, Gas-phase photocatalytic activity of spray-pyrolysis-synthesized TiO₂ thin films modified by increased amount of acetylacetone in precursor solution, Tallinn University of Technology School of Engineering, Department of Materials and Environmental Technology

Julia Komljuk, bakalaureusekraad, 2022, (juh) **Jekaterina Sydorenko**, Pihustuspürolüüsiga sünteesitud TiO₂ õhukeste kilede optimaalse sadestustemperatuuri leidmine fotokatalüütiliseks kasutamiseks, Tallinna Tehnikaülikool, Inseneriteaduskond, Materjali- ja keskkonnatehnoloogia instituut

Rasmus Tõniste, bakalaureusekraad, 2022, (juh) **Jekaterina Sydorenko**; Ilona Oja Acik, Isepuhastuvate pinnakatete väljatootamine, Tallinna Tehnikaülikool, Inseneriteaduskond, Materjali- ja keskkonnatehnoloogia instituut

Teaduspublikatsioonid

T. Dittrich, **J. Sydorenko**, N. Spalatu, N. H. Nickel, A. Mere, M. Krunks, I. Oja Acik. "Synthesis control of charge separation at anatase TiO₂ thin films studied by transient surface photovoltage spectroscopy", ACS Applied Materials & Interfaces journal, 14(38), 43163-43170, 2022, doi.org/10.1021/acsami.2c09032.

T. Olukan, **J. Sydorenko**, A. Katerski, M. Al Mahri, C-Y. Lai, A. Al-Hagri, S. Santos, M. Chiesa. "Insights into TiO₂ thin film photodegradation from Kelvin Probe AFM maps", Applied Physics Letters, 121(3), 031901, 2022, dx.doi.org/10.1063/5.0098788.

J. Sydorenko, A. Mere, M. Krunks, M. Krichevskaya, I. Oja Acik. "Transparent TiO₂ thin films with high photocatalytic activity for indoor air purification", RSC Advances, 12(55), 35531-35542, 2022, https://doi.org/10.1039/D2RA06488J.

J. Spiridonova, A. Mere, M. Krunks, M. Rosenberg, A. Kahru, M. Danilson, M. Krichevskaya, I. Oja Acik. "Enhanced visible and ultraviolet light-Induced gas-phase photocatalytic activity of TiO₂ thin films modified by increased amount of acetylacetone in precursor solution for spray pyrolysis", Catalysts, 10(9), 1011, 2020, doi.org/10.3390/catal10091011.

J. Spiridonova, A. Katerski, M. Danilson, M. Krichevskaya, M. Krunks, I. Oja Acik. "Effect of the titanium isopropoxide:acetylacetone molar ratio on the photocatalytic activity of TiO₂ thin films", *Molecules*, 24(23), 4326, 2019, doi.org/10.3390/molecules24234326.

Populaarteaduspublikatsioonid

- 2021, Aprill "Uudsed pinnakatted puhastavad õhu kahjulikest viirustest ja bakteritest" publikatsioon portaalis Novaator, ERR
<https://novaator.err.ee/1608169126/uudsed-pinnakatted-puhastavad-ohu-kahjulikest-viirustest-ja-bakteritest>
- 2021, Aprill "Innovative coatings for air purification from harmful viruses and bacteria" publikatsioon portaalis Research in Estonia, Novaator, ERR ingliskeelne tõlge.
<https://researchinestonia.eu/2021/04/27/innovative-coatings-clean-the-air-of-harmful-viruses-and-bacteria/>
- 2021, Aprill "Tallinna teadlased leiutasid õhku puhastavad pinnakatted" intervjuu portaalis Forte Delfi.
<https://forte.delfi.ee/artikkel/93199975/tallinna-teadlased-leiutasid-ohku-puhastavad-pinnakatted>
- 2021, Aprill "TalTech arendab isepuhastuvat titaandioksiid pinnakatet" intervjuu saates ETV+ Koφe+, vene keeles
<https://etvpluss.err.ee/1608192499/v-taltech-razrabotali-samoochiwajuweesja-pokrytie-na-osnove-dioksida-titana>

ISSN 2585-6901 (PDF)
ISBN 978-9949-83-955-1 (PDF)